Auxin and the nodule

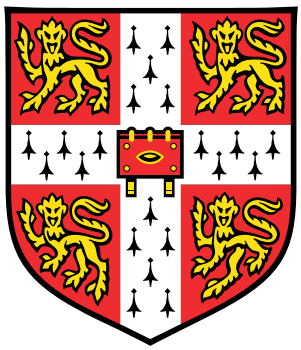

Ioannis Tamvakis

Sainsbury Lab

University of Cambridge

This dissertation is submitted for the degree of

Doctor of Philosophy

Darwin College

2021

To Ties..

Declaration

I hereby declare that except where specific reference is made to the work of others, the contents of this dissertation are original and have not been submitted in whole or in part for consideration for any other degree or qualification in this, or any other University. This dissertation is the result of my own work and includes nothing which is the outcome of work done in collaboration, except where specifically indicated in the text. This dissertation contains fewer than 65,000 words including appendices, bibliography, footnotes, tables and equations and has less than 150 figures. This dissertation is submitted for the degree of doctor of philosophy in Darwin College, Cambridge University, 2021.

Ioannis Tamvakis
2021

Acknowledgements

I would like to express my deep appreciation for the scientific interaction and friendship of Ross Carter, Nadia Radzman, Marie Bruser, Veronica Grieneisen and Stan Maree, Giuseppe Fracetti, Rea Kourounioti, John Fozard, Tjelvar Olsson, Eleni Soumpourou, Laila Moubayidin, Myriam Charpentier, Nuno Leitao, Leonie Luginbuehl, Guru Radhakrishnan, Henrik Ahl, Vasiliki Kanellaki, the Oldroyd group, the Jonsson group, and above all, the organogenesis team and its organiser, Jodi Lilley.

Chapter 2: I would like to thank the organogenesis team of the Oldroyd lab for their helpful suggestions and support.

Chapter 3: This chapter was done in collaboration with Jodi Lilley, Katharina Schiessl, Aaron Thomas and the whole organogenesis team, with help from Tjelvar Olsson and Guru Radhakrishnan.

Chapter 4: I would like to thank the organogenesis team, Sean Jones, Nadia Radzman and Katie Abley.

Chapter 5: Yucasin and Yucasin DF was kindly provided by Tomokazu Koshiba. Many thanks to Allan Downie for input on the alfalfa protocol.

This work was done in the labs of Giles Oldroyd, Veronica Grieneisen and Henrik Jonsson. I would like to express my deepest gratitude to them for giving me the opportunity to experience science in each of their unique labs. I would also like to thank BBSRC, ENSA and the Bill and Melinda Gates foundation for supporting science, in the pursue to deepen our scientific understanding of nature, to responsibly feed the world.

More friends that helped me develop during my time in the UK are named in the companion document "Antithesis" where important PhD parerga unrelated to nodule development reside, available on request.

Abstract

In this work we aim to characterise the role of the plant hormone auxin in the development of nitrogen-fixing, indeterminate legume nodules. More specifically we want to know the timing of, and the processes responsible for, the auxin signaling induction detected upon inoculation of the root of *Medicago truncatula* with its symbiotic rhizobium, *Sinorhizobium meliloti*. Using a variety of approaches, we uncover the role of local auxin biosynthesis in the initiation of the indeterminate nodule, and indicate how local auxin biosynthesis is necessary and sufficient for lateral organ induction in *M. truncatula*. By employing the use of dynamic models of auxin transport, we combine our results with previous studies into a unified understanding of the interactions between auxin biosynthesis, auxin transport, and gene regulatory networks driving nodule development.

Contents

List of Figures

Chapter 1

Introduction

1.1 The evolution of plant root symbioses

Symbiosis between different phyla is a recurring and important novelty of life[1]. In many cases, modification of development underpins symbiotic success. This holds true in many species across the kingdoms of life, from the general adaptations of mammals to host bacteria in their intestines to the specific adaptations of Acacia trees to host ant colonies on their branches[2]. Plants, specifically, are masters in forming symbioses. Among these, the ones that aim to increase the influx of bio-available nitrogen from the atmosphere are decisive for the lifecycle and biomass of many ecosystems on Earth, and are formed between plants and diazotrophic bacteria[3]. Examples include the symbiosis of Cycads and nitrogen-fixing cyanobacteria, inside collaroid roots[4], the symbiosis of actinorhizal plants with filamentous *Frankia* actinomycetes[5], the symbiosis of diazotrophic bacteria in the mucilage of aerial roots of Mexican maize[6], and the symbiosis of legumes and *Parasponia* with rhizobia. These plants have the capability to form developmental structures specifically designed to host the symbiont, which in many cases increases the rates of nitrogen-fixation greatly. Legumes are prime example of this, as they form specialized root organs, the nodules, in which they host rhizobia. Not all plants, however, are capable of forming such symbioses, and in many anthropogenic environments on earth there is a lack of nitrogen-fixing plants. This thesis aims to elucidate how symbiosis and plant development are interlinked in legume nodules, in the broadest sense possible. The work herein should help in engineering this symbiosis into cereals.

1.1.1 The two main symbioses

The most ancient and widespread symbiosis of land plants is with mycorrhiza. Starting as far back as the Devonian period[7], it is estimated that currently as much as 80% of plant species might engage in it[8]. During mycorrhization the plant provides to the fungus fixed carbon and gets in return water and mineral nutrients, effectively increasing root foraging. In the case of the symbiosis of plants with Arbuscular Mycorrhizal (AM) fungi of the phylum Glomeromycota, the fungal hyphae penetrate root cells and form branched structures inside them, called arbuscules, where resource exchange takes place. The fungal networks in many cases are essential for sufficient phosphate supply, and engage in sophisticated trading with the plant hosts[9].

Building on previous success, plants of the orders Fabales, Fagales, Rosales and Cucurbitales have managed to allow, instead of fungi, nitrogen fixing bacteria of the genus *Frankia,* or *Rhizobium*, to colonize their roots. Phylogenetic analyses have estimated that land plants became predisposed to form this symbiosis around 100 million years ago[10, 11]. Similarly to the AM symbiosis, the bacteria penetrate the root, either intercellularly or intracellularly. In many cases the root cells reinitiate cell divisions and form a host organ, the nodule, with specialized morphology. Rhizobia provide the plant with ammonium by fixing nitrogen directly from the atmosphere, and the plant in return sustains them with fixed carbon.

1.1.2 Switching symbiotic partner

Intimate chemical communication between the two symbionts is key for symbiotic success. Before and during AM symbiosis starving plant roots exude strigolactones, which the fungi recognize as chemical signals. The fungi from their part produce polysaccharides known as Mycorhization (Myc) factors that the plant roots perceive using the so-called Common Symbiosis Pathway[12]. Perception of these symbiont-derived polysaccharides is mediated by LysM-receptor-kinases at the plasma membrane. These receptors have been co-opted from chitin-perception of immunity signaling, and have been evolving to recognize a diverse array of Myc and Nodulation (Nod) factors[13]. In fact plants seem to recognize both chitin-oligosaccharides (COs) derived from the fungal cell wall and lipo-chito-oligosaccharides (LCOs) made by both types of symbionts, to recognize friend from foe[14]. Recently it was shown that fungal LCOs have a much more widespread role than previously anticipated in regulating fungal development, even in non-symbiotic fungi[15]. Switching symbiotic partner is mediated by the ability of the LysM receptors to recognize new molecular signatures[16]. The most important switch happened when plants learned to recognize rhizobia in increasing stringency. Nitrogen-fixing rhizobia have since evolved highly decorated LCOs called Nod

factors, which they produce upon perception of exuded flavonoids from plant roots[17, 18]. Plasmids containing the genes required for nitrogen fixation as well as the production of Nod factors can confer symbiont status to Agrobacteria[19, 20], so Nod factors could act to advertise to plants the existence of nitrogen fixing capabilities. Consequently, like in marketing, product personalization and brand loyalty can be of paramount importance. Gene duplication and neofunctionalisation of the LysM-receptors have equipped legumes with stringent and extremely sensitive recognition of LCOs from their symbiotic partner, of which they can be highly selective[14]. It was recently shown that cereals, under extreme nutrient deficiency, can recognize LCOs categorized as Nod factors with the same proclivity as Myc factors[21], so one can ponder as to what stopped cereals from evolving a nitrogen-fixing symbiosis.

Upon recognition of COs or LCOs by the LysM-receptor-kinases, in conjunction with a Leucine-Rich Repeat (LRR) - containing receptor kinase, a burst of reactive oxygen species (ROS) and influx of calcium across the plasma membrane (PM) happen, as well as induction of calcium oscilations at the nucleus[14, 22]. These are present in both AM and nodule symbiosis, and are realized by ion channels regulating synchronous counterflows of calcium and potassium across the nucleus and the endoplasmic reticulum (ER)[22]. This in turn leads to the activation of the Ca2+/calmodulin-dependent protein kinase (CCaMK), which decodes calcium oscillations and induces subsequent transcriptional cascades[23–25].

1.1.3 The nodule symbiosis

Successful molecular signaling between legumes and rhizobia leads to two processes that develop in parallel. The first one is the internalization of the bacteria, and the second one is the formation of the nodule primordium, where cells will be made, capable to host the bacteria. Internalization of the bacteria can be done in many ways, the most primitive being crack entry and extracellular infection of the site. In many legume species however, like *Medicago truncatula*, successful signaling leads to activation of chemotactic root hair growth, that leads to the tip of the root hair encircling the rhizobium and sealing it from the rhizosphere[26]. After this, major cytoskeletal, polar cargo transport, and signaling changes enable the plant cell to grow an “infection thread”, a tube that will pass from cell to cell in an elaborate process that requires cell to cell signaling, and transfer the rhizobia for internalization in specialized plant cells, where they differentiate and form symbiosomes[26].

Another novelty of the symbiosis with bacteria is the formation of the nodule, a lateral organ of the root specifically grown to host the bacteria. The importance of having an organ regulating the site of bacterial infection is easily apparent. The nodule acts to provide the bacterioids with enough space to occupy, while at the same time spatially restricting the bacteria within a tissue type capable of hosting them. It connects the bacteria with the plant vasculature

and the atmosphere, so that the necessary exchange of nutrients and gasses can occur. As a self regulated unit, it can itself be regulated in terms of numbers by whole-plant morphogenetic regulatory processes, such as the Autoregulation of Nodulation (AON)[27]. A number of different nodule types are recognized in different plant lineages, the main ones being the two appearing in legumes, the indeterminate (*Medicago sativa* (alfalfa), *Medicago truncatula* (barrel medic), *Pisum sativum* (pea), *Trifolium sp.* (clover) etc.) and determinate nodules *(Glycine max*(soybean), *Phaseolus sp.* (bean), *Lotus japonicus* (Japanese trefoil) etc.)[28], a classification that has nothing to do with legume phylogeny[29] . Outside the legume family, nodules are also present in the symbioses of some plants with actinomycetes of the genus Frankia, for example in the plant *Casuarina glauca*[30]. Parasponia of the Ulmacae family is also able to nodulate[31]. The angiosperm *Gunnera*, on the other hand, hosts *Nostoc* cyanobacteria inside infected glands at the base of its leaves[32]. Here we are specifically interested in the morphogenesis of the indeterminate and determinate nodules formed by the legume family. Classification in these two nodule types has to do with growth patterns[29]: In indeterminate nodules, the initial cell divisions happen in the pericycle, endodermis and inner cortex layers of the root, and then a new meristem surpasses the infected cells of the cortex and positions itself in the outer cortex, making this type of nodule capable of sustained growth, leading to an elongated shape with a cell differentiation gradient[33]. In determinate nodules this pattern inverts, with the first cell divisions happening in the mid or outer cortex[34] and briefly moving to inner cortex, with arrest of cell division when the domain of cell divisions reaches the vasculature, or non-sustained central cell divisions and radial expansion[35]. The last cells to differentiate are at the periphery of the determinate nodule[36]. Although Lateral Roots (LRs) and nodules appear to be related organs, there is a key difference in the way they are initiated. LRs have been shown to emerge from pre-patterned lateral root founder cells[37], whereas nodules do not seem to have a site preference, apart from the tissue type they emerge from. In some plants however, nodules appear to stem from LR initials and maintain a more primitive LR-like structure[38].

1.1.4 Root zone and tissues susceptible to nodulation

Legume nodules arise from a specific zone of the root, called the susceptibility zone. Already suggested by Nutman as the zone of the root where the root hairs grow (1948,[39]), the extent of the susceptibility zone was carefully measured by Bhuvaneswari *et al* in a series of publications[40–43]. In cowpea and soybean, the root was reported to have peak infectivity at the point of the root where the root hairs are just emerging (best spot for inoculation, BSFI), after flood inoculation with rhizobia. The vast majority of nodules grew in a region of the root with BSFI at the center of this region, and the distance between BSFI and root tip as the radius

of this region. Nodules were reported to grow on new growth of the root as well, after the point where the root tip was at the time of inoculation[40, 42]. Different legumes have different susceptibility zone profiles: Alfalfa and cowpea were reported to prefer to nodulate from the part of the root that has no root hairs at the time of inoculation. Alfalfa and white clover were able to also nodulate from parts where the root hairs had matured, compared to cowpea and soybean which did not. In *Medicago truncatula*, assessment of the susceptibility zone extent has been done by Mohd-Radzman *et al* [44] to measure the effect of MtCEP peptide on competency for nodulation. The results show that, similar to other legumes, nodules initiate at most 10mm away from the root tip (a point where root hairs have fully emerged), and that exogenous application of CEP peptide shifts nodule initiation to younger parts of the root. The question of what changes the extent and profile (in terms of infectivity) of the susceptibility zone is an important one, as it can identify endogenous pathways with which the plant can modulate nodule numbers.

Nodules initiate, apart from a specific zone, also from specific tissues. In *Medicago truncatula* and many other species the first cell divisions occur at the pericycle cells opposite protoxylem poles[33, 45], the same tissue part where lateral root initials are formed[46, 47]. In *Arabidopsis thaliana* these cells are the most sensitive to exogenous auxin application and divide readily[48]. Understanding how these cells start to divide in nodule initiation, in regards to the signal they receive as well as the main pathways involved should give us a clear perspective on the evolution of nodulation, with the main question being how the nodule is related to lateral roots and which point in lateral root development, if any, was exploited by evolution to link rhizobial infection to developmental processes. Elucidating the main components of both processes is not trivial since both are central to root function and thus heavily regulated and connected to many other aspects of root physiology. In recent years however, central components have been identified, which are both necessary and sufficient for nodule as well as LR initiation[49, 50]. In the next section we will dive deep into the developmental programs of the nodule to describe the key players involved in them.

1.2 Signaling and transcriptional regulation during nodule initiation

The first step of bacterial infection and host-symbiont signaling is perception of a Nod-factor signal through a heterodimeric LysM receptor kinase complex of *Medicago truncatula* Nod Factor Perception (MtNFP) and LysM domain-containing Receptor-Like Kinase (MtLYK3)[51] that leads to Does-not-Make-Infections-2 (MtDMI2)-mediated nuclear calcium oscilations[12].

These are decoded by the Calcium and Calmodulin-dependent protein Kinase (CCaMK) which forms an activated protein complex with, and phosphorylates, Interacting-Protein-of-DMI3 (MtIPD3) (or its functionally redundant copy IPD3-like)[52]. At this point the signal enters the gene regulatory network (GRN) of the plant cells, as IPD3 forms complexes with the transcription factors Nodulation-Signaling-Pathway-1 (MtNSP1) and MtNSP2[53, 54] bridged through binding with DELLA growth regulators[55], and can activate the expression of the master nodulation regulator Nodule-INception (NIN) by direct binding to its gene promoter[23], either by itself or in a complex. The NSPs are able to form other complexes as well, for example (in *Lotus japonicus*) with Interacting-Protein-of-NSP2 (IPN2), again targeting the *NIN* promoter and acting to promote or suppress its transcription based on the presence-absence of each transcription factor[56]. NIN originates from the NIN-Like-Protein (NLP) family of nitrate-responsive transcription factors which affect root growth GRNs in response to nitrate[57], a response which involves Calcium sensing as well, via the action of Calcium-dependent-Protein-Kinases (CPKs)[58]. On close inspection, it is apparent that NIN and NLPs bind to a similar motif: If I compare the *Arabidopsis thaliana* NLP6 consensus binding motif published by Konishi *et al*[59] to the consensus binding motif of *Lotus japonicus* NIN published by Soyano *et al* [60], I can observe similarities of the motif form CTT-N(10)-AAG. Other studies allow the suggestion that NIN is a derived form of NLPs, that has lost binding domains of NLPs important for the nitrate sensing cascade[61] but might have retained the capability to activate the same developmental programs[57, 58, 62, 63]. To summarize, the signaling and transcriptional cascade that leads to expression of NIN happens first in the epidermis, and it is essential for both infection and nodule organogenesis [60, 64, 65]. NIN, alongside ERF-Required-forNodulation-1 (ERN1) will go on to regulate genes crucial for infection thread formation, like Early-NODulin-11 (*ENOD11*), as well as the group of genes Rhizobium-directed-Polar-Growth (*RPG*), Vapyrin (*VPY*) and Lumpy-INfections (*LIN*), the proteins of which organize polar exocytosis and the cytosceletal connection between the nucleus and the tip of the infection thread[26] (Figure 1.1, left part). In the following section we will focus on NIN and nodule organogenesis.

1.2.1 Gene Regulatory Network of Nodulation (GRNN) and Cytokinin

Downstream of NIN expression, the most important and well characterized role in nodule initiation is held by cytokinin. Multiple studies show that cytokinin sensing through the Cytokinin-REceptor-1 (MtCRE1) is necessary and sufficient for nodule organogenesis[66–69]. Intriguingly, NIN does not sit downstream or upstream of cytokinin response, but rather at the same level: NIN directly induces the expression of *CRE1*[70], increasing cytokinin sensitivity, and on the other hand cytokinin signaling, through CRE1, induces the expression of

NIN[65–67, 71]. The elusive direct mechanistic link between cytokinin signaling and *NIN* was found recently in the form of Cytokinin Elements (CEs) which sit upwards of 15 kilobases away from the *NIN* transcriptional start site (TSS) in most nodulating species[72], a distance that might be indicative of the importance of regulating the magnitude of the possitive feedback between cytokinin and *NIN*, assuming regulatory magnitude is a function of distance (meaning, if they were closer to the TSS, the positive feedback might activate everything spontaneously). *NIN* is also indirectly activated by cytokinin through type B response regulators (RR-Bs) binding on the promoter of, and activating the expression of, *NSP2*[73]. As such there are two well established feedback loops. NIN directly upregulates *CRE1*, which in turn, in the presence of cytokinin, activates RR1, which upregulates *NIN*, directly by binding to the CEs, and indirectly through the upregulation of expression of NSP2 which activates the IPN2-NSP1-NSP2 complex to upregulate *NIN* (Figure 1.1, in red and orange). This positive feedback loop with a positive coherent feed forward loop embedded in it could be siting at the core of nodule organogenesis, as feedback loops are known to act as forcing structures in GRNs, creating a dynamic lockdown of the regulatory state[74]. The type of feed forward loop embedded is known to encode for a delay function that makes sure over time that the activating input signal is persistent before activating the downstream target[75], acting as a check, which could include the conditional nuclear relocalization of NSP2[53]. It is interesting to note that cytokinin biosynthesis, through activity of the enzymes LOnely-Guy-1 (MtLOG1) and IsoPentenyl-Transferase-3 (IPT3), is also locally upregulated during nodulation[76], at least through the action of KNOTTED1-like-homeobox-3 (MtKNOX3)[77], however upstream activators are elusive. Lastly, other notable targets of the type-B RRs activated during nodule cytokinin response are *CytoKinin-oXidase-1* (*CKX1*), the protein of which degrades cytokinin, the type-A *RR4*, the protein of which should inactivate CRE1[78–80], forming negative feedback loops on cytokinin signaling, keeping it in check, and *bHLH476*, encoding for a transcription factor that enhances organogenesis[73].

From the point of view of nodule initiation, ranking other parallel and downstream components of the GRNN is less clear. For example, it is known that ERN1/2 AP2/ERF transcription factors (TFs) are essential for nodulation, since the *Medicago truncatula ern1-ern2* double mutant is unable to initiate infection or nodule development[81]. In *Lotus japonicus*, *ERN1*, like *NIN*, is directly upregulated by CCaMK-IPD3[82], while in *Medicago truncatula ERN1* is directly upregulated by the GRAS TFs NSP1 and NSP2[83, 84]. ERNs directly regulate *ENOD11*, with ERN3 being a repressor and ERN1/2 being activators of this important nodulin gene for infection[85]. NSP1/2 are also directly upregulating *ENOD11*[54] in *Medicago*. NIN's role in regulating this module is less clear however, as there is evidence that NIN directly or indirectly represses *ENOD11* expression, [86], while at the same time it

is established that NIN directly upregulates *Nuclear-Factor-Ys* (*NF-Y*s)[60], the proteins of which in turn directly upregulate *ERN1*[84]. It is not known if the role of ERNs in nodule organogenesis is direct or if it is due to successful infection being a natural checkpoint of the process.

1.2.2 GRNN and Auxin

The rest of the regulatory network parts we will consider here will be delineated from the point of view of auxin signaling, as auxin is crucial for both nodule organogenesis[28, 30, 68, 112–115] and infection[116, 117]. Briefly, during infection we have the upregulation of the Auxin-Response-Factor-16 (*ARF16*) around infection threads, whose mutant in *Medicago truncatula* is resistant to infection. In terms of organogenesis, to study auxin dynamics we have to take into account the mobile nature of this principal plant hormone. Auxin has a complex relationship with its transport, which can lead to spatial patterning and morphogenesis[118], and it has been proposed that, in indeterminate nodulators, auxin accumulates proximal to the site of infection due to decreased acropetal polar auxin transport (PAT), either by local increase in flavonoids[18, 112, 119], or another unknown signal that inhibits PAT, which could conceivably be cytokinin[105, 120]. In *Medicago truncatula*, CRE1-dependent upregulation of flavonoid biosynthesis genes inhibits acropetal auxin transport, and external application of flavonoids can rescue nodulation in the *cre1* mutant[68](Figure 1.1, in deep blue). In determinate nodulators however, auxin transport inhibition is not required for nodule organogenesis[113, 121], and flavonoids seem to only act in their regular role in plant-rhizobium communication as rhizobial *NOD* gene inducers[17, 121]. In *Lotus japonicus* auxin accumulation comes about by the expression of the auxin biosynthesis gene Tryptophan-Aminotransferase-of-*Arabidopsis thaliana* (*TAA*)[114]. We show in chapter 3 and 4 that, in *Medicago truncatula*, we also have the expression of auxin biosynthesis genes of the *YUCCA* (*YUC*) family, early during nodule initiation[50], in agreement with previous gene expression studies[122]. How these genes are induced downstream of NIN is not known. One possibility is that STYLISH TFs, the genes of which are known to be directly upregulated in *Medicago truncatula* by NF-Y[93], are upregulating *YUC* genes, as they are known to do in *Arabidopsis thaliana* and *Physcomitrella*[94–96]. Another possibility is that auxin biosynthesis is regulated directly or indirectly by Lateral-organ-Boundaries-Domain (LBD) transcription factors, auxin upregulated master regulators of lateral roots[90–92]. *LBD16* was recently shown to be directly upregulated by NIN both in *Medicago truncatula* and in *Lotus japonicus*([49, 50], and more evidence in chapter 5). Yet another possibility is that meristem master regulators PLETHORA (PLT) TFs are regulating *YUCCA*s, as they are redundantly involved in nodule meristem maintenance[97, 98]. PLTs are known in *Arabidopsis thaliana* to be slowly up-

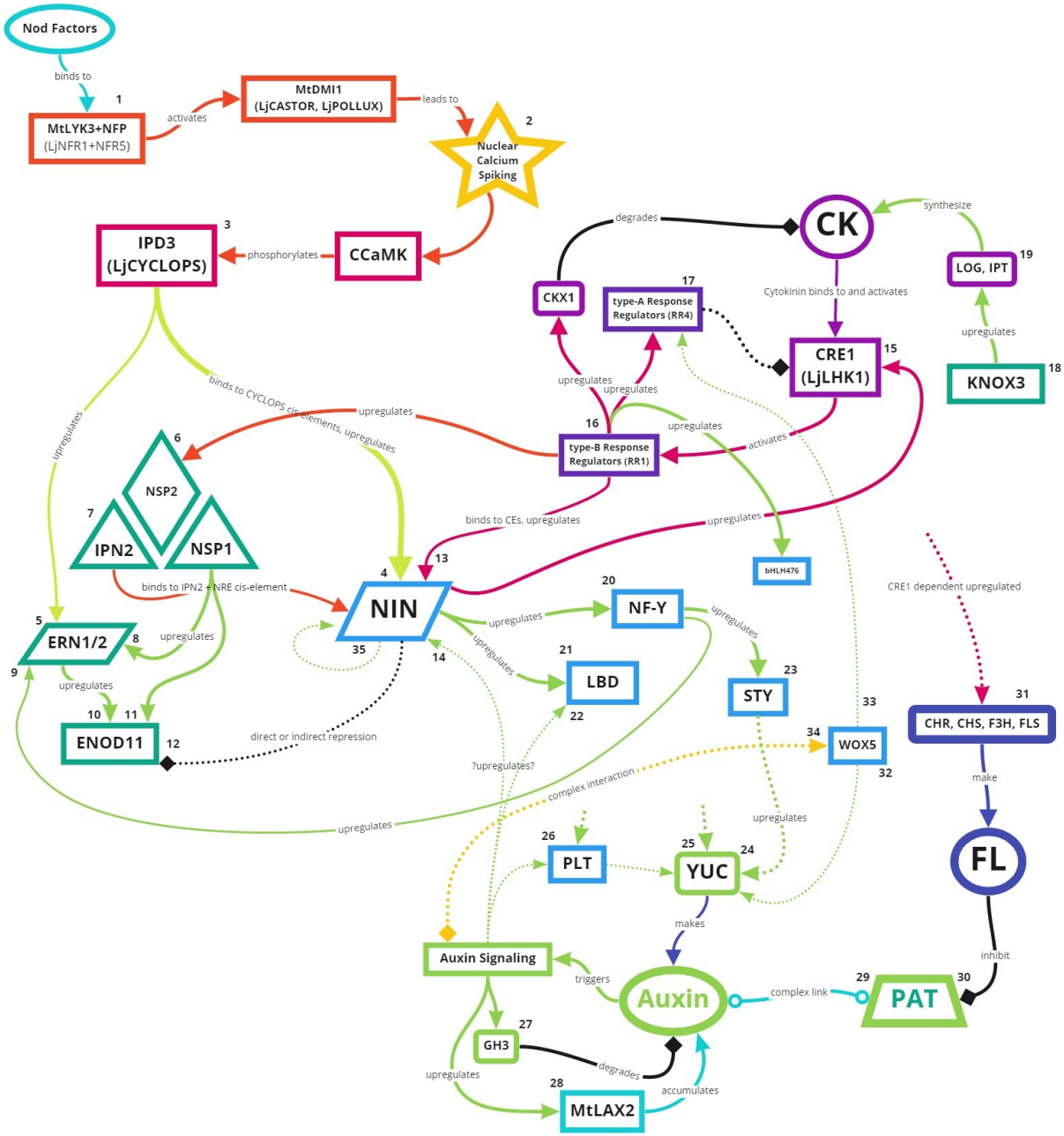

Figure 1.1: Gene Regulatory Network of Nodulation, derived from literature. Solid edges denote regulatory interactions with substantial experimental support. Dashed edges denote incomplete information or regulatory interactions known from non-legume species. 1:[51, 87], 2:[88], 3:[52], 4:[23], 5:[23, 82], 6:[73], 7:[56], 8:[83, 84], 9:[84], 10:[85], 11:[54], 12:[86], 13:[72], 14:[89](more support in chapter 3), 15:[70], 16:[73], 17:[78–80], 18:[77], 19:[76], 20:[60], 21:[49, 50], 22:[90–92], 23:[93], 24:[94–96], 25: see chapter 3, 26:[97–101], 27:[68, 91], 28:[102], 29:[103–105], 30:[68], 31:[68], 32:[106–109], 33:[110], 34:[111], 35:[72].

regulated by auxin signaling[99] and to create a feedback by directly upregulating *YUCCA*s [100, 101]. Lateral roots need PLTs to form properly, with two groups delineated, early expressed AtPLTs 3, 5 and 7, and late AtPLTs 1, 2 and 4[123]. It remains to be seen how these TFs are induced and function during nodule formation and maintenance. Lastly, the important root meristem regulator WUSCHEL-related-homeobox-5 (WOX5) is implicated in nodule development[97]. It has been shown both in *Arabidopsis thaliana* and *Medicago truncatula* that *WOX5* is auxin inducible[106–109], and that , in *Arabidopsis thaliana*, WOX5 is driving auxin biosynthesis through expression of *AtYUC1*[111]. WOX5 was recently shown to upregulate type-A *RR*s in *Medicago truncatula*[110], but WOX/WUSCHELs are known to directly downregulate *ARRs* in *Arabidopsis thaliana* meristems[124] so more work is needed. It is interesting to note that WOX TFs are known to drive stem cell programs and define meristematic regions through direct interaction with conserved co-factors of the HAiry-Meristem (HAM) family[125](GRAS domain TFs), of which NSP2 is a member. They also repress local auxin signaling by upregulating *IAA*s[111] as well as via histone modification and repression of important auxin signaling genes[126] and thus act to maintain high auxin levels and low auxin sensitivity at stem cell regions, taking the role of an auxin response rheostat[126]. Auxin signaling during nodule development might then feedback positively to *NIN* expression, as there is evidence that auxin treatment of Glycine roots upregulates *NIN* ([89], more evidence in the results). This potentially puts NIN as a key regulator of a second positive feedback between NIN and auxin signaling, as well as a coupler of signaling activation of the two major plant hormones, auxin and cytokinin(Figure 1.1, right part). More work is needed to show if this is the case.

Lastly, no review of TFs involved in nodule development can be complete without mentioning the enigmatic action of *NOOT-BOP-COCH-Like* (*NBCL*) genes in sustaining nodule identity. In *Medicago truncatula*, *nodule-root1* (*Mtnoot1*) mutant has impaired nodule meristem maintenance, leading to the decoupling of the peripheral vascular meristems to the central one, loss of meristem identity, and formation of lateral roots from the peripheral vascular meristems[127]. This result has also been demonstrated in *Pisum sativum* (pea) ortholog *cochleata1* (*Pscoch1*) mutant[128], and in *Lotus japonicus Ljnbcl1* mutant[129], making this TF's action conserved across nodule types, with concomitant floral phenotypes.

We can appreciate how powerful the above GRNN is in making nodules when we consider how genetic induction of its components can give nodules in the absence of rhizobia. Gain-of-function (GOF) mutants of *CCamK* can give spontaneous cortical cell proliferation without calcium spiking[130], and so do constitutively active and expressed *NIN*[60], *NF-Y*[60] and phosphomimetic *CYCLOPS*[23]. GOF Mutations of *CRE1 - LHK* (*snf2*) are able to produce spontaneous fully formed nodules.[24, 71]. All of these are accompanied by a local increase

in auxin signaling[115]. On the whole, nodule initiation and maintenance involves a GRN where most components can be found in other plant developmental processes, but has unique wiring that presumably contributes to the unique patterning and shape of the nodule.

1.3 Auxin and cytokinin in plant development and nodulation

As we have seen above, the two main plant hormones, auxin and cytokinin, are heavily involved in the creation of the nodule. This comes with no surprise, as just application of these two hormones together can induce callus formation in many plant species[131], and so are expected to have a role in the *de-novo* organ formation process of nodule initiation. Historically, it was proposed as early as 1936 by Thimann[132], that the nodule is an active auxin-producing center, based on the amount of auxin that can be extracted. Thimann proposed rhizobia as the source of auxin, a position later elaborated by Libbenga et al (1973,[133]), who suggested cell divisions occur due to both auxin and cytokinin produced by rhizobia, when the rhizobia reach tissues with high concentration of stimulatory host factors. Cytokinin has been shown for more than 60 years now to induce cortical cell divisions[134], is able to induce nodule formation[67, 71, 135–138] and is certainly produced by rhizobia[139, 140]. While cytokinin and auxin[30, 141–144] secretion by bacteria can alter root development, and one can think that this might have facilitated early nodule symbiosis evolution, in that case plants have taken back control of nodule development, as pure Nod factors alone can trigger nodule formation[145]. Looking at the larger picture of hormonal regulation of plant development should provide a foundation to understand how hormones might be implicated in nodule development.

1.3.1 Auxin and cytokinin in plant development

Normally when we talk about auxin we refer to indole-3-acetic acid, but auxins are a group of tryptophan-derived compounds that regulate plant patterning and morphogenesis. They act mainly through changing gene expression via the TRANSPORT INHIBITOR RESPONSE 1 (TIR1) - related auxin signaling pathway[146]. The core of this pathway consists of a signaling cascade where, upon perception of auxin by its receptor domain, TIR1 ubiquitinates AUXIN/INDOLE-3-ACETIC ACID (Aux/IAA) proteins, causing their degradation. Normally Aux/IAA bind and inhibit AUXIN RESPONSE FACTORS (ARFs), TFs that heavily regulate gene expression. In this way auxin application releases ARFs to bind to their targets[147] and detectable change in transcript abundance can occur within 5 minutes[148]. Auxin however

affects cell physiology in other ways as well. Recently, TIR1-dependent non transcriptional auxin effects on cell expansion[149] were reported, which involve coupling of auxin influx and calcium signaling at the plasma membrane[150], an effect that could explain auxin involvement in root hair growth[151], a process known to be heavily regulated by cyclic nucleotide-gated channels (CNGCs) forming oscillating, emergently tip-focused calcium gradients[152]. Another line of research suggests that interdigitation of pavement-cells happen through auxin perception at the plasma membrane by auxin binding protein 1 (ABP1) and recruitment of the cytoskeleton by emerging RHO OF PLANTS (ROP) protein domains[153]. Lastly, parallel auxin signaling pathways exist, as TRANSMEMBRANE KINASE 1 (TMK1) can perceive auxin at the plasma membrane and then translocate to the nucleus and phosphorylate non-canonical IAAs, as identified in *Arabidopsis thaliana* apical hooks[154].

Auxin transport is an elaborate process heavily expanded by evolution. Auxin, as a weak acid, is apolar in the cell wall, where the pH is close to 5.5. Thus it does not interact with the cell PM and can pass into the cytoplasm. There, due to the neutral pH, auxin molecules shed the proton and become polar, and are unable to get out of the cell by passive diffusion. As such, plant cells are regarded to act as acid traps, and this mechanism is believed to govern the underlying dynamics of auxin localization in plant tissues, with all the above being called the "chemiosmotic model"[155]. Polar auxin transport (PAT) appears to be the evolutionary adaptation addressing these issues of hormone developmental regulation of large body plans[156]. Auxin is known to be actively polarly transported in plant tissues, following a pattern, in my opinion, reminiscent of an inverted Benard convection cell: in cortical tissues it flows towards the top of the plant, towards all shoot meristems, and there it is redirected in the inner, vascular tissues, and is transported to root meristems, where it is deflected again to the cortical tissues. Auxin transport is directed by an intricate system of polar exporters, apolar importers and transport facilitators, at the cellular and subcellular level, able to produce Byzantine patterning dynamics on plant tissues[157–161]. Prime examples of patterning processes directed by auxin in plant tissues are the establishment of the root pole in the embryo[162], the emergence of new organs in the shoot apical meristem and their connection to the existing vasculature[163], and vein formation in leaves[164]. Auxin accumulation triggers developmental change in plant tissues[165], mainly through the rapid induction of gene expression by the Aux/IAA- and ARF-dependent auxin signaling pathway, described above. The main protein families that modulate auxin transport between different compartments and through the plasma membrane, as research in *Arabidopsis thaliana* has shown, are the influx transporters of the AUX1-LAX family, the efflux transporters of the PIN family, and the ATP-symporters of the PGP family. We will discuss these transporter families in the section about auxin transport in the nodule.

The role of auxin in the formation and development of lateral shoot and root organs is well established in *Arabidopsis thaliana*, however is heavily context-dependent. In the shoot apical meristem (SAM) emergence of auxin maxima at the peripheral zone (PZ) is solely directed by auxin transport[118, 166], where phenomenologically PIN proteins polarise towards cells with high auxin concentration, creating a positive feedback that patterns new primordia. The positioning of these is phyllotaxis, which, after millennia of mathematicians trying to decipher the origin of its beauty, can now be mechanistically understood[167, 168]. In the case of shoot bud outgrowth, auxin transport also plays a key role, whereby it is activated and connects the bud to the vasculature only when the right signals come along, which can be the loss of the main auxin stream from the dominant apical meristem[169], cytokinin[170], sugars[171], stringolactone, or all of the above[172]. In the root meristem (RM), auxin is an instructive gradient for cell elongation and differentiation, at least through the concentration coupling with PLETHORA TFs[99]. The auxin gradient is maintained through polar auxin transport that forms a fountain with a reflux loop[158]. The peak of auxin concentration coincides with the stem cell niche, but this positioning is maintained by auxin biosynthesis, as its abolition shifts the peak to the root tip[173]. Modulation of auxin concentration at the sides of the RM due to laterally differential transport rates induced by root environmental perception gives rise to root tropisms[174]. Lateral root initials are patterned through an oscillation of auxin signaling at the differentiation front of the pericycle[175], opposite xylem poles. The mechanism behind this periodic priming is not yet sufficiently explained, but it seems to be dependent on differential auxin loading of the large cells arriving periodically at the shootward end of the RM[176]. During aquisition of lateral root initials fate an auxin signaling coherent feed-forward loop upregulates *PIN3*[177], and later an asymmetric cell division occurs, mediated by auxin upregulated LBD16[178]. For the subsequent step of lateral root emergence auxin signaling is again required, through regulation of auxin biosynthesis gene *YUC4* by B3 TFs LEAFY COTYLEDON 2 (LEC2) and FUSCA3 (FUS3)[179].

Cytokinins are a group of compounds synthesized from adenine. In the first step of synthesis, IPT enzymes make iP-type cytokinins. These are then converted by cytochrome P450 CYP735A enzyme to zeatin-type cytokinins[69]. Both types are transported through the vasculature to act in different tissues, trans-zeatin-types from root to shoot via the xylem, and iP-type from shoot to root through the phloem[180]. In the last step, LOG enzymes produce free base, active cytokinin. Cytokinin signaling is a multistep phosphorelay system[181] involving histidine kinases (HKs) that have a cytokinin receptor domain, authentic histidine phosphotransferases (AHPs) and type-B RRs[182]. In the SAM, cytokinin regulates central zone (CZ) and meristem size, through a positive feedback with SHOOTMERISTEMLESS (STM), a KNOX family TF, which at the same time downregulates gibberellin acid

(GA) and upregulates cytokinin biosynthesis[183]. Cytokinin signaling is integrated into the WUS patterning system responsible for the width of the CZ and placement and size of the stem cell domain[184], as cytokinin upregulates *WUS*, and, through negative regulators of cytokinin signaling type-A RRs, also upregulates *Clavata-3*, expressing a spatially patterned WUS repressor[185]. Auxin interferes with cytokinin regulation of the WUS patterning system by downregulating the same *ARR*s through MONOPTEROS (MP) auxin response factor [185]. This action is overall considered to connect the two hormones in synergy in the SAM, while the opposite interaction is observed during root pole specification and in the root meristem, where auxin stimulates the expression of ARRs[186]. Auxin in the SAM, however, has higher concentration in the Peripheral Zone (PZ) where organs initiate, and there the interaction with cytokinin is considered antagonistic, by to the least supression of *STM*[187]. For the purpose of probing the role of cytokinin in nodule organogenesis, it is interesting to note that, in *Arabidopsis thaliana*, nitrate availability in the root modulates production of cytokinin precursors, which act as long range signals and get converted in the SAM by LOG enzymes to cytokinin, which in turn modulates shoot organogenesis rate[188]. In the root meristem (RM), cytokinins inhibit root growth, in contrast to their action in the SAM. This happens through cytokinin local action in the differentiation front of the RM, which, when increased, acts to shift the front rootward and retard main root growth[189, 190]. This is done at least in part through antagonistic interaction, activation by cytokinin and repression by auxin, of the *IAA SHORT HYPOCOTYL 2* (*SHY2*) expression, the protein of which in turn represses *PIN*s and *IPT*s[190, 191]. Cytokinin, in *Arabidopsis thaliana*, also regulates root branching, by inhibition of lateral root initiation[192].

1.3.2 Cytokinin in nodule development

There has been considerable research on the hormonal mechanisms leading to the initiation of the nodule primordium. Cytokinin and auxin have central roles in the reprogramming of cells of the pericycle, endodermis and inner cortex to undergo cell divisions. The cytokinin Histidine Kinase (HK) receptor mutant *Mtcre1*, (*Ljlhk1* in *Lotus japonicus*) has unaffected epidermal responses to rhizobia, but no transition to cell divisions and no primordium, suggesting that cytokinin signaling is crucial for nodule organogenesis[66, 67]. The *cre1* mutant is able however to produce very few nodules[67, 68], and redundant activity of other HKs in the process has been shown in both *Medicago truncatula*[193] and *Lotus japonicus*[194]. On the other hand, gain-of-function mutants of *CRE1* (or the analogous gain-of-function (GOF) *snf2* mutant of *LHK1* in *L.j.*) are prone to spontaneously produce nodule-like structures in the absence of bacteria[114, 195]. In addition, as discussed already above, cytokinin application in wild-type legume roots can induce cortical cell divisions and the expression of Nod

genes[38, 43, 71, 196], and can lead to fully formed nodules[135, 197]. Some rhizobial species secrete CK-like compounds affecting root development in soybean[139, 140], and addition of a gene involved in the secretion of trans-zeatin can rescue the ability of *nod-* rhizobia mutants to induce nodule organogenesis, but not infection thread formation[198]. These results, taken together, suggest that cytokinin and its signaling is involved in the initial steps of nodule organogenesis, in a manner analogous to the reported role of cytokinin in the *Arabidopsis thaliana* embryo, where it directs stem cell specification at the root pole through the action of B-type ARR proteins[186]. Detailed analyses on the spatiotemporal dynamics of cytokinin responses during nodule initiation are lacking, but a dual sensor for auxin and cytokinin has shown that different tissues of the mature nodule can be distinguished on the basis of signaling ratios between the two hormones[199]. At the same time, although upregulation of cytokinin synthesis genes (*MtLOG1,2*, *LjIPT3*) upon infection has been shown[27, 76, 200, 201], and nodulation is hampered in the respective mutants[76, 202], the mechanism by which cytokinin signaling is augmented in the first 10 hours after inoculation is not properly understood, apart from the upregulation of *CRE1* by NIN[70]. Measurements of cytokinin concentration in *Medicago truncatula* after application of LCOs show an increase in bioactive cytokinins within 3 hours, the expression of CK biosynthesis genes is upregulated, and the majority of the transcriptional changes at this point in time depend on the activity of CRE1[203]. These results indicate a possible central role of the hypothesized cytokinin signaling feedback with NIN in the early response to rhizobia, and point to the need of better characterization of these early responses, to understand if cytokinin signaling feedbacks can play the role of the elusive signal from the epidermis to the pericycle, responsible for nodule initiation[105]. It has been proposed that accumulation of auxin via inhibition of polar auxin transport is mediated by CRE1-dependent production of auxin-transport-altering flavonoids and/or CK itself[18, 28, 33, 68, 103–105, 112].

1.3.3 Auxin transport in plant and nodule development

Auxin transport has the ability to pattern plant tissues[118, 204], and has been proposed to be responsible for auxin accumulation and signaling during nodule development[18, 28, 205, 206]. In order to better understand auxin transport during nodule initiation, we will present the main auxin transporter protein families and published results on their activity during nodule development.

The auxin transporters that we focus the least here are the phosphoglycoproteins (PGPs, otherwise known as ABCBs) of the ATP binding cassette transporter family (ABC). PGP mutants result in reduced auxin transport and growth, and PGPs are capable of import as well as export of auxin from the plant cell[207, 208]. The role of PGPs in auxin transport

is believed to be supplemental, limited to reinforcing existing auxin fluxes defined by other transporters[209], and stabilizing PM efflux complexes in ”lipid rafts”[208]. In nodulation two PGPs have been identified to be highly upregulated upon infection, named AMN2 and AMN3. Phenotypic analysis of the double mutant, however, did not show any nodulation phenotype[210].

The AUX1 family comprises of auxin importers with high affinity to auxin, that have distinct roles in plant development[211]. The AUX1-LAX proteins are largely homogeneously distributed in the plasma membrane. Their morphogenetic importance is that via differential expression between cell types (or cells of the same type with differential responses to external stimuli), they affect the directionality of auxin transport and the accumulation of the hormone[212, 213]. For example, expression and PM localization of AtAUX1 is observed at the L1 epidermal layer in the shoot apical meristem, where it serves to position and stabilize new primordia by restricting auxin diffusion to the inner layers[163]. On the other hand, AtLAX2 regulates vascular development[211]. In *Medicago truncatula*, five LAXes have been identified [214]. They have been shown to be upregulated during nodule formation and to localize in the nodule primordium and mature nodule veins. They play a role in auxin accumulation at the nodule meristem, and mutants of these transporters have reduced nodulation[102, 210, 215].

The PIN proteins are exporters of auxin that have striking mutant phenotypes. In *Arabidopsis thaliana*, mutants of *AtPIN1* are unable to produce phyllotaxis, and have shoots growing upwards like a pin (hence the name)[216]. AtPIN2 mutants on the other hand exhibit a strong agravitropic phenotype[186]. All PINs have a basic structure of two hydrophobic domains of 5 transmembrane helices and a variable hydrophilic region in the middle. The family can be subdivided into two groups based on the contents of the hydrophilic loop[217]: class I with a very short hydrophilic loop and class II with a long one (AtPIN1-4 and AtPIN7). The hydrophilic loop affects localization of the protein. Long PINs undergo constitutive cycling between the PM and endosomal compartments[218] creating clusters of high concentration[219]. Their correct positioning plays an important role in the directionality of auxin transport[165]. The molecular components underlying the different modalities of PIN polarity is a field of considerable research and controversy. The auxin receptor ABP1 has been proposed to mediate fast reactions like the rapid inhibition of clathrin-mediated endocytosis of PINs from the plasma membrane, and to function in cytoskeletal rearrangements mediated by ROP GTPases. [220, 221]. Its role however in plant development has been disputed[222]. Short PINs, on the other hand, localize in the endomembranes and, for example in the case of AtPIN5 (ortholog of *Medicago truncatula* MtPIN9) which is localized in the ER, have been suggested to control auxin homeostasis in the cell[223] through their action in compartmentalizing auxin in the

ER, where auxin can be inactivated by conjugation.

Long PINs appear to have functional redundancy in *Arabidopsis thaliana*, as they have overlapping domains of expression, can functionally replace each other when localized in the same side of a cell, and their promoter activity is flexibly regulated leading to ectopic expression of homologs in At*pin* mutants[224]. The long AtPIN1 (the closest homologs of which in *Medicago truncatula* are MtPIN4, MtPIN5 and MtPIN10[225]), is expressed in *Arabidopsis thaliana* in the apical part of the embryo proper, the shoot apical meristem and developing organs and in the vascular system. AtPIN7 is expressed in the basal part of the embryo and in the root tip. AtPIN2 (*Medicago truncatula* homologs MtPIN2 and MtPIN7), AtPIN3 and AtPIN4 (homologs MtPIN3 and MtPIN1) are also expressed in the root tip, where they take part in the maintenance of the "reflux loop"[158]. The expression topology of the *Arabidopsis thaliana* short PINs can be summarized as ubiquitously expressed for AtPIN5 (*Medicago truncatula* ortholog MtPIN9), and in the male gametophyte for AtPIN8[224]. It is interesting to note that there is a second family of putative auxin transporters that resemble in activity the short PINs, the PILS[226], but they do not seem to play a role in intercellular auxin transport.

One interesting difference in the set of PINs that *Medicago truncatula* possesses is that it has MtPIN10, an ortholog of the "sister of PIN1" SoPIN1 clade, present in monocots like Brachypodium[227], that is missing in *Arabidopsis thaliana*. The SoPIN1s are a class of PINs related to AtPIN1 that seem to have undergone subfunctionalization: In *Arabidopsis thaliana*, the creation of a new auxin maximum at the shoot apical meristem surface as well as the connection of it to the existing vasculature is mediated by initial polar auxin transport towards the emergent maximum by AtPIN1 and subsequent canalization of auxin from the maximum to the vasculature by the same PIN, its repolarization mediated by the upregulation of MAB4 and the action of PINOID[228]. In contrast, in Brachypodium, the formation of the maximum is mediated by a SoPIN1, and the canalization by PIN1a and PIN1b[227]. Thus, it is possible that MtPIN10 acts in a similar fashion, mediating the creation of auxin maxima, by pointing "up the auxin gradient"[157]. Analysis of the *Mtpin10* mutant showed that indeed PIN10 acts to create the auxin maxima at the leaf primordia and leaf and flower margins[229, 230]. Cross complementation with AtPIN1 however shows that they are functional orthologs. Since MtPIN10 is upregulated during nodulation[67, 68], it is interesting to explore if it has a role in the creation of an auxin maximum at the nodule primordium. Preliminary results show that MtPIN10 polarizes towards new primordia and its mutant has a mild phenotype in the extent of nodule primordium cell division domain(Ting Ting Xiao, unpublished results from her thesis[231]). To date, there is no published work on assessing the polarity and localization of PINs in the nodulation of legumes. There is, however, a detailed study of the localization of PINs and LAXes in the nodules of *Casuarina glauca*[30], where it was found that AUX1 ex-

pression in infected cells and PIN1 expression in uninfected cells, in conjunction with possible auxin production by the Frankia symbiont, acted to restrict and accumulate auxin in infected cells.

A number of studies have determined the expression changes that PINs undergo under nodulation. *MtPIN10* has been reported to be mildly upregulated 6hpi(hours post inoculation), something that does not happen in the *cre1* mutant[68], and be mildly inducible as early as 3hpt(hours post treatment) under nod factor treatment[67]. MtPIN2 is expressed in the uninoculated root in the epidermis and cortex, but has an extremely low expression level in the differentiation zone[232]]. Upon infection, it has been reported to be expressed (with a 5-fold change) as early as 24hpi[68]. It has been observed in developing nodules at 72hpi localized at the side of the primordium, and it is present in the base of nodules as well as LRs, possibly to divert auxin from vasculature to the new organ (or vice versa). Although it is present throughout LR development at the tip of the LR, it is absent in mature nodules[232]. *MtPIN4* is also upregulated upon inoculation 3-6hpi [67, 68]. The short MtPIN9 (ortholog of the ER-localized AtPIN5) shows a quick and consistent downregulation upon infection. It is also strongly downregulated in response to short-term cytokinin treatment[67]. In this study, we will hypothesize that PIN9 affects auxin availability in the susceptibility zone, and test for possible effects on susceptibility zone span and nodule numbers. We will also probe the localization and polarity of MtPIN2 and MtPIN9, to provide groundwork on assessing how the cortical auxin stream is affected by nodulation.

Two other approaches worth mentioning in understanding the effect of PINs on nodulation are RNAi silencing of *PIN* translation[232] and using anti-PIN antibodies[30, 67]. Silencing *MtPINs 1-4* respectively, with detected cross-silencing, led to a drop in nodule numbers upon infection, but no detectable changes in root morphology. Using antibodies, PIN localization was detected to be highest in inner cortical cells close to the root tip, but the authors do not report on PIN localization at the susceptibility zone or in the young nodule primordia. Interestingly, PINs were more abundant in the *cre1* mutant, suggesting a connection between steady state auxin transport dynamics and cytokinin signaling. All in all, PINs show promise as being important in nodule development.

1.3.3.1 Nodule initiation affects auxin flow, and *vice versa*

Studies have shown that in order to understand auxin localization in plant tissues, a detailed analysis of its transport has to be carried out[157, 158, 233], and, in some cases, auxin sources and sinks can be thought to have negligible effects on the local auxin levels[104, 158]. This seems to be especially true for the domains of the plant where the activity of auxin transporters is high, for example in the meristems. In the case of the nodule, there has been considerable

research into understanding how the initial auxin signaling activation - accumulation, crucial for the development of both determinate and indeterminate nodule primordia[33, 115, 196], comes about. One approach, favored by many labs, takes the form of assessing the root-level changes in major auxin flows (acropetal, basipetal) under nodulation[18, 67, 68, 112, 113, 121, 205, 234]. Acropetal auxin transport is thought to be mediated by the vasculature and inner cortex, whereas the basipetal is considered to take place in tissues close to the root epidermis[235]. Using radiolabeled IAA, auxin transport can be assessed by application at the root tip or at a cut made above the inoculation point in the root, and measurement above or below the site of spot inoculation, respectively, or at the middle. In *Vicia sativa* (indeterminate nodules), rhizobia and nod factors inhibit auxin transport within 24hpi[234]. In the same study, a time course of the auxin transport changes showed that rhizobia inhibit acropetal polar auxin transport (PAT) from 16hpi onwards. Acropetal PAT inhibition from 24hpi onwards was also observed in *Medicago truncatula* (indeterminate nodules)[18, 68, 205]. Interestingly, an increase in basipetal auxin transport (in the order of 200%) after inoculation has been shown[68],. No inhibition of auxin transport was detected in *Lotus japonicus* (determinate nodules) before nodule initiation[113](24hpi), but increase of acropetal auxin transport was detected at 48hpi. These results point to a difference in PAT changes during initiation of determinate and indeterminate nodules, and have led to the formation of the hypothesis that, at least in indeterminate nodules, auxin accumulation at the site of nodule primordium formation comes about by alterations in auxin transport.

This hypothesis is supported by experiments that show that, in a reverse manner, disturbing auxin flow can cause nodule initiation. When polar auxin transport inhibitors (PATIs) are applied to the root of legume species forming indeterminate nodules, pseudonodules are formed[68, 198, 236–240], i.e. uninfected nodule-like structures that express genes specific to nodule symbiosis[198] even in *nsp2* and *nin* mutants[237]. Proposing PAT alterations as a common legume strategy for auxin accumulation fails however due to PATIs failure to produce pseudonodules in species forming determinate nodules [241–243], where they can even inhibit nodule formation in rhizobium inoculated plants[241]. It is interesting to note that PATIs can also not produce pseudonodules in the *Medicago truncatula* ethylene insensitive *sickle1-1* mutant[237]. PATIs commonly used to induce pseudonodules are naphthylphthalamic acid (NPA) as well as 2,3,5-triiodobenzoic acid (TIBA), which both inhibit auxin transport, by similar methods[244]. NPA, a flavonol analog, controls dimerization of PINs and affects their ability to direct auxin efflux protein complexes[245], and binds to PGPs[246]. TIBA has been shown to bind at the same protein as NPA[247], but, unlike NPA, is thought to be polarly transported similarly to IAA[248]. Since TIBA reduces acropetal auxin transport both in *Medicago truncatula* and *Lotus japonicus*[242], which make nodules of different type, but

produces pseudonodules only in *Medicago truncatula*, more work is required to understand PAT's role in *Medicago truncatula* nodule development.

1.3.4 Auxin signaling in indeterminate nodules

A complementary approach to study auxin dynamics in nodulation is through the use of auxin reporters on nodulation experiments. Two reporter types have been extensively used to date, based on the auxin responsive *GH3* promoter (*pGH3*, normally the promoter of the auxin responsive gene encoding for the auxin degradation enzyme GH3[249]), or based on the promoter *DR5*, which consists of repeated auxin responsive elements (AuxREs), targeted upon auxin signaling by the ARF transcription factors[250]. Pivotal results have shown that using a *pGH3:GUS* (auxin induced β-*Glucuronidase* (*GUS*) gene) auxin reporter DNA construct to transform *Trifolium repens* (indeterminate nodulator) can uncover elaborate auxin responses during nodulation[112]. Spot inoculating roots of transgenic plants led to a reported decrease of the *pGH3* signal at the cortex and vasculature, locally and acropetally of the inoculation site, 5hpi and 10hpi. After these timepoints, the authors reported an increase of the signal both locally at the cortex, and the reappearance of the signal at the vasculature acropetally from the site of inoculation, at 20hpi. At 30 hpi, they report an increase of cortical and vascular local signal all around the root at the site of inoculation, and at 50hpi a signal only at the first dividing cells. These results point to alteration of auxin levels not only at the site of inoculation 20hpi onwards, but also basipetally and acropetally from the site before that, leading the authors to suggest that auxin transport is affected by inoculation, resulting in early changes of auxin levels throughout the root. A formal statistical analysis of the results is lacking however, and a statistical analysis by us on these published data showed that the reported alterations at 5hpi and 10hpi are not strictly statistically significant, due to low percentages of samples with altered phenotypes and low numbers of replicates([112],table 2 of the article). The authors show however that similar alterations to the *pGH3* signal can come about by local application of the flavonol quercetin or NPA, leading them to suggest that alterations in PAT come about early during nodulation, possibly by the polar auxin transport inhibition action of locally produced flavonoids on the vascular acropetal auxin stream[112, 119]. Application of Nod-factors, however, led to a different pattern, where there was an auxin (*pGH3*) minimum at the site of local treatment 20hpt, which subsequently inverted to an increased signal in the general area at 30hpt. Its important in my opinion to reevaluate these results and the timing of the auxin response perturbations, since from these results 20 years of research into auxin transport during nodule initiation stem from, mainly due to how fast these responses are reported to be, and how they alter vascular auxin reporter profiles. Using the auxin reporter *pDR5:GUS* in transgenic roots of *Medicago truncatula* [232], a similar auxin pattern of higher

vascular signal at and above the inoculation site has been observed, albeit at the later timepoint of 72h after flood inoculation. These observational results are lacking any form of quantification. In a different study[68], the *GH3* promoter was used to investigate auxin signaling changes in transgenic roots of *Medicago truncatula* wild type (WT) and *cre1* mutant. The authors show that, upon infection, a cortical *pGH3* signal can be observed as early as 24hpi (and not at 6hpi), with a concomitant increase in the directly measured auxin IAA at the spot of infection, as measured by mass spectrometry, and a decrease in acropetal auxin transport and increase in basipetal auxin transport. These effects were not present in the *cre1* mutant under inoculation, but, interestingly, the *pGH3* signal in the root hairs was present as in WT. In conclusion, results from auxin reporters in plants making indeterminate nodules show that there is an accumulation of auxin 20hpi onwards at the site of inoculation, and alterations of auxin levels and presumably auxin fluxes at the root level with a pivot at the inoculation site. There is some probability of this happening before 20hpi. Although the alterations in auxin levels and transport are consistent among studies after 24hpi, before that timepoint conclusive evidence of such processes being present at the site of infection is lacking.

1.3.5 Auxin signaling in determinate nodules

Studies of auxin signaling - accumulation upon nodulation in plants making determinate nodules paint a different picture. In soybean, *pDR5:GUS* (auxin induced β-Glucuronidase) studies showed no alteration in the auxin signal at 8 hours post inoculation (hpi) compared to control[121]. While alterations in PAT and severe reduction in nodulation were observed when key isoflavone biosynthetic genes were silenced using an RNAi method, nodulation was rescued by isoflavone-hypersensitive rhizobia or purified Nod-factors, indicating that modulation of PAT via production of flavonoids was not essential for nodulation. The authors of this study conclude that it is flavonoid induction of Nod-factors in bacteria that explains the RNAi-silencing phenotype, rather than flavonoid modulation of PAT. In *Lotus japonicus*, *pGH3:GUS* and *pGH3:GFP* (auxin induced Green Fluorescent Protein (GFP)) reporters provided evidence of auxin signaling and possible auxin accumulation in the outer cortex[113] upon inoculation. Spot inoculation of the *pGH3:GUS* showed staining linked to cortical cell divisions, 2-5dpi. Staining was higher at the outer cortex and in the main root vasculature directly in contact with the nodule primordium. Nod factor application showed no signal 6hpt, and a slight auxin signal at the spot of application 24hpt, accompanied by a relative decrease of auxin signal at the root tip. In a different study[241], the *pGH3* signal was again detected in the outer cortex, at 2dpi, with no effect on the GUS staining auxin signal of the vasculature above and below the nodule primordium. All in all, auxin signaling and possible accumulation can be detected early during nodule organogenesis, it appears to be localized and concurrent with cell divi-

sions, and in different legume families might come about by, or/and have different effects on, auxin localization and flow across the whole root.

1.3.6 Computational nodule auxin transport

Computational modeling studies of polar auxin transport (PAT) have proven indispensable in the characterization and understanding of the emergence of auxin patterning by different transporter spatial arrangements and polarity feedbacks[146, 163, 169, 213, 251–256]. Only one such line of research, spanning several publications[33, 103–105] has been carried out for the characterization of auxin dynamics during indeterminate nodule organogenesis. Using a 2-dimensional representation of a longitudinal slice of the susceptibility zone of *Medicago truncatula*, where auxin and auxin transport dynamics are modeled expicitly, the authors start from a simulation setup that portrays what they presume are the native dynamics of auxin diffusion and transport. The setup is an adaptation of the first model used to study the root auxin reflux loop[158]. In this setup each cell is represented by a homogeneous subdomain of the 2D plane, and between the cells there is explicit apoplastic connected space. Then they consider how the concentration of auxin in each point of the space changes through time. In order to do this the authors use partial differential equations describing auxin diffusion inside the cells and in the apoplast, and varied permeability, "auxin transport", at the interface between the cell and the apoplast, which are extrapolated by how PIN proteins position in microscopic observations of the *Arabidopsis thaliana* root[158]. This is due to lack of comprehensive characterization of any *Medicago truncatula* PIN localization, to date. With this simple model they then test how different alterations of PAT at the site of infection can produce a local auxin maximum, and how the profile of this maximum is. They find that between the three different hypotheses of PAT alterations (increased auxin influx, decreased efflux, local auxin biosynthesis) the most parsimonious is the decrease in local auxin efflux, leading to auxin accumulation in specific simulated inner root tissues. The authors also produce a modeling description of how diffusion of a mobile signal from the site of infection that inhibits auxin efflux leads to the formation of a local auxin maximum[105]. They propose that this model captures the essential features of how auxin accumulates early during nodule organogenesis, and indicate that *in planta* such a signal could be cytokinin or flavonoids. Indeed, both hormone classes are known to alter auxin transport. In *Arabidopsis thaliana*, cytokinin (CK) signaling through the action of Cytokinin Response Factor (CRF) TFs is able to directly alter PIN expression[257], and CK redirects PINs for lytic degradation through a branch of fast CK signaling that does not involve transcription[120, 258]. Flavonoids have been shown to regulate the activity of ABCB auxin transporters[259], and to act as PATIs like NPA[260]. There are, however, a number of inconsistencies between the model and experimental data. First, the model makes

the prediction that basipetal auxin transport is inhibited in cortical tissues, and this is how auxin accumulates. This precludes possible inhibition of vascular acropetal auxin flows[105]. Experimental results, though, show a 2-fold increase of basipetal auxin transport 24hpi in *Medicago truncatula*[68]. Secondly, PIN localization studies at the susceptibility zone are lacking, so the authors use efflux transport rates deduced from studies of the elongation zone of *Arabidopsis thaliana*, or, as a test for model robustness, 10-times less. Both these assumptions might be inaccurate, and experimental studies are needed to assess the localization and abundance of auxin transporters at the site of inoculation. At the same time, although the authors point to a decrease of efflux as the mechanism for auxin accumulation, an increase in transcription of PINs has been observed in response to infection[67, 68]. Thirdly, the model assumes a static polar efflux pattern, that does not change due to auxin perturbations. Although this might be true in the differentiated tissue of the susceptibility zone, reorientation of auxin transport machinery due to changes in auxin concentration is a regular occurrence in plant tissues[228, 261]. Including this possibility in the model might introduce complexity that could hamper the experimental-modeling cycle, but might drastically alter the outcome of the study, especially the reported incapability of local auxin biosynthesis to give rise to auxin accumulation and a subsequent primordium. There is a clear need to study if and how, in reality, PAT is affected by infection.

1.4 Outstanding questions and research objectives

At the beginning of my PhD there was considerable lack of knowledge as to how symbiosis signaling recruits auxin to drive nodule formation. Most reviews of the literature suggested that the two nodule types have different ways to recruit auxin[28], something that would be interesting to elaborate on if both types have a common evolutionary origin[10].Thus we focused on two main questions, **when** can we first detect auxin signaling during nodule initiation, **and how** does it come about. I wanted to put the models, predicting auxin transport to be responsible for auxin accumulation, to the test. I designed experiments to test their assumptions and their results, as directly as possible, to inform the next modeling cycle. For a start I wanted to see if cortical auxin flow at the site of infection was enough to provide auxin for a new primordium. I also wanted to provide the first *Medicago truncatula* GFP-tagged PINs to directly observe their behavior during nodule formation, to see if model predictions of transport reduction held true. Understanding when auxin signaling appears can give us a clue as to how it happens, by comparing the timing to gene expression. To this end I worked with others to prepare a detailed timecourse of gene expression changes during the first steps of nodule development by RNA-seq transcriptomics. Concurrently I measured auxin signaling changes

in time using our new *Medicago truncatula* auxin reporter lines. By comparing the timing of gene expression with the timing of auxin signaling we were able to show that changes in auxin transport might be subsequent to auxin accumulation, and that auxin biosynthesis might be actually responsible for initial auxin accumulation. After this discovery my objective was to put our new hypothesis to the test by perturbing auxin biosynthesis. I also modeled the process to better understand how auxin biosynthesis, although potentially at the core of nodule initiation for both nodule types, might affect differently auxin transport in the primordia of the two nodule types.

Chapter 2

Auxin transport during nodule organogenesis

2.1 Introduction

It is known for more than 30 years that chemicals that act as polar auxin transport inhibitors (PATIs) are able to produce pseudonodules in legumes[68, 198, 237–240]. This has led to the proposition of the hypothesis that auxin transport inhibition underpins the formation of an auxin signaling maximum and initiation of the cell cycle in natural nodule formation[28, 34, 67, 68, 112, 119, 198, 242, 262]. A natural first step is to replicate the results on pseudonodule formation using PATIs. I then test how local application of auxin or auxin transport inhibitors affect auxin signaling in stably transformed *Medicago truncatula pDR5:GFP-NLS* auxin reporter line, and compare the response to the timing and intensity of the natural auxin maximum formed during nodule initiation. These experiments aim to test the hypothesis proposed previously that inhibition of cortical auxin flow gives rise to the nodule auxin maximum [33, 103, 104]. We also tag *Medicago truncatula* auxin transporters PIN2 and PIN9 with GFP in order to observe their localization patterns and ask if they are relevant for nodulation. Two *pin9* mutant lines were also tested for nodulation phenotypes. The results suggest that auxin transport is active through the region where a nodule appears, however, local cortical inhibition of auxin transport does not seem to be a plausible hypothesis for the creation of a local auxin maximum.

2.2 Results

For the purpose of this study, I selected newly developed *Medicago truncatula* plants stably transformed with the auxin responsive marker *pDR5:GFP-NLS* (Green Fluorescent Protein with Nuclear Localisation Signal driven by *Direct Repeat 5* auxin sensitive promoter) for high fluorescence and response. Our reporter line showed comparable auxin response patterns to *Medicago truncatula pDR5:GUS* lines as well as *DR5:GFP* reporter lines of other plants, where an auxin response maximum is observed in the root meristem as well as lateral root primordia. We also developed from first principles a *Medicago truncatula* GFP-DII-NLS auxin degradable protein construct, as well as a full R2D2 ratiometric auxin sensor[263], which passed all auxin sensitivity tests (for more information and microscopy pictures see Methods 9). However, I was unable to use the DII based auxin sensors in this study due to delay in making a stably transformed *Medicago truncatula* line, a task delegated to another lab.

2.2.1 Flood application of Polar auxin transport inhibitors produces pseudonodules

I treated the roots of 4 day old *Medicago truncatula pDR5:GFP-NLS* as well as wild-type (Jester) seedlings grown on plates with flood application of polar auxin transport inhibitors (PATIs) (see Methods 1) . I used water solutions of naphthylphthalamic acid (NPA) 200μM as well as 2,3,5-triiodobenzoic acid (TIBA) 200μM. Root growth was assessed by epifluorescent microscopy of *pDR5:GFP-NLS* seedlings as well as plain observation of wild-type (Jester line) seedlings. Careful observation of the *pDR5:GFP-NLS* signal did not show drastic changes 6 - 48 hours post treatment (hpt), except from a perceived mild increase in the GFP signal at the region where the root tip used to be at the start of the application of the inhibitors, in both NPA and TIBA treated roots, compared to *pDR5:GFP-NLS* seedlings grown on normal medium (control case). I observed a slight loss of fluorescence in treated roots at 4 days post treatment, compared to control. 6 days after application there was an increase of GFP signal across the root, and abnormalities on the surface of the roots. At 13 days post treatment I observed lateral structures emerging from the roots, some of which resembled nodules (Figure 2.1), compared to control root systems where none emerged. Lateral structures were much more prevalent and dense 3 weeks post treatment in TIBA treated roots (Figure 2.1 B-C) compared to NPA treated roots. Although many of the structures resemble the pseudonodules reported in the literature, I also report a great number of stunted lateral roots, round structures resembling nodules but with root hairs emerging, as well as some instances where a structure resembling a nodule changed fate and a lateral root emerged from within (Figures 2.1 D-E).

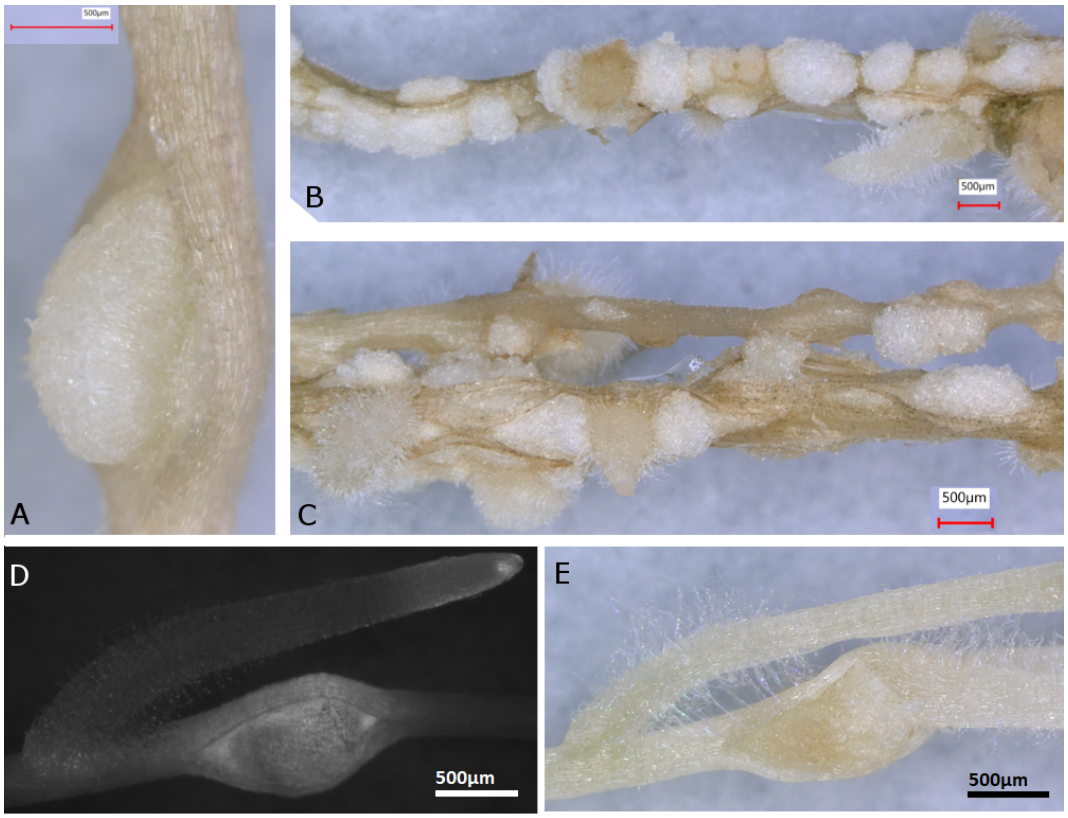

Figure 2.1: TIBA and NPA produce pseudonodules**: A,B,C** *Medicago truncatula* roots flood-treated with TIBA 200µM, 3weeks post treatment. Pseudonodules and abnormal lateral structures were present in all root systems (replicate N=18 root systems, control N=20). **D** Fluorescent microscopy picture of pseudonodule created by flood-treatment of NPA 200µM in *pDR5:GFP-NLS*, 13dpt. These structures were rare, with two such structures found in N=14 root sustems. **E** Same pseudonodule as in D, 3wpt, normal stereoscopic picture. A lateral root emerged from the pseudonodule.

2.2.2 Local perturbation of auxin dynamics in the susceptibility zone

Although root-level auxin transport perturbation is able to produce pseudonodules, as seen in the previous section, there is a need for experiments to address if this is the process by which auxin maximum formation occurs during normal nodule initiation. To better understand how auxin signaling at the cortex of the susceptibility zone of *Medicago truncatula* roots responds to different local chemical perturbations, I treated *pDR5:GFP-NLS* seedlings with water droplets containing different chemicals that could affect auxin signaling and transport (Methods 13). 24 hours post treatment I observed the changes in auxin signaling of the treated region of the root using fluorescent stereoscopy. I then quantified the local auxin response by calculating the ratio of fluorescence of the region of the root under the droplet to the regions of the root above and bellow the droplet (Figure 2.4 B, Methods 6). Preliminary results showed that local application of a water droplet on the susceptibility zone with 6-Benzylaminopurine (BAP) (10μM or 100μM), a cytokinin analogue, did not produce a consistent auxin response, but Nod-factor(10μM) or BAP+Nod-factor treatment elicited a mild epidermal auxin response, compared to control treatment with a water droplet. Application of GR24 (1μM), a strigolactone, did not produce an auxin response. In three formal experiments, local application of NPA 100μM or TIBA 100μM did not produce a discernible auxin response as measured by the fluorescence ratio of the droplet region to neighboring regions of the root, as compared to the fluorescence ratio of water droplet negative control (Figure 2.2). Although PATI application had no effect, I confirmed that application of NPA should be able to internalize PINs, in the relevant timescale and concentration, by testing, in a different experiment, the effect of NPA on *PIN2-GFP* transgenic roots treated with NPA (Figure 2.5 G, more results in section 2.2.4). In contrast to the results of PATIs, local application of Indole-3-acetic acid (IAA, auxin) 1μM on *pDR5:GFP-NLS* seedling roots produced a significant change in the fluorescent signal ratio (Figure 2.2 A). Application of auxin was enough to elicit a cortical auxin response, whereas inhibition of auxin transport through the cortex was not.

2.2.3 Auxin signaling maximum during nodule initiation

I used the new *pDR5:GFP-NLS* reporter line to observe and quantify the auxin response of *Medicago truncatula* seedling roots to local application of rhizobia, under nitrogen starved conditions. I treated 4 day old *Medicago truncatula* seedlings with water droplets containing diluted *Sinorhizobium meliloti* liquid culture that produces Nod-factors already, due to the addition of luteolin (Methods 4). I then observed the local auxin response under confocal, inverted, and epifluorescence microscopes. Observation under an inverted microscope showed an early epidermal as well as cortical auxin response, visible from around 12 hpi onwards

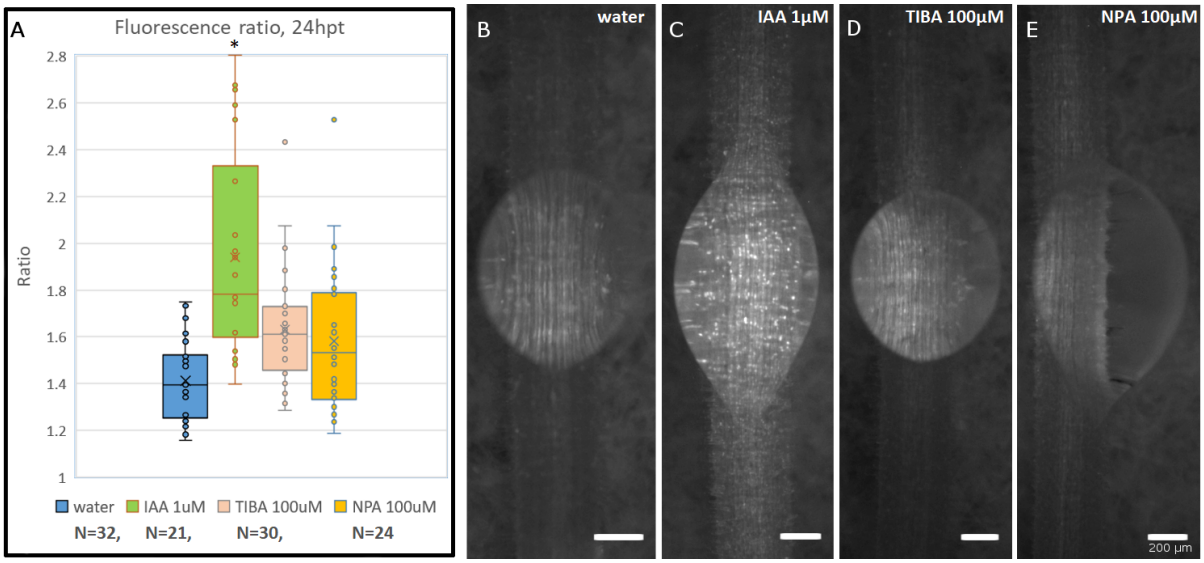

Figure 2.2: Local application of auxin transport inhibitors does not cause cortical auxin response**: A** Fluorescence ratio of the root region inside the droplet, to the average fluorescence of the root above and bellow the droplet, in *pDR5:GFP-NLS* seedling roots inoculated at the SZ with different chemicals by droplet spot treatment, 24 hours post treatment (hpt). The asterisk denotes statistically significant increase of the ratio when IAA 1µM is applied compared to control water treatment (Student's t-test, p-value<0.05). No significant difference was observed between the other two groups and control. **B-E** Representative fluorescent stereoscopy pictures of the different treatments, at 24hpt: water, IAA 1µM, TIBA 100µM, NPA 100µM. All scale bars denote 200µm.

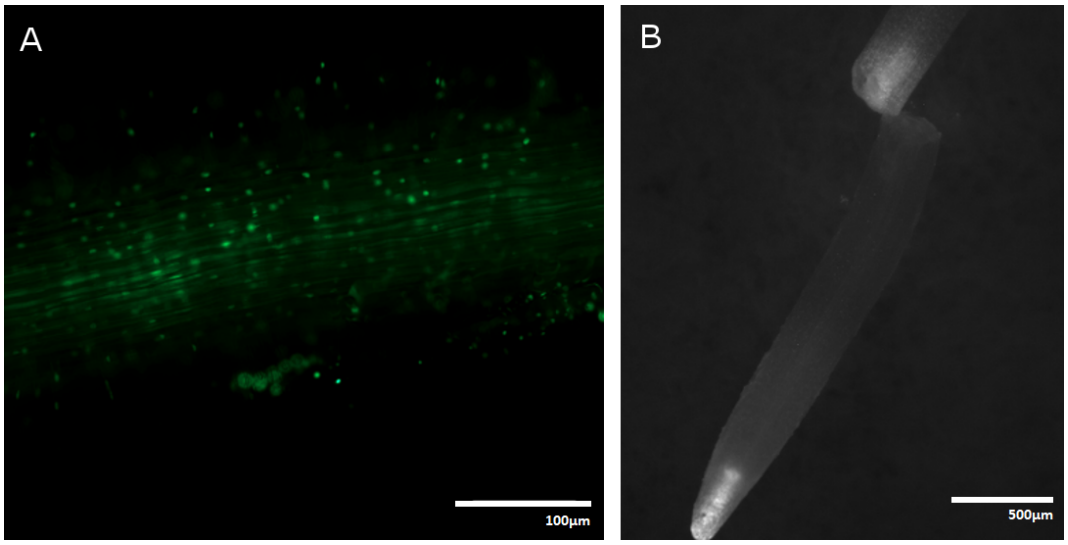

Figure 2.3: *pDR5:GFP-NLS* response under different conditions**:** **A** Fluorescent microscopy picture of a *pDR5:GFP-NLS* seedling root susceptibility zone 12 hours post spot inoculation. Fluorescent nuclei at the periphery belong to root hairs, but nuclei from deeper tissues can be seen in the central region as well. **B** Root from the same reporter line that was cut, instead of being spot inoculated, 22hpc. Picture by fluorescent stereoscopy, white depicting fluorescence intensity. Accumulation of an auxin signal can be observed in the vasculature above the cut.

(Figure 2.3 A). I could first detect an auxin response in the inoculated root hairs, visible from around 8hpi, and then response in the deeper tissues, from 12hpi onwards, forming a distinct auxin maximum in the inoculated region (Figure 2.4 B).

To understand if the auxin response is due to accumulation of auxin due to disruption of auxin flows through the inoculated region, in a different experiment, I cut the root at the susceptibility zone and tracked the auxin response in the cut area. I observed a clear signal in the side of the cut which is closer to the shoot, first in the vasculature at around 6 hours, and then in both vasculature and cortex, in all the roots (representative Figure 2.3 B at 22 hours post cut). Interestingly I did not observe any signal at the lower side of the cut, either at the vasculature or cortex (N=24). These results support the empirical model of auxin transport through the root where auxin is transported from shoot to root through the vasculature, and retrograde flow through the cortex is negligible far from the root tip. The timescale of presumed accumulation of auxin, responsible for this result, is similar to the one of the auxin maximum forming during nodule initiation.

Next, I quantified the appearance of the auxin maximum during local spot inoculation and natural nodule initiation, by recording the fluorescence of the *pDR5:GFP-NLS* line under the epifluorescent stereoscope, in time. I used again the simple metric to quantify the intensity

of the auxin response maximum, by comparing the total fluorescence of the inoculated region to that of the regions directly above and below, and calculating the ratio (Figure 2.4 B). With this metric I can quantify how much the inoculated region "stands out" compared to the two neighboring regions. Seedling roots were treated locally with different droplets, as per spot inoculation protocol (Methods 4). Negative control mock treatment of the root susceptibility zone of *Medicago truncatula pDR5:GFP-NLS* seedlings with a water droplet not containing rhizobia gives consistently a fluorescence ratio a bit above 1 (Figure 2.4 A and 2.2 A). This is due to a light focusing effect where the droplet acts as a lens under the microscope, increasing locally the perceived fluorescence level. Spot-treating *Medicago truncatula pDR5:GFP-NLS* seedlings with water droplets containing IAA auxin 2,5μM (positive control) gives a quick and clear fluorescent signal compared to water control, visible and significant already in 1 hour, with a maximum at 6 hours, which declines after that timepoint (Figure 2.4 A). This result shows that the *pDR5:GFP-NLS* reporter line is highly responsive and should give a good indication for the timing of any auxin responses. Spot inoculation of *Medicago truncatula pDR5:GFP-NLS* seedlings with rhizobia water solution produces an auxin maximum that slowly diverges significantly from mock negative control at about 8 hours post inoculation. Then a clear, observable difference in local fluorescence develops in all roots tested, that includes a clear cortical auxin response, at 14 hours post inoculation. The auxin response maximum of the nodule primordium becomes extremely pronounced after 48 hours, surpassing the maximal response of the auxin treatment.

2.2.4 Towards characterization of two *Medicago truncatula* PINs involved in nodulation

In order to understand how auxin transport is implicated in nodule initiation, PIN auxin transporters related to the process have been identified previously [18, 30, 67, 68, 232]. However, to date there has been no published research on the localization of individual *Medicago truncatula* PINs. This is due to the complexity involved in inserting a GFP tag in the PIN protein. PIN proteins comprise of two regions on either end, of 5 transmembrane domains, and a middle region of variable complexity that is intracellular. Successful GFP insertion tagging of PINs has only being reported for the middle intracellular region, for long PINs, and the last intracellular region between the last two transmembrane domains for a short PIN[223, 264–268]. The middle region of the protein is functional due to the existence of multiple phosphorylation sites [269], and thus incorrect tagging can lead to localization defects of the transporter. I aligned all reported successful GFP tagged PINs from the literature with *Medicago truncatula* PINs and identified, and ranked , for all *Medicago truncatula* PINs, all possible GFP insertion sites

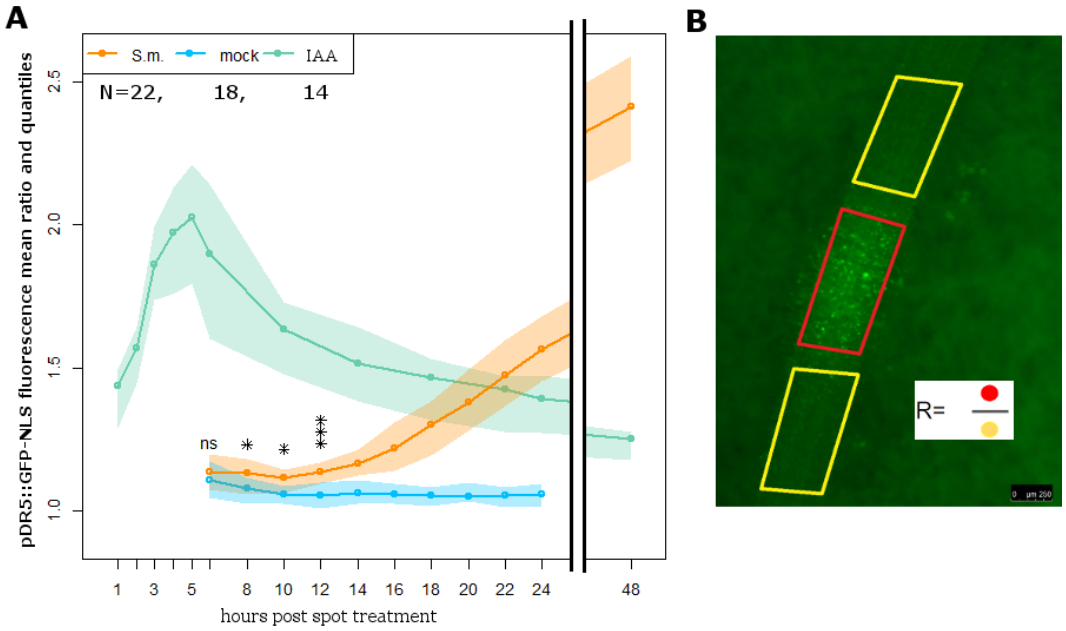

Figure 2.4: Auxin signaling during nodule initiation**:** **A** Auxin signaling response measured with *pDR5:GFP-NLS* fluorescence intensity at the site of spot inoculation compared to neighboring non-inoculated areas of the root. Spot treatments included S. meliloti inoculation solution (orange), 2.5 μM IAA (green), and mock inoculation solution (blue). Shading indicates 25-75% quantiles and asterisks indicate significant differences between S. meliloti and mock treatment at the specific timepoints (student's t test, * P<0.05, *** P<0.001). At all timepoints in S. meliloti treatments after 12 hpi, as well as all the IAA timepoints, there is significant difference to the mock treatment with a P-value less than 0.001, but this is not denoted in the plot for simplicity. The plot is contracted between the 24 and 48 hours post inoculation timepoints. **B** Example of a *pDR5:GFP-NLS* root, spot inoculated with S. meliloti, at 24hpi. Red and yellow rectangles indicate the regions of the root used for calculating the fluorescence intensity ratio (R) which is recorded in **A**.

based on sequence similarity and successful insertions at their orthologs and closest homologs (Methods 7). I identified two *Medicago truncatula* PINs as important for nodulation to carry forward for GFP-tagging, *Medicago truncatula* PIN2, ortholog of *Arabidopsis thaliana* PIN2, which is a long PIN known to be involved in cortical basipetal polar auxin transport and to be upregulated during inoculation[68, 232], and *Medicago truncatula* PIN9, homolog of *Arabidopsis thaliana* short PINs, known for their role in sequestering auxin in the ER[223]. PIN9 has been repeatedly reported to be downregulated during nodule initiation[67]. For both PINs I compared the results from 3 different tagging positions and successfully identified the one that performed best and gave plausible results in respect to the literature. I also analyzed the activity of the respective PIN promoters using *promoter-GUS* (β-*Glucuronidase*) expression analysis (Methods 21) in transformed nodulating roots. All DNA constructs can be found in Methods 22.

The *Medicago truncatula PIN2* promoter is highly active in root tips, with expression not extending beyond the differentiation zone (Figure 2.3 A-C), according to *promoter-GUS* transgenic root staining. In nodules the *PIN2* promoter is moderately active at the base of the nodule, the vasculature, and the meristem. Fusing GFP (more specifically the eGFP "Venus") at position 361 of the PIN2 protein revealed, through confocal microscopy of transgenic roots, a basipetal polar localization of the transporter in epidermal and outer cortical tissues of the meristem (Figure 2.3 D-E). This is comparable to what has been reported for the *Arabidopsis thaliana* PIN2 transporter localization[266]. NPA treatment of constitutively expressing *PIN2-GFP* transgenic roots for 20h led to internalization of PIN2-GFP and formation of so-called BFA bodies[270] (Figure 2.3 G) as well as loss of polarity. Careful observation of *PIN2-GFP* transformed roots showed that, in 4 out of 5 roots visualized, the domain where *pPIN2:PIN2-GFP* could be detected extended well beyond the differentiation zone (Figure 2.3 H). This lead me to suppose that although PIN2 is expressed in meristems, it remains in (and is cycled to) the cell membrane as the cells mature.

Medicago truncatula PIN9 expression and localization was different than those of *PIN2*. *Promoter-GUS* analysis of *pPIN9* using transgenic, flood inoculated roots showed mild expression in the root stele and columella. In nodules *PIN9* is expressed in vasculature and the meristematic zone of the nodule (Figure 2.4 A-B). Regarding PIN9 protein localization, I identified position 331 of the PIN9 protein as a GFP fusion site that gives natural protein localization, compared to studies from Arabidopsis[223]. DNA constructs generated by this approach can be found in Methods 22. I generated transgenic roots with DNA constructs where PIN9 was fused with Venus (GFP) in position 331 and was driven by an *Arabidopsis thaliana Ubiquitin* promoter, *pAtUBI10*. I then observed PIN9 localization using confocal microscopy (Methods 19). *Medicago truncatula* PIN9-331Venus localizes perinuclearly and

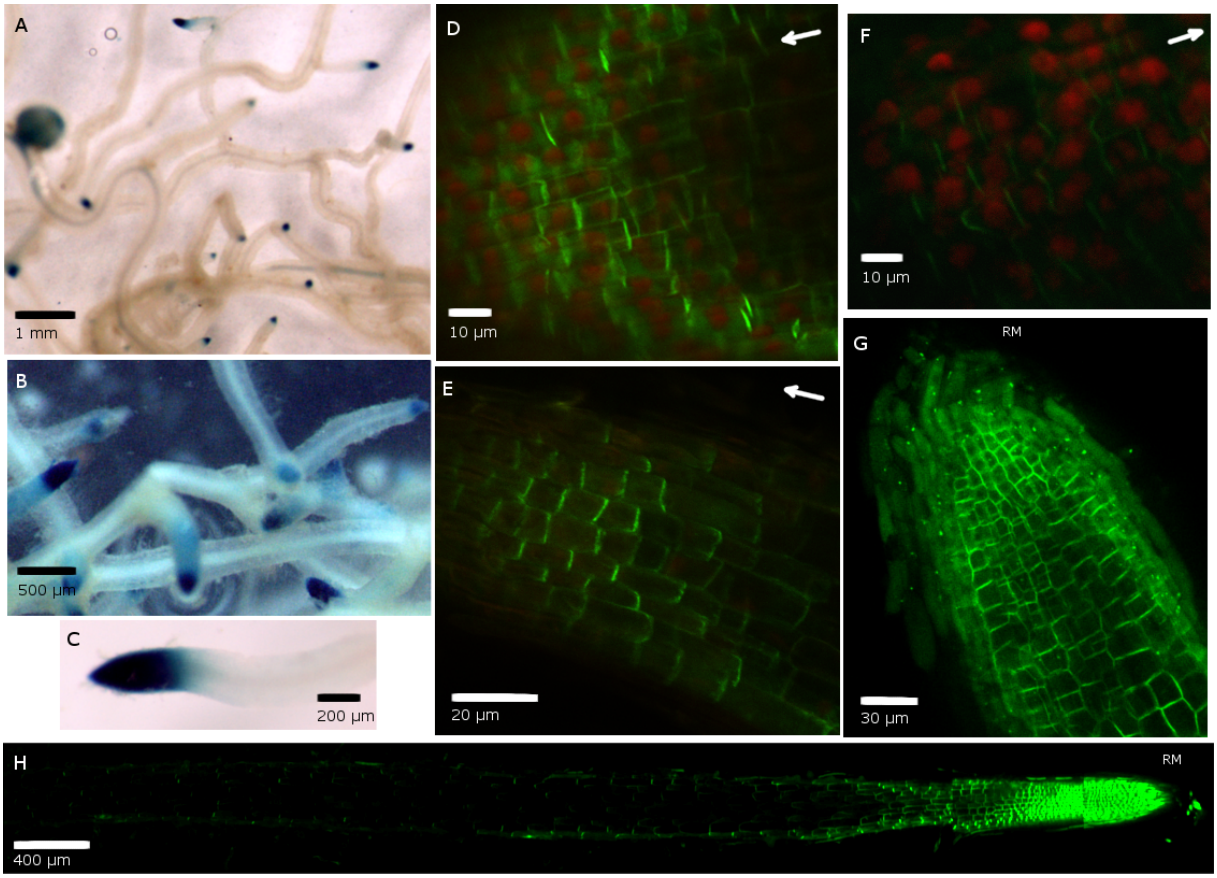

Figure 2.5: MtPIN2 expression and localization**: A,B,C** Activity of the *MtPIN2* promoter in nodulating transgenic roots transformed with the *pPIN2:GUS* DNA construct. Pictures of β-Glucuronidase staining and subsequent bright-field microscopy of transgenic roots. **D,E** Confocal microscopy of outer cell layers (epidermal and cortical) of transgenic root tip expressing a *AtUBI10:NLS-mCherry_pLjUBI1:MtPIN2-361VENUS* construct. White arrows denote direction towards the Root Meristem (RM). **F** Same observation as in D, but with *PIN2-VENUS* being expressed under its own native *pPIN2* promoter, showing clear basipetal polar plasma membrane localization. **G** Confocal microscopy of same transgenic roots as in D, 20 hours after flood treatment with NPA 100µM. Notice the change to apolar PM localization and internalization of PIN2 into "BFA bodies" in epidermal tissues. **H** Example composite confocal tile picture of variable focal planes of the same transgenic root as in F, using high sensitivity settings, showing how *pPIN2:PIN2-VENUS* can be detected in the epidermis well into the differentiation zone of the root, with basipetal polar PM positioning similar to AtPIN2 in *Arabidopsis thaliana*.

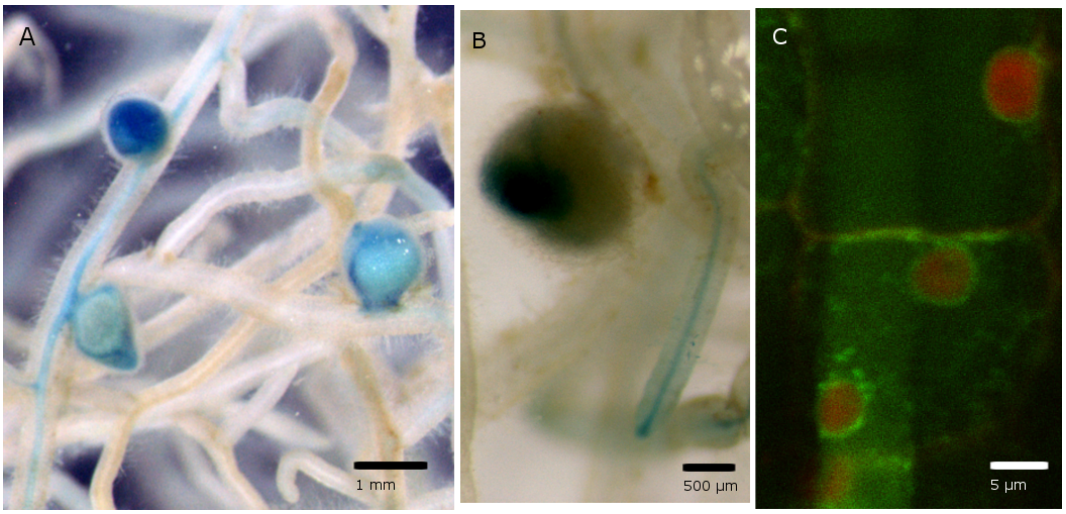

Figure 2.6: MtPIN9 expression and localization**: A,B** Bright field images of nodulating transgenic roots expressing the β-*Glucuronidase* gene under the control of the *MtPIN9* promoter. Visualization of the promoter activity is done using GUS staining. **C** Confocal fluorescent microscopy of transgenic root expressing *pAtUBI10:NLS-mCherry_pLjUBI1:MtPIN9-331VENUS* DNA construct, where nuclei are visualized by nuclear localized mCherry (red fluorescent protein, in red), and in green we visualize PIN9.

at the ER. I detected a faint localization at the plasma membrane as well (Figure 2.4 C). This indicates a role of PIN9 in cellular auxin homeostasis and invites further investigation.

2.2.5 The *pin9* mutant has no nodule phenotype

In order to understand if PIN9 is involved in nodule development I identified and characterized two *pin9* mutant lines. These are mutants from the Noble foundation Tnt1 insertion mutant database with transposon insertions at the first exon of the *PIN9* open reading frame (Figure 2.5 A). Both mutants were tested for changes in nodule initiation capability across the susceptibility zone, and overall nodule density, compared to the same line genotyped to be homozygous for the wild type (WT) gene. Using a spot inoculation protocol (Methods 4), I inoculated with rhizobia the susceptibility zone of WT and *pin9* either at the site of new emergent root hairs, which is considered the best spot for inoculation using this method, or at different intervals from the root tip, in order to understand if the mutant has altered susceptibility zone extent compared to WT. Neither of these experiments showed a statistically significant difference in the propensity of the mutants to make nodules compared to wild-type plants (Figure 2.5 B-C), either when the plants were grown on normal spot-inoculation medium (Methods 4) or on medium lacking aminoethoxyvinylglycine (AVG). I then compared nodule densities between flood inoculated wild-type roots and the two *pin9* mutants when the plants were grown

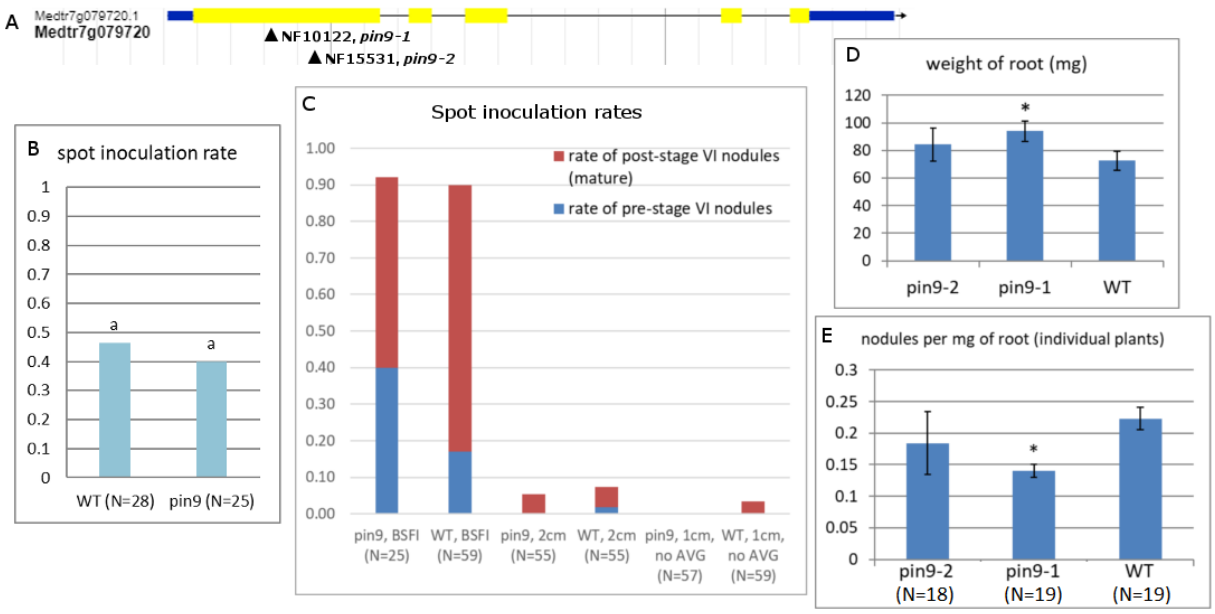

Figure 2.7: Lack of nodulation phenotype in *pin9* mutant**:** **A** Tnt1 insertion positions at the *MtPIN9* genomic region for the two mutant lines generated. **B** Spot inoculation rate of wild type (WT) and *pin9* mutant line at the susceptibility zone. **C** Spot inoculation rates of WT and *pin9* mutant at different positions of the root. First two categories compare the inoculation at the Best Spot For Inoculation (BSFI) i.e. the susceptibility zone, 7mm from the root tip. The middle two categories compare the inoculation rate 2cm away from the root tip. The last two categories compare the inoculation rate at 1cm, in a medium lacking aminoethoxyvinylglycine (AVG, see Methods 4). **D** Whole root weight of 3 weeks old seedlings of the two *pin9* mutant lines compared to WT. **E** Nodules per mg of root tissue for the two *pin9* mutant lines compared to WT. All significant (p-value<0.05) comparisons are denoted with an asterisk.

in sand (Methods 5). I found a statistically significant reduction in the number of nodules per miligram of wet root system weight in *pin9-1* compared to wild-type, but no difference in *pin9-2* compared to wild-type. This was attributed to higher root system weight in *pin9-1* plants compared to WT. The results were not consistent between the two mutant lines so I report no effect of *PIN9* gene mutation on nodule numbers.

2.3 Discussion

There seems to be an elusive link between auxin transport perturbation and nodule initiation. Polar auxin transport inhibitors are conclusively able to induce the formation of pseudonodules, in species forming indeterminate nodules [68, 198, 237–240], but not in species forming determinate nodules [241–243], and induce only indeterminate pseudonodules in a species able to produce both types of nodules[242]. Real nodules also conclusively perturb auxin

transport. During the formation of indeterminate nodules there is acropetal auxin transport inhibition[18, 67, 68, 112, 205, 234, 242], but no inhibition during determinate nodule formation[113, 121, 242]. Lets make for a moment a gross simplification and reassess these results. We can say that most of acropetal auxin transport passes through the vasculature on its way to the root tip. We can also say that indeterminate nodules form from vascular tissues and tissues proximal to the vasculature, whereas determinate nodules do not, they form from cortical tissues. These results say that "vascular" (initiated also in the vasculature) nodules reduce vascular auxin flow, and reduction of vascular flow induces "vascular" nodules. But which comes first? Also, why "cortical" (initiated strictly in the cortex) nodules, which presumably have very similar developmental program involving NIN[11, 201] due to a common evolutionary root, are not induced by auxin transport blockage and do not cause one?

One possible explanation is that auxin transport through the cortex is much lower than that of the vasculature, making the feedbacks between nodule formation and auxin accumulation due to blockage negligible. If this is the case, determinate nodules that initiate in the cortex will not be artificially induced by auxin transport blockage, simply because there is not enough auxin transport through the cortex in order for the blockage to produce a sufficient auxin maximum. In this study I observe PIN2 being present in the cortex of the susceptibility zone (Figure 2.5 H), but cutting the root produces an auxin maximum due to vascular flow and no maximum due to cortical flow (Figure 2.3 B). Recent results on the *Medicago truncatula pin2* mutant, reporting on the absence of any nodulation phenotype, corroborate on how PIN2 is not involved in nodulation or that its possible action is compensated by other PINs[271]. Local application of PATIs also did not produce a cortical auxin maximum (Figure 2.2). All these could mean that transverse planes, through the susceptibility zone main root axis, are not in an equilibrium in respect to auxin flows through them, with the vascular flow of auxin towards the root tip being the predominant flow, and further, that the lower part of the root is a net auxin sink, assuming slow growth dynamics. Further experimental study on local auxin flows should help test this hypothesis. Taking everything together, there is little evidence supporting the hypothesis that nodule initiation involves a cortical auxin flow restriction.

Inferring causality to the correlation between "vascular" nodule initiation and vascular auxin flow blockage might be done by comparing the timing of the two processes, ignoring feedbacks for a moment. If the accumulation of auxin during nodule initiation comes subsequent to the published timing of vascular auxin transport blockage, we should lean towards blockage causing the nodule. If its the other way around in time, we should lean towards the initiation of the nodule causing a blockage. In my hands, timing the emergence of the auxin maximum in *Medicago truncatula* gave a strong signal of divergence from buffer treatment 8-12 hours post inoculation. To put in contrast this result, accurate in time studies of cytosceletal

changes early during nodulation of *Medicago sativa* and *truncatula*[45], show the first microtubular cytoskeleton rearrangements to occur 16-18hpi in pericycle cells positioned opposite protoxylem poles, and first cortical cell activation at 18-24hpi facing these pericycle cells, all possibly mediated by altered auxin levels in these cells. Most studies of auxin transport, although coarse in timepoints, agree that in indeterminate nodulators there is a detectable change occurring at 24hpi[18, 67, 68, 112, 205, 234, 242]. This leads me to propose that there is first an auxin maximum occuring, then changes in the phase of the nodule initials, then vascular auxin transport blockage. My proposal, however, cannot explain how the *Medicago truncatula* cre1 mutant can be rescued by PATIs and flavonoids[68], or that indeed PATIs can perturb the root to produce, among other things, pseudonodules (Figure 2.1). Ideally, a combined approach where we can test auxin signaling via fluorescent reporters as well as observe the dynamics of transported auxin, possibly using fluorescent[173] and radiotracer auxin analogs and visualization methods (when available), would be able to discern auxin accumulation due to auxin transport blockage from other means.

Chapter 3

Transcriptional signature of nodule initiation

3.1 Introduction

Important parallels can be drawn between nodule developmental programs and those of other plant meristems[97]. The nodule, however, uses these programs to attain new and diverse morphologies[29]. Identifying the key patterning and morphogenesis processes taking place during nodule formation should shed light into the function and evolution of this organ, and can guide engineering of a similar organ in crop cereals. To this end we identified the timing of nodule initiation during spot inoculation, and tracked in high temporal resolution the transcriptional divergence underpinning it, using RNA sequencing and subsequent verification of important targets revealed. The timing of this process was compared to the auxin signaling I detected in chapter 2. In this chapter we will focus on presenting key gene families that are involved in nodule formation. Many results herein are interwoven with our publication[50].

3.2 Results

3.2.1 Spot inoculation reveals the extent of the susceptibility zone

During the development of our spot-inoculation protocol (Methods 4), I became interested in identifying the extent of the susceptibility zone in the roots of *Medicago truncatula*, in our hands. First, I wanted to pinpoint the positions in the root where we have maximal inoculation efficiency, to facilitate subsequent experiments. In addition I wanted to find where in the root inoculation rate was close to 50% under our spot inoculation protocol, in order to better compare mutants that might have a phenotype in susceptibility zone extent, as presented for

the *pin9* mutant in chapter 2. Thirdly, I was interested in figuring out how far from the RM nodules can appear, to give an indication as to if cortical auxin flow, which as we have seen in chapter 2 diminishes away from the RM, would affect nodule formation. The results presented below are all generated in experiments where roots are grown on agar medium that contains the ethylene biosynthesis inhibitor aminoethoxyvinylglycine (AVG) which elongates seedling roots and enhances nodulation[272].

To characterize the profile of the susceptibility zone, 7 day old *Medicago truncatula* (Jester ecotype) seedlings were spot inoculated with droplets containing rhizobia (Figure 3.1, A-C), at different intervals from the root tip. The results presented below (Figure 3.1-D) are combined from two full experiments, one where the intervals were set at 1, 1.5, 2, 2.5, 3 cm , and one where the intervals were set at 1, 2, 2.5, 3, 4, 5 cm away from the root tip. Both experiments had sufficient statistical power to show significantly different inoculation rates across the susceptibility zone (Methods 10). Under these growth conditions, there was a sigmoidal drop in the infectivity of the root with the midpoint around 2cm away from the root tip. In addition it was observed that nodules did not grow as fast when they were initiated away from the root tip compared to closer to the root tip. It is interesting however that nodules were induced as far away from the root tip as 3 centimeters. For comparison, the width of the root was measured to be around 400 micrometers, and the differentiation zone to be less than 7mm away from the tip, as 7mm is typically where new root hairs start their development. Thus the nodules do not need close proximity to the RM to initiate, under our experimental conditions.

3.2.2 Time course of gene expression during nodule initiation

We used the high efficiency of spot inoculation to measure local changes in gene expression in inoculated root segments. The roots were treated with droplets containing rhizobia prepared to infect (see Methods 4), or mock treatment. Then ~3mm root segments containing the inoculation spot were collected at different time intervals, and RNA was extracted, then sent for sequencing and subsequent identification of differentially regulated genes (DEGs) compared to mock (see Methods 20 for the full protocol and statistical tests).

In the initial experiment, we detected a drastic change in the number of genes differentially regulated between 8 and 16 hours post inoculation (hpi) (Figure 3.2 A). Moreover, at 16hpi many genes related to auxin and plant development were differentially expressed, whereas at 8hpi they were not. The timing of this transcriptional divergence coincided with the timing of the auxin maximum formation detected on the *pDR5:GFP-NLS* seedlings revealed in the previous chapter, and was not characterized before in detail by other labs, possibly due to the difficulty of performing an experiment with a 12h interval step. To better understand the order

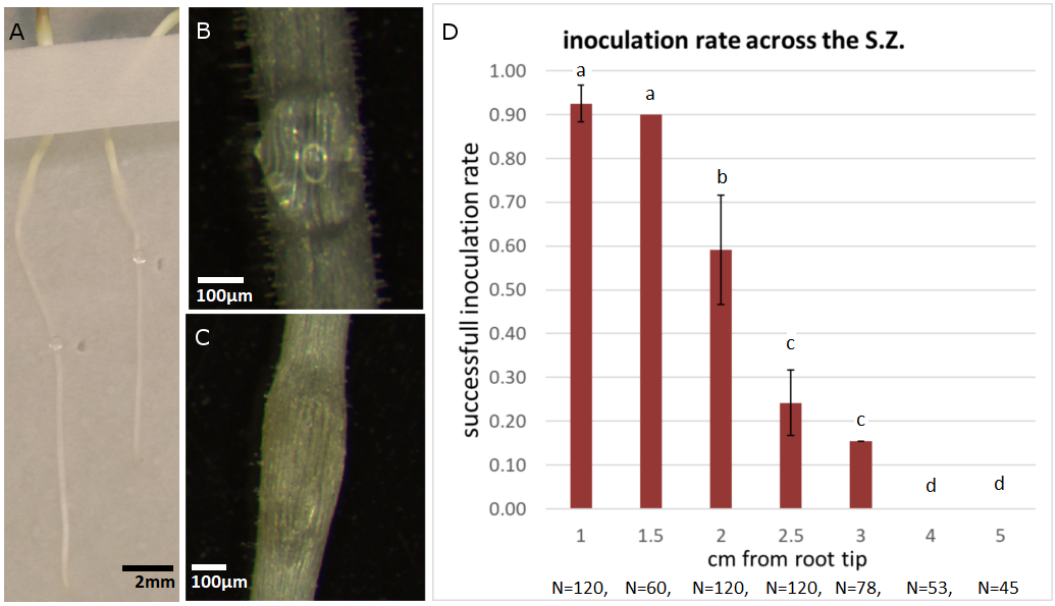

Figure 3.1: Spot inoculation rate profile of the root susceptibility zone**: A** Spot inoculation of *Medicago truncatula* seedling roots. First, seeding roots are grown on agar plates with filter paper cover on the agar. Then, the susceptibility zone is found via stereo microscopy and marked by puncturing the filter paper, next to it, using a syringe. After that, water droplets containing rhizobia are placed on this region, where the root hairs first emerge and help the droplet to remain standing. **B** Close-up of droplet used for spot inoculation, sitting on emerging root hairs. **C** Developing nodule at the inoculated spot, 6 days post inoculation (dpi). **D** Successful inoculation rate at different intervals from the root tip, showing the extent of the susceptibility zone under our growth conditions. Letters above the bars denote groupings of statistically significant differences among groups based on chi-squared test with Marascuilo procedure.

of events between these two time-points, we generated more time-points at 10, 12 and 14hpi in a follow up experiment. The combined results showed a clear progressive induction of gene expression, where we could observe different steps of nodule organogenesis (Figure 3.2 B). I used the Phytozome platform[273] to find all the family members of gene families I was interested in exploring their expression. I will first discuss the backbone of our discoveries related to auxin, and then dive deeper in the different gene families we looked into.

Expression of the central nodulation transcription factor (TF) NIN (gene identifier Medtr5g099060) was detected from 8hpi onward, along with NF-YA [274] (Medtr1g056530), and PLT3 (Medtr5g031880), a PLETHORA family member known from *Arabidopsis thaliana* to be a central hub in the post-wounding root regeneration gene regulatory network (GRN)[275]. In subsequent time-points we have the detection of transcripts for 3 LBD TFs at 10hpi (LBD16:Medtr7g096530, Medtr4g083680) and 12 hpi (LBD11:Medtr4g060950), who are central regulators of lateral root initiation[90–92]. We also detected the expression of at least 5 type-A Response Regulators (RRs) at and after 10hpi, indicating that cytokinin signaling is active in this period of nodule initiation (Figure 3.4). Interestingly, no member of the cytokinin biosynthesis enzyme families *LOG* and *IPT* was expressed before 16hpi, but the cytokinin degrading *CKX* enzyme family was highly expressed from 8hpi onwards (e.g.Medtr2g039410 and Medtr4g126150), indicating an active negative feedback loop regulation on cytokinin levels caused by active cytokinin signaling. Surprisingly, we detected induction of 3 auxin biosynthesis genes of the *YUCCA* family sequentially at 12, 14 and 16hpi, which after phylogenetic analysis (Figure 3.3) and comparison with *Arabidopsis thaliana* ortholog expression profiles using the Expressologs database[276] I named *YUC8* (Medtr7g099330, *YUC5* in our publication), *YUC2* (Medtr6g086870) and *YUC1* (Medtr3g109520), respectively. Interestingly, according to *Medicago truncatula* Plant eFP browser[277], *YUC8* is highly expressed specifically in nodules. Subsequent to this, at 16hpi, we have the differential expression of many genes related to auxin transport, transport modulation and auxin degradation. The ones that stand out are *PIN1* (Medtr4g084870), *PIN2* (Medtr4g127100), *PIN9* (Medtr7g079720, down-regulated), *LAX2* (Medtr7g067450), many auxin responsive *GH3*s (e.g. *GH3.6*:Medtr5g016320) and a *PINOID* (*PID*, Medtr8g089420) which expresses a protein regulating PIN localization by PIN phosphorylation[269, 278]. GH3, PID and PIN1 up-regulation pointed to an orchestrated response to auxin accumulation, which happens in the same way in the shoot apical meristem when a new auxin maximum forms[228]. At 16hpi we have cells entering the cell cycle, as many members of the indicator families *CYCLIN-A* and *CDC20* are expressed from then on (Figure 3.4). Thus we formed the hypothesis that there are 3 steps in the induction of auxin responses in nodule initiation. First there is expression of TFs central to organogenesis at 8 and 10hpi, second an induction of auxin biosynthesis at 12 and 14hpi that causes auxin ac-

cumulation, which at a third stage causes a response of a suite of auxin responsive genes at 16hpi. If this is true I reasoned that I should be able to detect auxin signaling at this time-point by statistical tests for enrichment of auxin responsive elements in the set of promoters of differentially regulated genes, compared to a random promoter set. Thus I next explored which signals promote this transcriptional divergence by using bioinformatic analyses of the promoters of all differentially expressed gene sets at different timepoints.

3.2.3 Detection of cytokinin response and a subsequent auxin response

To test the hypothesis of a general auxin response at 16hpi, I asked the question if and when there is a statistically significant enrichment for auxin responsive elements (AuxREs) in the promoters of differentially regulated genes, at different time-points up to and including 16hpi (see Methods 8B), compared to random sets of promoters. To this end I assembled a database of the promoter sequences of all *Medicago truncatula* genes, using Phytozome[273]. I also assembled a collection of AuxRE and type-A RR motif profiles, based on the AuxREs used in *DR5* and *DR5v2* auxin reporters[263] and the *Arabidopsis thaliana* cytokinin response regulator ARR1 and ARR2 binding motifs from the Jaspar database[279]. I used the RR motifs to detect and place in time a possible cytokinin response. I then tested, using the Analysis of Motif Enrichment (AME) tool of the MEME suite[280], in each time-point, for enrichment of AuxRE - ARR motifs in the upstream regions of genes detected to change expression, compared to upstream regions of a random set of genes (Methods 8B). I detected a highly significant enrichment for AuxRE motifs in the promoter sets of genes both up-regulated (adjusted p-value $< 10^{-7}$) and down-regulated (adj. p-value $< 10^{-4}$) at 16hpi, and not before. I could however detect significant enrichment for ARR1 in the promoters of up-regulated genes at 12hpi (p-value $< 10^{-3}$), and ARR2 in the promoters of up-regulated genes at 14hpi (p-value $< 10^{-4}$), only. These results point to a cytokinin response being active at 12 and 14hpi, that correlates with type-A *RR* gene up-regulation, and a subsequent auxin response at 16hpi (Figure 3.2-B). In a second approach, all the promoter sequences of *Medicago truncatula* genes were ranked in respect to the abundance of AuxREs in them. I then investigated how the 60 highest ranked genes in this list changed expression nodule timecourse RNA-seq data set. None of these genes was differentially regulated before 16hpi, and some were up-regulated at 16hpi and onward. I find these results to corroborate on our placement of the onset of auxin signaling at 16hpi, and to suggest that auxin biosynthesis precedes auxin accumulation. I will discuss more results from this type of motif analysis in section 3.2.5 below.

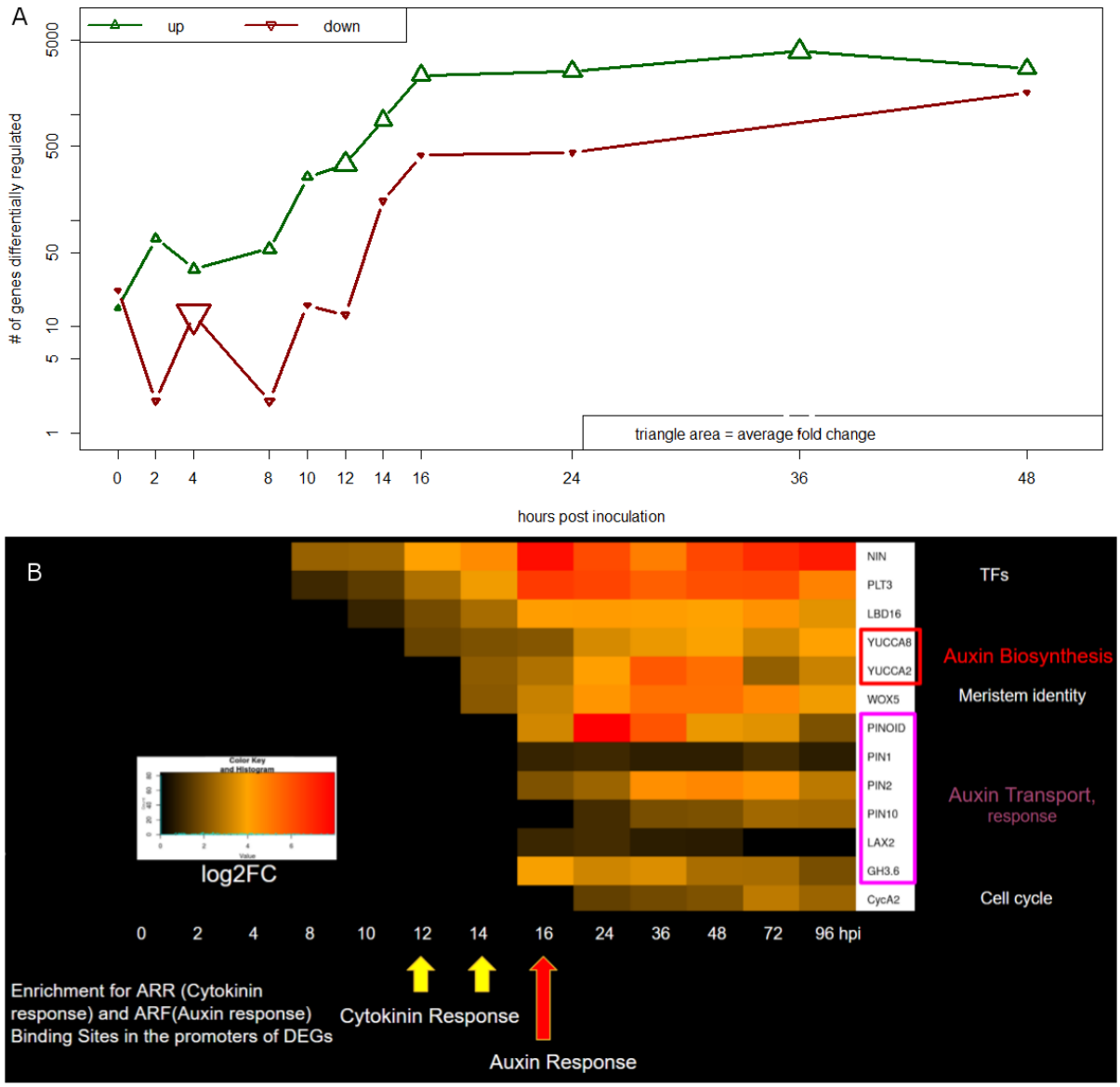

Figure 3.2: Transcriptional signature of nodule initiation**:** **A** Log-plot of the number of up-regulated (green) and down-regulated (red) genes during nodule initiation, as measured by RNA-seq. The triangle area corresponds to the average fold change of the group of genes at each time-point. **B** Heatmap of the up-regulation of selected group of genes of the same data set as in (A). Under the heatmap I denote the time-points where I discovered first a significant enrichment for cytokinin and auxin response elements in the set of promoters of differentially regulated genes compared to promoters of a random set of *Medicago truncatula* genes.

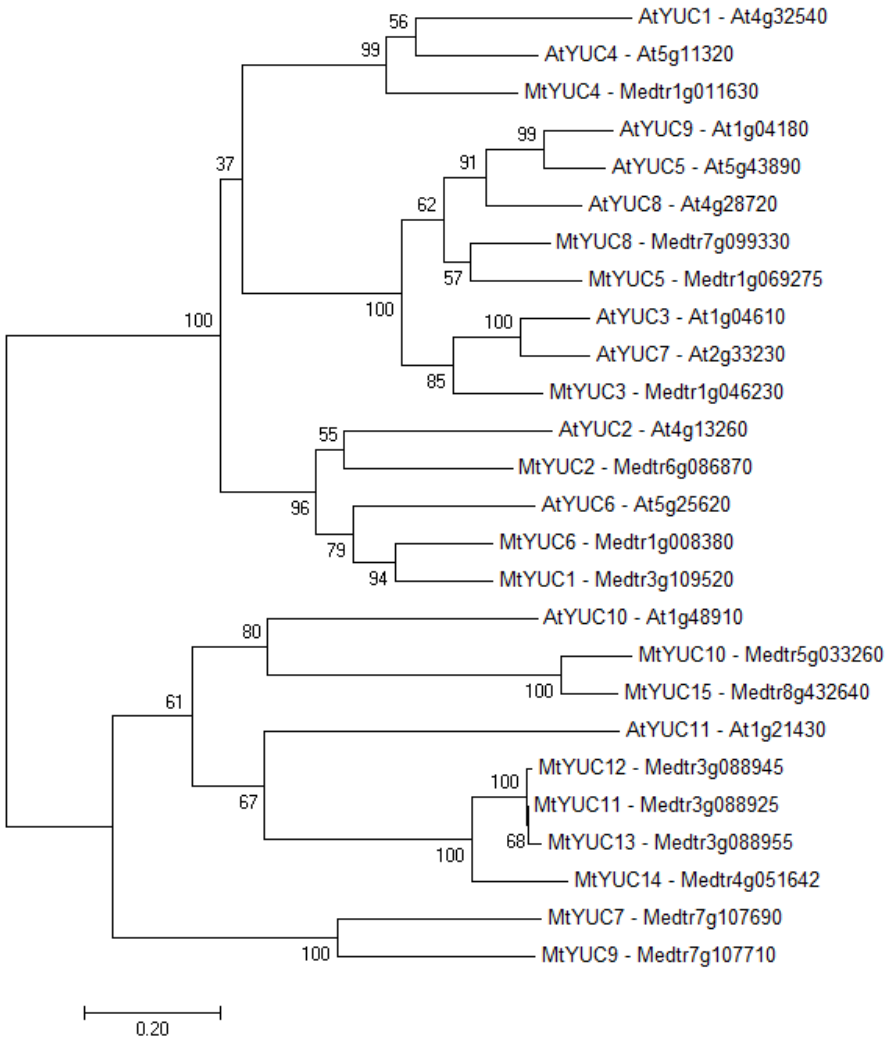

Figure 3.3: Phylogenetic tree of *Arabidopsis thaliana* and *Medicago truncatula* YUCCA proteins (Methods 14).

3.2.4 Exploring other gene families with active regulation

Looking at how different gene families involved in plant organogenesis are regulated during nodule initiation proved to be highly informative to understand how this organ comes to be and how its initiation relates to that of other organs (Figure 3.4, 3.5). Starting with the *PLETHORA* gene family, which are important *APETALA2-domain* transcription factors[100, 281], we can observe an early sequential induction of *MtPLT3* (8hpi) and *MtPLT5* (16hpi, Medtr4g127930) expression, then induction of *MtPLT1* (Medtr2g098180) and *MtPLT4* (Medtr7g080460, otherwise known as *BABYBOOM*) expression, at 24hpi. This is highly analogous to induction of lateral root primordia in *Arabidopsis thaliana*, where we have AtPLT3,5,7 as early inducers of late *AtPLT*1,2 and 4[123]. *MtPLT2* (Medtr4g06537) expression however is not generally induced, except for a transient down-regulation at 48hpi. Due to the fact that *Arabidopsis thaliana PLT1,2,3,4* promoters have been reported to give the same expression patterns as their respective *Medicago truncatula* ones[98], we expected this gene family to not be involved in nodule specific patterning processes, rather, to be induced by them. Since we know that *NIN* is a central regulator of nodule development, and that *NIN* is part of the *NLP* family that regulates root branching[57, 58], the exciting possibility that NIN and NLPs regulate *PLTs* in the same way became apparent. In order to test the plausibility of this hypothesis, I scanned the promoters of *Arabidopsis thaliana* and *Medicago truncatula PLTs* for NIN binding sites[60], which I find to be similar to AtNLP ones[59], using the Find Individual Motif Occurrences (FIMO) tool of the MEME suite. I indeed found multiple possible NIN binding sites in the 3kb promoter sequences of *AtPLT1-4* and *MtPLT1-4*, with the ones with the highest similarity score being motifs at approximately -130bp from the transcription start site (TSS) of *AtPLT2*, and motifs in the promoter of *MtPLT2*, *MtPLT1* and before the TSS of *MtPLT3*. However, few motifs of low similarity were expected to be found by chance alone. Thus I concluded that regulation of *PLT*s from NIN and NLPs cannot be ruled out. I devised transactivation experiments to test for possible cross-regulation between MtPLT3 and MtNIN (see chapter 4, section 4.2.2).

The gene families I would like to discuss next is other families related to auxin. The *Small Auxin-Up RNA* (*SAUR*) gene family encodes for proteins which have many functions in cell growth, with the main characterized one being the promotion of cell expansion[282] through interaction and inhibition of membrane bound PP2C.D family phosphatases, which inhibit an acid growth mechanism[283]. Most *SAUR* promoters are known to have AuxREs[284, 285]. The *SAUR* gene family in *Medicago truncatula* is very large[286], however, we did not detect any member being expressed before 16hpi, in agreement with my placement of the auxin response, with some members being highly induced from 16hpi onward (e.g. Medtr3g113310, Figure 3.4). There is the exception of *MtSAUR1* (Medtr8g094980), which has a mild up-

regulation at 10 and 12 hpi, previously reported to be related to epidermal response to infection[117]. Differential regulation of genes from the *Aux/IAA* and *ARF* families was also exclusive to 16hpi onward, with a general trend of *IAA*s being mildly up-regulated and *ARF*s being mildly down-regulated. I next looked at the Tryptophan-Aminotransferase-of-*Arabidopsis* (TAA) family of enzymes, responsible for the first step in auxin synthesis. Although implicated in nodule development in *Lotus japonicus*[114], the earliest expression of any *TAA* was detected here to be at 24hpi (Medtr3g077250), which led us to believe that they are not implicated in the initial auxin accumulation. Due to the sequential role of TAAs and YUCCAs in auxin production, any of them could be the bottleneck of auxin production metabolic flux, and in this case it seems to be YUCCAs. The Dioxygenase for auxin oxidation (DAO) family, in contrast to the previous ones, irreversibly inactivates auxin by oxidation[287], and, interestingly, is highly up-regulated from 10hpi (Medtr7g063730, Medtr4g074130, Medtr3g088745 and others). This is an interesting result, as it points to auxin production as well as degradation precluding transcriptional regulation of canonical auxin transport during nodule initiation. A *UDP-glucosyltransferase* (Medtr7g080935), that inactivates auxin precursors, was coexpressed with *DAO*s. In terms of auxin transport, the main results were discussed above, however I did not discuss the curious case of the *PGP/ABCB* transporter gene expression. Two of them, namely *MtAMN3* (Medtr8g022270) and *MtAMN2* (Medtr4g081190) are highly expressed from 2hpi and 10 hpi onward, respectively. The double mutant however did not have a phenotype[210]. It remains to be seen what is their role in nodulation. Another auxin transport family are the PIN-Like transporters (PILs)[226], which seem to act in intracellular auxin transport. In our data set, none of these genes were expressed before 16hpi, and some where mildly down-regulated after that. This indicates no change in PIL mediated auxin compartmentalization in the new organ, a result that could be generalized, as the same expression down-regulation is seen in *MtPIN9*, the protein of which is also acting in auxin compartmentalization[223] (discussed in chapter 2).

Next we will look at gene families that could be implicated in the early expression of *YUCCA* genes. It could be that *YUC*s are directly up-regulated by NIN, PLTs[281], or WOXs[126]. However, as presented above, LOB TFs are our leading hypothesis for induction of auxin biosynthesis (presented by our lab in [50]). This could be a direct regulation, or indirect, through STYLISH (STY) TFs [94, 95] which can also be up-regulated by NF-Ys[93]. At the time of writing this thesis, convincing results were published showing STY TFs involved in up-regulating *YUC*s in the post-initial cell division stage, helping in nodule emergence[288]. The cause of the initial up-regulation of *YUC*s, however, is not resolved yet. Looking at our data set, no *STY* family member is up-regulated before 16hpi, and we observe a gradual expression induction of 6 *STY*s by 36hpi (Medtr4g099070 and Medtr5g089750 early, Medtr8g076620

and Medtr1g023230 late important ones), indeed pointing to a delayed role of STYs[288] in nodule emergence. Clues as to what could be inducing the early *YUC* expression can be found if we look in WOX- related TFs. From the *WUSCHEL* family[126], 2 genes are differentially regulated early during nodule initiation. *MtWOX5* (Medtr5g081990) is up-regulated at 14hpi, and another *WOX* (Medtr3g115620) is up-regulated at 16hpi. Could it be that early up-regulation of *YUC*s have to do with WOX and its interactors? For one, we already know that NSP2 is important for nodulation, but its underappreciated that it's HAIRY MERISTEM (HAM) homologs in *Arabidopsis thaliana* are interacting with WOX to regulate stem cell nieces[125]. Recently I surveyed the expression of *Leafy Cotyledon* (*LEC*) family, which WOX regulates[289]. In *Arabidopsis thaliana*, LEC1 is an NF-YB subunit, and it acts together with LEC2 during early embryogenesis to induce, among other things, embryo identity, auxin biosynthesis[290] and somatic embryogenesis[291], a result that holds in *Medicago truncatula* as well[292]. Overexpression of *LEC2* can induce totipotency in many species, at least in part through *YUCCA* induction[293, 294], and BBM stem cell-related activity is through this TF as well[295]. I identified a *LEC* homolog, Medtr7g105370, to be highly expressed from 10hpi onward, and invite more research on the possibility of the corresponding TF being part of the network regulating early *YUC* induction. Overall, This TF could be the missing piece of the puzzle of how NF-YA1 could regulate *YUCCA*s, as from the NF-YA family we have *MtNFY-A1* (*HAP2*) (Medtr1g056530) only being expressed from 8hpi, and from the *NF-YB* family we have *MtNF-YB16* (Medtr4g119500) only being highly up-regulated from 12hpi onward. All the data corresponding to the observations discussed here can be found in the supplementary list of differentially expressed genes in our group publication[50], as well as Figures 3.4 and 3.5.

Lastly, I would like to make some observations about how nodule initiation relates to other plant developmental processes. Nodule initiation does not seem to involve the expression of the *NO TRANSMITTING TRACT* (*NTT*) and its paralogs, as we detected only one of them being lowly and briefly expressed only at 16hpi (Medtr2g090745) and a general family down-regulation after. These genes are necessary for the initiation of the root meristem in the *Arabidopsis thaliana* embryo, and distal cell fate at the RM, and their missexpression can transform other stem cell populations to a distal stem cell fate[296]. It stands to reason then that nodule initiation does not require this family, and suppression of their expression might help in keeping nodule identity. Another stem cell developmental process I can compare the nodules with is the spontaneous organ formation in the leaves of the *kanadi1-kanadi2 Arabidopsis thaliana* mutant, where run-away *YUCCA* expression re-polarizes the leaf tissue and induces the formation of outgrowths[297]. Outgrowth formation is dependent on CUP-SHAPED COTYLEDON (CUC) TFs, which are locally co-expressed with YUCs, redirect

PIN localization, and give directionality to growth, in this setting. CUCs are generally responsible for shaping multiple organs via margin dissection[298, 299]. Our data set indicates that the large *Medicago truncatula* CUC family is broadly and consistently down-regulated in the nodule. This could suggest that the globular shape of this organ might involve suppression of this and other families of shaping factors, and that YUCCA action does not require them in the nodule to form a proximal auxin maximum. We cannot rule out, however, that regulation is spatially heterogeneous in the region we probe, cancelling out over the whole tissue sample. In the future, comparing the gene regulatory network state of the nodule to that of other organs[300] could lead to an understanding of how this organ attains it's unique "inverted" organization, where, I suggest, infectable cortical tissue takes central position, and vasculature forms peripherally, a testament to the evolvability and plasticity of plant development.

3.2.5 Bioinformatic analyses of the RNA-seq data set

Our data set gives a unique opportunity to characterize nodule development through both holistic and targeted bioinformatic approaches. I found these approaches to be complementary and informative to our main research question of how is auxin involved in nodule initiation, to the least by placing processes relating to auxin in time among other developmental events. To prepare our data set, first I sorted the differentially expressed genes by expression across time-points and extracted annotation for these genes. For this I used a custom-made web scraper program that extracted the community annotation for *Medicago truncatula* genome v4 (Mt4.0) provided by JCVI[301], as well as annotations of respective *Arabidopsis thaliana* homologs from Phytozome[273]. I opted for three types of analyses to the data set. Our first type of analysis was a literature search to identify interesting targets highly and quickly differentially regulated throughout the datapoints for further research. The second approach was to perform gene ontology enrichment tests for the sets of up-regulated and down-regulated genes in each time-point (Methods 18). The third approach was to test the same groups of genes for motif enrichment of known TF binding sites in their promoter sequences, or to find novel motifs in these promoters and test for enrichment in comparison to a random set of *Medicago truncatula* promoters (Methods 8A).

Looking at early up-regulated genes revealed a number of interesting targets for further research. From the very few (9 in total) genes up-regulated consistently from 2hpi and all the time-points onward, most express proteins which seem to be defence related, according to annotation, for example a putative ankyrin repeat-like protein (Medtr6g027840) that has a possible relation to ABA signaling, a salicylic acid carboxyl methyltransferase (Medtr6g056070), a tyrosine kinase (Medtr4g129010) and an LRR receptor-like kinase (Medtr5g026760). All fold-change gene expression values can be found in Figure 3.5. A pectate lyase (Medtr3g086320)

expressed could be related to the breakdown of the cell wall to remodel for root hair extention and curling. I also detected a high up-regulation of expression of a hypothetical protein (Medtr5g005290) that has no known *Arabidopsis thaliana* homologs, but is part of a big legume family of hypothetical proteins of unknown function, based on a HMMER search. Lastly, I identified a subtilisin-like serine protease (Medtr4g102400) whose *Arabidopsis thaliana* homolog is involved in stomatal lineage development[302]. Many *WRKY* transcription factor genes (Medtr7g071120, Medtr3g090860, Medtr4g007060) were expressed specifically on this time-point, which pinpoints to an active stress response[303]. Looking at the set of genes up-regulated from 4hpi onward also reveals defence related responses, corroborated by GO tests (see below). We have the expression of a possible exochitinase (glycoside hydrolase Medtr4g116990), a defensin (Medtr8g012795), and a cell wall remodeling DUF642 family protein (Medtr4g039720). Two more completely unknown proteins, with no *Arabidopsis thaliana* homologs, were found to be expressed (Medtr4g088510, Medtr8g040940). Between the time-points of 2hpi and 4hpi I found a number of genes that were first highly up-regulated and then highly down-regulated (e.g. Medtr8g479250, Medtr1g090957, Medtr4g117610), with one encoding for a cyanogenic beta-glucosidase (Medtr4g015420) which releases hydrogen cyanide [304](Figure 3.5). This could indicate that between these points in time the plants decides if the inoculum is a friend or foe. Interestingly, I did not find a single gene that was down-regulated early and throughout our datapoints. All the above indicate a stage between 0-8hpi where the GRN of the plant reconfigures from a pure defence response to a symbiotic decision, where symbiosis suppresses other responses the plant might have initiated.

Gene Ontology enrichment for the sets of differentially regulated genes (Methods 18) was next employed to better understand which cellular components, processes and molecular functions are activated in each timepoint of nodule induction. For this we used the agriGO analysis toolkit[305] (full analysis description in Methods 18). The results complemented the general observations I made above. I will present only the highly significant results to make it this section easier for the reader. At 4hpi the set of genes up-regulated by more than 2-fold yielded significant results for enrichment in *response to stimulus* and *response to stress* GO categories. At 8hpi, up-regulated genes were enriched in *transport*, *establishment of localization* and other categories related to transmembrane movement of substances, which might be related to the infection process taking place. At 10hpi we have *response to chemical stimulus* and *oxidative stress*, *heme*, *tetrapyrrole*, *iron ion* and *calcium ion binding* categories, which are also enriched in the 12hpi up-regulated group, where we have the addition of *cell wall biogenesis*, *phosphorelay signal transduction system*, *nitrogen metabolic process regulation*, *kinases*, *regulation of transcription*, *RNA metabolism* and *macromolecule biosynthesis* categories. At these time-points I could make sense of these results by relating them to the calcium

Figure 3.4: Expression fold change during nodule formation of selected genes. All data reported are significant and have FDR corrected p-values less than 0.05. Gene family members with non significant expression changes (n.s.) are omitted.

group	gene ID	gene name/description	2hpi	4	8	10	12	14	16	24	36	48	72	96hpi
	Medtr5g099060	NIN	n.s.	n.s.	5.1	5.3	17.3	24.6	203.2	70.8	30.9	76.6	119.6	166.5
	Medtr1g056530	NF-YA1, HAP2	n.s.	n.s.	8.2	4.6	12.1	38.4	355.4	232.8	288.3	690.7	571.4	673.8
	Medtr5g031880	MtPLT3	n.s.	n.s.	2.0	2.8	6.5	13.5	93.7	80.8	51.4	67.1	70.5	28.8
	Medtr4g060950	LBD11	n.s.	n.s.	n.s.	n.s.	4.1	4.0	7.3	10.4	10.7	7.8	7.2	2.9
	Medtr4g083680	LBD4	n.s.	n.s.	n.s.	1.7	2.9	2.6	6.0	2.9	1.9	2.0	1.6	n.s.
	Medtr7g096530	LBD16	n.s.	n.s.	n.s.	1.8	3.6	6.1	18.4	19.0	18.1	16.9	22.1	11.5
ARRs	Medtr3g015490	ARR-related	n.s.	n.s.	n.s.	2.1	3.1	3.6	5.4	2.8	2.0	n.s.	n.s.	n.s.
	Medtr3g078613	ARR-related	n.s.	n.s.	n.s.	1.7	2.4	2.0	5.0	2.7	2.1	1.4	n.s.	1.3
	Medtr5g036480	ARR4	n.s.	n.s.	n.s.	2.1	3.7	2.2	4.2	1.5	n.s.	n.s.	n.s.	n.s.
	Medtr7g490310	ARR-related	n.s.	n.s.	n.s.	1.5	1.8	n.s.	2.7	1.9	1.5	1.3	n.s.	n.s.
	Medtr8g038620	ARR11	n.s.	n.s.	n.s.	2.8	5.1	6.4	34.5	9.7	11.4	7.7	10.6	7.0
LOG	Medtr7g101290	LOG1	n.s.	n.s.	n.s.	n.s.	n.s.	n.s.	136.5	12.4	4.8	2.7	9.1	8.1
IPTs	Medtr2g022140	IPT-related	n.s.	n.s.	n.s.	n.s.	n.s.	n.s.	12.6	5.7	2.5	3.7	2.1	n.s.
	Medtr1g110590	IPT1	n.s.	n.s.	n.s.	n.s.	n.s.	n.s.	n.s.	n.s.	17.4	15.1	166.2	43.8
	Medtr4g117330	IPT-related	n.s.	n.s.	n.s.	n.s.	n.s.	n.s.	13.2	2.8	2.2	1.9	2.8	2.5
CKXs	Medtr2g039410	CKX-related	n.s.	n.s.	2.5	3.1	7.7	8.5	8.4	5.2	1.5	n.s.	2.8	2.6
	Medtr4g126150	CKX-related	n.s.	n.s.	n.s.	6.8	25.3	339.6	80.7	17.7	10.8	26.8	31.5	19.0
YUCs	Medtr7g099330	MtYUC8	n.s.	n.s.	n.s.	n.s.	3.1	3.9	4.3	10.0	12.8	15.2	9.3	17.3
	Medtr6g086870	MtYUC2	n.s.	n.s.	n.s.	n.s.	n.s.	4.6	6.6	17.9	57.1	40.1	4.9	8.8
	Medtr3g109520	MtYUC1	n.s.	n.s.	n.s.	n.s.	n.s.	n.s.	2.6	2.4	3.6	2.6	n.s.	n.s.
PINs	Medtr4g084870	PIN1	n.s.	n.s.	n.s.	n.s.	n.s.	n.s.	1.8	2.0	1.7	1.7	2.2	1.6
	Medtr4g127100	PIN2	n.s.	n.s.	n.s.	n.s.	n.s.	n.s.	4.0	5.4	23.4	26.7	21.1	7.6
	Medtr1g030890	PIN3	n.s.	n.s.	n.s.	n.s.	n.s.	n.s.	n.s.	n.s.	-1.6	-1.6	-2.6	-3.4
	Medtr1g029190	PIN6	n.s.	n.s.	n.s.	n.s.	n.s.	n.s.	n.s.	1.9	8.1	6.0	4.2	1.9
	Medtr7g079720	PIN9	n.s.	n.s.	n.s.	n.s.	n.s.	n.s.	-3.8	-3.8	-6.6	-2.8	-3.2	n.s.
	Medtr7g089360	PIN10	n.s.	n.s.	n.s.	-1.4	n.s.	n.s.	n.s.	2.1	3.7	3.8	5.6	5.5
LAXs	Medtr5g082220	LAX1	n.s.	n.s.	n.s.	n.s.	n.s.	n.s.	n.s.	1.6	1.5	1.4	1.3	n.s.
	Medtr7g067450	LAX2	n.s.	n.s.	n.s.	n.s.	n.s.	n.s.	1.9	2.1	1.6	1.6	n.s.	-1.3
GH3s	Medtr5g016320	GH3.6	1.6	n.s.	n.s.	n.s.	n.s.	n.s.	14.4	9.1	10.7	6.2	6.1	3.7
	Medtr8g027955	GH3-related	n.s.	n.s.	n.s.	n.s.	n.s.	n.s.	-1.8	-2.1	-2.3	-2.1	-2.4	-1.9
	Medtr8g027920	GH3-related	n.s.	n.s.	n.s.	n.s.	n.s.	n.s.	-1.8	n.s.	-1.9	n.s.	n.s.	1.6
	Medtr8g467000	GH3-related	n.s.	n.s.	n.s.	-1.3	n.s.	n.s.	-1.4	-1.3	-1.9	-1.6	-1.6	-1.6
	Medtr7g094190	GH3.7	n.s.	n.s.	n.s.	n.s.	n.s.	n.s.	1.4	n.s.	1.4	1.3	1.4	1.5
	Medtr1g088765	GH3.2	n.s.	n.s.	n.s.	-1.8	n.s.	n.s.	n.s.	n.s.	-1.7	-2.3	-2.0	-2.7
	Medtr7g117110	GH3.9	n.s.	n.s.	n.s.	n.s.	n.s.	n.s.	n.s.	-1.2	-1.5	-1.4	-1.4	-1.5
	Medtr0035s0150	GH3-related	n.s.	n.s.	n.s.	n.s.	n.s.	n.s.	n.s.	2.3	2.8	2.5	5.3	3.4
PIDs	Medtr2g018990	PID-related	n.s.	n.s.	n.s.	n.s.	n.s.	n.s.	n.s.	n.s.	2.4	n.s.	1.6	1.9
	Medtr8g089420	PID	n.s.	n.s.	n.s.	n.s.	n.s.	n.s.	9.6	253.0	61.0	12.6	11.3	3.8
	Medtr4g113790	PID2-related	n.s.	n.s.	n.s.	n.s.	n.s.	n.s.	n.s.	n.s.	3.6	3.9	15.2	17.3
Cyclins	Medtr2g102550	CycA2	n.s.	n.s.	n.s.	n.s.	n.s.	n.s.	n.s.	2.9	3.4	4.0	7.6	5.3
	Medtr3g102530	Cyclin-related	n.s.	n.s.	n.s.	n.s.	n.s.	n.s.	2.5	2.3	3.4	3.6	3.0	4.8
	Medtr3g102520	Cyclin-related	n.s.	n.s.	n.s.	n.s.	n.s.	n.s.	2.9	4.0	5.0	4.5	3.9	5.1
	Medtr3g100710	Cyclin-related	n.s.	n.s.	n.s.	n.s.	n.s.	n.s.	1.4	1.4	1.8	1.6	n.s.	n.s.
D Cyclins	Medtr4g094942	Cyclin-D3-2-related	n.s.	n.s.	n.s.	n.s.	n.s.	n.s.	n.s.	1.8	2.5	2.2	2.3	2.9
	Medtr5g035360	Cyclin-D1-1-related	n.s.	n.s.	n.s.	n.s.	n.s.	n.s.	n.s.	n.s.	-1.3	-1.5	-2.3	-1.5
	Medtr3g100710	Cyclin-D4-1-related	n.s.	n.s.	n.s.	n.s.	n.s.	n.s.	1.4	1.4	1.8	1.6	n.s.	n.s.
	Medtr5g032550	Cyclin-D2-1-related	n.s.	n.s.	n.s.	n.s.	n.s.	n.s.	n.s.	n.s.	1.6	1.3	n.s.	1.6
	Medtr3g102310	Cyclin-related	n.s.	n.s.	n.s.	n.s.	n.s.	n.s.	n.s.	n.s.	-1.6	n.s.	1.5	1.8
	Medtr1g107535	Cyclin-D3-1-related	n.s.	n.s.	n.s.	n.s.	n.s.	n.s.	n.s.	1.9	1.7	2.2	3.5	2.9
CDC20 related,	Medtr3g051690	CDC20-related	n.s.	n.s.	n.s.	n.s.	n.s.	n.s.	3.6	4.3	2.9	2.3	2.8	2.7
anaphase	Medtr3g067940	CCS52a-related	n.s.	n.s.	n.s.	n.s.	n.s.	n.s.	n.s.	1.4	2.5	3.0	6.1	5.0
specific	Medtr7g034625	CDC20-related	n.s.	n.s.	n.s.	n.s.	n.s.	n.s.	n.s.	3.5	4.6	3.6	8.8	7.5
	Medtr1g054300	WD-40 repeat prot.	n.s.	n.s.	n.s.	n.s.	n.s.	n.s.	2.7	2.7	2.4	1.7	n.s.	1.5
	Medtr4g102510	FIZZY-related	n.s.	n.s.	n.s.	n.s.	n.s.	n.s.	1.4	1.3	1.5	n.s.	n.s.	1.4
PLTs	Medtr2g098180	PLT1	n.s.	n.s.	n.s.	n.s.	n.s.	n.s.	n.s.	3.3	n.s.	n.s.	7.5	4.0
	Medtr4g065370	PLT2	n.s.	n.s.	n.s.	n.s.	n.s.	n.s.	n.s.	n.s.	n.s.	-18.3	n.s.	n.s.
	Medtr5g031880	PLT3	n.s.	n.s.	2.0	2.8	6.5	13.5	93.7	80.8	51.4	67.1	70.5	28.8
	Medtr7g080460	PLT4	n.s.	n.s.	n.s.	n.s.	n.s.	n.s.	n.s.	6.4	n.s.	4.5	15.2	5.2
	Medtr4g127930	PLT5	n.s.	n.s.	n.s.	n.s.	n.s.	n.s.	3.6	3.5	3.1	2.7	3.7	2.9
	Medtr8g068510	PLT7	n.s.	n.s.	n.s.	n.s.	n.s.	n.s.	n.s.	n.s.	n.s.	n.s.	n.s.	n.s.
SAURs	Medtr8g094980	SAUR1	n.s.	n.s.	n.s.	1.7	2.1	n.s.	n.s.	1.4	n.s.	n.s.	n.s.	-1.4
	Medtr3g113310	SAUR-related	n.s.	n.s.	n.s.	n.s.	n.s.	n.s.	61.7	138.8	512.7	237.6	881.6	276.8
	Medtr3g092220	SAUR-related	n.s.	n.s.	n.s.	n.s.	n.s.	n.s.	-1.6	-1.4	-2.1	-1.7	-2.0	-2.1
	Medtr2g044020	SAUR-related	n.s.	n.s.	n.s.	n.s.	n.s.	n.s.	3.6	n.s.	n.s.	2.0	3.6	7.7
	Medtr4g005320	SAUR-related	n.s.	n.s.	n.s.	n.s.	n.s.	n.s.	6.9	n.s.	n.s.	n.s.	n.s.	n.s.
	Medtr8g022440	SAUR-related	n.s.	n.s.	n.s.	n.s.	n.s.	n.s.	-1.7	-1.6	-2.3	-1.8	-4.1	-2.9
	Medtr4g072190	SAUR-related	n.s.	n.s.	n.s.	n.s.	n.s.	n.s.	3.7	2.5	1.9	2.8	3.2	2.5
	Medtr7g051910	SAUR-related	n.s.	n.s.	n.s.	n.s.	n.s.	n.s.	-1.6	-1.5	-2.2	-1.9	-2.7	-2.7
	Medtr8g026730	SAUR-related	n.s.	n.s.	n.s.	n.s.	n.s.	n.s.	1.8	2.1	1.4	n.s.	n.s.	-2.0

Figure 3.5: Expression fold change during nodule formation of selected genes . (continued)

group	gene ID	gene name/description	2hpi	4	8	10	12	14	16	24	36	48	72	96hpi
Aux/IAAs	Medtr1g080860	IAA16-related	n.s.	n.s.	n.s.	n.s.	n.s.	n.s.	-1.5	-1.5	-1.8	-1.7	-1.8	-1.8
	Medtr4g115070	IAA9	n.s.	n.s.	n.s.	n.s.	n.s.	n.s.	1.8	1.4	1.8	1.6	1.5	n.s.
	Medtr1g093240	IAA14-related	n.s.	n.s.	n.s.	n.s.	n.s.	n.s.	1.4	2.2	3.2	3.2	2.5	2.3
	Medtr8g067530	IAA9	n.s.	n.s.	n.s.	n.s.	n.s.	n.s.	1.4	1.6	2.1	1.9	2.4	2.0
	Medtr4g011880	IAA19-related	n.s.	n.s.	n.s.	n.s.	n.s.	n.s.	1.7	3.4	2.2	n.s.	n.s.	n.s.
	Medtr4g115075	IAA-related	n.s.	n.s.	n.s.	n.s.	n.s.	n.s.	n.s.	3.9	21.2	55.7	16.6	21.1
	Medtr8g014520	IAA18	n.s.	n.s.	n.s.	n.s.	n.s.	n.s.	n.s.	-1.6	-2.0	-2.0	-2.0	-1.5
	Medtr1g093350	IAA1-related	n.s.	n.s.	n.s.	n.s.	n.s.	n.s.	n.s.	1.5	1.7	1.4	1.5	n.s.
ARFs	Medtr1g094960	ARF10-related	n.s.	n.s.	n.s.	n.s.	n.s.	n.s.	8.5	5.4	6.9	5.3	3.9	3.4
	Medtr2g093740	ARF4	n.s.	n.s.	n.s.	n.s.	n.s.	n.s.	-1.6	-1.5	-1.8	n.s.	n.s.	-1.9
	Medtr4g021580	ARF12-related	n.s.	n.s.	n.s.	n.s.	n.s.	n.s.	-1.4	-1.4	-1.4	-1.3	n.s.	n.s.
	Medtr4g124900	ARF19-related	n.s.	n.s.	n.s.	n.s.	n.s.	n.s.	-1.4	-1.7	-2.2	-1.5	n.s.	-1.5
	Medtr2g043250	ARF19-related	n.s.	n.s.	n.s.	n.s.	n.s.	n.s.	1.3	1.6	2.2	1.9	2.2	1.6
	Medtr3g064050	ARF8	n.s.	n.s.	n.s.	n.s.	n.s.	n.s.	1.4	1.5	2.4	2.0	1.6	n.s.
	Medtr5g076270	ARF8	n.s.	n.s.	n.s.	n.s.	n.s.	n.s.	n.s.	1.4	1.5	1.4	n.s.	n.s.
	Medtr8g100050	ARF2	n.s.	n.s.	n.s.	n.s.	n.s.	n.s.	n.s.	-1.3	-1.3	-1.4	n.s.	n.s.
	Medtr1g024025	ARF5	n.s.	n.s.	n.s.	n.s.	n.s.	n.s.	n.s.	1.3	2.0	2.5	3.6	3.4
TAAs	Medtr4g105220	TAA-related	n.s.	n.s.	n.s.	n.s.	n.s.	n.s.	n.s.	n.s.	-1.6	n.s.	n.s.	1.8
	Medtr3g077250	TAA-related	n.s.	n.s.	n.s.	n.s.	n.s.	n.s.	n.s.	1.8	1.6	1.3	n.s.	n.s.
	Medtr5g033510	TAA1-related	n.s.	n.s.	n.s.	n.s.	n.s.	n.s.	n.s.	n.s.	n.s.	n.s.	n.s.	3.6
DAOs	Medtr7g063730	DAO-related	n.s.	n.s.	n.s.	6.7	193.4	493.2	2215.1	381.3	2117.2	2176.5	2370.1	5145.6
	Medtr2g068960	DAO-related	n.s.	n.s.	n.s.	n.s.	n.s.	n.s.	57.0	10.2	47.1	n.s.	2.9	13.2
	Medtr4g074130	DAO-related	n.s.	n.s.	n.s.	4.3	10.8	15.4	39.8	12.6	43.1	78.0	86.0	66.0
	Medtr2g069020	DAO-related	n.s.	n.s.	n.s.	n.s.	n.s.	2.7	2.9	3.1	21.9	22.9	29.4	126.7
	Medtr3g088745	DAO-related	n.s.	n.s.	n.s.	54.7	52.8	134.5	975.7	523.9	600.6	426.5	694.5	600.8
	Medtr4g132770	DAO-related	n.s.	n.s.	n.s.	n.s.	n.s.	n.s.	14.9	26.9	51.9	63.0	91.2	131.2
	Medtr4g132765	DAO-related	n.s.	n.s.	n.s.	n.s.	n.s.	n.s.	13.0	27.2	116.0	136.6	205.1	859.7
	Medtr7g080935	UDP-glucosyltransferase	n.s.	n.s.	n.s.	6.6	10.5	117.4	37.7	56.3	69.7	63.7	119.4	104.1
AMNs	Medtr4g081190	AMN2	n.s.	n.s.	n.s.	11.0	160.5	219.6	283.5	150.3	775.4	60.1	164.8	479.7
(ABCBs)	Medtr8g022270	AMN3	4.5	4.2	9.0	27.6	81.3	82.5	141.9	27.7	62.6	14.0	56.1	31.0
PILS	Medtr8g006780	PILS-related	n.s.	n.s.	n.s.	n.s.	n.s.	n.s.	-2.4	-1.7	-3.1	-2.1	-3.2	-3.3
	Medtr5g024970	PILS-related	n.s.	n.s.	n.s.	n.s.	n.s.	n.s.	-2.1	-1.8	-3.1	-2.4	-3.4	-3.7
	Medtr5g024660	PILS-related	n.s.	n.s.	n.s.	n.s.	n.s.	n.s.	n.s.	-1.5	-3.1	-1.8	-2.7	-2.3
	Medtr5g024640	PILS-related	n.s.	n.s.	n.s.	n.s.	n.s.	n.s.	n.s.	-1.9	-4.0	-2.2	-2.5	-2.0
STYs	Medtr8g076620	STY-SHI-related	n.s.	n.s.	n.s.	n.s.	n.s.	n.s.	n.s.	23.3	38.9	96.9	130.8	55.0
	Medtr5g089750	STY-SHI-related	n.s.	n.s.	n.s.	n.s.	n.s.	n.s.	1.6	2.1	6.4	7.7	14.1	14.2
	Medtr4g099070	STY-SHI-related	n.s.	n.s.	n.s.	n.s.	n.s.	n.s.	1.9	1.8	2.6	1.8	n.s.	1.5
	Medtr3g014660	STY-SHI-related	n.s.	n.s.	n.s.	n.s.	n.s.	n.s.	n.s.	n.s.	2.2	2.9	3.3	4.6
	Medtr1g023230	STY-SHI-related	n.s.	n.s.	n.s.	n.s.	n.s.	n.s.	n.s.	4.3	16.2	35.2	19.7	12.1
	Medtr5g021130	STY-SHI-related	n.s.	n.s.	n.s.	n.s.	n.s.	n.s.	n.s.	n.s.	3.6	8.6	14.1	9.0
	Medtr4g071110	STY-SHI-related	n.s.	n.s.	n.s.	n.s.	n.s.	n.s.	n.s.	n.s.	n.s.	n.s.	7.9	20.9
	Medtr8g039110	STY-SHI-related	n.s.	n.s.	n.s.	n.s.	n.s.	n.s.	n.s.	n.s.	n.s.	n.s.	96.3	265.5
	Medtr0363s0040	STY-SHI-related	n.s.	n.s.	n.s.	n.s.	n.s.	n.s.	n.s.	n.s.	n.s.	n.s.	22.3	10.5
WOXs	Medtr5g081990	MtWOX5	n.s.	n.s.	n.s.	n.s.	n.s.	4.4	8.6	21.0	39.1	38.8	25.7	13.6
	Medtr3g115620	WOX-related	n.s.	n.s.	n.s.	n.s.	n.s.	n.s.	1.8	2.0	2.3	2.1	1.4	n.s.
LEC-related	Medtr4g119500	NF-YB16, AtLEC1 related	n.s.	n.s.	n.s.	n.s.	45.1	235.1	295.7	499.0	558.9	124.1	48.8	203.6
	Medtr7g105370	LEC2-related	n.s.	n.s.	n.s.	5.1	9.7	39.4	75.8	224.1	194.4	174.2	231.1	683.1
NTT-WIP2	Medtr2g090745	NTT-related	n.s.	n.s.	n.s.	n.s.	n.s.	n.s.	1.6	n.s.	-1.2	n.s.	-2.2	-2.4
related	Medtr1g016010	NTT-related	n.s.	n.s.	n.s.	n.s.	n.s.	n.s.	-1.9	-1.6	-2.0	-1.8	-1.5	-1.4
CUCs	Medtr2g064470	CUC-related	n.s.	n.s.	n.s.	n.s.	n.s.	n.s.	-1.4	-1.6	-1.7	-1.6	-1.7	-1.4
	Medtr7g100990	CUC-related	n.s.	n.s.	n.s.	n.s.	n.s.	n.s.	-2.9	n.s.	n.s.	-2.3	-4.0	-3.3
	Medtr7g085260	CUC-related	n.s.	n.s.	n.s.	n.s.	n.s.	n.s.	n.s.	-1.4	-2.0	-1.9	-2.0	-1.9
	Medtr7g097090	CUC-related	n.s.	n.s.	n.s.	n.s.	n.s.	n.s.	-1.9	-2.4	-3.6	-2.4	-3.0	-2.8
	Medtr6g032770	CUC-related	n.s.	n.s.	n.s.	n.s.	n.s.	n.s.	-1.6	-1.5	-2.4	-1.5	n.s.	-1.7
	Medtr4g108760	CUC-related	n.s.	n.s.	n.s.	n.s.	n.s.	n.s.	-2.4	-2.2	-3.3	-2.4	-3.6	-3.8
early expressed	Medtr6g027840	ankyrin repeat RF-like	2.8	2.6	3.4	11.0	43.4	24.7	23.6	16.4	20.8	11.6	6.3	10.2
genes	Medtr6g056070	SA carboxyl methyltransferase	4.2	2.4	3.2	4.2	9.0	6.4	16.1	4.7	12.4	7.3	8.4	34.1
	Medtr4g129010	tyrosine kinase	17.8	16.1	20.1	12.6	89.3	230.3	497.4	158.0	38.6	15.7	16.5	17.4
	Medtr5g026760	LRR receptor-like kinase	9.8	5.9	n.s.	14.3	145.5	108.9	123.5	45.9	101.7	63.7	77.5	78.5
	Medtr3g086320	pectate lyase	14.5	84.6	45.3	39.1	1852.2	586.4	5234.2	4642.3	4261.8	821.0	5853.7	9142.0
	Medtr5g005290	hypothetical protein	55.1	29.1	n.s.	29.3	258.1	343.1	855.4	518.6	374.3	205.4	231.5	295.7
	Medtr4g102400	subtilisin-like serine protease	3.7	2.0	3.9	6.8	21.5	34.6	98.1	102.6	127.1	139.4	71.4	222.6
early expressed	Medtr7g071120	WRKY1-related	2.0	n.s.	n.s.	n.s.	n.s.	n.s.	1.7	n.s.	n.s.	-1.4	n.s.	n.s.
WRKYs	Medtr3g090860	WRKY-related	5.3	n.s.	n.s.	n.s.	n.s.	n.s.	n.s.	9.4	5.5	2.4	n.s.	n.s.
	Medtr4g007060	WRKY40-related	1.7	n.s.	n.s.	n.s.	n.s.	n.s.	n.s.	n.s.	-1.4	n.s.	n.s.	n.s.
early expressed	Medtr4g116990	glycoside hydrolase	n.s.	3.5	5.1	17.0	48.7	51.3	680.4	46.6	131.7	104.0	22.5	51.2
genes	Medtr8g012795	Defensin-related	n.s.	26.2	46.6	9.5	2096.7	728.4	649.5	286.2	507.5	102.1	609.3	27.9
	Medtr4g039720	DUF642-related	n.s.	17.5	107.6	24.7	902.7	1072.6	284.8	419.9	116.9	12.2	8.4	20.9
legume-specific	Medtr4g088510	hypothetical protein	n.s.	17.3	21.8	11.8	120.0	238.2	3844.0	4914.4	3502.4	1491.4	1842.4	984.2
	Medtr8g040940	hypothetical protein	n.s.	92.8	92.0	13.2	713.6	728.2	779.6	1672.7	2381.6	214.0	3337.1	604.2
early pulse	Medtr8g479250	RAD60-SUMO-like	113.5	-399.1	n.s.	n.s.	n.s.	n.s.	n.s.	n.s.	n.s.	n.s.	n.s.	n.s.
	Medtr1g090957	legume lectin domain-related	90.4	-576.0	n.s.	n.s.	n.s.	n.s.	n.s.	n.s.	n.s.	n.s.	n.s.	n.s.
	Medtr4g117610	Primary-amine oxidase	30.9	-32.7	n.s.	n.s.	n.s.	n.s.	n.s.	n.s.	n.s.	n.s.	n.s.	n.s.
	Medtr4g015420	cyanogenic beta-glycosidase	10.7	-94.0	n.s.	n.s.	n.s.	n.s.	n.s.	n.s.	n.s.	n.s.	n.s.	n.s.
SOSEKIs	Medtr1g115370	SOK-related	n.s.	n.s.	n.s.	n.s.	2.6	4.3	4.5	5.6	10.2	11.6	4.7	3.0
	Medtr2g062310	SOK-related	n.s.	n.s.	n.s.	n.s.	n.s.	n.s.	n.s.	18.9	18.4	38.0	126.1	499.8
	Medtr4g063130	SOK-related	n.s.	n.s.	n.s.	n.s.	n.s.	n.s.	n.s.	1.7	7.4	5.2	7.8	3.5

and cytokinin signaling involved in nodule initiation. At 14hpi up-regulated genes are related to *ribosome biogenesis*, *ribonucleoprotein complex biogenesis*, *RNA processing*, *ncRNA*, *cell wall*, *chemical stimulus response* and *RNA modification*, among others. Interestingly, down-regulated genes by more than 2-fold are here specific to GO categories, mainly "*response to oxidative stress*", *"response to chemical stimulus*" and *"peroxidase activity*". At 16hpi and 24 hpi, GO enrichment is extremely diverse, indicating drastic changes in cellular state. Most of the previous GO terms are present in the results, with many more related to generic cell proliferation processes, including chromatin remodeling. At 16hpi genes down-regulated by more than 2.2-fold are enriched for *anion transport*, *oxidation reduction*, *terpene synthase* and *carbon-oxygen lyase* categories. At 24hpi I also tested the set of 5-fold+ up-regulated genes, which were shown to be enriched in *ethylene metabolic process*, *cellular alkene metabolism*, *alkene biosynthesis*, *cell wall biogenesis*, and *aspartate metabolism* categories. Summarizing these results is difficult, apart from underlying a bleak outlook for the sleep schedule of the nodule researcher: nodule initiation makes all the important developmental decisions around 12 hours post inoculation, making this a hard process for one person to take data for. I realized that this could have been an unknown bias in previous studies, where there is a frequent choice of no time-points sampled between 6hpi and 24 hpi.

Next I will explore results regarding the transcription factor binding sites present in the promoters of differentially regulated genes. I wanted to ask the general question of which TFs could be responsible for the expression changes we observe at different time-points. After assembling a database of 3kb *Medicago truncatula* promoters, and a database of known TF BS motifs, there were two approaches that I found interesting to explore, based on if the motifs we are looking for are previously unknown, or known. In the first case, I asked the question whether there is an unknown motif present in the sets of promoters of differentially regulated genes but relatively absent in random sets of promoters, using multiple approaches available from the MEME suite (Methods 8A). In the second, I assumed conservation of the TF binding motifs between *Arabidopsis thaliana* and *Medicago truncatula* and used the extensive databases that exist for *Arabidopsis thaliana* TFs provided by the MEME suite, as well as motifs characterized in the literature relevant to nodule development, to ask again if any TF BS is enriched in the set of the promoters of the genes we observe to be up-regulated or down-regulated at each time-point, compared to random sets of promoters (Methods 8B). To prepare all input files for analyses using the MEME suite, I used scripts written in Perl programming language, whereas for the automation of the multiple analyses required for all timepoints I used scripts written in Bash shell scripting language.

In the first approach, where I try to find unknown enriched motifs (Methods 8A), results were hard to interpret due to multiple TF BSs being similar to the enriched motifs found *de-*

novo. Older pipelines of the MEME suite I used were also prone to overfitting, as they could find significant results even in the negative control case of finding enriched motifs between two groups of randomly selected promoters. There were however some results that were statistically significant across all different methods, and I will discuss these here. I found a predicted enriched motif in the promoters of genes up-regulated at 4hpi that bares resemblance to the GCC-box BS of *Arabidopsis thaliana* Ethylene-Responsive element binding Factor 1 (ERF1)[306] (GCCGGCC motif of figure 3.6 B, enrichment test E-value 0.0018, similarity test p-value 0.003, also enriched in 12hpi up-regulated promoters, p-value<0.004). This motif could be the BS of ERN1[82]. I also found a very interesting palindromic motif (Figure 3.6 C) (p-value <0.05), enriched in other time-points as well, that I later discovered was already inferred by a similar bioinformatic study to be implicated in the mycorrhization process in *Medicago truncatula* (element Myc1)[307]. It has no known TFs binding to it. Across the intermediate time-points, MEME detected enrichment for long stretches of DNA consisting of A, T and C motifs that could be related to the activity of promiscuous TFs NF-Y[308] (CCAAT) and NSP1[54] (AATTT). At 16hpi up-regulated promoters, STREME was able to detect enrichment for a motif similar to the one *Arabidopsis thaliana* STYLISH1 (STY1) binds to (enrichment p-value 0.02, similarity p-value 0.04, motif presented in figure 3.6-D), which corroborates to the expression of the *STY* family at and after 16hpi we presented above, and the late role of STYs in nodule initiation. More *de-novo* motif results are available and will not be discussed here, and point to the amenability of our data set to upstream TF detection and GRN inference approaches.

The second approach I used was more straight-forward: I assembled a database of *Arabidopsis thaliana* TF BSs (JASPAR[279] and *Arabidopsis thaliana* PDB[309]), and combined it with motifs important for nodule development that I reverse-engineered from published motif logos: NSP1[54], NIN[60], PLT[281], NF-Y[308], AINTEGUMENTA (ANT)[310], PIN-formed Cytokinin Response Element (PCRE)[257] and all possible Auxin Response Elements, gaped (with all possible middle gaps from literature) or not[311]. I then assumed conservation of these motifs between *Arabidopsis thaliana* and *Medicago truncatula*, and tested for enrichment of these motifs in the different groups of differentially regulated gene promoters, compared to random sets of *Medicago truncatula* promoters. The results revealed which TF families might be responsible for the early transcriptional divergence of nodule symbiosis (Figure 3.6 A). The earliest detected TF BSs included those of WRKYs , which was interestingly in agreement with the expression of *WRKY* family members at the same time, described earlier in this chapter (Figure 3.5), and give more impetus to the idea of an early defence response at around 4hpi. This result also shows the internal consistency of the results of this approach to other results from our dataset. NSP1 BS was enriched throughout our

A	0hpi	2hpi	4hpi	8hpi	10hpi	12hpi	14hpi	16hpi	random
up	-	WRKY (-2) YAB NSP1 (-3)	ERFs (-2) NSP1 (-2)	NSP1 (-2)	WOX (-5) AHLs (-6) KAN1 YAB ERF NSP1 (-2)	WOX (-4) AHLs ERFs YAB KAN1 ARR1 NSP1 (-5) NFY (-2)	WOX13 (-9) AHLs NSP1 (-4) YAB KAN1 ARR2 ERFs NFY (-2)	ERFs(-17) NSP1 (-10) AuxREs (-7) ANT AHLs (-6) SPL NIN (-6) PLT (-2) ...	-
down	-	-	-	-	AHLs (-8) YAB ATHB NSP1	NAC	-	AHLs (-50) HD-ZIPs (-40) Zinc fingers (-26) PIFs TCPs AP3 NSP1 (-14) NIN (-5) AuxREs (-4) ANT ...	-

(corrected **p-value** order of magnitude in parentheses)

NSP1 Hirsh *et al*,2009
NIN Soyano *et al*,2013
PLT Santuari *et al*,2016
NFY Petroni *et al*,2012

ANT Nole Wilson *et al*,2000
PCRE Simaskova *et al*, 2015
JASPAR DB
ArabidopsisPDB

AuxRE from pDR5

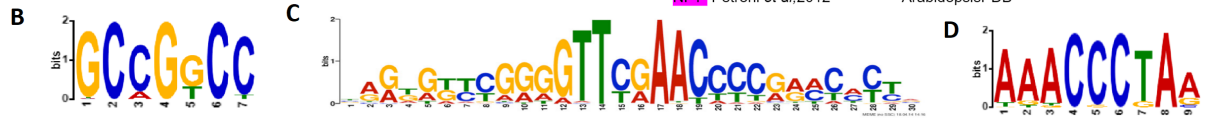

Figure 3.6: Enrichment for transcription factor binding sites in promoter sets of differentially regulated genes during nodule initiation**:** **A** Enrichment of known TF BSs in sets of promoters of up-regulated and down-regulated genes, compared to random sets. The number in parenthesis represents the exponent of the corresponding p-value (e.g. -8 denotes p-value < 1E-8). **B** Discovered motif enriched in 4hpi up-regulated promoters, similar to AtERF1 BS. **C** Palindromic motif discovered and enriched in multiple time-points. **D** Motif discovered/enriched in 16hpi up-regulated promoters, similar to the AtSTY1 BS motif.

time-points, which shows how this TF might be underlying a broad transcriptional facilitation during symbiosis[82]. The detection of BSs for NF-Ys at 12hpi and 14hpi coincides with the expression of both NF-YA1 and NF-YB16 subunits and corroborates to these TFs having an important role in this intermediary step of nodule initiation. WOX BSs are also detected at the same time-points, and more or less coincide with *WOX5* expression, and, in conjunction with ARR BS detection and expression give us the idea that around 12hpi we have totipotency and stem cell identity specification for a subset of cells. Finally at 16hpi I detect a plethora of TF BSs to be enriched, indicating that many different developmental programs are induced. Interestingly, both PLT and NIN BSs are only enriched in 16hpi promoters, which might indicate that these two TFs are regulatory hubs, not themselves involved in broad transcriptional regulation. Clearly more work is needed to connect detected motifs with active TFs of nodule initiation, however, motif enrichment gives us another valuable layer of information. It suggests independently that the order of events are an initial stress response, followed by reconfiguration of the transcriptional state, leading to a cytokinin response/stem cell identity state, driving an auxin response stage that coincides with broad transcriptional reprogramming.

I would like to also report a tangential discovery related to the regulation of NIN. I attempted to independently confirm from first principles the results of cytokinin element motif conservation in the *NIN* promoter, reported recently by Liu *et al*[72]. I instead unexpectedly discovered apparent conservation of auxin response elements. More specifically, I performed a small scale study where I aligned the full *NIN* promoter sequences of *Medicago truncatula*, *Lotus japonicus* and *Cicer arietinum* using the ProCoffee algorithm[312] of the T-Coffee software suite[313]. The settings used where the defaults for this approach, provided by the suite (only mode=procoffee for command flags). These three species where chosen due to the simple availability of full promoter sequence data (from previous gene end to transcriptional start site (TSS) of NIN) from the Phytozome database. The region that showed the highest detectable conservation, both in terms of size and similarity, by using this simple approach, was a 40bp region centered around 332bp upstream of the *Medicago truncatula NIN* transcriptional start site (Figure 3.7). This region happens to be detected for these species by Liu *et al*[72] as well (Figure 3 in their publication, the peak of conservation closest to the TSS), but its not the focus of their study. I then compared the *Medicago truncatula* conserved sequence with the binding sites present in my database of *Arabidopsis thaliana* TF BSs, presented in the previous paragraph. To this end I used the FIMO tool of the MEME suite, with default settings. The results indicated that, if the conserved region has a regulatory role, the most likely candidates for binding are transcription factors of the Zinc finger, Cys2His2-like fold (C2H2) type, of the INDETERMINATE-DOMAIN (IDD) family, since binding motifs of members of this family from *Arabidopsis thaliana* match to this region, e.g. IDD5 (AT2G02070,

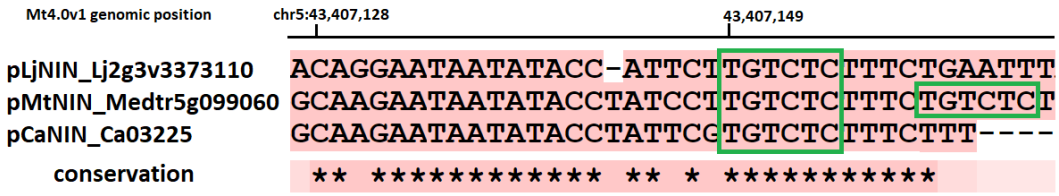

Figure 3.7: AuxREs in p*NIN*s: Small segment of the alignment of NIN promoters of *Lotus japonicus, Medicago truncatula* and *Cicer arietinum,* exhibiting high levels of sequence similarity. Highlighted are conserved putative auxin response elements that sit 334bp upstream of *MtNIN* transcription start site.

motif ID "C2H2_tnt.IDD5_colamp_a_m1", p-value=1.77e-06, q-value=0.00018), IDD11 (q-value=0.00015), IDD4 (q-value=0.0004) and others. These TFs are known to be involved in root development, acting together with SHORT-ROOT and SCARECROW [314]. Upon close inspection of the conserved sequence, in addition, I identified auxin responsive elements (AuxREs, TGTCTC sequence), as originaly defined by studies culminating in the creation of the first version of the *Direct-Repeat 5 (DR5*) auxin sensor[263, 315] (highlighted regions in Figure 3.7). This was not detected by the FIMO tool due to the AuxREs being short in size, leading to a low significance score. This result indicated possible regulation of NIN by auxin signaling, which was later demonstrated experimentaly in *Glycine max* by another group[89]. It invites further study on which TFs bind to this NIN promoter region during nodule initiation.

3.3 Discussion

In this chapter I described the results of what I believe is the best transcriptomics data set for nodule development to date. Due to the careful choice of time-points our team was able to identify key genes sufficient in driving nodule initiation[50], with many more lurking to be discovered. The main conclusions of this study is that up-regulation of auxin biosynthesis genes can be detected before auxin signaling, pointing to a previously unknown process by which the nodule initiates, which I will further elucidate in the next chapters. Supported by my bioinformatic analyses, as I presented above, our data set tells a story of an initial stress response, followed by reconfiguration of the transcriptional state, leading to a cytokinin response/stem cell identity state, driving an auxin response stage that coincides with broad transcriptional reprogramming. These results help us answer both when and how auxin accumulates in the *Medicago truncatula* nodule. Generation of and comparison to an identical data set in *Lotus japonicus* would help us delineate the commonalities in nodule initiation, and can be combined with phylogenomic methods recently developed to understand nodu-

lation in legumes through gene and promoter conservation ([11] and Jean Keller, personal communication). I also showed through identification of regulatory motifs that our data set is amenable to GRN inference systems biology approaches, and I invite more work to be done in this direction, analogous to studies in *Arabidopsis thaliana*[316]. This work might include clustering of genes by expression patterns, to better detect TF BSs responsible for regulation of each cluster, and connection of these binding sites with the *Medicago truncatula* homologs expressed. Complementary work by high-throughput TF-promoter binding inference between important promoters and active TFs can delineate the central part of the connectivity graph of the GRNN, as it was recently done for wounded root regeneration in *Arabidopsis thaliana*, where it was shown that PLT3 and LBDs were the most central regulatory hubs[275]. A first step towards this direction will be presented in the next chapter, where I use transactivation assays to understand which TFs regulate the YUCCA promoters.

One concern we have regarding our data set is the use of aminoethoxyvinylglycine (AVG), an ethylene biosynthesis inhibitor, in the growth medium, as previously stated. The *Medicago truncatula* ethylene insensitive *sickle1-1* mutant[237] which has a mutation in the ethylene signaling EIN2 gene, is a "supernodulator" under normal conditions, but does not make pseudonodules under PATI application[237]. This means that under AVG growth conditions the root might be unable to form a nodule using PAT changes, instead responding/compensating with up-regulation of auxin biosynthesis. Indeed, ethylene has a complex relationship with auxin biosynthesis and somatic embryogenesis, as there is evidence that down-regulation of ethylene biosynthesis in *Arabidopsis thaliana* is required for YUCCA expression[317]. This interaction must be resolved in future work. Another limitation is that, due to the sampling of the whole root segment, it is impossible for our data set to distinguish between epidermal and cortical responses, which we know from previous studies to differ markedly ([117] and [122] in comparison to our data set, also [318]). This limitation could be overcome by new methods of single cell transcriptomics of root cells[319] coupled to mapping and visualizing how the cells progress through the transcriptional cell-state space, using the measured differences in mature and immature RNA pools to identify the individual cell state eigenvector (from which transcriptional state, to which state, the cell is going)[320, 321]. This approach provides the exciting opportunity to identify transcriptionally the nodule tissue types, their fate-map and organization in actual and transcriptional state space, and possibly the concomitant changes in rhizobial differentiation.

Chapter 4

Experiments and models of auxin dynamics reveal how auxin biosynthesis could be responsible for nodule organogenesis

4.1 Introduction

In previous chapters I indicated the extensive volume of research on the interactions between auxin transport and indeterminate nodule development [18, 28, 67, 68, 112, 205, 206, 242, 271, 322], which lead these authors to the hypothesis that polar auxin transport (PAT) inhibition underpins nodule initiation[28, 206]. These earlier works consider the correlation between experimentally shown PAT perturbations and nodule development to imply causation from the first to the second. This causal hypothesis is supported by the ability of PAT inhibitors (PATIs) to induce pseudonodule development[18, 198, 236–240], and the ability of PATIs and flavonoids to rescue the *cre1* mutant[68]. This hypothesis finds theoretical support in a series of exemplary models of auxin transport by Deinum *et al*[33, 103–105] which have allowed us for the first time to conceptualize how auxin might accumulate in initiating nodules. In these models, three scenarios are first compared: symbiotic signaling either inhibiting the local magnitude of transport, increasing local auxin influx, or increasing local auxin biosynthesis[33, 103, 104]. These models indicate, assuming their assumptions are correct, that auxin transport inhibition is the most, and auxin biosynthesis is the least likely scenario for auxin accumulation, and the authors go on to describe how a diffusive signal of epidermal origin inhibiting local auxin transport can account for auxin maximum formation in nodule initiation[105]. This result is

heavily dependent, in my opinion, on the simplifying assumption by the authors that auxin transport polarity is unaffected by changes in auxin concentration. Changes in direction of transport, or feedbacks between a higher concentration of auxin to transport, are ignored. Our collective experimental results on auxin biosynthesis initiating nodule formation are, superficially at least, incompatible with these models and hypotheses on the role of auxin transport in nodule formation[18, 28, 33, 68, 103–105, 112, 119, 203, 205, 206, 322]. I wanted to resolve the apparent incompatibilities by understanding, first, why the earlier models[103–105] ranked the auxin biosynthesis hypothesis as the least likely. A careful examination of the models shows, and the authors indicate themselves, that in all of these models simulated local auxin biosynthesis in response to symbiotic signaling does not lead to auxin accumulation due to auxin transport keeping the local levels of auxin low[103]. In these models, the authors use the simplifying assumption that auxin transport magnitude and polarity is unaffected by changes in auxin levels. Both this result and this assumption have been put into question in earlier chapters. In chapter 2 I showed how local auxin application, as a proxy for auxin biosynthesis, can easily produce an auxin response (Figure 2.2 A, C) that takes at least 48 hours to reset back to normal (Figure 2.4, green line), presumably through PAT. In chapter 3 I showed how auxin biosynthesis upregulation precedes in time a bioinformatically detected auxin response that involves the majority of PAT components (*e.g.* *PIN*s and *PINOID*, Figure 3.2 B). As such I believe that perturbation of auxin transport as a response to increased auxin levels due to local auxin biosynthesis cannot be overlooked as an important mode of action of auxin biosynthesis on plant form. Thus I focused on the feedbacks between auxin levels and PAT, overlooked by a simplifying omission in previous studies[18, 28, 33, 68, 103–105, 112, 119, 203, 205, 206, 322], to explore alternative models of auxin and PAT dynamics during nodulation that could describe better what we observe in the real nodule primordium.

Interactions between local auxin levels/fluxes and PAT changes in plants is an active area of research, with many feedbacks proposed through the years (central publications in my opinion: [118, 157, 159, 233, 255, 261, 323–325]). Original work by Mitchison on how self-amplification of auxin flux can lead to vein formation[233, 253, 326] has been expanded to possibly include shoot meristem auxin maxima formation[159]. On the other hand, up-the-gradient, concentration-based models where PINs orient towards the neighboring cells with the highest auxin content can also explain SAM auxin maxima[118, 157]. Both feedbacks can be combined to explain shoot organ formation, where up-the-gradient effects on PAT repolarization can make the epidermal auxin maximum, and a flux based feedback in underlying tissues can make the vein connection[261]. Flux-based feedbacks could be implemented in plants by sensing intracellular auxin concentration at the plasma membrane[160, 323]. Competition for auxin binding and sensing at the extracellular side of the PM and feedback to PIN

orientation could also in principle recapitulate concerted PAT dynamics[162, 324, 327]. Extracellular auxin sensing and unidirectional flux counting have been combined in recent models that can reproduce all basic PAT patterning we observe *in planta[325].* Lastly, a model where plant cells have internal polarity as animal cells do, and auxin and PAT mediates tissue-level polarity coordination has been proposed[255]. All of these feedback models have high explanatory power in respect to how plants perform *de-novo* auxin patterning, but nearly all of them lack a thorough mechanistic mapping to actual molecular components that can affect PIN positioning in the ways they propose. Results addressing this knowledge gap are only recently emerging[328], and most likely involve multiple pathways affecting PIN polarity [220, 221, 329].

In this chapter first I will explore where and how YUCCAs are expressed in the developing nodule, and if indeed local auxin biosynthesis is capable of initiating lateral structures or not, by direct experiments. Then, for the purpose of studying how auxin biosynthesis might contribute to the observed PAT dynamics, I chose one of the dynamical PAT models presented in the introduction, the intracellular partitioning model for plant tissue cell polarity[255, 297], to ask the question, how would localized auxin production affect PAT during nodule initiation. This is the first step in using active-feedback PAT models to understand nodule development, which opens the possibility of the opposite route as well. This particular model was used by Abley *et al* to understand how spontaneous YUCCA expression in the abaxial epidermis of the leaves of the *kanadi1 kanadi2 Arabidopsis thaliana* mutant reorganizes the proximodistal PIN polarity field and gives rise, in concert with auxin importer expression, to auxin maxima driving formation of outgrowths[297], a situation which is analogous to what we observe in the nodule, both in terms of auxin biosynthesis (chapter 3, this chapter) and AUX/LAX expression[102]. The intracellular partitioning model, which in many regards behaves similarly to a with-the-flux model[159, 255, 297], describes a set of rules[255] in which auxin acts as a mediator molecule to align, in the tissue scale, each individual cell's partitions of cellular components. These rules give rise to the PAT field spontaneously organizing with a direction from auxin sources to sinks. We will use this model bellow to make predictions about PAT changes during nodule initiation.

4.2 Results

4.2.1 Auxin biosynthesis is sufficient for lateral organ induction

In the previous chapter we showed how early expression of *YUCCA* auxin biosynthesis genes in response to symbiotic signaling precedes in time an auxin signaling response. We wanted

to know in which root tissues this expression of *YUC* occurs, and what its effect might be to root organogenesis. To this end we first generated plasmids containing the β-*Glucuronidase* gene driven by *YUC2* and *YUC5* promoters (*pYUC2:GUS* and *pYUC5:GUS*, *YUC5* is named *YUC8* in our publication), then generated *Medicago truncatula* transgenic roots in which these plasmids were inserted using *Agrobacterium rhizogenes*-mediated hairy root transformation (Methods 3). This was a group effort with postdoctoral scientist, Jodi Lilley. We then infected the transgenic root systems with *Sinorhizobium melilotii* transformed with the β-*Galactosidase* (*LacZ*) gene, using flood inoculation (Methods 5). Successful infection events were detected by dual GUS-Magenta staining for the gene promoter and bacteria respectively (Methods 21). Resulting stained nodule primordia were visualized with multiple microscopy techniques (Methods 19). For both *pYUC2* and *pYUC5* promoters we found identical activation at the vascular-pericycle tissues proximal to the successful early infection event. Interestingly, the expression domain stayed at the base of the developing nodule, with expansion into the nodule vasculature in mature nodules (Figure 4.1, first column, adopted from our publication[50]). This expression pattern suggests a specific role of auxin biosynthesis in nodule organogenesis and not rhizobium infection.

Next we wanted to know if auxin biosynthesis is sufficient for lateral organ development. We designed DNA constructs for hairy root transformation where the *YUC2* coding sequence was under the regulation of a dexamethasone (DEX) inducible system[330]. When transgenic roots were grown, having no apparent initial phenotype, and then transfered to DEX containing medium, we observed lateral organs growing from many positions of the transgenic roots at the same time (Figure 4.1, second column). Microscopic observation of these root outgrowths revealed short, "stubby" lateral-root-like structures that grow recursively from mature, differentiated tissue (Figure 4.1, third column). These results show conclusively that, in *Medicago truncatula,* auxin biosynthesis upregulation is sufficient for lateral organ induction.

The global effect of our DEX induction protocol does not help in understanding if local *YUC* expression is sufficient for local lateral organ induction. To test if it would be possible to induce locally gene expression by local application of DEX, I placed DEX-infused paper clippings on root systems transformed for DEX-inducible GFP expression. The results showed that, in agreement with previous studies[330], DEX induction could not be locally restricted, as subsequent microscopical observation showed, the whole root system concurrently becoming homogeneously fluorescent. In order to make a locally inducible system in *Medicago truncatula* hairy roots, I designed and used DNA constructs based on the β-estradiol inducible system[331], which in principle could restrict gene expression at the desired part of the root where β-estradiol is applied, and the desired tissue type, through tissue-specific promoters. These studies were not concluded, but showed great promise, which in the future could help

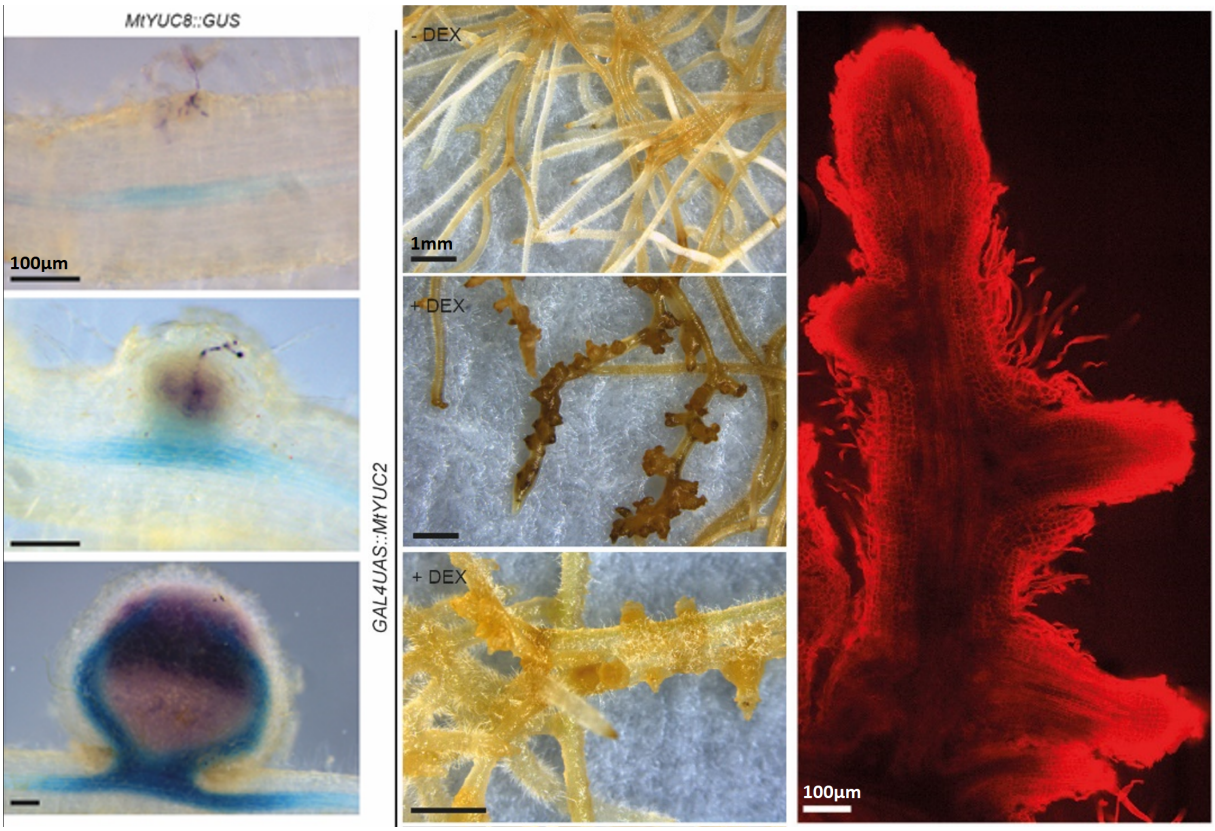

Figure 4.1: YUCCA enzymes are expressed in the nodule and are sufficient to induce lateral structures: **First column:** *pYUC8:GUS* staining (blue) in transgenic roots inoculated with *Sinorhizobium melilotii LacZ* bacteria (stained purple). **Second column:** DEX induction of *YUC2* gene in transgenic roots produces lateral organs. **Third column:** Confocal microscopy of a lateral organ produced, stained with propidium iodine. Image by Katarina Schiessl. Images adopted from our common publication, produced by a group effort[50]. Scale bars represent 100 µm in first and third column, 1mm in second column of pictures.

test gene expression effects on different positions of the susceptibility zone.

In the previous chapter we uncovered a potential overlap, during nodule organogenesis, of cytokinin signaling with auxin biosynthesis, with the latter, as we showed above, being able to induce de-novo organ formation. This coupling could be mediated by NIN, as we have seen in the general introduction. In a parallel study we asked the general question, how interaction between the two hormones could lead to tissue patterning (together with Sean Jones, all information can be found in his master thesis). More specifically, we were interested how transcriptional regulation of enzymes involved in auxin and cytokinin production and degradation, by auxin and cytokinin signaling, could lead to tissue patterning, by constructing the full set of Golden Gate modules that encode for *HormonalSignalingPromoter:EnzymeCodingRegion* scheme (example interaction using these modules in Figure 4.2 E). For hormonal signaling promoters we used *pDR5* (auxin activated) and *pTCS* (cytokinin activated), whereas for enzyme coding genes we used a set of *IPT*s, *LOG*s, *CYP735A* and *CKX*s, and *YUC*s, *TAA*s and *GH3*s (Methods 22). The modules generated included fusions of any of these promoters to any of these genes. First we validated the ability of these enzymes to perturb the auxin-cytokinin balance. To do so we expressed them individually, accompanied in the same Golden Gate DNA construct by auxin-cytokinin reporter modules (nuclear localized eGFP and mCherry fluorescent proteins driven by *pDR5* and *pTCS* respectively) and a constitutively expressed nuclear localised CFP (mTurquoise2), in transfected *Nicotiana benthamiana* leaves. We then generated confocal images of the transfected regions, identified the nuclei based on CFP fluorescence, and measured, per nucleus, the ratio of eGFP to mCherry fluorescence in the region of the nucleus, as a proxy for the signaling balance between the two hormones (Sean Jones, Master Thesis entitled "Investigating Reaction-Diffusion Patterns of Auxin and Cytokinin in Nicotiana leaves", also Figure 4.2 A,B). For this we used the FIJI image processing application. We then compared the values obtained to the same measurements from control constructs bearing only the reporter modules. The validation step indicated that expression of these enzymes in *Nicotiana benthamiana* leaves was enough to shift the balance between the signaling activation of the two hormonal pathways in the direction expected (Figure 4.2 B). This was especially true in the case of expressing the MtYUC2 used in above studies involving DEX (Figure 4.2 B, *pNos:YUC*). We then arranged the interactions between the two hormones to represent the self- and hetero-interactions between an activator and an inhibitor in reaction diffusion systems[332, 333] (example Figure 4.2 E). We tested the ability of these constructs to create spatial patterns of hormone activation by transfection of *Nicotiana benthamiana* leaves, compared to control constructs that code only for auxin and cytokinin reporters, by analysing the spatial arrangement of hormonal signaling ratios of Tobacco leaf cells. The full array of DNA constructs made for this purpose can be found in Methods 22. Although the results

of this approach are interesting and inconclusive as of yet, they are beyond the scope of this section, and can be found in the Master thesis of my student, Sean Jones. I used the same library of DNA constructs, however, to make *Medicago truncatula* transgenic roots. This was done to test if any of the set of interactions we encoded for had a morphogenic ability in the root. Interestingly, two constructs, both encoding solely for *pTCS:YUC* in conjunction with reporter modules, developed roots with aberrant lateral structures proximal to the RM (Figure 4.2 C,D, EC19245 in Methods 22). The zone where these ectopic lateral cell proliferations grew was just beyond the differentiation zone of the RM, where cytokinin signaling is known to be active[190]. This result is a further evidence that, in *Medicago truncatula*, coupling cytokinin signaling to auxin biosynthesis is sufficient to induce cortical cell proliferation, and suggests that NIN acts as a conditional coupler between the two. This result was replicated for the construct EC19245, which was able to produce a small number of these structures (Figure 4.2 C,D), compared to a control construct expressing only reporter modules (EC19241) that did not produce any structure of this type, as expected. I have never observed a lateral outgrowth so close to the root meristem in *Medicago truncatula* normal roots.

4.2.2 Towards characterising the GRNN upstream of *YUCCA* expression

In order to understand how *YUCCA* upregulation comes about in such an early stage of nodule initiation, I used a transactivation assay protocol described previously[334], refined by our lab member Nadia Radzman and implemented in Golden Gate cloning (Methods 16), to understand which transcription factors (TFs) regulate *YUC* promoters. The approach is based on differential expression of two different Luciferases, one under regulation of a constitutive promoter, and one under the promoter of choice. We also expressed the TF of choice from the same DNA construct, fused to GFP (more specifically the enhanced GFP called Venus) (Figure 4.3, example DNA construct in the middle) to see if it will affect the activation of the promoter of choice relative to that of the constitutive promoter. For comparison, we made corresponding Golden Gate DNA constructs without the transcription factor, instead just GFP (Venus) in its place, as our negative control (Figure 4.3 B). We then transform *Nicotiana benthamiana* leaves using Agro-infiltration with *Agrobacterium tumefaciens* carrying these plasmids. We verify TF nuclear localization using confocal microscopy and then collect material to test for differential luminescence between the two Luciferases using a luminometer. I designed in a combinatorial fashion, using Golden Gate, DNA constructs to test all possible transactivation interactions between the NIN, LBD16, PLT3 TFs, and *pYUC3*, *pYUC2*, *pYUC5* (*YUC8* in previous chapter), *pLBD16*, *pNFYA8*, *pPLT3* and *pIAA9* promoters. I also designed constructs coexpressing PLT3 and NIN, to test for differences between individual and combined activity of these TFs. Not all constructs were successful, however, and many

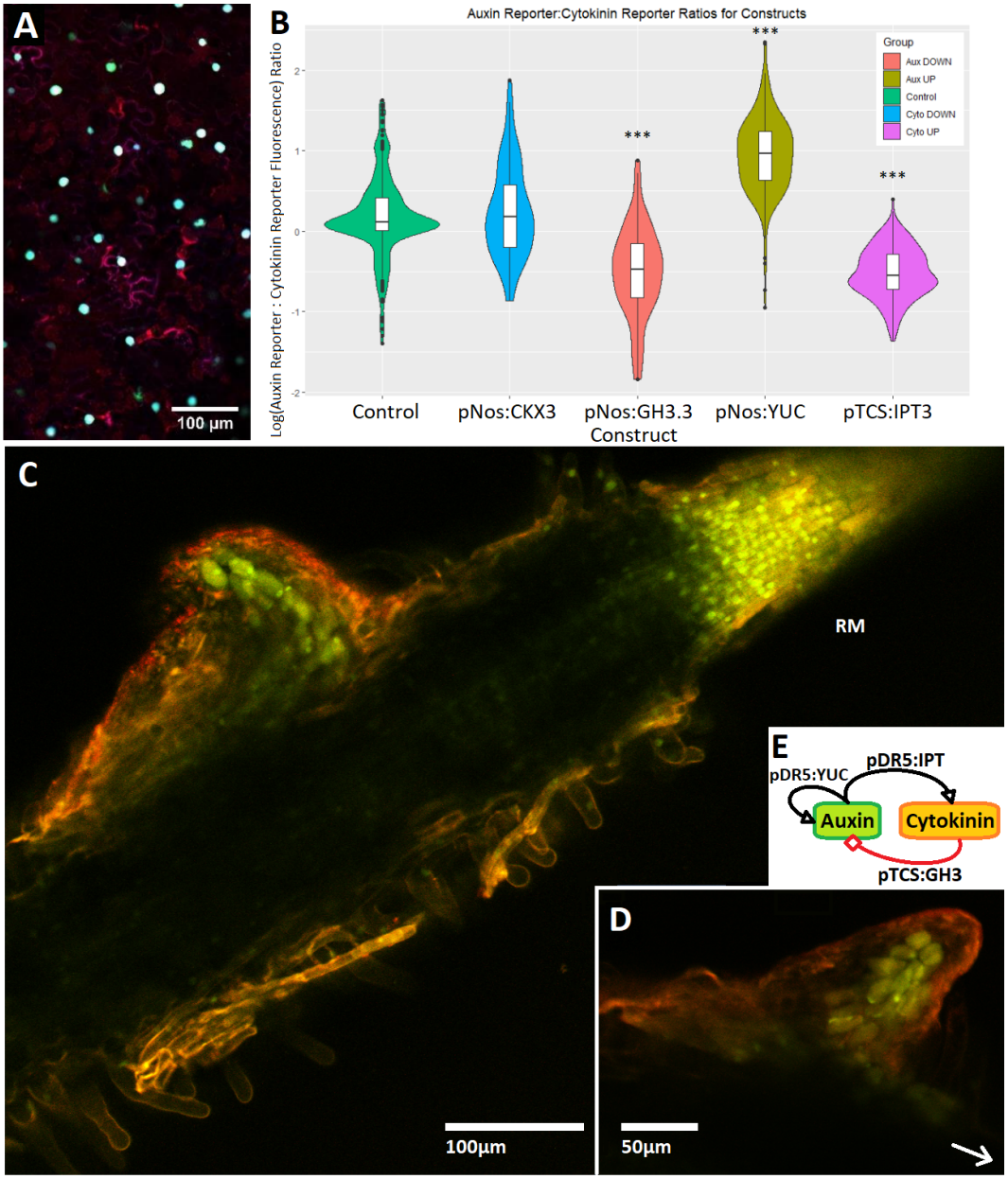

Figure 4.2: Cytokinin induction of YUCCA gives lateral organ: **A** Confocal microscopy picture of Tobacco leaf transformed with EC19258_S53_pL2B_pDR5:NLS-eGFP_pTCS:NLS-mCherry_pNos:mTurq2-NLS2_p35s:P19_pTCS:LjIPT3 DNA construct, composite of all fluorescent channels. The nuclear localized CFP (mTurquoise2-NLS2) serves to identify and isolate individual nuclear regions, using the FIJI image processing software, in order to then quantify the fluorescence of eGFP and mCherry, and calculate, per nucleus, the fluorescence ratio, a proxy of the relative activity of auxin and cytokinin signaling pathways. **B** Violin Plot of the logarithmic ratios between eGFP and mCherry channel fluorescence intensity, measured for a population of nuclei in the aforementioned confocal microscopy pictures, for DNA constructs that contain the different enzyme modules (x-axis). Each violin-box plot contains pooled data for 3 biological replicates, consisting of, on average, 24 analyzed nuclei. The stars denote statistically significant difference to the control (Tukey HSD, *** = p-value < 0.001). The plot was made by Sean Jones and the data come from our collaborative work. **C** Confocal microscopy picture of transgenic root meristem expressing EC19245_pDR5:NLS-eGFP_pTCS:NLS-mCherry_**pTCS:YUC**, with non-canonical lateral structure emerging proximal to the RM. **D** Another instance of a lateral structure, proximal to the RM, in a different transgenic root system. Arrow denotes the direction to the root meristem (RM). **E** Example engineered interaction network between auxin and cytokinin, resembling by design the Activator-Inhibitor Reaction Diffusion model of Gierer-Meinhardt[333].

failed in different stages of development. Successful constructs and their corresponding controls can be found in Methods 22. I report here the results which have passed all quality tests and I have sufficient data and statistical power for. Both NIN and PLT3, fused to Venus GFP, when expressed in *N. benthamiana* leaves, showed nuclear localization, as expected (Figure 4.3 A,C), which was markedly different localization than when GFP was expressed alone, in our negative control case (Figure 4.3 B). When PLT3-Venus was expressed, I observed a downregulation of the p*YUC3* promoter, as well as downregulation of the p*YUC5* promoter (Figure 4.3 D,F), compared to the control case where only Venus was expressed, as measured by differential luminosity of the two Luciferases. *YUC3* (Medtr1g046230) was identified in the previous chapter as a third *YUC* expressed in later stages of nodule development. This effect of PLT3 on pYUCs was surprising, given that PLTs are known to have a positive role on YUC expression in the *Arabidopsis thaliana* RM[99, 281]. On the other hand, I found that expression of NIN-Venus has no significant effect on the expression levels of p*YUC2* and p*YUC5*, but it activates the *LBD16* promoter (Figure 4.3 E-G). The results are summarized in figure 4.3H, and suggest that, individually, neither PLT3 nor NIN are responsible for the early upregulation of *YUC*s during nodule initiation, which I described in the previous chapter. Both these transcription factors though were successful in altering Luciferase gene expression levels in our transactivation experiment.

4.2.3 A model of auxin transport during nodule initiation

For the purpose of this study, I chose one of the dynamical PAT models presented in the introduction, the intracellular partitioning model for plant tissue cell polarity[255, 297], to ask the question, how would localized auxin production affect PAT during nodule initiation. With the help of Katie Abley, I set up a 2-dimensional simulation aiming to represent the longitudinal section of the part in the susceptibility zone where a nodule appears, spanning from the center axis of the root to the epidermis, for a length of 12 cells. The simulation domain is similar to the ones previously used[103–105], and was chosen to be this way for ease of comparison with models published previously. There is one difference however, previous studies have considered a full longitudinal section, from epidermis to epidermis, whereas here I consider only half a section, from epidermis to the center root axis. This choice was made to facilitate the emergence of a "reflux loop" polarity field[158], resembling what we know for PAT in this region, from initial boundary conditions of auxin flow. The starting setup for the simulation (mathematical rules, parameter setup, and algorithmic implementation) of the PAT field is identical to the setup used for the indirect coupling model of figure 9D of Abley *et al,* 2016[297] (article supplementary source code 12, see Methods 17). I then included auxin sources and sinks at the boundary of my simulation domain, to represent how auxin enters

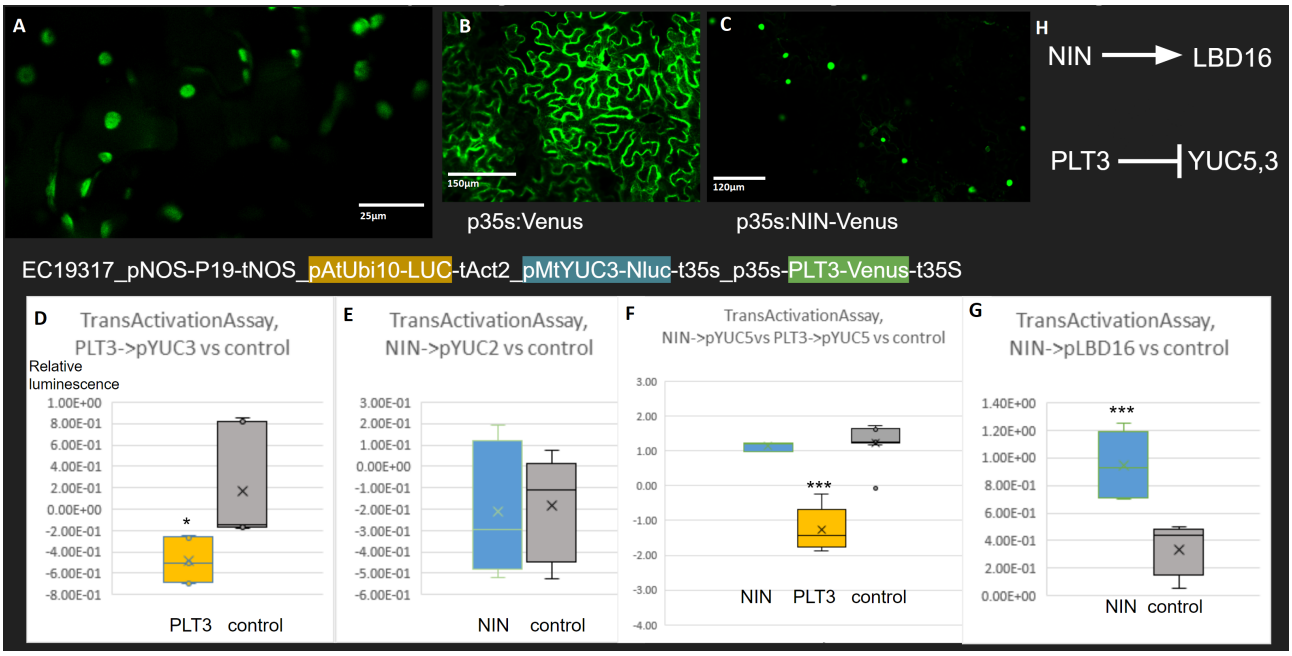

Figure 4.3: Transactivation Assay reveals regulatory interactions between NIN, PLT and *YUC*: **A** Confocal microscopy picture of *Nicotiana benthamiana* leaf transformed with the EC19317 construct containing PLT3-Venus fusion protein, confirming its nuclear localization. The full construct, indicated bellow the picture, is designed for testing for transactivation of the promoter by the TF, by comparing the relative fluorescence between constitutively expressed Luciferase (LUC) and NanoLuc Luciferase (Nluc) expressed by the promoter in question. **B** Picture of negative control construct containing only Venus. **C** Picture of NIN-Venus, also showing nuclear localization. **D-G** Transactivation assay results for the action of PLT3 (yellow) and NIN (blue) TFs on the promoters of *YUC3, YUC2, YUC5* and *LBD16*, compared to control (gray). The plots are relative luminescence values for the two Luciferases, with 3 biological replicates and 3 technical replicates per condition. Stars denote significant difference of relative luminescence compared to control, according to Student's t-test. (*=p-value<0.05, ***=p-value<0.0001) **H** Summary of results in the form of regulatory interaction graph.

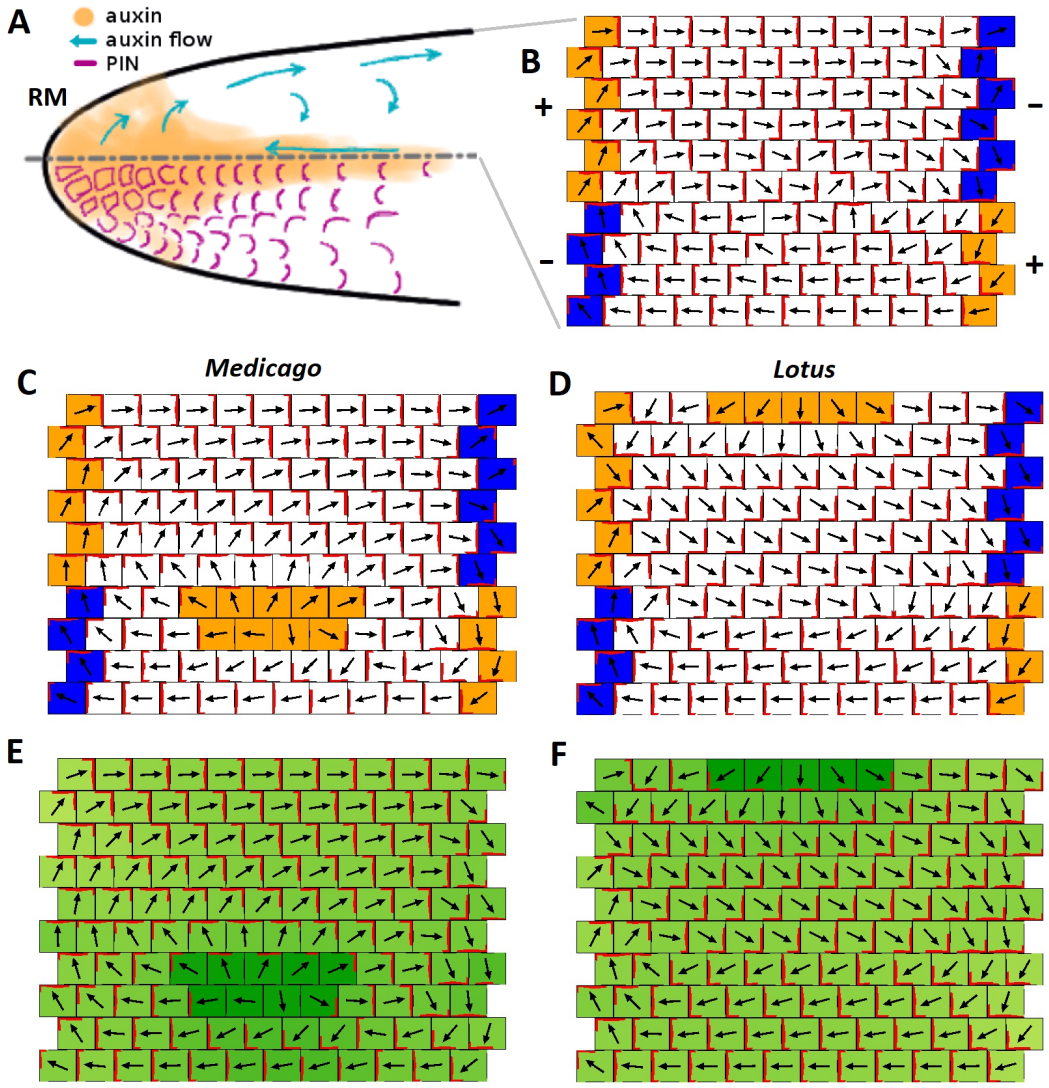

Figure 4.4: Intracellular partitioning model and nodule initiation**:** **A** Schematic of root meristem auxin concentration and flow (upper part), and PIN orientation(lower part). **B** 2D stable simulation result of the cortical and vascular flow of a susceptibility zone root segment. The result resembles the expected auxin transport through the region. In orange we have auxin sources (influx of auxin from outside the simulation domain). In blue we have auxin sinks (outflux). In red we have PIN localization. The arrow denotes cell polarity in terms of intracellular partitioning and auxin transport[297]. **C** Simulation result after introducing local auxin biosynthesis (orange cells) in and around pericycle cells, as in the case of *Medicago truncatula* nodule initiation. Note the disruption of vascular auxin flow. **D** Same situation as in C, but here we have the introduction of auxin biosynthesis in the epidermis, as in the case of *Lotus japonicus* nodule initiation. **E-F** Auxin concentration profiles for C and D, respectively. Green intensity denotes auxin concentration.

and leaves the simulated root segment, with a rootward direction in the vasculature, but with a shootward direction in the cortex. I then simulated the model dynamics to recreate a stable local reflux loop configuration (Figure 4.4 B). The next step was to ask what happens to auxin concentration and auxin flux in this simulated environment, if I introduce auxin biosynthesis, either at the pericycle cells, similarly to indeterminate nodule initiation, or at the epidermis, similarly to determinate nodule initiation[34, 113, 241]. Introducing auxin biosynthesis in these different positions had a similar effect in the auxin profile, in that cells producing auxin could retain a higher auxin concentration, as expected (Figure 4.4 E-F). The effect on the repolarization of the intracellular partitioning and PAT field, however, was very different for the two cases (Figure 4.4 C-D). Auxin production in the pericycle cells led to disruption of the auxin flow through the vasculature, with many vascular cells shootwards of the activated ones changing completely polarity orientation and countering the normal flow (Figure 4.4 C). This indicates that initiation of indeterminate nodules in deeper tissues could be the cause for the acropetal auxin flow disruption previously shown experimentally to occur 24 hours post inoculation and later [18, 67, 68, 112, 205, 234, 242]. If auxin production appears in the epidermis, however, there was no effect on vascular auxin flow (Figure 4.4 D), also in agreement with experimental studies in determinate nodulators[113, 121, 242]. Videos for the two simulation cases can be found here and here.

One interesting prediction this model makes is the difference in polarity orientation in the mid- and inner-cortex layers. In the case of the indeterminate nodule these layers are pointing outwards towards the epidermis, whereas in the determinate nodule they point inwards towards the vasculature. This prediction can be tested experimentally by timecourse microscopy of polar cell components. A notable candidate for this type of study is BASL, a polarity regulator of the asymmetric divisions of *Arabidopsis thaliana* stomatal-lineage cells[335]. Ectopic expression of this protein in root cells marks the basal side of the cell. Continuous ectopic expression however affects cell growth and can hinder natural progression of root maturation ([335], personal communication with the authors). PINs and ROPs are also candidates. Recently, a new family of polar proteins was characterized, the SOSEKIs[336], who resemble animal Dishevelled polarity regulators, which reveal an apical-basal polarity field existing in plants, independent or upstream of PIN orientation. During LR induction, SOSEKIs (SOKs) are expressed early and mark the first periclinal divisions and polarity changes associated with the new LR[336]. I investigated the timeline of gene expression of the *Medicago truncatula SOSEKI* family in nodulation and was surprised to find one *MtSOK* (Medtr1g115370) being expressed early, from 12hpi onwards (Figure 3.5, end). Two more *SOKs* (Medtr2g062310 highly expressed, Medtr4g063130), were expressed 24hpi onwards. DNA constructs for fluorescent tagging for these SOKs have been already designed and synthesized, and can be

provided to test, in *Medicago truncatula* and *Lotus japonicus* transgenic roots, the hypothesis of opposite polarity orientation of the inner cortex during nodule development of the two nodule types.

4.3 Discussion

In this chapter we provided evidence of auxin biosynthesis being sufficient to induce lateral organ organogenesis in *Medicago truncatula* roots. Moreover, we showed that cytokinin signaling, when coupled in such a way as to freely induce auxin biosynthesis, is able to induce organogenesis of root lateral structures in the differentiation zone of the *Medicago truncatula* root meristem. I then investigated upstream regulation of *YUCCA* auxin biosynthesis genes active during nodule initiation, using a transactivation methodology that can be easily expanded to include all known transcription factors that are active during this process. The way by which auxin biosynthesis genes are induced early in *Medicago truncatula* nodules, however, is still elusive. The hypothesis of auxin biosynthesis supporting the initiation of all legume nodule types is the simplest when we consider nodule evolution. It suggests auxin biosynthesis was at the center of nodule development throughout evolutionary history, but it has different effects on PAT (Figure 4.5). In the case of the indeterminate nodule, auxin biosynthesis is capable of initiating cell division, but it also affects vascular auxin flow, an effect that must have a positive feedback on auxin levels and nodule induction. It remains to be seen if this feedback is needed for natural initiation, regardless if artificial initiation through PAT inhibition is possible for this nodule type[18, 198, 236–240], perhaps due to the cells capable of transitioning to nodule identity residing in an area of high auxin flux and being auxin sensitive. In the case of the determinate nodule, on the other hand, local auxin biosynthesis is sufficient for nodule induction, and does not involve/need/affect auxin transport perturbation (Summary Figure 4.5). The alternative hypothesis of nodule initiation through polar auxin transport reduction[28, 206] implies more steps in the changes required for the evolution of the two nodule types, since there is evidence that determinate nodules do not employ this method to initiate[113, 121, 242]. The conceptual framework used to compare the two hypotheses is enriched by our model, which can act as a first step in a modeling study of different proposed PAT feedbacks predicting the local polarity changes during the naturally inducible symbiosis initiation, and comparing the results with experiments involving SOSEKI proteins (see section above). Our model is by no means close to the reality of nodule initiation, it merely provides an alternative view to the ones previously proposed[33, 103–105, 206]. For the purpose of comparing the different models, I have set-up, in consultation with Henrik Jonsson, Ross Carter and Nadia Radzman, graph models of longitudinal and transversal sections of the *Medicago truncatula* suscepti-

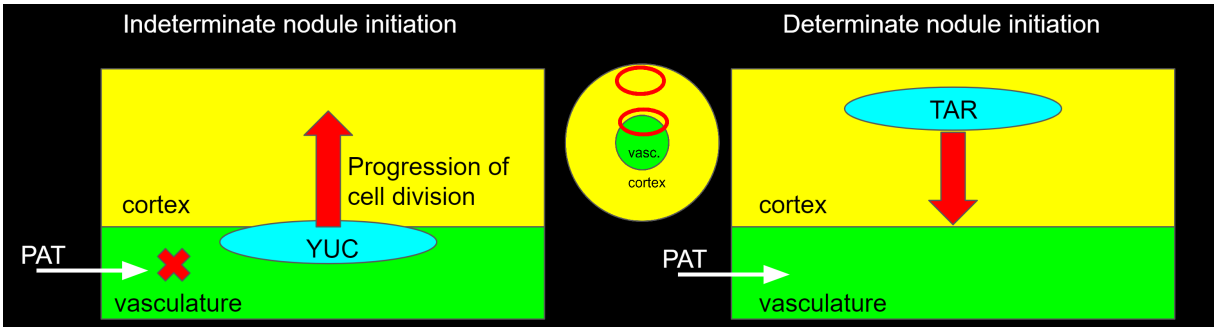

Figure 4.5: Model of auxin biosynthesis and formation of different nodule types: Simple summary model schematic depicting the differences in how auxin biosynthesis might be implicated in nodule initiation between indeterminate - determinate nodule types. 2-D longitudinal half-section of the root segment under nodule initiation. Auxin biosynthesis by YUCCA enzymes and subsequent changes might affect auxin transport through the vasculature during the development of the indeterminate nodule (left). In contrast, during determinate nodule development activity of TAR enzymes initiates the nodule but does not affect vascular (acropetal) auxin transport(right). The central diagram (transversal section of the root) depicts how nodule initiation in different positions can have different effects on PAT purely due to geometric considerations (area of effect) and proximity to the vasculature, where PAT is high. If nodule primordia of both types have the same footprint in the transversal section of the root, the footprint can be much smaller when compared to the area of the cortex than when compared to the area of the vasculature. As such, their respective effects on auxin flow can be of drastically different scale.

bility zone, with realistic cell dimensions, that can be implemented in the Organism-Tissue Simulator software package[337, 338]. They are available on request for future studies.

Chapter 5

Auxin biosynthesis inhibition suppresses nodule development

5.1 Introduction

In the previous chapters I described how auxin biosynthesis is upregulated early during nodule development, and how artificial induction of auxin biosynthesis readily gives rise to lateral root structures. In this chapter I will investigate how much auxin biosynthesis contributes to indeterminate nodule development by inhibiting its activity using multiple approaches. While perturbation of root auxin transport using polar auxin transport inhibitors has been studied extensively in relation to nodule initiation[68, 198, 237–240], the effect of perturbing auxin biosynthesis, using auxin biosynthesis inhibitors, has been scantly and only recently studied[339]. Due to the central part of auxin biosynthesis in plant development, any experiment that focuses on the activity of YUCCA auxin biosynthesis enzymes during nodule initiation ideally would be designed to perturb the activity only locally. With this in mind I first designed experiments using Yucasin[340], a potent competitive inhibitor of the enzymatic conversion of indole-3–pyruvic acid (IPyA) to IAA by YUC. The aim was to use Yucasin co-applied with rhizobium spot inoculation to test for effects on nodule initiation rates. This experiment was not possible due to Yucasin affecting the growth of the bacteria at the concentration required, as tested by overnight growth levels in the presence of different Yucasin concentrations (Methods 11). I circumvented this problem using 2 approaches. Firstly, I enlarged the set of YUCCA inhibitors with the use of Yucasin difluorinated analog (YucDF, 5-[2,6-difluorophenyl]-2,4-dihydro-[1,2,4]-triazole-3-thione), a more potent and stable Yucasin analog[341], as well as 4-phenoxyphenylboronic acid (PPBo) and 4-biphenylboronic acid (BBo), all potent YUCCA inhibitors[342]. I tested the effect of these inhibitors on rhizobial growth and found no de-

tectable - significant inhibition in the respective concentrations used therein (Methods 11). Secondly, I aimed to circumvent the use of rhizobia all-together, by local induction of nodule development using Nod-factors. Earlier observations on the *DR5* auxin signaling reporter line showed that in *Medicago truncatula* an epidermal auxin response can be observed in response to Nod-factor local application (chapter 2), but a cortical response is rare, and nodule development has never occurred, to my knowledge, in any lab. In *Medicago sativa* (alfalfa), however, Nod-factors are known to induce nodule organogenesis, as this is how Nod-factors were conclusively shown to be the primary and sufficient symbiotic signal[145], an event occurring possibly due to autotetraploidy affecting the gene regulatory network of nodulation of this species[343]. Thus for our purposes I developed a Nod-factor spot-treatment protocol for efficient local nodule induction on *Medicago sativa* seedling roots (Figure 5.2 B, Methods 15). I used this protocol to assess the role of auxin biosynthesis inhibition in nodule initiation in rhizobia-free conditions. Lastly, I generated a knockout *yucca2-yucca8* double mutant and investigated the effects of these mutations on nodulation.

5.2 Results

5.2.1 YUCCA inhibitors affect nodule initiation

I will first discuss what happens to *Medicago* nodulation capability if I apply YUCCA auxin biosynthesis inhibitors in the root growth medium. I grew *Medicago truncatula* (Jester ecotype) seedlings on nitrogen-depleted agar medium containing aminoethoxyvinylglycine (AVG) (as per spot inoculation protocol, Methods 4) with or without YucDF, PPBo or BBo, in concentrations that do not affect bacterial growth but had small phenotypic effects on root growth, as expected (see Methods 11, 12). When each seedling root was spot inoculated (droplet treatment containing *S.meliloti*), spot inoculation rates of roots grown on YUCCA-inhibitor containing mediums was significantly lower compared to seedlings grown on normal spot inoculation medium (Fisher exact test, as well as Chi-square test with correction, on inoculation rates, Figure 5.1). The experiment was performed 4 times with significant results similar to the ones presented. Interestingly, in one experiment I included a group of treatments with the polar auxin transport inhibitor 2,3,5-triiodobenzoic acid (TIBA, in concentrations 400nM, 1μM or 10μM) to compare its effects with YUCCA inhibitors. Results showed that addition of TIBA in the agar growth medium also statistically significantly and efficiently suppresses spot inoculation rates compared to control (3 nodules per 30 seedlings in TIBA 400nM treatment, 5n./78s. in TIBA 1μM, 0n./30s. in TIBA 10μM, all compared to control 56n./66s.) This result stands in apparent contrast to the pseudonodule-inducing capability of TIBA (chapter 2). In

all main experiments, when nodule initiation was suppressed by application of YUCCA inhibitors in the growth medium, unexpectedly, I observed the emergence of lateral roots (LRs) instead of nodules from the spot inoculation position, in low frequencies (Figure 5.1, in green). I investigated if this was due to nodules reverting to LR fate under YUCCA inhibition by performing the negative control experiment of spot inoculation just with bacterial growth medium without rhizobia (Figure 5.1, left side of the bar plot). This experiment showed that, under these conditions, the roots respond with a low frequency to water spot inoculation by creating a local lateral root, an effect known as hydropatterning[344]. This residual effect is masked by symbiotic signaling in the normal inoculation case. Interestingly, I attempted to rescue the nodule inhibition by YUCCA inhibitors by co-application of 2,4-dichlorophenoxyacetic acid 7μM (2,4D, stable synthetic auxin analog), or other auxin analogs (IAA 200nM or 2μM or 20μM, NAA 2μM), to the inoculation medium. This led to drastic local increases of LR organogenesis but not to nodule initiation rescue (Figure 5.1, right side).

A similar and complementing line of experiments I next performed tested the effect of YUCCA inhibitors on the induction of *Medicago sativa* (alfalfa) nodules using local root application of Nod-factors. Alfalfa seedlings were grown on normal spot inoculation medium or medium containing YUCCA inhibitors, then spot treated with Nod factors, which were able to induce bacteria-free nodules at the site of spot application. Inclusion of YUCCA inhibitors in the growth medium significantly reduced the nodule induction efficiency during spot-treatment of *Medicago sativa* seedlings with 10 μM Nod-factor mix, compared the nodulation efficiency during spot treatment of seedlings grown on normal medium (Chi-square test with Marascuilo correction, Figure 5.2, Methods 15). The experiment was validated by a repeat experiment, however a third experiment did not produce significant results, but had the same trend. In higher YucDF and BBo concentrations of YUCCA inhibitor application I observed a concomitant retardation of transition to mature nodules, with only root hair extension and pre-stage VI (unemerged) nodule development (stages of nodule development defined by Xiao *et al*[33]) (Figure 5.2 A). These results help to rule out the possibility that inhibition of nodule formation by YUCCA inhibitors, observed in earlier experiments on *Medicago truncatula* seedlings, is caused by possible off-target effects of YUCCA inhibitors on rhizobial growth and infectivity.

5.2.2 Local application of YUCCA inhibitors

Regarding the experimental results described in the previous section does not help us rule out the following hypothesis: Auxin is transported to the nodule initiation location from reservoirs in different parts of the root, and YUCCA inhibitors deplete these reservoirs, suppressing nodulation. Local application of YUCCA inhibitors would help us rule out the possibility that

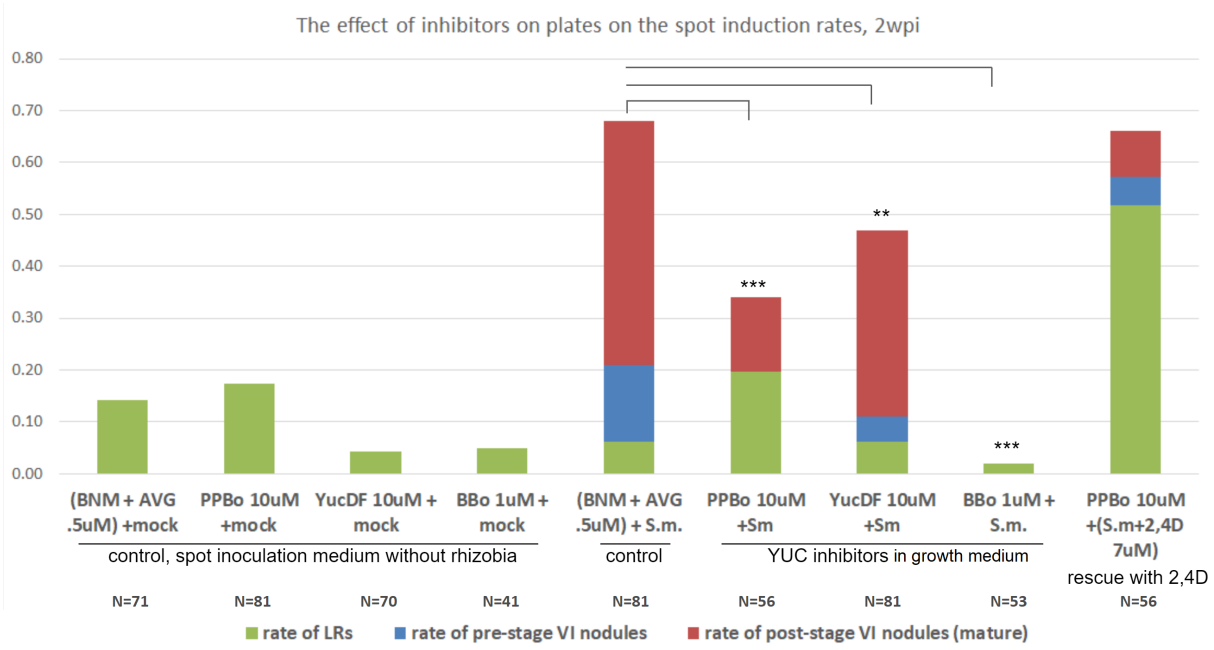

Figure 5.1: Effect of auxin biosynthesis inhibition in spot inoculation: Rates of immature (in blue), mature (emerged, in red)[33] nodules and lateral roots (in green) appearing on roots of *Medicago truncatula* seedlings grown on BNM+AVG media containing different YUCCA inhibitors, 2 weeks post spot inoculation of *Sinorhizobium meliloti* or mock spot treatment. The treatment categories and number of replicates per treatment are as follows: Mock spot inoculation treatment (absence of any rhizobia from inoculum) of seedlings grown on standard Buffer Nodulation Medium (BNM) agar plates with the addition of aminoethoxyvinylglycine (AVG) 0.5μM (our normal growth medium, N=71). Mock spot inoculation of seedlings grown on BNM+AVG normal growth medium with the addition of 4-phenoxyphenylboronic acid (PPBo) 10μM on the medium (N=81), or YucasinDF (YucDF) 10μM (N=70), or 4-biphenylboronic acid (BBo) 1μM (N=41). Spot inoculation of *Sinorhizobium meliloti* (S.m.) on seedlings grown on normal BNM+AVG agar medium (N=81), or normal medium with the addition of PPBo 10μM (N=56), or YucDF 10μM (N=81), or BBo 1μM (N=53). In the last category seedlings grown on normal medium with the addition of PPBo 10μM are spot inoculated with standard S.m. inoculation solution where 2,4-dichlorophenoxyacetic acid (2,4D) synthetic auxin has been added to a final concentration of 7μM (N=56). Stars denote significant difference in nodulation rates between the two categories as measured by one-tailed Fisher exact test, with two stars representing a p-value less than 0.001 and three stars a p-value less than 0.0001.

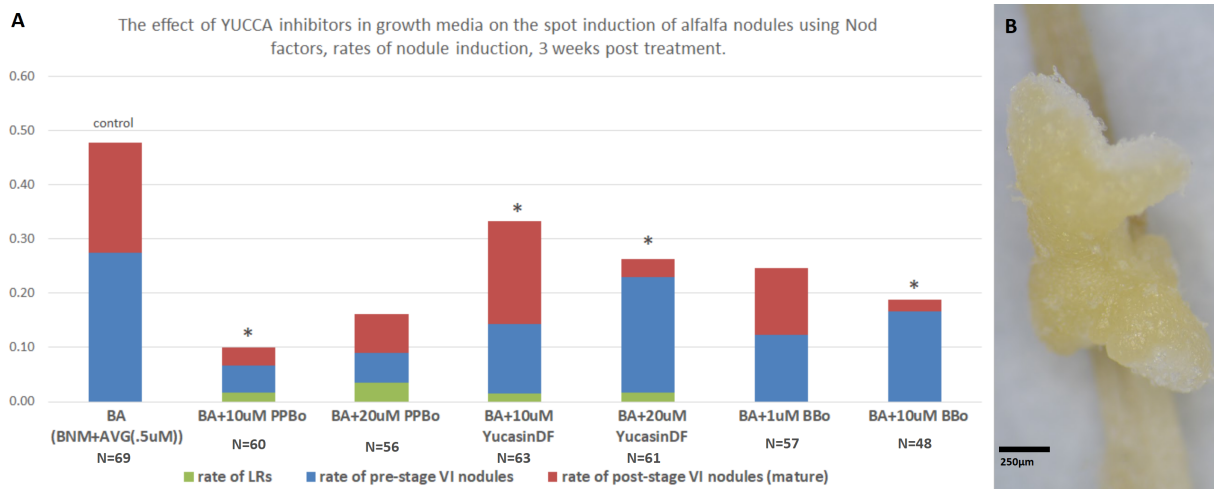

Figure 5.2: Effect of auxin biosynthesis inhibition on *Medicago sativa* Nod-factor-induced nodulation rates**:** **A** Rates of immature (in blue) and mature (in terms of development, in red) nodules on alfalfa roots grown on different YUCCA inhibitor-containing media, spot-treated with Nod-factors, 3 weeks post treatment. The first treatment is spot treatment with Nod-factors (10 µM Nod-factor mix) of alfalfa seedlings grown on normal Buffer Nodulation Medium (BNM) agar plates with the addition of aminoethoxyvinylglycine (AVG) 0.5µM (Normal spot-inoculation medium, denoted as BA) (N=69). All other treatments are different only with regard to the addition of individual YUCCA inhibitors in the growth medium: 4-phenoxyphenylboronic acid (PPBo) 10µM (N=60) or 20µM (N=56), YucasinDF 10µM (N=63) or 20µM (N=61), 4-biphenylboronic acid (BBo) 1µM (N=57) or 10µM (N=48). Stars denote significant reduction (p-value < 0.05) in nodulation rates compared to the control group according to a chi-square test with Marascuilo correction. **B** Example alfalfa nodule spot-induced by local application of a water droplet containing Nod-factors.

the observed inhibition of nodulation by inclusion of YUCCA auxin biosynthesis inhibitors in the growth medium (section 5.2.1) comes about via broad effects of YUCCA inhibitors on the apical meristem and/or global root auxin biosynthesis and IAA availability across the whole root. With this in mind, a third line of experiments focused on inhibition of auxin biosynthesis only at the site of nodule initiation, by local application of YUCCA inhibitors. This was achieved by co-treatment of YUCCA inhibitors with the Nod-factor-containing solution during spot nodule induction in *Medicago sativa* (alfalfa), or co-treatment with rhizobia during spot inoculation of *Medicago truncatula*. For spot inoculation of *Medicago truncatula* I experimented with addition of Yucasin 10μM or PPBo 10μM in the inoculum. For co-treatment of YUCCA inhibitors with Nod-factors on alfalfa seedling roots, I experimented with addition of PPBo 50μM or 500μM, Yucasin 500μM or BBo 500μM addition to the local treatment solution containing Nod-factors. Results from alfalfa showed that, during local spot co-treatment of YUCCA inhibitors and Nod-factors, a general trend of inhibition of the mature nodule stage occurs across different YUCCA inhibitor co-treatments compared to control. Moreover, nodule induction can be significantly suppressed when I co-apply high concentrations of PPBo with the Nod-factor containing spot treatment medium, compared to the control case where only Nod-factors are applied (PPBo 500μM, p-val<0,05 - Chi-square test with Marascuilo correction, control N=68 seedlings, replicate N=67 seedings. control nodules=47, replicate nodules=1). These results however were not significant across all 4 replicate experiments, and this consistent significant result in high PPBo concentration might be due to chemical toxicity. Similar inconsistency in results was observed in 3 experiments of co-treatment of YUCCA inhibitors and rhizobia during spot inoculation of *Medicago truncatula*, albeit there was a trend of mild inhibition of nodule initiation. Overall, local addition of auxin biosynthesis inhibitors at the site of nodule initiation of both species did not consistently inhibit nodulation. This leads us to believe that a careful assessment of the penetrability of these chemicals into plant tissues must be performed, possibly using fluorescent tracer compounds with similar molecular weight and chemical attributes, in order to better understand how fast and far these chemicals can penetrate the root tissues, in comparison to the symbiotic signal. Thus far we have not found a replicable experiment in which suppression of auxin biosynthesis can be targeted only at the site of nodule initiation, in order to test the hypothesis that local auxin biosynthesis drives nodule formation.

5.2.3 Reduction in nodule numbers in the *yucca2-yucca8* double mutant

Auxin biosynthesis is a highly localized process, and the expression patterns of different *YUCCA*s can assign to them different roles in plant development[179, 293, 317]. By investigating the tissue specificity of *MtYUC8* expression using the BAR *Medicago truncatula* eFP

Browser[276], I was able to find that *YUC8* is highly expressed in nodules, compared to other tissues (Figure 5.3 B). With this in mind, we hypothesized that knockout mutants of *YUC8* and *YUC2*, expressed early during nodule development (as presented in chapter 3), could exhibit nodule-specific developmental phenotypes. I generated *yuc2* and *yuc8* homozygous mutants from Noble Tnt1 transposon insertion lines NF4544 and NF14406, respectively (Figure 5.3 A). These single mutants did not show any significant phenotype in terms of nodule numbers, when grown on nutrient replete soil, after 3 week flood inoculation with rhizobia, compared to wild type control lines. This could be due to redundancy between these two coexpressed auxin biosynthesis genes, so I crossed the two lines to make the *yuc2,8* double mutant. Crossing yielded a low number of viable seeds, and was successful only when the *yuc2* mutant was providing the pollen, itself an observation I could not find a causing hypothesis for. These seeds yielded a small number of *yuc2,8* homozygous double mutant plants, of which most died early from stunted growth and fungal infection. Two of these plants showed a striking extreme dwarf phenotype (Figure 5.3 D) where a 5 month old plant did not reach a height of more than 4 centimeters, but was capable of reaching maturity and developing extremely small flowers and pods, and a normal sized seed. Genotyping, however, revealed one homozygous double mutant plant that had close to normal growth, putting these phenotypic observations into question, due to their variability. Normal growth could be explained by compensation by other YUCCAs, upregulated in this plant only, thus further study is required. This plant provided seeds to test for nodulation capability. Flood inoculation and subsequent nodulation efficiency testing of background *Medicago truncatula* strain R108 plants versus *yuc2,8* F2 (second generation) plants showed a significant reduction in nodule numbers per root system in the double mutant (Student's t-test, p-value<0.05, Figure 5.3 C). This finding further supports the hypothesis that auxin biosynthesis plays a role in nodule development.

5.3 Discussion

The results I presented in this chapter support the hypothesis that auxin biosynthesis via the Indole-3-Pyruvic Acid (IPyA) pathway, mediated by the activity of YUCCA enzymes, contributes to nodule development. Two approaches, one knocking out both *YUCCA* genes implicated in early activation of auxin biosynthesis during nodule development, and a second, inhibiting the activity of all YUCCA enzymes by application of chemical inhibitors, lead to reduction in nodule numbers. Interestingly, knocking out both *YUCCA2* and *YUCCA*8 genes led to a variable dwarf phenotype that is similar to the ones of *yucca* mutants in *Arabidopsis thaliana*[101]. The local auxin maximum of nodule initiation (described in chapter 2), can be assisted by local auxin biosynthesis, distal auxin biosynthesis and transport to the nodule

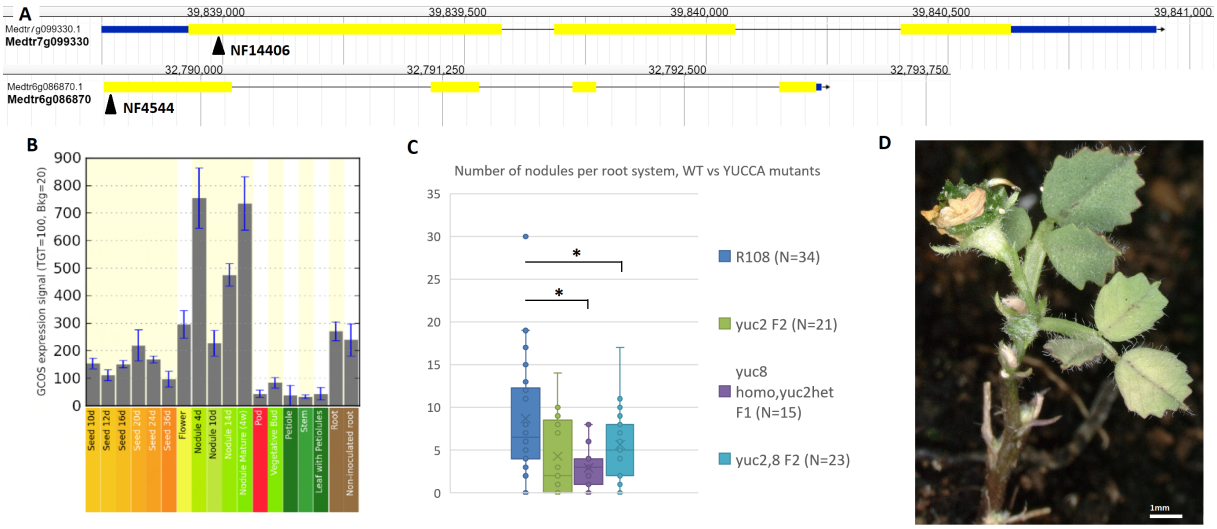

Figure 5.3: Reduced nodulation in the *yuc2,8* mutant**:** **A** Tnt1 insertion mutant positions for *yuc8* (Noble Foundation line NF14406, insertion in Medtr7g099330 gene) and *yuc2* (NF4544, Medtr6g086870). **B** Absolute expression levels of the *YUC8* gene across different tissues, according to the *Medicago truncatula* eFP Browser[276]. Note the high expression levels in nodules. **C** Nodule numbers in flood inoculated root systems of different genotypes, 3 weeks post inoculation. The genotypes used are the wild-type control R108 (N=34 root systems), a second generation *yuc2* mutant population (N=21), a first generation segregating population of daughter plants of a self-pollinated *yuc8* homozygous - *yuc2* heterozygous double mutant (N=15), and a second generation population of a *yuc2-yuc8* double homozygous mutant that was able to produce seeds (N=23). Stars denote significant reduction in nodule numbers per root system compared to wild-type (Student's t-test, p-value<0.05). **D** One case of the variable phenotype of the *yuc2,8* double mutant, showing extreme dwarfism after 5 months of growth.

initiation site, or anything in between these two scenarios. In support of the first scenario, in the previous chapter we provided evidence of local expression of auxin biosynthesis genes. In this chapter I did not succeed to locally suppress auxin biosynthesis, only showing that global root inhibition of auxin biosynthesis inhibits nodule formation. Since auxin is transported, we cannot rule out that the results presented in this chapter can be explained by the second scenario, where inhibition of auxin production in, for example, established meristems, limits the available auxin molecules that can be transported to the new organ. After all, studies in *Arabidopsis thaliana* show that application of Yucasin depletes auxin from the root meristem, and that there is a substantial contribution to the maintenance of the auxin maximum there by auxin biosynthesis[173]. A third interesting hypothesis is that the effects of auxin biosynthesis inhibitors on nodulation rates that we observe have to do with the reported role of auxin biosynthesis on root hair curling and rhizobial infection. In *Lotus japonicus* it has been shown that auxin biosynthesis via to the least *LjTAR1* is contributing to auxin accumulation and response in root hairs, during early Nod-factor perception, important for the infection process[339]. If auxin biosynthesis has a similar role in the infection process of *Medicago truncatula*, the results we report of lower nodulation when we apply auxin biosynthesis inhibitors could be explained via the effect of the inhibitors in the availability of auxin in root hairs undergoing infection. Going forward, it is clear that due to the mobile nature of auxin, a toolset for local perturbation of auxin dynamics needs to be created (see also chapter 4). Stable transformation of *Medicago truncatula* with our auxin signaling reporter R2D2 (Methods 9) could also set the stage for experiments on the roles of of auxin biosynthesis in the infection process and nodule organogenesis.

Chapter 6

General Discussion

Our approach in studying auxin dynamics during nodule development, presented in this thesis, gets its power from the homogeneity of growth and treatment conditions across all experiments performed. *Medicago truncatula* seedlings were grown on the same medium, treated identically across experiments at the same area of the susceptibility zone (which we characterized in chapter 3), and experimented upon at the same time post germination, when we measured changes in gene expression by spot inoculation (chapter 3), when we observed the emerging auxin response using the DR5 reporter line (chapter 2), when we spot-treated chemicals perturbing auxin concentration and flux (chapter 2, chapter 5), and when we cut the root to observe the timing of auxin accumulation due to flux obstruction (chapter 2). As such the timing of the root responses could be brought into focus and be compared, and we were able to ask our main research question, namely, when does auxin accumulate post inoculation, and how - by which order of events. In our hands, timing the emergence of the auxin maximum in *Medicago truncatula* gave a strong signal of divergence from buffer treatment 8-12 hours post inoculation, with a cortical response being visible 12hpi onwards (chapter 2), coinciding in time with the expression of auxin biosynthesis genes *YUCCA2* and *YUCCA8* (chapter 3). Complementing this result, accurate in time studies of cytosceletal changes early during nodulation of *Medicago sativa* and *truncatula*[45], show the first microtubular cytoskeleton rearrangements to occur 16-18hpi in pericycle cells positioned opposite protoxylem poles, and first cortical cell activation at 18-24hpi facing these pericycle cells, all possibly mediated by altered auxin levels in these cells. Most studies of acropetal auxin transport, although coarse in timepoints, agree that in indeterminate nodulators there is a detectable change occurring at 24hpi[18, 67, 68, 112, 205, 234, 242]. Although we did not make direct measurements of the same kind, we can propose that in order for the observed auxin signal to be attributed to local acropetal auxin flux reduction, inhibition would have to be immediate after inoculation (informed by cut root observations of chapter 2), and certainly could not be attributed, alter-

natively, to a cortical auxin flow reduction (spot treatment with PATIs, chapter 2). This leads us to propose that there is first an auxin maximum occurring, then changes in the cell-cycle phase of the nodule initials, then vascular auxin transport blockage.

The auxin maximum we observed can now be placed in the context of the symbiotic transcriptional response, by our painstakingly accurate transcriptomic dataset for nodule development (chapter 3). Due to the careful choice of timepoints our team was able to identify key genes sufficient in driving nodule initiation (published in [50]), with many more lurking to be discovered. The main conclusions of this study is that upregulation of auxin biosynthesis genes can be detected before auxin signaling, pointing to a previously unknown process by which the indeterminate nodule initiates. Supported by my bioinformatic analyses, our dataset tells a story of an initial stress response (0-8 hours post inoculation), followed by reconfiguration of the transcriptional state (around 8hpi), leading to a cytokinin response - stem cell identity - auxin biosynthesis stage (10-14hpi), driving an auxin response stage that coincides with broad transcriptional reprogramming (16hpi). There is also an indication that NIN, already known to bring about a symbiosis-inducible positive feedback with cytokinin signaling[65–67, 70–73], is implicated in a symbiotic-conditional positive feedback with auxin signaling as well, via indirect upregulation of auxin biosynthesis, and auxin responsive elements in the NIN promoter (chapter 3), and could mediate a totipotency inducing positive interaction between the two major plant hormones (chapter 1). These results help us answer both when and how auxin accumulates in the *Medicago truncatula* nodule. Generation of and comparison to an identical dataset in *Lotus japonicus* would help us delineate the commonalities in nodule initiation between the two nodule types, and can be combined with phylogenomic methods[11]. I also showed, through identification of regulatory motifs, that our dataset is amenable to GRN inference systems biology approaches (chapter 3), and I invite more work to be done in this direction, analogous to studies in *Arabidopsis thaliana*[316]. Complementary work by high-throughput TF-promoter binding inference between important promoters and active TFs can delineate the central part of the connectivity graph of the gene regulatory network of nodulation, as it was recently done for wounded root regeneration in *Arabidopsis thaliana*, where it was shown that PLT3 and LBDs were the most central regulatory hubs[275]. I made the first steps towards this direction by the use of transactivation assays (chapter 4), to understand which TFs regulate the YUCCA promoters, a method that can be easily expanded to include all known transcription factors that are active during early nodule induction. Results showed that, contrary to expectation, PLT3 was a repressor of *YUC* promoters, and that NIN directly upregulates the lateral organ inducing LBD16 transcription factor[49, 50, 90, 92]. The members of the gene regulatory network path(s) from NIN to YUCCA induction are still elusive however, although the candidate LEC transcription factor we recently uncovered (Medtr7g105370,

chapter 3) might be one of them[290–295].

We then moved on to show that auxin biosynthesis via the IPyA pathway, mediated by the activity of YUCCA enzymes, is sufficient to induce lateral organ organogenesis (chapter 4), and that, conversely, inhibition of YUC activity by either chemical inhibitors or creation of knockout *yuc* mutants inhibits nodule development (chapter 5). The hypothesis of auxin biosynthesis underlying initiation of all nodule types is compelling, as it would simplify the evolutionary trajectory of different nodule types: auxin biosynthesis was at the center of nodule development throughout evolutionary history, but it had different effects on PAT. In the case of the indeterminate nodule, auxin biosynthesis is capable of initiating cell division, but it also affects vascular auxin flow, an effect that must have a positive feedback on auxin levels and nodule induction. It remains to be seen if this feedback is needed for natural initiation, regardless if artificial initiation through PAT inhibition is possible for this nodule type[18, 198, 236–240], perhaps due to the cells capable of transitioning to nodule identity residing in an area of high auxin flux and being auxin sensitive. In the case of the determinate nodule, on the other hand, local auxin biosynthesis is sufficient for nodule induction, and does not involve/need/affect auxin transport perturbation. This conceptual framework is supported by our model, which can act as a first step in a modeling study of different proposed PAT feedbacks predicting the local polarity changes during the naturally inducible symbiosis initiation, and comparing the results with experiments (chapter 4). Our model is by no means close to the reality of auxin dynamics occuring during nodule initiation, it merely provides an alternative view to the ones previously proposed[33, 103–105, 206]. It gives predictions, however, about the changes in cell polarity involved in the initiation of the two nodule types, which could be investigated through experiments utilizing the polarity indicating SOSEKI proteins[336] we identified to be expressed during nodule initiation (chapter 4).

All in all, our work [50, 345] uncovers previously unknown interactions and feedbacks between the central symbiosis regulator NIN and a conserved lateral organ/root developmental program involving LBD16 and YUCCA-mediated auxin biosynthesis[90, 92] in *Medicago truncatula* nodule development. This result was independently and simultaneously shown to hold true in *Lotus japonicus* as well[49]. I believe that the insight of NIN, central inducer of nodule symbiosis[60, 64, 86, 195, 346, 347], possibly acting as a conditional coupler and inducer of both a cytokinin positive feedback response[65–67, 70–73] and a local auxin positive feedback response[49, 50, 89] is an important new point of view for how the legume gene regulatory network dynamically locks down the nodule symbiotic state[74] and subsequent nodule development. There are many important outstanding questions, however, about how the emerging nodule recruits related root developmental programs[33, 97, 98] involving WOX-CLV[106, 109–111, 124, 126, 188, 289, 337] and PLETHORA[98–101, 123, 281]

transcription factors, to uniquely pattern and establish itself in the root form. Not surprisingly, understanding the patterning and morphogenesis of the nodule delineates the general principles of plant development, and as such can be an important area of research with direct biotechnological applications.

Concluding remarks

The work presented across these chapters provides a shift in our understanding of nodule development. By uncovering the central role of auxin biosynthesis in driving indeterminate nodule organ formation, we can now propose that both indeterminate and determinate nodules initiate with the help of auxin biosynthesis, and that the evolution of determinate nodules might have come about by simply shifting the domain of where this is possible, through the expression of the TAA enzymes providing the precursor IPyA to YUCCAs in mid and outer root cortex[114, 339]. As such we can now appreciate how the nodule is self-regulated in terms of developmental potential in all ways needed, as it has its own cytokinin[69, 77] and auxin source. This notion is in line with an understanding of plant form as a colony of communal entities[146], and supports a view of the nodule as a separate/independent/self-sustaining developmental unit. Our results, at least superficially, go against the grain of a large number of reports supporting auxin transport changes as the cause for indeterminate nodule initiation[18, 28, 67, 68, 112, 205, 206, 242, 271, 322]. I attempted to unify our understanding of the interactions between auxin transport and biosynthesis during nodule initiation by means of the model presented in chapter 4, and anticipate great insights about plant development to emerge from this controversy. After all, nodule development is, in my opinion, one of the most profound naturally inducible modifications of plant development in response to a symbiont that we study. Wielding the processes underpinning it, through genetic engineering, would give a massive engineering potential[348].

Chapter 7

Materials and Methods

7.1 Plant material - growth conditions and media

We used *Medicago truncatula* Jester Jemalong cultivar, A17 Jemalong cultivar, and R108 for all experiments. Mutant lines obtained through the Noble foundation are derived from R108 background. Our *pDR5:GFP-NLS* line is derived from the A17 cultivar. All *Medicago* hairy root transformation, spot inoculation and gene expression experiments use the Jester cultivar. *Medicago sativa* seeds used were of the strain "lucerne" obtained through the company Brown Seeds.

We grow *Medicago* in controlled environment rooms at 23°C, with 16 hour photoperiod and light intensity of 300μmol m^{-2} s^{-1}, for all experiments. When bulking for seed, we grow *Medicago* in greenhouses with extra light supply in the winter.

The following media were used for plant and bacterial growth:

- Lysogeny Broth, Lennox (L) 1 litre: Tryptone 10 g, yeast extract 5 g, NaCl 5 g, D-Glucose 1 g. For solid medium +10 g Lab M No.1 agar.

- Luria-Bertani (LB) medium: Tryptone 10 g, yeast extract 5 g, NaCl 5 g. For solid medium +10 g Lab M No.1 agar.

- Rhizobium complete medium (TY): Tryptone 5 g, yeast extract 3 g, CaCl2(6H2O) 1.32 g. For solid medium +10 g Lab M No.1 agar.

- Rhizobium minimal medium (MM) 1 litre: VITS (vitamins) standard medium 5ml, NaGlu (sodium glutamate) 25ml, 3% Mannitol 10ml, Y medium addition to the final volume of 1 litre.

- Buffered Nodulation Medium (BNM) 1 litre: MES (2-(N-morpholino) ethanesulfonic acid) buffer 390 mg, CaSO4(2H2O) 344 mg, KH2PO4 0.125 g, MgSO4(7H2O) 122 mg, Na2EDTA 18.65 mg, FeSO4(7H2O) 13.9 mg, ZnSO4(7H2O) 4.6 mg, H3BO3 3.1 mg, MnSO4(H2O) 8.45 mg, Na2MoO4(2H2O) 0.25 mg, CuSO4(5H2O) 0.016 mg, CoCl2(6H2O) 0.025 mg, pH

6.0. For solid medium + 11.5 g Formedium agar. In most spot inoculation experiments we add aminoethoxyvinylglycine (AVG) to this medium to a final concentration of 500nM, then medium is noted as "BA", indicated in the text.

- Modified FP medium (modFP): CaCl2(2H2O) 0.1 g, MgSO4 0.12 g, KHPO4 0.01 g, Na2HPO4(12H2O) 0.150 g, ferric citrate 5 mg, H3BO3 2.86 g, MnSO4 2.03 g, ZnSO4(7H2O) 0.22 g, CuSO4(5H2O) 0.08 g, H2MoO4(4H2O) 0.08 g, NH4NO3 0.5 mM, Formedium agar 8 g, pH 6.0.

7.2 Methods

1. **Flood treatment with PATIs:** For flood treatment of *Medicago* roots with polar auxin transport inhibitors, I prepared water solutions of 200µM TIBA and 200µM NPA (final concentrations), from 50mM (in 100%DMSO) stock solutions. I then treated 7 days old seedlings plated in BNM, by flooding the roots with 1ml solution using a 1ml pipette, and then collecting the solution from the bottom of the plate using the same pipette.

2. **Golden Gate Cloning:** For making DNA constructs the Golden Gate cloning technique is used as presented here[349]. Level 2 constructs used in this study are indicated in Methods 22.

3. **Hairy root transformation** (HRT) protocol was performed similarly to Boisson *et al* [350]. In most experiments HRT was performed using the *Medicago truncatula* Jester Jemalong ecotype, the same we used for the generation of our RNAseq dataset. Regarding the seedlings used, 4 days prior to transformation, we scarify and sterilize the amount of seeds required for the experiment. Scarification is usually done using sand paper, however it is not required for the Jester seeds. We sterilize Jester seeds using Sodium hypochlorite (bleach) solution in the sterile conditions of the laminar flow hood, in 50ml Falcon tubes. We add 10ml standard bleach solution, rock the tube, leave for 4 minutes, then add 10ml sterile water and leave for another 4 minutes. After that we pour out the bleach and wash the tube with sterile water at least 10 times. The last wash is left in and we imbibe the seeds for 1 and a half hours. When sterility is a big concern, the seeds are divided in multiple Falcon tubes from the start, and we pipette a bit of the imbibition water to corresponding Liquid Broth (LB) plates to check for bacterial and fungal growth overnight and throw out corresponding Falcons when we see signs of contamination on the plates. After imbibition, Seeds are then plated on water agar plates, wrapped with micropore tape and aluminium foil, and placed upside down at 4°C to stratify and vernalize for 3 nights. The day before the transformation, we move the

seeds to room temperature to germinate, still upside down so that the roots will grow away from the agar. On the day of the transformation, in the laminar flow hood in sterile conditions, we take each seedling using forceps, cut 3mm off the tip of the seedling's root using a scalpel, then dip the new root tip in the *Agrobacterium rhizogenes* cultures of choice. We then move the seedlings in modified Fahraeus media (Mod FP) square plates with filter paper backing. We put 6-10 seedlings per plate, and place over the seedling roots a wet filter paper strip to hold them in place. We then wrap the plates with micropore tape and leave them in the growth room, vertically under the lights for 3 weeks. We place a sheet of kitchen roll paper over the plates so that the roots are not damaged by bright light.

Regarding the *Agrobacterium rhizogenes* cultures used, we normally start a bacterial pre-culture 2 days prior to transformation. We prepare 5ml Liquid Broth (LB) media universals with 25μg/mL Kanamycin, 20μg/mL Rifampicin, 50μg/mL Carbomycin. Then, in the laminar flow hood, we swab through the bacterial mats of *Agrobacterium rhizogenes* plates using a sterile toothpick, drop the toothpick in the universal, and grow the pre-cultures for 24h at 28°C. The bacteria we use are electrocompetent *Agrobacterium rhizogenes* strain 1193 that carry the DNA plasmids we transform with. The next day, we start the main cultures in 50ml Falcon tubes with 5ml LB medium with 25μg/mL Kanamycin, 20μg/mL Rifampicin, 50μg/mL Carbomycin, by transferring 1ml of pre-culture to 4ml of LB+antibiotics. At the day of transformation, we spin the Falcon tube cultures on 4200rmp for 3 minutes, remove the LB in sterile conditions, and re-suspend the cultures in 1ml sterile water which we place in a small Petri dish or a 6 -well culture dish for easy accessibility to dip the plant roots.

4. **Spot inoculation:** For spot inoculation of rhizobia on *Medicago* seedling roots is performed as per lab protocol, published in [50]. Briefly, a droplet of 1.4uL water solution containing rhizobia is applied at the site of root hair emergence, roughly 7mm away from the root tip. The droplet is a *Sinorhizobium meliloti* solution at a calculated OD 0.02, diluted in FP medium[351]. *S.m.* solution was made by first growing *S.m.* in preculture in MM media (Minimal Media, Y media with the addition of vitamins, sodium glutamate and mannitol) for 24h, then 16h in MM media + 3μM luteolin, for the induction of Nod factor production. The mock treatment is the same growth medium without the inclusion of bacteria (just MM+luteolin), treated with the same growth conditions and diluted in FP in identical way. We normally treat 7 day old seedlings, which are plated in BNM media + aminoethoxyvinylglycine (AVG) 500nM. Before treatment, we find the best spot for inoculation (BSFI) using a stereo microscope placed inside the flow hood and marking where the BSFI is for each individual root by puncturing a hole next

to it in the filter paper and growth medium using a sterile hypodermic needle. The spot is defined as the root segment closest to the root tip where we can clearly see more than 15 root hairs emerging, at a square segment of the root, with height equal to the width of the root. This normally coincides with the susceptibility zone, as root hairs emerge in bulk there, even under AVG treatment. Droplet placement is done using a special long thin and flexible pipette tip (Eppendorf), but can be also done with a thread dipped in the inoculum. All experiments in this thesis are performed with droplets placed on the roots and with all seedling plates carefully transferred in the growth room so that there is minimal droplet loss due to droplet water surface break.

5. **Flood inoculation**: For simple nodulation efficiency assessment of transgenic plant roots or mutants, flood inoculation was performed on plants grown in Terragreen : sharp sand mix (1:1) (Oil-DriCompany, Wisbech, UK)[50] , in P40 trays. Seeds are sterilized, imbibed, vernalized for 2 days, then left in room temperature for 1 day to sprout. Seedlings are then transferred to Terragreen-sharp sand 1:1 mix potting medium and plants are grown for another 2 days. After, inoculation is performed, by pouring 2ml of *S.m.* grown in TY medium overnight, diluted with water to a final OD of 0.02, in each root system. Nodule numbers per root system and root weight are measured at 2 weeks post inoculation (wpi). For the nodule phenotypic analysis of mutants, 20 plants are inoculated of each line, and average root weight and nodule numbers were counted at 14dpi.

6. ***pDR5:GFP-NLS* local fluorescence timecourse**: In the timecourse of auxin accumulation quantification, *pDR5:GFP-NLS* stably transformed *Medicago truncatula* seeds are grown and spot inoculated/ treated in BNM+AVG 500nM vertical plates, as per spot inoculation protocol (Methods 4, [50]). A total of 5 experiments were carried out, to extract the necessary data. The roots are assessed under a stereoscope inside the laminar flow hood for where the susceptible zone is, and marked with a prick next to the root at the filter paper under it, using a sterile hypodermic needle. After this, I either spot inoculate with rhizobia as per protocol, or treat with a droplet of 2,5μM IAA of the same volume (positive control), or mock treatment as per spot inoculation protocol, or Nod-factor 10^{-8}M treatment. Per experiment, ~60 plants were visualized for each treatment. Mock treatments were kept to a minimum in subsequent experiments, as the relevant data were gathered, and the *pDR5:GFP-NLS* line showed no response. The plants (mock and S.m. treatment) were in most experiments visualized between 6hpi and 24hpi, with a later timepoint at 48hpi and 54hpi in some experiments. Treatments with auxin were visualized 1-6hpt every hour, and every 4hours after that(as the main

response was found 3hpt) until 24hpi, and at 48hpi. I used simple statistical t-test for analyzing for divergence from the mock treatment. I tested the plants after 7 days for nodule emergence, and traced back to my data pictures to decide which plants I use for quantifying the auxin signal, since not all of them nodulated. For visualization of the timeline of auxin patterning (*pDR5:GFP-NLS*) the Leica M205FA stereo microscope is used, with standard GFP fluorescence settings across experiments. The pictures obtained are then compiled per growing root, and analyzed for mean fluorescence inside Regions of Interest (ROIs) using the FIJI software. At each timepoint picture, I quantify the following metric, "ratio of inside to mean outside fluorescence": I measure the mean fluorescence in the ROI consisting of a square with side length equal to the width of the root, positioned at the center of the zone of my droplet application of rhizobia. I measure then the mean fluorescence inside two identical in size ROIs, positioned again inside the root, apically and basally of the site of inoculation, 2 root widths away. I then calculate the ratio of the two measurements. This has the advantage of an internal normalization procedure, as each root and each experiment might give different fluorescence levels. This method is somewhat similar to one used by Pacios-Bras *et al*[113].

7. **Fluorescent PINs:** For generating Fluorescent PINs, I aligned all *Medicago truncatula* and *Arabidopsis thaliana* PINs and identified all the positions in the PIN protein sequence that have been used in the literature for insertion of a GFP tag. C or N-terminal tagging is not possible in these membrane-bound proteins, possibly due to the fact that both ends are extracellular. Most successfully tagged positions are in the middle large intracellular loop in the long PINs, and in the last short intracellular loop in the short PINs. I aligned the *Arabidopsis thaliana* PINs to the *Medicago truncatula* PINs using the MUSCLE and ClustalW plugin of Jalview. I identified 3 positions in MtPIN2 (361[268], 412[264], 455[266]) and 3 in MtPIN9 (181, 198[264], 331[223]) analogous to successful positions from literature of closely related AtPINs (see citations above). I inserted a Venus tag in the sequence with the addition of poly-A linkers, and requested a synthesized construct with this configuration. Resulting constructs were inserted in transgenic roots and visualized in the confocal microscope. 1 attempt in each MtPIN was successful, as judged by comparison of the protein localization and dynamics to the literature. The successful protein positions were 361 for MtPIN2([268], different tagging site than the attempt from Xiao *et al* [231], which I tried as well and in my hands showed abnormal localization) and 331 for MtPIN9[223] (last intracellular loop). Tagging positions for all *M.tr.* PINs have been identified, and, currently, some of them are in various stages of development and evaluation. Please contact me for further information and constructs.

8. **Motif analyses:** I use the MEME suite of tools[280] to address questions about the transcriptional control of the genes differentially regulated in our RNA-seq timecourse dataset. I downloaded the 3000bp upstream promoter sequences for all predicted genes of *Medicago truncatula* (genome version 4.1) from Phytozome[273]. The promoter length I chose was more than enough to cover most regulatory regions, as the upstream 500bp from the TSS have been indicated to contain most cis-regulatory motifs of the gene of interest, based on single nucleotide polymorphism distributions in *Arabidopsis thaliana* promoters[352]. I used the program "dust" from the suite to mask low-complexity regions in all the sequences. I assembled random sets of sequences of different sizes for negative control tests and for provision of control sets. I assembled a motif database consisting of many publicly available TF binding sites, most from *Arabidopsis thaliana*, by merging two publicly available databases: JASPAR Plants[279] and ArabidopsisPBM[309], both provided by the MEME suite, with the assumption that there is conservation of motifs between *Arabidopsis thaliana* and *Medicago truncatula*. I then added my own motifs by reverse engineering the motif profiles provided in the literature for many TFs interesting for nodulation, like NIN[347], PLT[281], NSP1[54], NFY[308], PCRE1[257] and the consensus knowledge from the field about AuxREs[263]. All motif files are available on request. To test and rank promoters for abundance of a motif I used the FIMO program of the suite. **A:** For analyses of enrichment with *de-novo* identified motifs, I ran the pipeline MEME->AME->FIMO with default settings (for short (<15) or long (>15bp) motif target lengths) and the aforementioned motif database as FIMO comparison. I also ran the same analyses with the new MEME differential enrichment mode, and STREME, with highly similar results between the three modes. The first pipeline method was prone to overfitting as judged by positive identification of enriched motifs when comparing random promoter groups to other random promoter groups. The later two methods showed the expected results in quality tests. **B:** Differential enrichment of known motifs was tested using the AME (Analysis of Motif Enrichment) tool of the MEME suite, using default settings. The tool was provided with a set of random control promoter sequences as control sequences, the number of which was at the same magnitude as the treatment set.

9. **MtR2D2 line development:** Together with Jodi Lilley we generated *Medicago truncatula*-specific GFP-DII-NLS fusion designs (successful ones = EC20866_pL1M-R3-pLjUBI1-mCherry-2xGS4xGS4xGS2xG-MtIAA27-KQ-RK-P177L-GAGA-NLS-t35S and EC20868_pL1M-R2-pLjUBI1-3xVenus-2xGS4xGS4xGS2xG-MtIAA27-KQ-RK-GAGA-NLS-t35S) which are different from the *Arabidopsis thaliana* versions in the order of the fusion protein components. All tests were carried out in the same fashion to the one

designed for *Arabidopsis thaliana*[263]. Briefly, I executed hairy root transformations using the R2D2 construct, and the resulting transgenic roots were tested for reporter auxin sensitivity, through a timeline of fluorescence microscopy carried out using confocal fluorescence microscopy. For each construct designed, I tested for a decrease of fluorescence in the auxin sensitive reporter channel compared to the fluorescence at the stable reporter channel, upon auxin treatment. The constructs that showed positive results were verified by a timecourse microscopy 5 minutes after 25μM IAA treatment, every 3 minutes for 2 hours, in triplicate. The results were analyzed in FIJI, via quantification of fluorescence in each channel for the region of interest. Results showed a clear exponential decay of the red channel signal (degradable mCherry-DII) with the green channel staying the same (GFP-stabilized-DII) (Figure 7.1). Data, results and constructs are available on request. Our MtR2D2 showed excellent expression patterns identical to its *Arabidopsis thaliana* counterpart (Figure 7.1).

10. **Susceptibility zone assessment:** For assessments of the extend of the susceptibility zone in *Medicago truncatula* seedling roots, one WT-homozygous and two *pin9*-homozygous mutant lines were spot inoculated at regular intervals away from the root tip (1, 2, 2.5, 3, 4, 5cm) as per spot inoculation protocol (Methods 5). For every spacepoint, 60 plants were inoculated, and the rate of successful infection was measured by counting presence-absence of nodules 10 days post inoculation. The results were analyzed using a chi-squared multiple statistical test with a Marascuilo correction, where appropriate, to distinguish differences among groups.

11. **YUCCA inhibitor effect on rhizobial growth:** I performed an experiment to test possible effects of Yucasin, PPBo and BBo on *Sinorhizobium meliloti* growth. Bacterial growth in liquid culture was tested overnight in 10ml vials of Minimal Media or TY with addition of Yucasin 100μM (final concentration), Yucasin 10μM, PPBo 100μM, PPBo 10μM, PPBo 1μM, BBo 100μM, BBo 10μM, BBo 1μM, and background DMSO, in triplicate, with identical inoculation of bacteria, in concentration and volume. OD600 of the culture was measured after 24h and 48h. Results showed transition to significant inhibition of bacterial growth due to high conscentration of the chemical added to occur in respective concentrations 10μM<Yucasin<100μM,10μM<PPBo<100μM, 1μM<BBo<10μM. Interestingly there was a small but significant promotion of rhizobial growth in low concentrations of PPBo (1μM).

12. **YUCCA inhibitor experiments:** Yucasin and YucasinDF was kindly provided by Tomokazu Koshiba (Tokyo Metropolitan University, personal communication) and diluted in 100%DMSO at 50mM stock solution. PPBo (4-phenoxyphenylboronic acid) and BBo (4-biphenylboronic

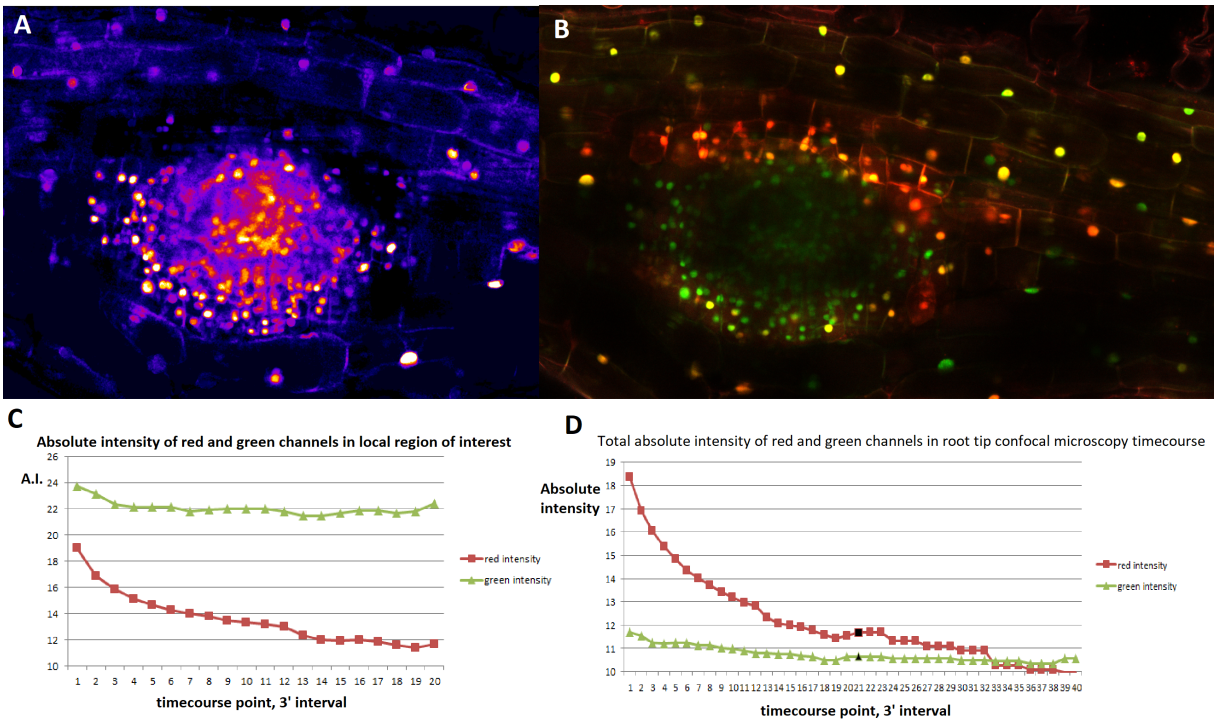

Figure 7.1: MtR2D2 generation**: A,B** Confocal microscopy of a lateral root in our generated R2D2 transgenic auxin sensor lines. On the left we have ratiometric pseudo-chromatic coloring based on the relative intensities for the green (stable DII) and red (auxin degradable DII) channel (FIJI LUT=fire). On the right we have the original picture. **C,D** Auxin induced degradation of mCherry-DII as opposed to GFP-stabilized-DII. 25μM auxin is applied on transgenic roots bearing the MtR2D2 construct, then a root is visualized using a 3 minute interval timecourse confocal microscopy. Fluorescence of the red channel and green channel is quantified in a region of interest in the root (C) or on a whole root tip picture (D).

acid)[339] was obtained, in consultation with Dugald Reid, through Sigma-Aldrich in powder form and diluted in 100% DMSO to 50mM final concentration stock solutions. Long term experiments showed that Yucasin was not chemically stable, and lost efficacy in 3 months, as indicated by the provider, so I used YucasinDF in later experiments. Great care must be taken when using all the inhibitors and especially the Yucasins to not expose them to heat above 50 degrees C, for example when adding them to the agar medium, as they can lose potency. The effect of these inhibitors on the growth of *Medicago sativa* and *truncatula* roots was assessed by measuring the growth of the seedling root in a 24h period, at the interval before the spot inoculation with *S.m.* or spot treatment with Nod-factors, and by overall assessment of the root systems during the experiments. Results showed that, in plants grown on BNM+AVG 500nM, addition of YucasinDF 10μM initially (first week) had no effect on root growth, but by the end of the experiment made the roots slightly longer, slightly agravitropic, with more lateral roots. The same final phenotype holds true on addition of BBo 1μM, but this chemical retarded root growth slightly initially. PPBo 1μM had no discernible effect on root growth, but PPBo 10μM slightly retarded root growth initially and led to more LRs eventually in the root systems. Under no scenario do these root systems show phenotypes that would indicate that general root development is inhibited, to attribute potential loss of nodule development to it. For assessment of nodulation efficiency in the different conditions, in each experiment between 50 and 80 seedlings were grown and inoculated for each condition as per spot inoculation protocol (Methods 4), with the spot being indicated additionally to the normal method by marking a small circle directly above it, on the clear plastic plate cover, with a pen. The nodules where scored for presence-absence and emergence (break of the epidermis) 8dpi and 2wpi (data shown). I used the Chi-square 2x5 test with Marascuilo 2x5 correction as the overall statistical test for significance of differences in the nodule presence-absence contingency table (data shown), and Fisher exact test for preliminary paired experiments leading up to the main experiments.

13. **Spot treatment with droplets** containing different chemicals was performed with the same protocol as in spot inoculation (Methods 5). Droplet composition is the following: BAP treatment= 6-Benzylaminopurine 10μM or 100μM in water, BAP+NF= 6-Benzylaminopurine 10μM and *S.m.* Nod-Factor 10μM in water, NF-mix= Nod-Factor 10μM + peptidoglycan (PGN) 0,05mg/ml and Acetazolamide 10μM in water (see Methods 15), IAA= Indole-3-acetic acid 1μM or 2.5μM in water, NPA= 1-naphthylphthalamic acid 100μM or 1mM in water with traces of DMSO from the stock, TIBA= 2,3,5-triiodobenzoic acid 100μM or 1mM in water with DMSO traces, Water= water with

DMSO traces, to control for DMSO in other treatments, GR24= 1-Methyl-2-oxindole 1μM in water.

14. **YUCCA phylogenetic tree**: The evolutionary history was inferred by using the Maximum Likelihood method based on the *Le Gascuel 2008* model[353]. The tree with the highest log likelihood (-10185.11) is shown. The percentage of trees in which the associated taxa clustered together is shown next to the branches. Initial tree(s) for the heuristic search were obtained automatically by applying Neighbor-Join and BioNJ algorithms to a matrix of pairwise distances estimated using a JTT model, and then selecting the topology with superior log likelihood value. A discrete Gamma distribution was used to model evolutionary rate differences among sites (5 categories (+G, parameter = 0.8746)). The tree is drawn to scale, with branch lengths measured in the number of substitutions per site. The analysis involved 26 amino acid sequences. All positions containing gaps and missing data were eliminated. There were a total of 363 positions in the final dataset. Evolutionary analyses were conducted in MEGA7 [354]. The phylogenetic tree presented in chapter 3 is part of a larger tree containing YUCCAs from multiple species, for better inference of phylogenomics. I included YUCCA sequences from the species *Medicago truncatula, Arabidopsis thaliana, Solanum lycopersicum, Populus trichocarpa, Glycine max, Brachypodium distachyon, Oryza sativa*, and *Physcomitrella patens* for outgroup.

15. **Spot treatment of** *Medicago sativa* (**alfalfa**) seedlings **with Nod-factor** solution was performed in identical way to Methods 5. The spot-treatment solution consists of water with purified *S.m.* Nod-factors at a final concentration of 10μM, kindly provided by Jongho Sun. If the nodule formation rate is low, treatment solution can be enriched to contain peptidoglycan (PGN) 0,05mg/ml and Acetazolamide 10μM , to increase the rate. Both were kindly provided by Jongho Sun and Feng Feng. Alfalfa seeds were obtained by Brown Seeds.

16. **Trans-Activation Assay** (TAA) was performed using the Agro-infiltration of tobacco leaves alternative method described here[334]. For more information on this protocol please consult Nadiatul (Nadia) A. Mohd-Radzman[44]. Briefly, the constructs indicated in the text where used to transform *Agrobacterium tumefaciens* , which was used to agro-infiltrate young (3 weeks post germination) *Nicotiana benthamiana* leaves. After 2 days, 1cm discs were cut out from the infection site and used for confocal verification of the localization of the transcription-factor-GFP fusion protein, or they were put in tubes with a small steel sphere, frozen using liquid nitrogen, ground using a tissue lyser (orbital shaker), vortexed in the presence of Passive Lysis Buffer, and the supernatant

was used for luciferase assay[334] (differential activity) using a 96-well luminometer.

17. **PAT Model:** The starting simulation environment is the one provided by figure 9D of Abley *et al,* 2016[297], which is provided in its entirety in the article supplementary source code 12 (https://doi.org/10.7554/eLife.18165.040). It is based in terms of implementation on the VVe modeling environment[355]. Code is available on request, and extensive documentation comes with the paper. The model represents a tissue using cell complexes (vertex graph model of multiple vertices representing intracellular space, membranes and walls), with many wall elements, and each vertex holds the local concentrations of chemicals. Chemicals explicitly considered in the simulation are polarizers (head *h* and base *b*) that interact with each other to give internal polarity to the cell by emergently separating their concentration peaks at opposite sides of the cell, and a mediator *m* which in this case represents auxin. The mediator interacts with the polarizers differentially, leading to coordination of the polarizer polarity across neighboring cells. Polarizer concentration affects mediator transport as well. The functions and parameters used for the interaction between chemicals can be found in the original publication[297]. I downloaded the source code zip directory provided above, and the model folders were opened in L-studio with VVe (downloaded from http://algorithmicbotany.org/virtual_laboratory/). I implemented modifications, which can be found, in concise form, in the following code:

```
// find updateOrganisers() call and replace it with
   updateOrganisersGiannis()=
        //updateOrganisers();
        updateOrganisersGiannis();   //Giannis

//add the updateOrganisersGiannis() function somewhere under the
   Model{}

void updateOrganisersGiannis(){
  if (time <1){
   forall const node& n in S:{
     if (n->type ==NT_CELL){
       if ((n->pos[0] < 3 and n->pos[1] < 9) || (n->pos[0] > 20 and n
          ->pos[1] > 9)) //create the plus organisers (auxin
          producers representing auxin influx at the boundary cells)
       {
         n->isPlus =true;
         n->production[2] = 2; //production rate can vary, 2 works
            for reflux loop creation
         std::cout << "position- n->pos[0]= " << n->pos[0] << ", and
```

```
            n->pos[1]= " << n->pos[1] << " became a plus organiser"
            << std::endl;
        }
        if ((n->pos[0] > 20 and n->pos[1] < 9) || (n->pos[0] < 3 and n
           ->pos[1] > 9)) // minus organisers creation(auxin sinks-
           auxin outflux at the boundary)
        {
          n->isMinus =true;
          n->degradation[2] = 2;  //degradation rate in outflux
              boundary cells
          std::cout << "position- n->pos[0]= " << n->pos[0] << ", and
              n->pos[1]= " << n->pos[1] << " became a minus organiser"
              << std::endl;
        }
      }
    }
    forall const cell& c in T.C:{
      if (((c->pos[0] < 3 and c->pos[1] < 9) || (c->pos[0] > 20 and c
         ->pos[1] > 9)) && c->type ==C_NORMAL)
      {
        c->isPlus =true;
        c->type = C_PLUS;
      }
      if (((c->pos[0] > 20 and c->pos[1] < 9) || (c->pos[0] < 3 and c
         ->pos[1] > 9)) && c->type ==C_NORMAL)
      {
        c->isMinus =true;
        c->type = C_MINUS;
      }
    }
  }

  if (time > 1200){//put some YUCCAs (auxin biosynthesis) working on
     the proximal to the infection vasculature
    forall const node& n in S:{
      if (n->type ==NT_CELL and n->isMinus ==false && (n->pos[0] > 7
         && n->pos[0] < 15 && n->pos[1] > 9 &&  n->pos[1] < 12))
      {
        n->isPlus = true;
        n->production[2] = 10;
        std::cout << "Position- n->pos[0]= " << n->pos[0] << ", and n
           ->pos[1]= " << n->pos[1] << " became a YUCCA plus
           organiser" << std::endl;
      }
```

```
    }
    forall const cell& c in T.C:{ // then, go through the tissue
       graph and change the properties of the cell so it can be drawn
      if (c->type ==C_NORMAL && c->isMinus ==false && (c->pos[0] > 7
         && c->pos[0] < 15 && c->pos[1] > 9 &&  c->pos[1] < 12))
      {
        c->isBasal =false;
        c->isPlus =true;
        c->type = C_PLUS;
        std::cout <<" setting a cell in tissue graph to be a YUCCA
           organiser, its position is:" <<c->pos <<std::endl;
      }
    }
  }
}

//change GridSize in the parameter file view.v to "GridSize:14 14"
```

Essentially, the changes presented above describe how the boundaries of the tissue have cells that produce and degrade auxin at a constant rate (presented in orange and blue color respectively in the simulation result figures), as a way to introduce boundary auxin fluxes in the simulation domain. These represent the vascular and cortical auxin flow. After 1200 simulation steps, which I identified in earlier simulations to be the time it takes for a reflux loop to form and stabilize, I introduce auxin production in central cells representing nodule initiation domains. Although I performed some parameter changes to test for stability of results, proving the result is robust to parameter changes, the parameters were kept the same as in the origin source code. The resulting code folder for *Medicago* simulations can be found here:Medicago, and for *Lotus* simulations here: Lotus. Please contact me for any queries.

18. **Gene Ontology:** GO enrichment was performed using the agriGO analysis toolkit[305]. I first assembled the lists of identifiers corresponding to the sets of upregulated and downregulated genes (separate lists) in each timepoint of our RNA-seq timecourse. I then used the available online analysis tool (http://bioinfo.cau.edu.cn/agriGO/analysis.php) to test for enrichment of GO terms in respect to suggested backgrounds or customized reference of random gene identifier sets. I used both Singular Enrichment Analysis and Parametric Analysis of Gene Set Enrichment tools and combined significant results for presentation in this thesis.

19. **Visualization** of R2D2, auxin, cytokinin reporter lines is performed either using a Zeiss 780 and 880 confocal microscope with 10x, 20x and 40x lenses, or a Leica M205FA

stereo microscope. GUS staining microscopy pictures were obtained using a Leica DM6000 compound microscope with 20X air objective and bright field settings. The lasers used for the excitation of GFP, Venus (eGFP) and mCherry are Argon laser emitting at 488 nm and DPSS 561-10 Yellow-Green laser emitting at 561nm. The fluorescence detection ranges used are 493-550nm for eGFP with a peak at 522nm and 578-694 for mCherry with a peak at 636nm.

20. **RNA-seq timecourse:** For spot inoculation and generation of transcriptomic timecourse of nodule development, roots were dissected to produce 2mm to 3mm segments of the spot of inoculation and mock spot treatment, at different timepoints after spot inoculation. About 50 to 60 segments were instantly frozen in liquid nitrogen and pooled to obtain 1 biological replicate, and 3-6 replicates per timepoint were analyzed. RNA was extracted using the RNeasy Micro Kit (Qiagen), the RNase free DNase kit (Qiagen) was used to remove genomic DNA. RNA sequencing (RNA-Seq) was performed by IMGM Laboratories (Martinsried, Germany). RNA-Seq libraries were prepared with the Illumina TruSeq® Stranded mRNA HT kit and sequencing of the libraries was performed on the Illumina NextSeq500 next generation sequencing system using the high output mode with 1 x 75 bp single-end read chemistry. The resulting reads from the raw fastq data were quality controlled and and mapped to the most recent M. truncatula reference genome version 4.0 (Mtv4.0) using the R package STAR. The counts and RPKM (Reads per kilobase per million mapped reads) values were calculated with featureCounts in R package Rsubread. Non-metric multidimensional scaling was exploited to account for outliers. Genes that show low expression throughout all samples were removed by measuring CPM (counts per million) values using R package edgeR. Differentially expressed genes (DEGs) were identified by pairwise comparisons of raw counts using the R package DESeq2 with the threshold of absolute fold change of over 1.5 and a false discovery rate (FDR) corrected p-value lower than 0.05.

21. **GUS staining**: We wash roots in water and fix them in 90% acetone for 1 hr, on ice. After that we replace acetone by a wash solution containing 50 mM phosphate buffer pH 7.2. The wash buffer is then replaced by a β-Glucuronidase (GUS) staining buffer containing 50 mM phosphate buffer pH 7.2, 0.5 mM K3Fe(CN)6 (potassium ferricyanide), 0.5 mM K4Fe(CN)6 (potassium ferrocyanide) and 2 mM X-Gluc (5-bromo-4-chloro-3-indolyl-beta-D-glucuronide, Melford), vacuum infiltrated for 15 min and incubated at 37°C overnight. For X-Gal staining, the tissue was washed in 50 mM phosphate buffer pH 7.2 and fixed in 2.5% glutaraldehyde by vacuum infiltration for 15 min and incubation at room temperature for 1 hr. Tissue was washed 3X in Z-buffer containing

100 mM phosphate buffer pH 7, 10 mM KCl, 1 mM MgCl2 and incubated in X-Gal staining buffer (Z-buffer supplemented with 5 mM K3Fe(CN)6, 5 mM K4Fe(CN)6 and 0.08% Magenta-GAL (5-Bromo-6-chloro-3-indolyl-B-D-galactopyranoside, Melford)) at 28°C overnight and washed with water 3 times. Tissue was cleared, stored and imaged in chloral hydrate solution. Images were obtained using a Leica DM6000 compound microscope 20X air objective with bright field settings.

22. Golden Gate DNA constructs used throughout this thesis are presented in Table 7.1 bellow.

Table 7.1: Golden Gate construct breakdown tables

ENSA Standard name, or experiment the constructs are used in	Backbone vector	Position 1	Position 2	Position 3	Position 4
PIN2 and PIN9 fluorescent protein reporters and promoter-GUS reporters (section 2.2.4, figure 2.5, 2.6)					
EC20520_pL2B_pAtUBI10::NLS-mCherry_pLjUBI1::gMtPIN2-361VENUS-20520	EC50506_pL2V-1	EC20488_pL1M-R1-pAtUBI10::NLS-mCherry-tNOS-20488	EC20490_pL1M-R2-pLjUBI1-gMtPIN2-361VENUS-t35S-20490	EC41744_pL1M-ELE-2-41744	
EC20523_pL2B_pAtUBI10::NLS-mCherry_pMtPIN2::gMtPIN2-361VENUS-20523	EC50506_pL2V-1	EC20488_pL1M-R1-pAtUBI10::NLS-mCherry-tNOS-20488	EC20493_pL1M-R2-pMtPIN2-gMtPIN2-361VENUS-tPIN2-20493	EC41744_pL1M-ELE-2-41744	
EC20871_pL2B_pAtUBI10::NLS-mCherry_pLjUBI1::gMtPIN9-331VENUS_20871	EC50506_pL2V-1	EC20488_pL1M-R1-pAtUBI10::NLS-mCherry-tNOS-20488	EC20498_pL1M-R2-pLjUBI1-gMtPIN9-331VENUS-t35S-20498	EC41744_pL1M-ELE-2-41744	
EC12029_pL2B_KAN_pMtPIN2::GUS_pAtUBI10::dsRed-12029	EC50506_pL2V-1	EC15029 pL1M-R1-pNOS-KAN-tNOS	EC11472_pL1M-R2-pMtPIN2-GUS-t35S-11472	EC15034 pL1M-R3-pAtUBI10-dsRed-tNOS	EC41766-pL1M-ELE-3-41766
EC12032_pL2B_KAN_pMtPIN9::GUS_pAtUBI10::dsRed-12032	EC50506_pL2V-1	EC15029 pL1M-R1-pNOS-KAN-tNOS	EC11474_pL1M-R2-pMtPIN9-GUS-t35S-11474	EC15034 pL1M-R3-pAtUBI10-dsRed-tNOS	EC41766-pL1M-ELE-3-41766

ENSA Standard name, or experiment the constructs are used in	Backbone vector	Position 1	Position 2	Position 3	Position 4	Position 5
Transactivation assay, successful constructs (section 4.2.2, figure 4.3)						
EC19317_pL2B-pYUC3:nLUC-p35S:PLT3-Venus	EC50506_pL2V-1	EC22799 pL1M-R1-pNOS-P19-tNOS	EC22800 pL1M-R2-pAtUbi10-LUC-tAct2	EC19303_pL1M-R3_pMtYUC3-Nluc-t35s	EC22805 pL1M-R4-p35s-PLT3-Venus-t35S	EC41780_pL1M-ELE-4-41780
EC19318_pL2B-pYUC3:nLUC-p35S:Venus	EC50506_pL2V-1	EC22799 pL1M-R1-pNOS-P19-tNOS	EC22800 pL1M-R2-pAtUbi10-LUC-tAct2	EC19303_pL1M-R3_pMtYUC3-Nluc-t35s	EC22806 pL1M-R4-p35s-Venus-t35S	EC41780_pL1M-ELE-4-41780
EC19319_pL2B-pYUC2:nLUC-p35S:NIN-Venus	EC50506_pL2V-1	EC22799 pL1M-R1-pNOS-P19-tNOS	EC22800 pL1M-R2-pAtUbi10-LUC-tAct2	EC19304_pL1M-R3_pMtYUC2-Nluc-t35s	EC22804 pL1M-R4-p35s-NIN-Venus-t35S	EC41780_pL1M-ELE-4-41780
EC19322_pL2B-pYUC2:nLUC-p35S:Venus	EC50506_pL2V-1	EC22799 pL1M-R1-pNOS-P19-tNOS	EC22800 pL1M-R2-pAtUbi10-LUC-tAct2	EC19304_pL1M-R3_pMtYUC2-Nluc-t35s	EC22806 pL1M-R4-p35s-Venus-t35S	EC41780_pL1M-ELE-4-41780
EC19323_pL2B-pYUC5:nLUC-p35S:NIN-Venus	EC50506_pL2V-1	EC22799 pL1M-R1-pNOS-P19-tNOS	EC22800 pL1M-R2-pAtUbi10-LUC-tAct2	EC19305_pL1M-R3_pMtYUC5-Nluc-t35s	EC22804 pL1M-R4-p35s-NIN-Venus-t35S	EC41780_pL1M-ELE-4-41780
EC19325_pL2B-pYUC5:nLUC-p35S:PLT3-Venus	EC50506_pL2V-1	EC22799 pL1M-R1-pNOS-P19-tNOS	EC22800 pL1M-R2-pAtUbi10-LUC-tAct2	EC19305_pL1M-R3_pMtYUC5-Nluc-t35s	EC22805 pL1M-R4-p35s-PLT3-Venus-t35S	EC41780_pL1M-ELE-4-41780
EC19326_pL2B-pYUC5:nLUC-p35S:Venus	EC50506_pL2V-1	EC22799 pL1M-R1-pNOS-P19-tNOS	EC22800 pL1M-R2-pAtUbi10-LUC-tAct2	EC19305_pL1M-R3_pMtYUC5-Nluc-t35s	EC22806 pL1M-R4-p35s-Venus-t35S	EC41780_pL1M-ELE-4-41780
EC19329_pL2B-pLBD16:nLUC-p35S:NIN-Venus	EC50506_pL2V-1	EC22799 pL1M-R1-pNOS-P19-tNOS	EC22800 pL1M-R2-pAtUbi10-LUC-tAct2	EC19306_pL1M-R3_pMtLBD16-Nluc-t35s	EC22804 pL1M-R4-p35s-NIN-Venus-t35S	EC41780_pL1M-ELE-4-41780
EC19330_pL2B-pLBD16:nLUC-p35S:Venus	EC50506_pL2V-1	EC22799 pL1M-R1-pNOS-P19-tNOS	EC22800 pL1M-R2-pAtUbi10-LUC-tAct2	EC19306_pL1M-R3_pMtLBD16-Nluc-t35s	EC22806 pL1M-R4-p35s-Venus-t35S	EC41780_pL1M-ELE-4-41780

ENSA Standard name, or experiment the constructs are used in	Backbone vector	Position 1	Position 2	Position 3	Position 4	Position 5
R2D2 auxin reporter (section 2.2, Methods 9)						
EC20865_pL2B_pNOS::KAN_pLjUBI1E7606606_pL2V-1 MtDII-NLS_pLjUBI1::mCherry-sMtDII-NLS_pAtUBI10::PM-cyPET_20865	EC15029 pL1M-R1-pNOS-KAN-tNOS	EC11950_pL1M-R2-pLjUBI1-VENUS-2xGS4xGS4xGS2xG-MtIAA27-KQ-RK-GAGA-NLS-t35S-11950	EC20866_pL1M-R3-pLjUBI1-mCherry-2xGS4xGS4xGS2xG-MtIAA27-KQ-RK-P177L-GAGA-NLS-t35S_20866	EC20547_pL1M-R4-pAtUBI10-PM-cyPET-tAgs-20547	EC41780-pL1M-ELE-4-41780	
EC21244_pL2B_pNOS::BASTA_pLjUBI1E7606606_pL2V-1 sMtDII-NLS_pLjUBI1::mCherry-MtDII-NLS	EC15324_pL1M-R1-pNOS-BAR-tNOS-15324	EC11950_pL1M-R2-pLjUBI1-VENUS-2xGS4xGS4xGS2xG-MtIAA27-KQ-RK-GAGA-NLS-t35S-11950	EC20866_pL1M-R3-pLjUBI1-mCherry-2xGS4xGS4xGS2xG-MtIAA27-KQ-RK-P177L-GAGA-NLS-t35S_20866	EC41766-pL1M-ELE-3-41766	x	
EC21245_pL2B_pNOS::BASTA_pLjUBI1E7606606_pL2V-1 sMtDII-NLS_pLjUBI1::mCherry-MtDII-NLS_pAtUBI10::PM-cyPET	EC15324_pL1M-R1-pNOS-BAR-tNOS-15324	EC11950_pL1M-R2-pLjUBI1-VENUS-2xGS4xGS4xGS2xG-MtIAA27-KQ-RK-GAGA-NLS-t35S-11950	EC20866_pL1M-R3-pLjUBI1-mCherry-2xGS4xGS4xGS2xG-MtIAA27-KQ-RK-P177L-GAGA-NLS-t35S_20866	EC20547_pL1M-R4-pAtUBI10-PM-cyPET-tAgs-20547	EC41780-pL1M-ELE-4-41780	
EC21246_pL2B_pNOS::BASTA_pLjUBI1E7606606_pL2V-1 sMtDII-NLS_pLjUBI1::mCherry-MtDII-NLS_pAtUBI10::PM-cyPET	EC15324_pL1M-R1-pNOS-BAR-tNOS-15324	EC20868_pL1M-R2-pLjUBI1-3xVenus-2xGS4xGS4xGS2xG-MtIAA27-KQ-RK-GAGA-NLS-t35S_20868	EC20866_pL1M-R3-pLjUBI1-mCherry-2xGS4xGS4xGS2xG-MtIAA27-KQ-RK-P177L-GAGA-NLS-t35S_20866	EC20547_pL1M-R4-pAtUBI10-PM-cyPET-tAgs-20547	EC41780-pL1M-ELE-4-41780	

ENSA Standard name, or experiment the constructs are used in	Backbone vector	Position 1	Position 2	Position 3	Position 4
Auxin and Cytokinin as Activator and Inhibitor in Reaction Diffusion, constructs (section 4.2.1)					
EC19240_S10_pL2B_pDR5-eGFP_pAtUBI10-mCherry_pAtUBI10-YUC	EC50506_pL2V-1	S1_pL1M-R1-pDR5-NLS-eGFP-TNos	S2_pL1M-R2-pAtUBI10-NLS-mCherry-T35S	S4_pL1M-R3-pAtUBI10-YUC-TNos	EC41766-pL1M-ELE-3-41766
EC19241_S13_pL2B_pDR5v2-eGFP_pTCS-mCherry	EC50506_pL2V-1	S6_pL1M-R1-pDR5v2-NLS-eGFP-TNos	S3_pL1M-R2-pTCS-NLS-mCherry-T35S	EC41744_pL1M-ELE-2-41744	
EC19242_S14_pL2B_pDR5-eGFP_pTCS-mCherry_pAtUBI10-YUC	EC50506_pL2V-1	S1_pL1M-R1-pDR5-NLS-eGFP-TNos	S3_pL1M-R2-pTCS-NLS-mCherry-T35S	S4_pL1M-R3-pAtUBI10-YUC-TNos	EC41766-pL1M-ELE-3-41766
EC19243_S15_pL2B_pDR5-eGFP_pTCS-mCherry_pDR5-YUC	EC50506_pL2V-1	S1_pL1M-R1-pDR5-NLS-eGFP-TNos	S3_pL1M-R2-pTCS-NLS-mCherry-T35S	S7_pL1M-R3-pDR5-YUC-TNos	EC41766-pL1M-ELE-3-41766
EC19244_S16_pL2B_pDR5-eGFP_pTCS-mCherry_pDR5v2-YUC	EC50506_pL2V-1	S1_pL1M-R1-pDR5-NLS-eGFP-TNos	S3_pL1M-R2-pTCS-NLS-mCherry-T35S	S8_pL1M-R3-pDR5v2-YUC-TNos	EC41766-pL1M-ELE-3-41766
EC19245_S17_pL2B_pDR5-eGFP_pTCS-mCherry_pTCS-YUC	EC50506_pL2V-1	S1_pL1M-R1-pDR5-NLS-eGFP-TNos	S3_pL1M-R2-pTCS-NLS-mCherry-T35S	S9_pL1M-R3-pTCS-YUC-TNos	EC41766-pL1M-ELE-3-41766
EC19246_S18_pL2B_pDR5v2-eGFP_pTCS-mCherry_pAtUBI10-YUC	EC50506_pL2V-1	S6_pL1M-R1-pDR5v2-NLS-eGFP-TNos	S3_pL1M-R2-pTCS-NLS-mCherry-T35S	S4_pL1M-R3-pAtUBI10-YUC-TNos	EC41766-pL1M-ELE-3-41766
EC19247_S19_pL2B_pDR5v2-eGFP_pTCS-mCherry_pDR5-YUC	EC50506_pL2V-1	S6_pL1M-R1-pDR5v2-NLS-eGFP-TNos	S3_pL1M-R2-pTCS-NLS-mCherry-T35S	S7_pL1M-R3-pDR5-YUC-TNos	EC41766-pL1M-ELE-3-41766
EC19248_S20_pL2B_pDR5v2-eGFP_pTCS-mCherry_pDR5v2-YUC	EC50506_pL2V-1	S6_pL1M-R1-pDR5v2-NLS-eGFP-TNos	S3_pL1M-R2-pTCS-NLS-mCherry-T35S	S8_pL1M-R3-pDR5v2-YUC-TNos	EC41766-pL1M-ELE-3-41766
EC19249_S21_pL2B_pDR5v2-eGFP_pTCS-mCherry_pTCS-YUC	EC50506_pL2V-1	S1_pL1M-R1-pDR5-NLS-eGFP-TNos	S3_pL1M-R2-pTCS-NLS-mCherry-T35S	S4_pL1M-R3-pAtUBI10-YUC-TNos	EC41766-pL1M-ELE-3-41766

ENSA Standard name, or experiment the constructs are used in	Backbone vector	Position 1	Position 2	Position 3	Position 4	Position 5	Position 6
Auxin and Cytokinin as Activator and Inhibitor in Reaction Diffusion, constructs (section 4.2.1)							
EC19256_S45_pL2B_pDR5-eGFP_pTCS-mCherry_pNos-mTurq2_p35s-P19_pDR5-LjIPT3	EC50506_pL2V-1	S1_pL1M-R1-pDR5-NLS-eGFP-TNos	S3_pL1M-R2-pTCS-NLS-mCherry-T35S	S22_pL1M-R3-pNos-mTurq2-NLS2-tNOS	S23_pL1M-R4-p35S-P19-tHsp	S29_pL1M-R5-pDR5-LjIPT3-t35s	EC41800_pL1M-ELE-5-41800
EC19257_S47_pL2B_pDR5-eGFP_pTCS-mCherry_pNos-mTurq2_p35s-P19_pDR5-CKX3	EC50506_pL2V-1	S1_pL1M-R1-pDR5-NLS-eGFP-TNos	S3_pL1M-R2-pTCS-NLS-mCherry-T35S	S22_pL1M-R3-pNos-mTurq2-NLS2-tNOS	S23_pL1M-R4-p35S-P19-tHsp	S31_pL1M-R5-pDR5-CKX3-t35s	EC41800_pL1M-ELE-5-41800
EC19258_S53_pL2B_pDR5-eGFP_pTCS-mCherry_pNos-mTurq2_p35s-P19_pTCS-LjIPT3	EC50506_pL2V-1	S1_pL1M-R1-pDR5-NLS-eGFP-TNos	S3_pL1M-R2-pTCS-NLS-mCherry-T35S	S22_pL1M-R3-pNos-mTurq2-NLS2-tNOS	S23_pL1M-R4-p35S-P19-tHsp	S37_pL1M-R5-pTCS-LjIPT3-t35s	EC41800_pL1M-ELE-5-41800
EC19259_S55_pL2B_pDR5-eGFP_pTCS-mCherry_pNos-mTurq2_p35s-P19_pTCS-CKX3	EC50506_pL2V-1	S1_pL1M-R1-pDR5-NLS-eGFP-TNos	S3_pL1M-R2-pTCS-NLS-mCherry-T35S	S22_pL1M-R3-pNos-mTurq2-NLS2-tNOS	S23_pL1M-R4-p35S-P19-tHsp	S39_pL1M-R5-pTCS-CKX3-t35s	EC41800_pL1M-ELE-5-41800
EC19266_S68_pL2B_pDR5-eGFP_pTCS-mCherry_pNos-mTurq2_p35s-P19	EC50506_pL2V-1	S1_pL1M-R1-pDR5-NLS-eGFP-TNos	S3_pL1M-R2-pTCS-NLS-mCherry-T35S	S22_pL1M-R3-pNos-mTurq2-NLS2-tNOS	S23_pL1M-R4-p35S-P19-tHsp	EC41780_pL1M-ELE-4-41780	
EC19267_S74_pL2B_pDR5-eGFP_pTCS-mCherry_pNos-mTurq2_p35s-P19_pNos-IPT3	EC50506_pL2V-1	S1_pL1M-R1-pDR5-NLS-eGFP-TNos	S3_pL1M-R2-pTCS-NLS-mCherry-T35S	S22_pL1M-R3-pNos-mTurq2-NLS2-tNOS	S23_pL1M-R4-p35S-P19-tHsp	S61_pL1M-R5-pNos-IPT3-t35s	EC41800_pL1M-ELE-5-41800
EC19268_S76_pL2B_pDR5-eGFP_pTCS-mCherry_pNos-mTurq2_p35s-P19_PNos-CKX3	EC50506_pL2V-1	S1_pL1M-R1-pDR5-NLS-eGFP-TNos	S3_pL1M-R2-pTCS-NLS-mCherry-T35S	S22_pL1M-R3-pNos-mTurq2-NLS2-tNOS	S23_pL1M-R4-p35S-P19-tHsp	S63_pL1M-R5-pNos-CKX3-t35S	EC41800_pL1M-ELE-5-41800
EC19269_S77_pL2B_pDR5-eGFP_pTCS-mCherry_pNos-mTurq2_p35s-P19_pNos-GH3.1	EC50506_pL2V-1	S1_pL1M-R1-pDR5-NLS-eGFP-TNos	S3_pL1M-R2-pTCS-NLS-mCherry-T35S	S22_pL1M-R3-pNos-mTurq2-NLS2-tNOS	S23_pL1M-R4-p35S-P19-tHsp	S64_pL1M-R5-pNos-GH3.1-t35S	EC41800_pL1M-ELE-5-41800

ENSA Standard name, or experiment the constructs are used in	Backbone vector	Position 1	Position 2	Position 3	Position 4	Position 5	Position 6
Auxin and Cytokinin as Activator and Inhibitor in Reaction Diffusion, constructs (section 4.2.1)							
EC19270_S78_pL2B_pDR5-eGFP_pTCS-mCherry_pNos-mTurq2_p35s-P19_pNos-GH3.3	EC50506_pL2V-1	S1_pL1M-R1-pDR5-NLS-eGFP-TNos	S3_pL1M-R2-pTCS-NLS-mCherry-T35S	S22_pL1M-R3-pNos-mTurq2-NLS2-tNOS	S23_pL1M-R4-p35S-P19-tHsp	S65_pL1M-R5-pNos-GH3.3-t35S	EC41800_pL1M-ELE-5-41800
EC19271_S82_pL2B_pDR5-eGFP_pTCS-mCherry_pNos-mTurq2_p35s-P19_pDR5-CKX3_pTCS-GH3.3	EC50506_pL2V-1	S1_pL1M-R1-pDR5-NLS-eGFP-TNos	S3_pL1M-R2-pTCS-NLS-mCherry-T35S	S22_pL1M-R3-pNos-mTurq2-NLS2-tNOS	S23_pL1M-R4-p35S-P19-tHsp	S31_pL1M-R5-pDR5-CKX3-t35s	S66_pL1M-R6-pTCS-GH3.3-tHsp
EC19281_S92_pL2B_pDR5-eGFP_pTCS-mCherry_pNos-mTurq2_p35s-P19_pDR5-LjIPT3_pTCS-GH3.3-ELB6	EC50506_pL2V-1	S1_pL1M-R1-pDR5-NLS-eGFP-TNos	S3_pL1M-R2-pTCS-NLS-mCherry-T35S	S22_pL1M-R3-pNos-mTurq2-NLS2-tNOS	S23_pL1M-R4-p35S-P19-tHsp	S29_pL1M-R5-pDR5-LjIPT3-t35s	S66_pL1M-R6-pTCS-GH3.3-tHsp
EC19282_S93_pL2B_pDR5-eGFP_pTCS-mCherry_pNos-mTurq2_p35s-P19_pDR5-CKX3_pTCS-Medtr6g(Yuc)-ELB6	EC50506_pL2V-1	S1_pL1M-R1-pDR5-NLS-eGFP-TNos	S3_pL1M-R2-pTCS-NLS-mCherry-T35S	S22_pL1M-R3-pNos-mTurq2-NLS2-tNOS	S23_pL1M-R4-p35S-P19-tHsp	S31_pL1M-R5-pDR5-CKX3-t35s	S89_pL1M-R6-pTCS-Medtr6g086879(YUC)-t35s
EC19283_S94_pL2B_pDR5-eGFP_pTCS-mCherry_pNos-mTurq2_p35s-P19_pDR5-LjIPT3_pTCS-Medtr6g(Yuc)-ELB-6	EC50506_pL2V-1	S1_pL1M-R1-pDR5-NLS-eGFP-TNos	S3_pL1M-R2-pTCS-NLS-mCherry-T35S	S22_pL1M-R3-pNos-mTurq2-NLS2-tNOS	S23_pL1M-R4-p35S-P19-tHsp	S29_pL1M-R5-pDR5-LjIPT3-t35s	S89_pL1M-R6-pTCS-Medtr6g086879(YUC)-t35s
EC19284_S98_pL2B_pDR5-eGFP_pTCS-mCherry_pNos-mTurq2_p35s-P19_pDR5-LjIPT3_pTCS-Medtr6g(Yuc)-ELE-6	EC50506_pL2V-1	S1_pL1M-R1-pDR5-NLS-eGFP-TNos	S3_pL1M-R2-pTCS-NLS-mCherry-T35S	S22_pL1M-R3-pNos-mTurq2-NLS2-tNOS	S23_pL1M-R4-p35S-P19-tHsp	S29_pL1M-R5-pDR5-LjIPT3-t35s	S89_pL1M-R6-pTCS-Medtr6g086879(YUC)-t35s
EC19285_S99_pL2B_pDR5-eGFP_pTCS-mCherry_pNos-mTurq2_p35s-P19_pDR5-CKX3_pTCS-Medtr6g(Yuc)-ELE6	EC50506_pL2V-1	S1_pL1M-R1-pDR5-NLS-eGFP-TNos	S3_pL1M-R2-pTCS-NLS-mCherry-T35S	S22_pL1M-R3-pNos-mTurq2-NLS2-tNOS	S23_pL1M-R4-p35S-P19-tHsp	S31_pL1M-R5-pDR5-CKX3-t35s	S89_pL1M-R6-pTCS-Medtr6g086879(YUC)-t35s

ENSA Standard name, or experiment the constructs are used in	Backbone vector	Position 1	Position 2	Position 3	Position 4	Position 5	Position 6
Auxin and Cytokinin as Activator and Inhibitor in Reaction Diffusion, constructs (section 4.2.1)							
EC19286_S100_pL2B_pDR5-eGFP_pTCS-mCherry_pNos-mTurq2_p35s-P19_pDR5-LjIPT3_pTCS-GH3.3-ELE6	EC50506_pL2V-1	S1_pL1M-R1-pDR5-NLS-eGFP-TNos	S3_pL1M-R2-pTCS-NLS-mCherry-T35S	S22_pL1M-R3-pNos-mTurq2-NLS2-tNOS	S23_pL1M-R4-p35S-P19-tHsp	S29_pL1M-R5-pDR5-LjIPT3-t35s	S66_pL1M-R6-pTCS-GH3.3-tHsp
EC19287_S101_pL2B_pDR5-eGFP_pTCS-mCherry_pNos-mTurq2_p35s-P19_pNos-Medtr6g(Yuc)	EC50506_pL2V-1	S1_pL1M-R1-pDR5-NLS-eGFP-TNos	S3_pL1M-R2-pTCS-NLS-mCherry-T35S	S22_pL1M-R3-pNos-mTurq2-NLS2-tNOS	S23_pL1M-R4-p35S-P19-tHsp	S88_pL1M-R5-pNos-Medtr6g(Yuc)-t35s	EC41800_pL1M-ELE-5-41800
EC19288_S102_pL2.2_pDR5-eGFP_pTCS-mCherry_pNos-mTurq2_p35s-P19_pDR5-LjIPT3_pTCS-GH3.3_pDR5-Medtr6g(Yuc)-ELE-7	S92_pL2B_pDR5-eGFP_pTCS-mCherry_pNos-mTurq2_p35s-P19_pDR5-LjIPT3_pTCS-GH3.3-ELB6	S90_pL1M-R7-pDR5-Medtr6g(Yuc)-tNos	ELE7				
EC19289_S103_pL2.2_pDR5-eGFP_pTCS-mCherry_pNos-mTurq2_p35s-P19_pDR5-CKX3_pTCS-Medtr6g(Yuc)_pTCS-ljIPT3_ELE-7	S93_pL2B_pDR5-eGFP_pTCS-mCherry_pNos-mTurq2_p35s-P19_pDR5-CKX3_pTCS-Medtr6g(Yuc)-ELB6	S91_pL1M-R7-pTCS-ljIPT3-tNos	ELE7				
EC19240_S10_pL2B_pDR5-eGFP_pAtUBI10-mCherry_pAtUBI10-YUC	EC50506_pL2V-1	S1_pL1M-R1-pDR5-NLS-eGFP-TNos	S2_pL1M-R2-pAtUBI10-NLS-mCherry-T35S	S4_pL1M-R3-pAtUBI10-YUC-TNos	EC41766-pL1M-ELE-3-41766		
EC19241_S13_pL2B_pDR5v2-eGFP_pTCS-mCherry	EC50506_pL2V-1	S6_pL1M-R1-pDR5v2-NLS-eGFP-TNos	S3_pL1M-R2-pTCS-NLS-mCherry-T35S	EC41744_pL1M-ELE-2-41745			
EC19242_S14_pL2B_pDR5-eGFP_pTCS-mCherry_pAtUBI10-YUC	EC50506_pL2V-1	S1_pL1M-R1-pDR5-NLS-eGFP-TNos	S3_pL1M-R2-pTCS-NLS-mCherry-T35S	S4_pL1M-R3-pAtUBI10-YUC-TNos	EC41766-pL1M-ELE-3-41766		

ENSA Standard name, or experiment the constructs are used in	Backbone vector	Position 1	Position 2	Position 3	Position 4
Auxin and Cytokinin as Activator and Inhibitor in Reaction Diffusion, constructs (section 4.2.1)					
EC19243_S15_pL2B_pDR5-eGFP_pTCS-mCherry_pDR5-YUC	EC50506_pL2V-1	S1_pL1M-R1-pDR5-NLS-eGFP-TNos	S3_pL1M-R2-pTCS-NLS-mCherry-T35S	S7_pL1M-R3-pDR5-YUC-TNos	EC41766-pL1M-ELE-3-41766
EC19244_S16_pL2B_pDR5-eGFP_pTCS-mCherry_pDR5v2-YUC	EC50506_pL2V-1	S1_pL1M-R1-pDR5-NLS-eGFP-TNos	S3_pL1M-R2-pTCS-NLS-mCherry-T35S	S8_pL1M-R3-pDR5v2-YUC-TNos	EC41766-pL1M-ELE-3-41766
EC19245_S17_pL2B_pDR5-eGFP_pTCS-mCherry_pTCS-YUC	EC50506_pL2V-1	S1_pL1M-R1-pDR5-NLS-eGFP-TNos	S3_pL1M-R2-pTCS-NLS-mCherry-T35S	S9_pL1M-R3-pTCS-YUC-TNos	EC41766-pL1M-ELE-3-41766
EC19246_S18_pL2B_pDR5v2-eGFP_pTCS-mCherry_pAtUBI10-YUC	EC50506_pL2V-1	S6_pL1M-R1-pDR5v2-NLS-eGFP-TNos	S3_pL1M-R2-pTCS-NLS-mCherry-T35S	S4_pL1M-R3-pAtUBI10-YUC-TNos	EC41766-pL1M-ELE-3-41766
EC19247_S19_pL2B_pDR5v2-eGFP_pTCS-mCherry_pDR5-YUC	EC50506_pL2V-1	S6_pL1M-R1-pDR5v2-NLS-eGFP-TNos	S3_pL1M-R2-pTCS-NLS-mCherry-T35S	S7_pL1M-R3-pDR5-YUC-TNos	EC41766-pL1M-ELE-3-41766
EC19248_S20_pL2B_pDR5v2-eGFP_pTCS-mCherry_pDR5v2-YUC	EC50506_pL2V-1	S6_pL1M-R1-pDR5v2-NLS-eGFP-TNos	S3_pL1M-R2-pTCS-NLS-mCherry-T35S	S8_pL1M-R3-pDR5v2-YUC-TNos	EC41766-pL1M-ELE-3-41766
EC19249_S21_pL2B_pDR5v2-eGFP_pTCS-mCherry_pTCS-YUC	EC50506_pL2V-1	S1_pL1M-R1-pDR5-NLS-eGFP-TNos	S3_pL1M-R2-pTCS-NLS-mCherry-T35S	S4_pL1M-R3-pAtUBI10-YUC-TNos	EC41766-pL1M-ELE-3-41766
EC21207_pL2B_pDR5-GH3_pTCS-IPT_pDR5-IPT_pTCS-YUC_pDR5-NLS-eGFP_pTCS-NLS-mCherry					
EC21208_pL2B_pDR5-YUC_pTCS-CKX_pDR5-IPT_pTCS-YUC_pDR5-NLS-eGFP_pTCS-NLS-mCherry					
EC21209_pL2B_pDR5-GH3_pTCS-IPT_pDR5-CKX_pTCS-GH3_pDR5-NLS-eGFP_pTCS-NLS-mCherry					
EC21210_pL2B_pDR5-YUC_pTCS-CKX_pDR5-CKX_pTCS-GH3_pDR5-NLS-eGFP_pTCS-NLS-mCherry					

References

[1] Lynn Margulis. Genetic and evolutionary consequences of symbiosis. *Experimental parasitology*, 39(2):277–349, 1976.

[2] Daniel H Janzen. Interaction of the bull's-horn acacia (acacia cornigera l.) with an ant inhabitant (pseudomyrmex ferruginea f. smith) in eastern mexico. *Univ. Kansas Sci. Bull*, 47:315–558, 1967.

[3] Cory C Cleveland, Alan R Townsend, David S Schimel, Hank Fisher, Robert W Howarth, Lars O Hedin, Steven S Perakis, Erika F Latty, Joseph C Von Fischer, Adrien Elseroad, et al. Global patterns of terrestrial biological nitrogen (n2) fixation in natural ecosystems. *Global biogeochemical cycles*, 13(2):623–645, 1999.

[4] J Halliday and JS Pate. Symbiotic nitrogen fixation by coralloid roots of the cycad macrozamia riedlei: physiological characteristics and ecological significance. *Functional Plant Biology*, 3(3):349–358, 1976.

[5] DAVID R Benson and WB Silvester. Biology of frankia strains, actinomycete symbionts of actinorhizal plants. *Microbiology and Molecular Biology Reviews*, 57(2):293–319, 1993.

[6] Allen Van Deynze, Pablo Zamora, Pierre-Marc Delaux, Cristobal Heitmann, Dhileepkumar Jayaraman, Shanmugam Rajasekar, Danielle Graham, Junko Maeda, Donald Gibson, Kevin D Schwartz, et al. Nitrogen fixation in a landrace of maize is supported by a mucilage-associated diazotrophic microbiota. *PLoS biology*, 16(8):e2006352, 2018.

[7] Thomas N Taylor, Winfried Remy, Hagen Hass, and Hans Kerp. Fossil arbuscular mycorrhizae from the early devonian. *Mycologia*, 87(4):560–573, 1995.

[8] Andreas Brachmann and Martin Parniske. The most widespread symbiosis on earth. *PLoS Biol*, 4(7):e239, 2006.

[9] Anouk van 't Padje, Gijsbert DA Werner, and E Toby Kiers. Mycorrhizal fungi control value of phosphorus in trade symbiosis with host roots when exposed to abrupt "crashes" and "booms" of resource availability. *New Phytologist*, 2020.

[10] Gijsbert DA Werner, William K Cornwell, Janet I Sprent, Jens Kattge, and E Toby Kiers. A single evolutionary innovation drives the deep evolution of symbiotic n 2-fixation in angiosperms. *Nature communications*, 5(1):1–9, 2014.

[11] Maximilian Griesmann, Yue Chang, Xin Liu, Yue Song, Georg Haberer, Matthew B Crook, Benjamin Billault-Penneteau, Dominique Lauressergues, Jean Keller, Leandro Imanishi, et al. Phylogenomics reveals multiple losses of nitrogen-fixing root nodule symbiosis. *Science*, 361(6398), 2018.

[12] Giles ED Oldroyd. Speak, friend, and enter: signalling systems that promote beneficial symbiotic associations in plants. *Nature Reviews Microbiology*, 11(4):252–263, 2013.

[13] Zoltan Bozsoki, Kira Gysel, Simon B Hansen, Damiano Lironi, Christina Krönauer, Feng Feng, Noor de Jong, Maria Vinther, Manoj Kamble, Mikkel B Thygesen, et al. Ligand-recognizing motifs in plant lysm receptors are major determinants of specificity. *Science*, 369(6504):663–670, 2020.

[14] Feng Feng, Jongho Sun, Guru V Radhakrishnan, Tak Lee, Zoltán Bozsóki, Sébastien Fort, Aleksander Gavrin, Kira Gysel, Mikkel B Thygesen, Kasper Røjkjær Andersen, et al. A combination of chitooligosaccharide and lipochitooligosaccharide recognition promotes arbuscular mycorrhizal associations in medicago truncatula. *Nature communications*, 10(1):1–12, 2019.

[15] Tomás Allen Rush, Virginie Puech-Pagès, Adeline Bascaules, Patricia Jargeat, Fabienne Maillet, Alexandra Haouy, Arthur Quymanh Maes, Cristobal Carrera Carriel, Devanshi Khokhani, Michelle Keller-Pearson, et al. Lipo-chitooligosaccharides as regulatory signals of fungal growth and development. *Nature communications*, 11(1):1–10, 2020.

[16] Rik Op Den Camp, Arend Streng, Stéphane De Mita, Qingqin Cao, Elisa Polone, Wei Liu, Jetty SS Ammiraju, Dave Kudrna, Rod Wing, Andreas Untergasser, et al. Lysm-type mycorrhizal receptor recruited for rhizobium symbiosis in nonlegume parasponia. *Science*, 331(6019):909–912, 2011.

[17] Senthil Subramanian, Gary Stacey, and Oliver Yu. Distinct, crucial roles of flavonoids during legume nodulation. *Trends in plant science*, 12(7):282–285, 2007.

[18] Anton P Wasson, Flavia I Pellerone, and Ulrike Mathesius. Silencing the flavonoid pathway in medicago truncatula inhibits root nodule formation and prevents auxin transport regulation by rhizobia. *The Plant Cell*, 18(7):1617–1629, 2006.

[19] A Kondorosi, E Kondorosi, CE Pankhurst, WJ Broughton, and Zs Banfalvi. Mobilization of a rhizobium meliloti megaplasmid carrying nodulation and nitrogen fixation genes into other rhizobia and agrobacterium. *Molecular and General Genetics MGG*, 188(3):433–439, 1982.

[20] ESPERANZA Martínez, R Palacios, and F Sanchez. Nitrogen-fixing nodules induced by agrobacterium tumefaciens harboring rhizobium phaseoli plasmids. *Journal of bacteriology*, 169(6):2828–2834, 1987.

[21] Jongho Sun, Feng Feng, and Giles Oldroyd. Recognition of chitooctamers and lipochitooligosaccharides activate symbiosis signaling in plants. In *2019 IS-MPMI XVIII Congress*. ISMPMI, 2019.

[22] Myriam Charpentier, Jongho Sun, Teresa Vaz Martins, Guru V Radhakrishnan, Kim Findlay, Eleni Soumpourou, Julien Thouin, Anne-Aliénor Véry, Dale Sanders, Richard J Morris, et al. Nuclear-localized cyclic nucleotide–gated channels mediate symbiotic calcium oscillations. *Science*, 352(6289):1102–1105, 2016.

[23] Sylvia Singh, Katja Katzer, Jayne Lambert, Marion Cerri, and Martin Parniske. Cyclops, a dna-binding transcriptional activator, orchestrates symbiotic root nodule development. *Cell host & microbe*, 15(2):139–152, 2014.

[24] Leila Tirichine, Niels Sandal, Lene H Madsen, Simona Radutoiu, Anita S Albrektsen, Shusei Sato, Erika Asamizu, Satoshi Tabata, and Jens Stougaard. A gain-of-function mutation in a cytokinin receptor triggers spontaneous root nodule organogenesis. *Science*, 315(5808):104–107, 2007.

[25] Teruyuki Hayashi, Mari Banba, Yoshikazu Shimoda, Hiroshi Kouchi, Makoto Hayashi, and Haruko Imaizumi-Anraku. A dominant function of ccamk in intracellular accommodation of bacterial and fungal endosymbionts. *The Plant Journal*, 63(1):141–154, 2010.

[26] Cheng-Wu Liu, Andrew Breakspear, Nicola Stacey, Kim Findlay, Jin Nakashima, Karunakaran Ramakrishnan, Miaoxia Liu, Fang Xie, Gabriella Endre, Fernanda de Carvalho-Niebel, et al. A protein complex required for polar growth of rhizobial infection threads. *Nature communications*, 10(1):1–17, 2019.

[27] Takema Sasaki, Takuya Suzaki, Takashi Soyano, Mikiko Kojima, Hitoshi Sakakibara, and Masayoshi Kawaguchi. Shoot-derived cytokinins systemically regulate root nodulation. *Nature communications*, 5, 2014.

[28] Ulrike Mathesius. Goldacre paper: Auxin: at the root of nodule development? *Functional Plant Biology*, 35(8):651–668, 2008.

[29] Janet I Sprent, Julie Ardley, and Euan K James. Biogeography of nodulated legumes and their nitrogen-fixing symbionts. *New Phytologist*, 2017.

[30] Francine Perrine-Walker, Patrick Doumas, Mikael Lucas, Virginie Vaissayre, Nicholas J Beauchemin, Leah R Band, Jérome Chopard, Amandine Crabos, Geneviève Conejero, Benjamin Péret, et al. Auxin carriers localization drives auxin accumulation in plant cells infected by frankia in casuarina glauca actinorhizal nodules. *Plant physiology*, 154(3):1372–1380, 2010.

[31] Rene Geurts, Ting Ting Xiao, and Barbara Reinhold-Hurek. What does it take to evolve a nitrogen-fixing endosymbiosis? *Trends in plant science*, 21(3):199–208, 2016.

[32] Howard T Bonnett and Warwick B Silvester. Specificity in the gunnera-nostoc endosymbiosis. *New Phytologist*, pages 121–128, 1981.

[33] Ting Ting Xiao, Stefan Schilderink, Sjef Moling, Eva E Deinum, Eva Kondorosi, Henk Franssen, Olga Kulikova, Andreas Niebel, and Ton Bisseling. Fate map of medicago truncatula root nodules. *Development*, 141(18):3517–3528, 2014.

[34] ANN M HIRSCH. Developmental biology of legume nodulation. *New Phytologist*, 122(2):211–237, 1992.

[35] Marie Turner, Narasimha Rao Nizampatnam, Mathieu Baron, Stéphanie Coppin, Suresh Damodaran, Sajag Adhikari, Shivaram Poigai Arunachalam, Oliver Yu, and Senthil Subramanian. Ectopic expression of mir160 results in auxin hypersensitivity, cytokinin hyposensitivity, and inhibition of symbiotic nodule development in soybean. *Plant physiology*, 162(4):2042–2055, 2013.

[36] Eduardo J Patriarca, Rosarita Tate, Elena Fedorova, Anna Riccio, Roberto Defez, and Maurizio Iaccarino. Down-regulation of the rhizobium ntr system in the determinate nodule of phaseolus vulgaris identifies a specific developmental zone. *Molecular plant-microbe interactions: MPMI (USA)*, 1996.

[37] Jaimie M Van Norman, Wei Xuan, Tom Beeckman, and Philip N Benfey. To branch or not to branch: the role of pre-patterning in lateral root formation. *Development*, 140(21):4301–4310, 2013.

[38] Ann M Hirsch, Thomas A LaRue, and Jeff Doyle. Is the legume nodule a modified root or stem or an organ sui generis? *Critical Reviews in Plant Sciences*, 16(4):361–392, 1997.

[39] PS Nutman. Physiological studies on nodule formation. ii. *The influence of delayed inoculation on the rate of nodula-NEMATODES—-RHIZOBIUM RELATIONSHIPS Taha, Raski*, 211, 1949.

[40] TV Bhuvaneswari, Arvind A Bhagwat, and Wolfgang D Bauer. Transient susceptibility of root cells in four common legumes to nodulation by rhizobia. *Plant Physiology*, 68(5):1144–1149, 1981.

[41] TV Bhuvaneswari, KK Mills, DEBORAH K Crist, WILLIAM R Evans, and WOLFGANG D Bauer. Effects of culture age on symbiotic infectivity of rhizobium japonicum. *Journal of bacteriology*, 153(1):443–451, 1983.

[42] TV Bhuvaneswari, Andrew P Lesniak, and Wolfgang D Bauer. Efficiency of nodule initiation in cowpea and soybean. *Plant physiology*, 86(4):1210–1215, 1988.

[43] Wolfgang D Bauer, TV Bhuvaneswari, Harry E Calvert, IJ Law, Nasir SA Malik, and SJ Vesper. Recognition and infection by slow-growing rhizobia. In *Nitrogen fixation research progress*, pages 247–253. Springer, 1985.

[44] Nadiatul A Mohd-Radzman, Carole Laffont, Ariel Ivanovici, Neha Patel, Dugald Reid, Jens Stougaard, Florian Frugier, Nijat Imin, and Michael A Djordjevic. Different pathways act downstream of the cep peptide receptor cra2 to regulate lateral root and nodule development. *Plant Physiology*, 171(4):2536–2548, 2016.

[45] AC Timmers, Marie-Christine Auriac, and Georges Truchet. Refined analysis of early symbiotic steps of the rhizobium-medicago interaction in relationship with microtubular cytoskeleton rearrangements. *Development*, 126(16):3617–3628, 1999.

[46] Joseph G Dubrovsky, Peter W Doerner, Adán Colón-Carmona, and Thomas L Rost. Pericycle cell proliferation and lateral root initiation in arabidopsis. *Plant physiology*, 124(4):1648–1657, 2000.

[47] Sandra Bensmihen. Lateral root formation and patterning in medicago truncatula. *The Model Legume Medicago truncatula*, pages 130–135, 2019.

[48] Marta J Laskowski, Mary E Williams, H Chad Nusbaum, and Ian M Sussex. Formation of lateral root meristems is a two-stage process. *Development*, 121(10):3303–3310, 1995.

[49] Takashi Soyano, Yoshikazu Shimoda, Masayoshi Kawaguchi, and Makoto Hayashi. A shared gene drives lateral root development and root nodule symbiosis pathways in lotus. *Science*, 366(6468):1021–1023, 2019.

[50] Katharina Schiessl, Jodi LS Lilley, Tak Lee, Ioannis Tamvakis, Wouter Kohlen, Paul C Bailey, Aaron Thomas, Jakub Luptak, Karunakaran Ramakrishnan, Matthew D Carpenter, et al. Nodule inception recruits the lateral root developmental program for symbiotic nodule organogenesis in medicago truncatula. *Current Biology*, 29(21):3657–3668, 2019.

[51] Esben B Madsen, Meritxell Antolín-Llovera, Christina Grossmann, Juanying Ye, Syndi Vieweg, Angelique Broghammer, Lene Krusell, Simona Radutoiu, Ole N Jensen, Jens Stougaard, et al. Autophosphorylation is essential for the in vivo function of the lotus japonicus nod factor receptor 1 and receptor-mediated signalling in cooperation with nod factor receptor 5. *The Plant Journal*, 65(3):404–417, 2011.

[52] Yue Jin, Zixuan Chen, Jun Yang, Kirankumar S Mysore, Jiangqi Wen, Jirong Huang, Nan Yu, and Ertao Wang. Ipd3 and ipd3l function redundantly in rhizobial and mycorrhizal symbioses. *Frontiers in Plant Science*, 9:267, 2018.

[53] Péter Kaló, Cynthia Gleason, Anne Edwards, John Marsh, Raka M Mitra, Sibylle Hirsch, Júlia Jakab, Sarah Sims, Sharon R Long, Jane Rogers, et al. Nodulation signaling in legumes requires nsp2, a member of the gras family of transcriptional regulators. *Science*, 308(5729):1786–1789, 2005.

[54] Sibylle Hirsch, Jiyoung Kim, Alfonso Muñoz, Anne B Heckmann, J Allan Downie, and Giles ED Oldroyd. Gras proteins form a dna binding complex to induce gene expression during nodulation signaling in medicago truncatula. *The Plant Cell*, 21(2):545–557, 2009.

[55] Yue Jin, Huan Liu, Dexian Luo, Nan Yu, Wentao Dong, Chao Wang, Xiaowei Zhang, Huiling Dai, Jun Yang, and Ertao Wang. Della proteins are common components of

symbiotic rhizobial and mycorrhizal signalling pathways. *Nature communications*, 7(1):1–14, 2016.

[56] Aifang Xiao, Haixiang Yu, Yuqian Fan, Heng Kang, Yaping Ren, Xiaoqin Huang, Xiumei Gao, Chao Wang, Zhongming Zhang, Hui Zhu, et al. Transcriptional regulation of nin expression by ipn2 is required for root nodule symbiosis in lotus japonicus. *New Phytologist*, 227(2):513–528, 2020.

[57] José M Alvarez, Anna-Lena Schinke, Matthew D Brooks, Angelo Pasquino, Lauriebeth Leonelli, Kranthi Varala, Alaeddine Safi, Gabriel Krouk, Anne Krapp, and Gloria M Coruzzi. Transient genome-wide interactions of the master transcription factor nlp7 initiate a rapid nitrogen-response cascade. *Nature communications*, 11(1):1–13, 2020.

[58] Kun-hsiang Liu, Yajie Niu, Mineko Konishi, Yue Wu, Hao Du, Hoo Sun Chung, Lei Li, Marie Boudsocq, Matthew McCormack, Shugo Maekawa, et al. Discovery of nitrate–cpk–nlp signalling in central nutrient–growth networks. *Nature*, 545(7654):311–316, 2017.

[59] Mineko Konishi and Shuichi Yanagisawa. An nlp-binding site in the 3'flanking region of the nitrate reductase gene confers nitrate-inducible expression in arabidopsis thaliana (l.) heynh. *Soil Science and Plant Nutrition*, 59(4):612–620, 2013.

[60] Takashi Soyano, Hiroshi Kouchi, Atsuko Hirota, and Makoto Hayashi. Nodule inception directly targets nf-y subunit genes to regulate essential processes of root nodule development in lotus japonicus. *PLoS Genet*, 9(3):e1003352, 2013.

[61] Mineko Konishi and Shuichi Yanagisawa. The role of protein-protein interactions mediated by the pb1 domain of nlp transcription factors in nitrate-inducible gene expression. *BMC plant biology*, 19(1):1–12, 2019.

[62] Jieyu Liu and Ton Bisseling. Evolution of nin and nin-like genes in relation to nodule symbiosis. *Genes*, 11(7):777, 2020.

[63] Peizhu Guan, Juan-José Ripoll, Renhou Wang, Lam Vuong, Lindsay J Bailey-Steinitz, Dening Ye, and Nigel M Crawford. Interacting tcp and nlp transcription factors control plant responses to nitrate availability. *Proceedings of the National Academy of Sciences*, 114(9):2419–2424, 2017.

[64] Tatiana Vernié, Jiyoung Kim, Lisa Frances, Yiliang Ding, Jongho Sun, Dian Guan, Andreas Niebel, Miriam L Gifford, Fernanda de Carvalho-Niebel, and Giles ED Oldroyd.

The nin transcription factor coordinates diverse nodulation programs in different tissues of the medicago truncatula root. *The Plant Cell*, 27(12):3410–3424, 2015.

[65] Leif Schauser, Andreas Roussis, Jiri Stiller, and Jens Stougaard. A plant regulator controlling development of symbiotic root nodules. *Nature*, 402(6758):191–195, 1999.

[66] Jeremy D Murray, Bogumil J Karas, Shusei Sato, Satoshi Tabata, Lisa Amyot, and Krzysztof Szczyglowski. A cytokinin perception mutant colonized by rhizobium in the absence of nodule organogenesis. *Science*, 315(5808):101–104, 2007.

[67] Julie Plet, Anton Wasson, Federico Ariel, Christine Le Signor, David Baker, Ulrike Mathesius, Martin Crespi, and Florian Frugier. Mtcre1-dependent cytokinin signaling integrates bacterial and plant cues to coordinate symbiotic nodule organogenesis in medicago truncatula. *The Plant Journal*, 65(4):622–633, 2011.

[68] Jason Liang Pin Ng, Samira Hassan, Thy T Truong, Charles H Hocart, Carole Laffont, Florian Frugier, and Ulrike Mathesius. Flavonoids and auxin transport inhibitors rescue symbiotic nodulation in the medicago truncatula cytokinin perception mutant cre1. *The Plant Cell*, 27(8):2210–2226, 2015.

[69] Dugald Reid, Marcin Nadzieja, Ondřej Novák, Anne B Heckmann, Niels Sandal, and Jens Stougaard. Cytokinin biosynthesis promotes cortical cell responses during nodule development. *Plant Physiology*, 175(1):361–375, 2017.

[70] Jie-shun Lin, Xiaolin Li, Zhenpeng Luo, Kirankumar S Mysore, Jiangqi Wen, and Fang Xie. Nin interacts with nlps to mediate nitrate inhibition of nodulation in medicago truncatula. *Nature plants*, 4(11):942–952, 2018.

[71] Anne Birgitte Heckmann, Niels Sandal, Anita Søndergaard Bek, Lene Heegaard Madsen, Anna Jurkiewicz, Mette Wibroe Nielsen, Leila Tirichine, and Jens Stougaard. Cytokinin induction of root nodule primordia in lotus japonicus is regulated by a mechanism operating in the root cortex. *Molecular plant-microbe interactions*, 24(11):1385–1395, 2011.

[72] Jieyu Liu, Luuk Rutten, Erik Limpens, Tjitse Van Der Molen, Robin Van Velzen, Rujin Chen, Yuhui Chen, Rene Geurts, Wouter Kohlen, Olga Kulikova, et al. A remote cis-regulatory region is required for nin expression in the pericycle to initiate nodule primordium formation in medicago truncatula. *The Plant Cell*, 31(1):68–83, 2019.

[73] Federico Ariel, Marianne Brault-Hernandez, Carole Laffont, Emeline Huault, Mathias Brault, Julie Plet, Michael Moison, Sandrine Blanchet, Jean Laurent Ichanté, Mireille

Chabaud, et al. Two direct targets of cytokinin signaling regulate symbiotic nodulation in medicago truncatula. *The Plant Cell*, 24(9):3838–3852, 2012.

[74] Eric H Davidson. Emerging properties of animal gene regulatory networks. *Nature*, 468(7326):911–920, 2010.

[75] Shmoolik Mangan and Uri Alon. Structure and function of the feed-forward loop network motif. *Proceedings of the National Academy of Sciences*, 100(21):11980–11985, 2003.

[76] Virginie Mortier, Anton Wasson, Pavel Jaworek, Annick De Keyser, Martijn Decroos, Marcelle Holsters, Petr Tarkowski, Ulrike Mathesius, and Sofie Goormachtig. Role of lonely guy genes in indeterminate nodulation on medicago truncatula. *New Phytologist*, 202(2):582–593, 2014.

[77] Mahboobeh Azarakhsh, Andrey M Rumyantsev, Maria A Lebedeva, and Lyudmila A Lutova. Cytokinin biosynthesis genes expressed during nodule organogenesis are directly regulated by the knox3 protein in medicago truncatula. *PloS one*, 15(4):e0232352, 2020.

[78] Peter Doerner. Plant meristems: Cytokinins-the alpha and omega of the meristem. *Current Biology*, 17(9):R321–R323, 2007.

[79] Tatiana Vernié, Sandra Moreau, Françoise de Billy, Julie Plet, Jean-Philippe Combier, Christian Rogers, Giles Oldroyd, Florian Frugier, Andreas Niebel, and Pascal Gamas. Efd is an erf transcription factor involved in the control of nodule number and differentiation in medicago truncatula. *The Plant Cell*, 20(10):2696–2713, 2008.

[80] Fernando J Ferreira and Joseph J Kieber. Cytokinin signaling. *Current opinion in plant biology*, 8(5):518–525, 2005.

[81] Marion R Cerri, Lisa Frances, Audrey Kelner, Joëlle Fournier, Patrick H Middleton, Marie-Christine Auriac, Kirankumar S Mysore, Jiangqi Wen, Monique Erard, David G Barker, et al. The symbiosis-related ern transcription factors act in concert to coordinate rhizobial host root infection. *Plant Physiology*, 171(2):1037–1054, 2016.

[82] Marion R Cerri, Quanhui Wang, Paul Stolz, Jessica Folgmann, Lisa Frances, Katja Katzer, Xiaolin Li, Anne B Heckmann, Trevor L Wang, J Allan Downie, et al. The ern1 transcription factor gene is a target of the ccamk/cyclops complex and controls rhizobial infection in lotus japonicus. *New Phytologist*, 215(1):323–337, 2017.

[83] Marion R Cerri, Lisa Frances, Tom Laloum, Marie-Christine Auriac, Andreas Niebel, Giles ED Oldroyd, David G Barker, Joëlle Fournier, and Fernanda de Carvalho-Niebel. Medicago truncatula ern transcription factors: regulatory interplay with nsp1/nsp2 gras factors and expression dynamics throughout rhizobial infection. *Plant Physiology*, 160(4):2155–2172, 2012.

[84] Tom Laloum, Maël Baudin, Lisa Frances, Agnes Lepage, Benjamin Billault-Penneteau, Marion R Cerri, Federico Ariel, Marie-Françoise Jardinaud, Pascal Gamas, Fernanda de Carvalho-Niebel, et al. Two ccaat-box-binding transcription factors redundantly regulate early steps of the legume-rhizobia endosymbiosis. *The Plant Journal*, 79(5):757–768, 2014.

[85] Andry Andriankaja, Aurélien Boisson-Dernier, Lisa Frances, Laurent Sauviac, Alain Jauneau, David G Barker, and Fernanda de Carvalho-Niebel. Ap2-erf transcription factors mediate nod factor–dependent mt enod11 activation in root hairs via a novel cis-regulatory motif. *The Plant Cell*, 19(9):2866–2885, 2007.

[86] John F Marsh, Alexandra Rakocevic, Raka M Mitra, Lysiane Brocard, Jongho Sun, Alexis Eschstruth, Sharon R Long, Michael Schultze, Pascal Ratet, and Giles ED Oldroyd. Medicago truncatula nin is essential for rhizobial-independent nodule organogenesis induced by autoactive calcium/calmodulin-dependent protein kinase. *Plant physiology*, 144(1):324–335, 2007.

[87] Patrick Smit, Erik Limpens, Rene Geurts, Elena Fedorova, Elena Dolgikh, Clare Gough, and Ton Bisseling. Medicago lyk3, an entry receptor in rhizobial nodulation factor signaling. *Plant physiology*, 145(1):183–191, 2007.

[88] Giles ED Oldroyd and J Allan Downie. Nuclear calcium changes at the core of symbiosis signalling. *Current opinion in plant biology*, 9(4):351–357, 2006.

[89] Youning Wang, Wei Yang, Yanyan Zuo, Lin Zhu, April H Hastwell, Liang Chen, Yinping Tian, Chao Su, Brett J Ferguson, and Xia Li. Gmyuc2a mediates auxin biosynthesis during root development and nodulation in soybean. *Journal of experimental botany*, 70(12):3165–3176, 2019.

[90] Yoko Okushima, Hidehiro Fukaki, Makoto Onoda, Athanasios Theologis, and Masao Tasaka. Arf7 and arf19 regulate lateral root formation via direct activation of lbd/asl genes in arabidopsis. *The Plant Cell*, 19(1):118–130, 2007.

[91] Violaine Herrbach, Ximena Chirinos, David Rengel, Kokoévi Agbevenou, Rémy Vincent, Stéphanie Pateyron, Stéphanie Huguet, Sandrine Balzergue, Asher Pasha, Nicholas Provart, et al. Nod factors potentiate auxin signaling for transcriptional regulation and lateral root formation in medicago truncatula. *Journal of experimental botany*, 68(3):569–583, 2017.

[92] Tatsuaki Goh, Koichi Toyokura, Nobutoshi Yamaguchi, Yoshie Okamoto, Takeo Uehara, Shutaro Kaneko, Yumiko Takebayashi, Hiroyuki Kasahara, Yoshifumi Ikeyama, Yoko Okushima, et al. Lateral root initiation requires the sequential induction of transcription factors lbd16 and puchi in arabidopsis thaliana. *New Phytologist*, 224(2):749–760, 2019.

[93] Md Shakhawat Hossain, Arina Shrestha, Sihui Zhong, Mandana Miri, Ryan S Austin, Shusei Sato, Loretta Ross, Terry Huebert, Alexandre Tromas, Ivone Torres-Jerez, et al. Lotus japonicus nf-ya1 plays an essential role during nodule differentiation and targets members of the shi/sty gene family. *Molecular plant-microbe interactions*, 29(12):950–964, 2016.

[94] D Magnus Eklund, Veronika Ståldal, Isabel Valsecchi, Izabela Cierlik, Caitriona Eriksson, Keiichiro Hiratsu, Masaru Ohme-Takagi, Jens F Sundström, Mattias Thelander, Inés Ezcurra, et al. The arabidopsis thaliana stylish1 protein acts as a transcriptional activator regulating auxin biosynthesis. *The Plant Cell*, 22(2):349–363, 2010.

[95] D Magnus Eklund, Mattias Thelander, Katarina Landberg, Veronika Ståldal, Anders Nilsson, Monika Johansson, Isabel Valsecchi, Eric RA Pederson, Mariusz Kowalczyk, Karin Ljung, et al. Homologues of the arabidopsis thaliana shi/sty/lrp1 genes control auxin biosynthesis and affect growth and development in the moss physcomitrella patens. *Development*, 137(8):1275–1284, 2010.

[96] Joel J Sohlberg, Mattias Myrenås, Sandra Kuusk, Ulf Lagercrantz, Mariusz Kowalczyk, Göran Sandberg, and Eva Sundberg. Sty1 regulates auxin homeostasis and affects apical–basal patterning of the arabidopsis gynoecium. *The Plant Journal*, 47(1):112–123, 2006.

[97] Henk J Franssen, Ting Ting Xiao, Olga Kulikova, Xi Wan, Ton Bisseling, Ben Scheres, and Renze Heidstra. Root developmental programs shape the medicago truncatula nodule meristem. *Development*, 142(17):2941–2950, 2015.

[98] Henk J Franssen, Olga Kulikova, Viola Willemsen, and Renze Heidstra. Cis-regulatory plethora promoter elements directing root and nodule expression are conserved be-

tween arabidopsis thaliana and medicago truncatula. *Plant Signaling & Behavior*, (just-accepted):00–00, 2017.

[99] Ari Pekka Mähönen, Kirsten Ten Tusscher, Riccardo Siligato, Ondřej Smetana, Sara Díaz-Triviño, Jarkko Salojärvi, Guy Wachsman, Kalika Prasad, Renze Heidstra, and Ben Scheres. Plethora gradient formation mechanism separates auxin responses. *Nature*, 515(7525):125–129, 2014.

[100] Carla Galinha, Hugo Hofhuis, Marijn Luijten, Viola Willemsen, Ikram Blilou, Renze Heidstra, and Ben Scheres. Plethora proteins as dose-dependent master regulators of arabidopsis root development. *Nature*, 449(7165):1053–1057, 2007.

[101] Violaine Pinon, Kalika Prasad, Stephen P Grigg, Gabino F Sanchez-Perez, and Ben Scheres. Local auxin biosynthesis regulation by plethora transcription factors controls phyllotaxis in arabidopsis. *Proceedings of the National Academy of Sciences*, 110(3):1107–1112, 2013.

[102] Sonali Roy, Fran C Robson, Jodi Lorraine Stewart Lilley, Chengwu Liu, Xiaofei Cheng, Jiangqi Wen, Caitlin Bone, Simon Walker, Jongho Sun, Donna Cousins, et al. Mtlax2, a functional homologue of the auxin importer ataux1, is required for nodule organogenesis. *Plant Physiology*, pages pp–01473, 2017.

[103] Eva E Deinum, René Geurts, Marijke Hartog, Ton Bisseling, and Bela M Mulder. Computational and experimental evidence that auxin accumulation in nodule and lateral root primordia occurs by different mechanisms, 2015.

[104] Eva Elisabeth Deinum, René Geurts, Ton Bisseling, and Bela M Mulder. Modeling a cortical auxin maximum for nodulation: different signatures of potential strategies. *Frontiers in plant science*, 3:96, 2012.

[105] Eva E Deinum, Wouter Kohlen, and René Geurts. Quantitative modelling of legume root nodule primordium induction by a diffusive signal of epidermal origin that inhibits auxin efflux. *BMC Plant Biology*, 16(1):254, 2016.

[106] Silvia Gonzali, Giacomo Novi, Elena Loreti, Fabio Paolicchi, Alessandra Poggi, Amedeo Alpi, and Pierdomenico Perata. A turanose-insensitive mutant suggests a role for wox5 in auxin homeostasis in arabidopsis thaliana. *The Plant Journal*, 44(4):633–645, 2005.

[107] Nijat Imin, Mahira Nizamidin, Tina Wu, and Barry G Rolfe. Factors involved in root formation in medicago truncatula. *Journal of experimental botany*, 58(3):439–451, 2007.

[108] S-K Chen, S Kurdyukov, A Kereszt, X-D Wang, PM Gresshoff, and RJ Rose. The association of homeobox gene expression with stem cell formation and morphogenesis in cultured medicago truncatula. *Planta*, 230(4):827–840, 2009.

[109] Maria A Osipova, Virginie Mortier, Kirill N Demchenko, Victor E Tsyganov, Igor A Tikhonovich, Ludmila A Lutova, Elena A Dolgikh, and Sofie Goormachtig. Wuschel-related homeobox5 gene expression and interaction of cle peptides with components of the systemic control add two pieces to the puzzle of autoregulation of nodulation. *Plant physiology*, 158(3):1329–1341, 2012.

[110] Anindya Kundu, Firoz Molla, and Maitrayee DasGupta. Turanose induced wox5 restores symbiosis in the medicago truncatula cytokinin perception mutant cre1. *bioRxiv*, page 830661, 2020.

[111] Huiyu Tian, Krzysztof Wabnik, Tiantian Niu, Hanbing Li, Qianqian Yu, Stephan Pollmann, Steffen Vanneste, Willy Govaerts, Jakub Rolčík, Markus Geisler, et al. Wox5–iaa17 feedback circuit-mediated cellular auxin response is crucial for the patterning of root stem cell niches in arabidopsis. *Molecular plant*, 7(2):277–289, 2014.

[112] Ulrike Mathesius, Helmi RM Schlaman, Herman P Spaink, Christ Of Sautter, Barry G Rolfe, and Michael A Djordjevic. Auxin transport inhibition precedes root nodule formation in white clover roots and is regulated by flavonoids and derivatives of chitin oligosaccharides. *The Plant Journal*, 14(1):23–34, 1998.

[113] Cristina Pacios-Bras, Helmi RM Schlaman, Kees Boot, Pieter Admiraal, Julio Mateos Langerak, Jens Stougaard, and Herman P Spaink. Auxin distribution in lotus japonicus during root nodule development. *Plant molecular biology*, 52(6):1169–1180, 2003.

[114] Takuya Suzaki, Koji Yano, Momoyo Ito, Yosuke Umehara, Norio Suganuma, and Masayoshi Kawaguchi. Positive and negative regulation of cortical cell division during root nodule development in lotus japonicus is accompanied by auxin response. *Development*, 139(21):3997–4006, 2012.

[115] Takuya Suzaki, Momoyo Ito, and Masayoshi Kawaguchi. Induction of localized auxin response during spontaneous nodule development in lotus japonicus. *Plant signaling & behavior*, 8(3):e23359, 2013.

[116] Andrew Breakspear, Chengwu Liu, Donna R Cousins, Sonali Roy, Dian Guan, and Jeremy D Murray. The role of hormones in rhizobial infection. *Biological Nitrogen Fixation*, pages 555–566, 2015.

[117] Andrew Breakspear, Chengwu Liu, Sonali Roy, Nicola Stacey, Christian Rogers, Martin Trick, Giulia Morieri, Kirankumar S Mysore, Jiangqi Wen, Giles ED Oldroyd, et al. The root hair "infectome" of medicago truncatula uncovers changes in cell cycle genes and reveals a requirement for auxin signaling in rhizobial infection. *The Plant Cell*, 26(12):4680–4701, 2014.

[118] Henrik Jönsson, Marcus G Heisler, Bruce E Shapiro, Elliot M Meyerowitz, and Eric Mjolsness. An auxin-driven polarized transport model for phyllotaxis. *Proceedings of the National Academy of Sciences*, 103(5):1633–1638, 2006.

[119] Ulrike Mathesius, Cathy Bayliss, Jeremy J Weinman, Helmi RM Schlaman, Herman P Spaink, Barry G Rolfe, Margaret E McCully, and Michael A Djordjevic. Flavonoids synthesized in cortical cells during nodule initiation are early developmental markers in white clover. *Molecular Plant-Microbe Interactions*, 11(12):1223–1232, 1998.

[120] Peter Marhavỳ, Jérôme Duclercq, Benjamin Weller, Elena Feraru, Agnieszka Bielach, Remko Offringa, Jiří Friml, Claus Schwechheimer, Angus Murphy, and Eva Benková. Cytokinin controls polarity of pin1-dependent auxin transport during lateral root organogenesis. *Current Biology*, 24(9):1031–1037, 2014.

[121] Senthil Subramanian, Gary Stacey, and Oliver Yu. Endogenous isoflavones are essential for the establishment of symbiosis between soybean and bradyrhizobium japonicum. *The Plant Journal*, 48(2):261–273, 2006.

[122] Marie-Françoise Jardinaud, Stéphane Boivin, Nathalie Rodde, Olivier Catrice, Anna Kisiala, Agnes Lepage, Sandra Moreau, Brice Roux, Ludovic Cottret, Erika Sallet, et al. A laser dissection-rnaseq analysis highlights the activation of cytokinin pathways by nod factors in the medicago truncatula root epidermis. *Plant physiology*, 171(3):2256–2276, 2016.

[123] Yujuan Du and Ben Scheres. Plethora transcription factors orchestrate de novo organ patterning during arabidopsis lateral root outgrowth. *Proceedings of the National Academy of Sciences*, 114(44):11709–11714, 2017.

[124] Andrea Leibfried, Jennifer PC To, Wolfgang Busch, Sandra Stehling, Andreas Kehle, Monika Demar, Joseph J Kieber, and Jan U Lohmann. Wuschel controls meris-

tem function by direct regulation of cytokinin-inducible response regulators. *Nature*, 438(7071):1172–1175, 2005.

[125] Yun Zhou, Xing Liu, Eric M Engstrom, Zachary L Nimchuk, Jose L Pruneda-Paz, Paul T Tarr, An Yan, Steve A Kay, and Elliot M Meyerowitz. Control of plant stem cell function by conserved interacting transcriptional regulators. *Nature*, 517(7534):377–380, 2015.

[126] Yanfei Ma, Andrej Miotk, Zoran Šutiković, Olga Ermakova, Christian Wenzl, Anna Medzihradszky, Christophe Gaillochet, Joachim Forner, Gözde Utan, Klaus Brackmann, et al. Wuschel acts as an auxin response rheostat to maintain apical stem cells in arabidopsis. *Nature communications*, 10(1):1–11, 2019.

[127] Jean-Malo Couzigou, Vladimir Zhukov, Samuel Mondy, Ghada Abu El Heba, Viviane Cosson, TH Noel Ellis, Mike Ambrose, Jiangqi Wen, Million Tadege, Igor Tikhonovich, et al. Nodule root and cochleata maintain nodule development and are legume orthologs of arabidopsis blade-on-petiole genes. *The Plant Cell*, 24(11):4498–4510, 2012.

[128] Brett J Ferguson and James B Reid. Cochleata: getting to the root of legume nodules. *Plant and cell physiology*, 46(9):1583–1589, 2005.

[129] Kévin Magne, Jeoffrey George, Ana Berbel Tornero, Blandine Broquet, Francisco Madueño, Stig U Andersen, and Pascal Ratet. Lotus japonicus noot-bop-coch-like 1 is essential for nodule, nectary, leaf and flower development. *The Plant Journal*, 94(5):880–894, 2018.

[130] Leïla Tirichine, Haruko Imaizumi-Anraku, Satoko Yoshida, Yasuhiro Murakami, Lene H Madsen, Hiroki Miwa, Tomomi Nakagawa, Niels Sandal, Anita S Albrektsen, Masayoshi Kawaguchi, et al. Deregulation of a ca 2+/calmodulin-dependent kinase leads to spontaneous nodule development. *Nature*, 441(7097):1153–1156, 2006.

[131] Shyamala Bhaskaran and Roberta H Smith. Regeneration in cereal tissue culture: a review. *Crop Science*, 30(6):1328–1337, 1990.

[132] Kenneth V Thimann. On the physiology of the formation of nodules on legume roots. *Proceedings of the National Academy of Sciences of the United States of America*, 22(8):511, 1936.

[133] KR Libbenga, F Van Iren, RJ Bogers, and MF Schraag-Lamers. The role of hormones and gradients in the initiation of cortex proliferation and nodule formation in pisum sativum l. *Planta*, 114(1):29–39, 1973.

[134] Nirmal Arora, Folke Skoog, and ON Allen. Kinetin-induced pseudonodules on tobacco roots. *American Journal of Botany*, 46(8):610–613, 1959.

[135] C Rodriguez-Barrueco and F BERMUDEZ CASTRO. Cytokinin-induced pseudonodules on alnus glutinosa. *Physiologia Plantarum*, 29(2):277–280, 1973.

[136] James B Cooper and Sharon R Long. Morphogenetic rescue of rhizobium meliloti nodulation mutants by trans-zeatin secretion. *The Plant Cell*, 6(2):215–225, 1994.

[137] Petra Bauer, Pascal Ratet, Martin D Crespi, Michael Schultze, and Adam Kondorosi. Nod factors and cytokinins induce similar cortical cell division, amyloplast deposition and msenod12a expression patterns in alfalfa roots. *The plant journal*, 10(1):91–105, 1996.

[138] Christopher Gauthier-Coles, Rosemary G White, and Ulrike Mathesius. Nodulating legumes are distinguished by a sensitivity to cytokinin in the root cortex leading to pseudonodule development. *Frontiers in plant science*, 9:1901, 2019.

[139] Donald A Phillips and John G Torrey. Studies on cytokinin production by rhizobium. *Plant Physiology*, 49(1):11–15, 1972.

[140] Dawn B Sturtevant and Barbara J Taller. Cytokinin production by bradyrhizobium japonicum. *Plant physiology*, 89(4):1247–1252, 1989.

[141] Youry Pii, Massimo Crimi, Giorgia Cremonese, Angelo Spena, and Tiziana Pandolfini. Auxin and nitric oxide control indeterminate nodule formation. *BMC Plant Biology*, 7(1):21, 2007.

[142] Serena Camerini, Beatrice Senatore, Enza Lonardo, Esther Imperlini, Carmen Bianco, Giancarlo Moschetti, Giuseppe L Rotino, Bruno Campion, and Roberto Defez. Introduction of a novel pathway for iaa biosynthesis to rhizobia alters vetch root nodule development. *Archives of Microbiology*, 190(1):67–77, 2008.

[143] NP Kefford, J Brockwell, and JA Zwar. The symbiotic synthesis of auxin by legumes and nodule bacteria and its eole in nodule development. *Australian Journal of Biological Sciences*, 13(4):456–467, 1960.

[144] Mart Theunis, Hajime Kobayashi, William J Broughton, and Els Prinsen. Flavonoids, nodd1, nodd2, and nod-box nb15 modulate expression of the y4wefg locus that is required for indole-3-acetic acid synthesis in rhizobium sp. strain ngr234. *Molecular Plant-Microbe Interactions*, 17(10):1153–1161, 2004.

[145] Georges Truchet, Philippe Roche, Patrice Lerouge, Jacques Vasse, Sylvie Camut, Françoise de Billy, Jean-Claude Promé, and Jean Dénarié. Sulphated lipooligosaccharide signals of rhizobium meliloti elicit root nodule organogenesis in alfalfa. *Nature*, 351(6328):670–673, 1991.

[146] Ottoline Leyser. Auxin, self-organisation, and the colonial nature of plants. *Current Biology*, 21(9):R331–R337, 2011.

[147] Ottoline Leyser. Auxin signaling. *Plant physiology*, 176(1):465–479, 2018.

[148] Bruce A McClure, Gretchen Hagen, Christopher S Brown, Melissa A Gee, and Tom J Guilfoyle. Transcription, organization, and sequence of an auxin-regulated gene cluster in soybean. *The Plant Cell*, 1(2):229–239, 1989.

[149] Matyáš Fendrych, Maria Akhmanova, Jack Merrin, Matouš Glanc, Shinya Hagihara, Koji Takahashi, Naoyuki Uchida, Keiko U Torii, and Jiří Friml. Rapid and reversible root growth inhibition by tir1 auxin signalling. *Nature plants*, 4(7):453–459, 2018.

[150] Julian Dindas, Sönke Scherzer, M Rob G Roelfsema, Katharina von Meyer, Heike M Müller, KAS Al-Rasheid, Klaus Palme, Petra Dietrich, Dirk Becker, Malcolm J Bennett, et al. Aux1-mediated root hair auxin influx governs scf tir1/afb-type ca 2+ signaling. *Nature communications*, 9(1):1–10, 2018.

[151] Rahul Bhosale, Jitender Giri, Bipin K Pandey, Ricardo FH Giehl, Anja Hartmann, Richard Traini, Jekaterina Truskina, Nicola Leftley, Meredith Hanlon, Kamal Swarup, et al. A mechanistic framework for auxin dependent arabidopsis root hair elongation to low external phosphate. *Nature communications*, 9(1):1–9, 2018.

[152] Christa Brost, Tanja Studtrucker, Ronny Reimann, Philipp Denninger, Jennifer Czekalla, Melanie Krebs, Ben Fabry, Karin Schumacher, Guido Grossmann, and Petra Dietrich. Multiple cyclic nucleotide-gated channels coordinate calcium oscillations and polar growth of root hairs. *The Plant Journal*, 99(5):910–923, 2019.

[153] Jisheng Chen, Fei Wang, Shiqin Zheng, Tongda Xu, and Zhenbiao Yang. Pavement cells: a model system for non-transcriptional auxin signalling and crosstalks. *Journal of experimental botany*, 66(16):4957–4970, 2015.

[154] Min Cao, Rong Chen, Pan Li, Yongqiang Yu, Rui Zheng, Danfeng Ge, Wei Zheng, Xuhui Wang, Yangtao Gu, Zuzana Gelová, et al. Tmk1-mediated auxin signalling regulates differential growth of the apical hook. *Nature*, 568(7751):240–243, 2019.

[155] Eric M Kramer and Malcolm J Bennett. Auxin transport: a field in flux. *Trends in plant science*, 11(8):382–386, 2006.

[156] MHM Goldsmith. The polar transport of auxin. *Annual Review of Plant Physiology*, 28(1):439–478, 1977.

[157] Richard S Smith, Soazig Guyomarc'h, Therese Mandel, Didier Reinhardt, Cris Kuhlemeier, and Przemyslaw Prusinkiewicz. A plausible model of phyllotaxis. *Proceedings of the National Academy of Sciences*, 103(5):1301–1306, 2006.

[158] Verônica A Grieneisen, Jian Xu, Athanasius FM Marée, Paulien Hogeweg, and Ben Scheres. Auxin transport is sufficient to generate a maximum and gradient guiding root growth. *Nature*, 449(7165):1008–1013, 2007.

[159] Szymon Stoma, Mikael Lucas, Jérôme Chopard, Marianne Schaedel, Jan Traas, and Christophe Godin. Flux-based transport enhancement as a plausible unifying mechanism for auxin transport in meristem development. *PLoS Comput Biol*, 4(10):e1000207, 2008.

[160] Klaartje van Berkel, Rob J de Boer, Ben Scheres, and Kirsten ten Tusscher. Polar auxin transport: models and mechanisms. *Development*, 140(11):2253–2268, 2013.

[161] Tom Bennett. Pin proteins and the evolution of plant development. *Trends in plant science*, 20(8):498–507, 2015.

[162] Krzysztof Wabnik, Hélène S Robert, Richard S Smith, and Jiří Friml. Modeling framework for the establishment of the apical-basal embryonic axis in plants. *Current Biology*, 23(24):2513–2518, 2013.

[163] Didier Reinhardt, Eva-Rachele Pesce, Pia Stieger, Therese Mandel, Kurt Baltensperger, Malcolm Bennett, Jan Traas, Jiří Friml, and Cris Kuhlemeier. Regulation of phyllotaxis by polar auxin transport. *Nature*, 426(6964):255–260, 2003.

[164] Megan G Sawchuk, Alexander Edgar, and Enrico Scarpella. Patterning of leaf vein networks by convergent auxin transport pathways. *PLoS Genet*, 9(2):e1003294, 2013.

[165] Steffen Vanneste and Jiří Friml. Auxin: a trigger for change in plant development. *Cell*, 136(6):1005–1016, 2009.

[166] Marcus G Heisler, Olivier Hamant, Pawel Krupinski, Magalie Uyttewaal, Carolyn Ohno, Henrik Jönsson, Jan Traas, and Elliot M Meyerowitz. Alignment between pin1 polarity and microtubule orientation in the shoot apical meristem reveals a tight coupling between morphogenesis and auxin transport. *PLoS biology*, 8(10):e1000516, 2010.

[167] Stephane Douady and Yves Couder. Phyllotaxis as a physical self-organized growth process. *Physical review letters*, 68(13):2098, 1992.

[168] Patrik Sahlin, Bo Söderberg, and Henrik Jönsson. Regulated transport as a mechanism for pattern generation: capabilities for phyllotaxis and beyond. *Journal of theoretical biology*, 258(1):60–70, 2009.

[169] Przemyslaw Prusinkiewicz, Scott Crawford, Richard S Smith, Karin Ljung, Tom Bennett, Veronica Ongaro, and Ottoline Leyser. Control of bud activation by an auxin transport switch. *Proceedings of the National Academy of Sciences*, 106(41):17431–17436, 2009.

[170] Tanya Waldie and Ottoline Leyser. Cytokinin targets auxin transport to promote shoot branching. *Plant physiology*, 177(2):803–818, 2018.

[171] Kumi Otori, Noriaki Tanabe, Masahiro Tamoi, and Shigeru Shigeoka. Sugar transporter protein 1 (stp1) contributes to regulation of the genes involved in shoot branching via carbon partitioning in arabidopsis. *Bioscience, biotechnology, and biochemistry*, 83(3):472–481, 2019.

[172] Francois F Barbier, Elizabeth A Dun, Stephanie C Kerr, Tinashe G Chabikwa, and Christine A Beveridge. An update on the signals controlling shoot branching. *Trends in plant science*, 24(3):220–236, 2019.

[173] Ken-ichiro Hayashi, Shouichi Nakamura, Shiho Fukunaga, Takeshi Nishimura, Mark K Jenness, Angus S Murphy, Hiroyasu Motose, Hiroshi Nozaki, Masahiko Furutani, and Takashi Aoyama. Auxin transport sites are visualized in planta using fluorescent auxin analogs. *Proceedings of the National Academy of Sciences*, 111(31):11557–11562, 2014.

[174] Thea van den Berg, Ruud A Korver, Christa Testerink, and Kirsten HWJ ten Tusscher. Modeling halotropism: a key role for root tip architecture and reflux loop remodeling in redistributing auxin. *Development*, 143(18):3350–3362, 2016.

[175] Miguel A Moreno-Risueno, Jaimie M Van Norman, Antonio Moreno, Jingyuan Zhang, Sebastian E Ahnert, and Philip N Benfey. Oscillating gene expression determines competence for periodic arabidopsis root branching. *Science*, 329(5997):1306–1311, 2010.

[176] JA Santos Teixeira and KH Ten Tusscher. The systems biology of lateral root formation: connecting the dots. *Molecular plant*, 12(6):784–803, 2019.

[177] Qian Chen, Yang Liu, Steven Maere, Eunkyoung Lee, Gert Van Isterdael, Zidian Xie, Wei Xuan, Jessica Lucas, Valya Vassileva, Saeko Kitakura, et al. A coherent transcriptional feed-forward motif model for mediating auxin-sensitive pin3 expression during lateral root development. *Nature communications*, 6(1):1–12, 2015.

[178] Benjamin Péret, Bert De Rybel, Ilda Casimiro, Eva Benková, Ranjan Swarup, Laurent Laplaze, Tom Beeckman, and Malcolm J Bennett. Arabidopsis lateral root development: an emerging story. *Trends in plant science*, 14(7):399–408, 2009.

[179] Li Ping Tang, Chao Zhou, Shan Shan Wang, Jia Yuan, Xian Sheng Zhang, and Ying Hua Su. Fusca 3 interacting with leafy cotyledon 2 controls lateral root formation through regulating yucca 4 gene expression in arabidopsis thaliana. *New Phytologist*, 213(4):1740–1754, 2017.

[180] Toru Kudo, Takatoshi Kiba, and Hitoshi Sakakibara. Metabolism and long-distance translocation of cytokinins. *Journal of integrative plant biology*, 52(1):53–60, 2010.

[181] Jennifer PC To and Joseph J Kieber. Cytokinin signaling: two-components and more. *Trends in plant science*, 13(2):85–92, 2008.

[182] Jian Feng, Chun Wang, Qingguo Chen, Hui Chen, Bo Ren, Xiaoming Li, and Jianru Zuo. S-nitrosylation of phosphotransfer proteins represses cytokinin signaling. *Nature Communications*, 4(1):1–9, 2013.

[183] Sophie Jasinski, Paolo Piazza, Judith Craft, Angela Hay, Lindsey Woolley, Ivo Rieu, Andrew Phillips, Peter Hedden, and Miltos Tsiantis. Knox action in arabidopsis is mediated by coordinate regulation of cytokinin and gibberellin activities. *Current Biology*, 15(17):1560–1565, 2005.

[184] G Venugopala Reddy and Elliot M Meyerowitz. Stem-cell homeostasis and growth dynamics can be uncoupled in the arabidopsis shoot apex. *Science*, 310(5748):663–667, 2005.

[185] Zhong Zhao, Stig U Andersen, Karin Ljung, Karel Dolezal, Andrej Miotk, Sebastian J Schultheiss, and Jan U Lohmann. Hormonal control of the shoot stem-cell niche. *Nature*, 465(7301):1089–1092, 2010.

[186] Bruno Müller and Jen Sheen. Cytokinin and auxin interaction in root stem-cell specification during early embryogenesis. *Nature*, 453(7198):1094–1097, 2008.

[187] Marcus G Heisler, Carolyn Ohno, Pradeep Das, Patrick Sieber, Gonehal V Reddy, Jeff A Long, and Elliot M Meyerowitz. Patterns of auxin transport and gene expression during primordium development revealed by live imaging of the arabidopsis inflorescence meristem. *Current biology*, 15(21):1899–1911, 2005.

[188] Benoit Landrein, Pau Formosa-Jordan, Alice Malivert, Christoph Schuster, Charles W Melnyk, Weibing Yang, Colin Turnbull, Elliot M Meyerowitz, James CW Locke, and Henrik Jönsson. Nitrate modulates stem cell dynamics in arabidopsis shoot meristems through cytokinins. *Proceedings of the National Academy of Sciences*, 115(6):1382–1387, 2018.

[189] Jacob Pieter Rutten and Kirsten ten Tusscher. In silico roots: room for growth. *Trends in plant science*, 24(3):250–262, 2019.

[190] Raffaele Dello Ioio, Francisco Scaglia Linhares, and Sabrina Sabatini. Emerging role of cytokinin as a regulator of cellular differentiation. *Current opinion in plant biology*, 11(1):23–27, 2008.

[191] Laila Moubayidin, Riccardo Di Mambro, and Sabrina Sabatini. Cytokinin–auxin crosstalk. *Trends in plant science*, 14(10):557–562, 2009.

[192] Tomáš Werner, Erika Nehnevajova, Ireen Köllmer, Ondřej Novák, Miroslav Strnad, Ute Krämer, and Thomas Schmülling. Root-specific reduction of cytokinin causes enhanced root growth, drought tolerance, and leaf mineral enrichment in arabidopsis and tobacco. *The Plant Cell*, 22(12):3905–3920, 2010.

[193] Stéphane Boivin, Théophile Kazmierczak, Mathias Brault, Jiangqi Wen, Pascal Gamas, Kirankumar S Mysore, and Florian Frugier. Different cytokinin histidine kinase receptors regulate nodule initiation as well as later nodule developmental stages in medicago truncatula. *Plant, cell & environment*, 39(10):2198–2209, 2016.

[194] Mark Held, Hongwei Hou, Mandana Miri, Christian Huynh, Loretta Ross, Md Shakhawat Hossain, Shusei Sato, Satoshi Tabata, Jillian Perry, Trevor L Wang,

et al. Lotus japonicus cytokinin receptors work partially redundantly to mediate nodule formation. *The Plant Cell*, 26(2):678–694, 2014.

[195] Giles ED Oldroyd and J Allan Downie. Coordinating nodule morphogenesis with rhizobial infection in legumes. *Annu. Rev. Plant Biol.*, 59:519–546, 2008.

[196] Ulrike Mathesius, Jeremy J Weinman, Barry G Rolfe, and Michael A Djordjevic. Rhizobia can induce nodules in white clover by "hijacking" mature cortical cells activated during lateral root development. *Molecular Plant-Microbe Interactions*, 13(2):170–182, 2000.

[197] Silvina Gonzalez-Rizzo, Martin Crespi, and Florian Frugier. The medicago truncatula cre1 cytokinin receptor regulates lateral root development and early symbiotic interaction with sinorhizobium meliloti. *The Plant Cell*, 18(10):2680–2693, 2006.

[198] AM Hirsch, TV Bhuvaneswari, JG Torrey, and T Bisseling. Early nodulin genes are induced in alfalfa root outgrowths elicited by auxin transport inhibitors. *Proceedings of the National Academy of Sciences*, 86(4):1244–1248, 1989.

[199] Jon Fisher, Paul Gaillard, Carl R Fellbaum, Senthil Subramanian, and Steve Smith. Quantitative 3d imaging of cell level auxin and cytokinin response ratios in soybean roots and nodules. *Plant, cell & environment*, 41(9):2080–2092, 2018.

[200] Sandra Moreau, Marion Verdenaud, Thomas Ott, Sebastien Letort, Françoise De Billy, Andreas Niebel, Jerome Gouzy, Fernanda de Carvalho-Niebel, and Pascal Gamas. Transcription reprogramming during root nodule development in medicago truncatula. *PLoS One*, 6(1):e16463, 2011.

[201] Takuya Suzaki and Masayoshi Kawaguchi. Root nodulation: a developmental program involving cell fate conversion triggered by symbiotic bacterial infection. *Current opinion in plant biology*, 21:16–22, 2014.

[202] Yaping Chen, Wei Chen, Xueliu Li, Huawu Jiang, Pingzhi Wu, Kuaifei Xia, Yali Yang, and Guojiang Wu. Knockdown of ljipt3 influences nodule development in lotus japonicus. *Plant and Cell Physiology*, page pct171, 2013.

[203] Arjan van Zeijl, Rik HM Op den Camp, Eva E Deinum, Tatsiana Charnikhova, Henk Franssen, Huub JM Op den Camp, Harro Bouwmeester, Wouter Kohlen, Ton Bisseling, and René Geurts. Rhizobium lipo-chitooligosaccharide signaling triggers accumulation of cytokinins in medicago truncatula roots. *Molecular plant*, 8(8):1213–1226, 2015.

[204] Richard S Smith and Emmanuelle M Bayer. Auxin transport-feedback models of patterning in plants. *Plant, cell & environment*, 32(9):1258–1271, 2009.

[205] Giel E van Noorden, John J Ross, James B Reid, Barry G Rolfe, and Ulrike Mathesius. Defective long-distance auxin transport regulation in the medicago truncatula super numeric nodules mutant. *Plant Physiology*, 140(4):1494–1506, 2006.

[206] Wouter Kohlen, Jason Liang Pin Ng, Eva E Deinum, and Ulrike Mathesius. Auxin transport, metabolism, and signalling during nodule initiation: indeterminate and determinate nodules. *Journal of Experimental Botany*, 69(2):229–244, 2018.

[207] Markus Geisler, H Üner Kolukisaoglu, Rodolphe Bouchard, Karla Billion, Joachim Berger, Beate Saal, Nathalie Frangne, Zsuzsanna Koncz-Kálmán, Csaba Koncz, Robert Dudler, et al. Twisted dwarf1, a unique plasma membrane-anchored immunophilin-like protein, interacts with arabidopsis multidrug resistance-like transporters atpgp1 and atpgp19. *Molecular biology of the cell*, 14(10):4238–4249, 2003.

[208] Markus Geisler, Joshua J Blakeslee, Rodolphe Bouchard, Ok Ran Lee, Vincent Vincenzetti, Anindita Bandyopadhyay, Boosaree Titapiwatanakun, Wendy Ann Peer, Aurelien Bailly, Elizabeth L Richards, et al. Cellular efflux of auxin catalyzed by the arabidopsis mdr/pgp transporter atpgp1. *The Plant Journal*, 44(2):179–194, 2005.

[209] Joshua J Blakeslee, Anindita Bandyopadhyay, Ok Ran Lee, Jozef Mravec, Boosaree Titapiwatanakun, Michael Sauer, Srinivas N Makam, Yan Cheng, Rodolphe Bouchard, Jiří Adamec, et al. Interactions among pin-formed and p-glycoprotein auxin transporters in arabidopsis. *The Plant Cell*, 19(1):131–147, 2007.

[210] Sonali Roy. *Analysis of gene expression, regulation and function of three symbiotic ABC subfamily-B transporters in Medicago truncatula*. PhD thesis, University of East Anglia, 2015.

[211] Benjamin Péret, Kamal Swarup, Alison Ferguson, Malvika Seth, Yaodong Yang, Stijn Dhondt, Nicholas James, Ilda Casimiro, Paula Perry, Adnan Syed, et al. Aux/lax genes encode a family of auxin influx transporters that perform distinct functions during arabidopsis development. *The Plant Cell*, 24(7):2874–2885, 2012.

[212] Kamal Swarup, Eva Benková, Ranjan Swarup, Ilda Casimiro, Benjamin Péret, Yaodong Yang, Geraint Parry, Erik Nielsen, Ive De Smet, Steffen Vanneste, et al. The auxin influx carrier lax3 promotes lateral root emergence. *Nature cell biology*, 10(8):946–954, 2008.

[213] Leah R Band, Darren M Wells, John A Fozard, Teodor Ghetiu, Andrew P French, Michael P Pound, Michael H Wilson, Lei Yu, Wenda Li, Hussein I Hijazi, et al. Systems analysis of auxin transport in the arabidopsis root apex. *The Plant Cell*, 26(3):862–875, 2014.

[214] EL Schnabel and J Frugoli. The pin and lax families of auxin transport genes in medicago truncatula. *Molecular genetics and genomics*, 272(4):420–432, 2004.

[215] Françoise de Billy, Cathy Grosjean, Sean May, Malcolm Bennett, and Julie V Cullimore. Expression studies on aux1-like genes in medicago truncatula suggest that auxin is required at two steps in early nodule development. *Molecular Plant-Microbe Interactions*, 14(3):267–277, 2001.

[216] Klaus Palme and Leo Gälweiler. Pin-pointing the molecular basis of auxin transport. *Current opinion in plant biology*, 2(5):375–381, 1999.

[217] E Zazimalova, P Krecek, P Skupa, K Hoyerova, and J Petrasek. Polar transport of the plant hormone auxin–the role of pin-formed (pin) proteins. *Cellular and molecular life sciences*, 64(13):1621–1637, 2007.

[218] Eva Zazimalova, Angus S Murphy, Haibing Yang, Klara Hoyerova, and Petr Hosek. Auxin transporters - why so many? *Cold Spring Harbor perspectives in biology*, 2(3):a001552, 2010.

[219] Jurgen Kleine-Vehn, Krzysztof Wabnik, Alexandre Martiniere, Lukasz Langowski, Katrin Willig, Satoshi Naramoto, Johannes Leitner, Hirokazu Tanaka, Stefan Jakobs, Stephanie Robert, et al. Recycling, clustering, and endocytosis jointly maintain pin auxin carrier polarity at the plasma membrane. *Molecular systems biology*, 7(1):540, 2011.

[220] Tongda Xu, Ning Dai, Jisheng Chen, Shingo Nagawa, Min Cao, Hongjiang Li, Zimin Zhou, Xu Chen, Riet De Rycke, Hana Rakusová, et al. Cell surface abp1-tmk auxin-sensing complex activates rop gtpase signaling. *Science*, 343(6174):1025–1028, 2014.

[221] Xu Chen, Satoshi Naramoto, Stephanie Robert, Ricardo Tejos, Christian Lofke, Deshu Lin, Zhenbiao Yang, and Jiri Friml. Abp1 and rop6 gtpase signaling regulate clathrin-mediated endocytosis in arabidopsis roots. *Current Biology*, 22(14):1326–1332, 2012.

[222] Yangbin Gao, Yi Zhang, Da Zhang, Xinhua Dai, Mark Estelle, and Yunde Zhao. Auxin binding protein 1 (abp1) is not required for either auxin signaling or arabidopsis development. *Proceedings of the National Academy of Sciences*, 112(7):2275–2280, 2015.

[223] Jozef Mravec, Petr Skupa, Aurelien Bailly, Klara Hoyerova, Pavel Krecek, Agnieszka Bielach, Jan Petrasek, Jing Zhang, Vassilena Gaykova, York-Dieter Stierhof, et al. Subcellular homeostasis of phytohormone auxin is mediated by the er-localized pin5 transporter. *Nature*, 459(7250):1136–1140, 2009.

[224] Pavel Krecek, Petr Skupa, Jiri Libus, Satoshi Naramoto, Ricardo Tejos, Jiří Friml, and Eva Zažímalová. The pin-formed (pin) protein family of auxin transporters. *Genome biology*, 10(12):249, 2009.

[225] Chenjia Shen, Runqing Yue, Youhuang Bai, Rong Feng, Tao Sun, Xiaofei Wang, Yanjun Yang, Shuanggui Tie, and Huizhong Wang. Identification and analysis of medicago truncatula auxin transporter gene families uncover their roles in responses to sinorhizobium meliloti infection. *Plant and Cell Physiology*, 56(10):1930–1943, 2015.

[226] Elke Barbez, Martin Kubeš, Jakub Rolčík, Chloé Béziat, Aleš Pěnčík, Bangjun Wang, Michel Ruiz Rosquete, Jinsheng Zhu, Petre I Dobrev, Yuree Lee, et al. A novel putative auxin carrier family regulates intracellular auxin homeostasis in plants. *Nature*, 485(7396):119–122, 2012.

[227] Devin L O'Connor, Adam Runions, Aaron Sluis, Jennifer Bragg, John P Vogel, Przemyslaw Prusinkiewicz, and Sarah Hake. A division in pin-mediated auxin patterning during organ initiation in grasses. *PLoS Comput Biol*, 10(1):e1003447, 2014.

[228] Masahiko Furutani, Yasukazu Nakano, and Masao Tasaka. Mab4-induced auxin sink generates local auxin gradients in arabidopsis organ formation. *Proceedings of the National Academy of Sciences*, 111(3):1198–1203, 2014.

[229] Jianling Peng and Rujin Chen. Auxin efflux transporter mtpin10 regulates compound leaf and flower development in medicago truncatula. *Plant signaling & behavior*, 6(10):1537–1544, 2011.

[230] Chuanen Zhou, Lu Han, Chunyan Hou, Alessandra Metelli, Liying Qi, Million Tadege, Kirankumar S Mysore, and Zeng-Yu Wang. Developmental analysis of a medicago truncatula smooth leaf margin1 mutant reveals context-dependent effects on compound leaf development. *The Plant Cell*, 23(6):2106–2124, 2011.

[231] Ting Ting Xiao. *Root and nodule: lateral organ development in N2-fixing plants*. Wageningen University, 2015.

[232] Xiuyan Huo, Elise Schnabel, Kelley Hughes, and Julia Frugoli. Rnai phenotypes and the localization of a protein:: Gus fusion imply a role for medicago truncatula pin genes in nodulation. *Journal of Plant Growth Regulation*, 25(2):156–165, 2006.

[233] GJ Mitchison. The dynamics of auxin transport. *Proceedings of the Royal Society of London B: Biological Sciences*, 209(1177):489–511, 1980.

[234] Kees JM Boot, Anton AN van Brussel, Teun Tak, Herman P Spaink, and Jan W Kijne. Lipochitin oligosaccharides from rhizobium leguminosarum bv. viciae reduce auxin transport capacity in vicia sativa subsp. nigra roots. *Molecular Plant-Microbe Interactions*, 12(10):839–844, 1999.

[235] Seiji Tsurumi and Yoriko Ohwaki. Transport of 14c-lableled indoleacetic acid in vicia root segments. *Plant and Cell Physiology*, 19(7):1195–1206, 1978.

[236] Ethel K Allen, ON Allen, and AS Newman. Pseudonodulation of leguminous plants induced by 2-bromo-3, 5-dichlorobenzoic acid. *American Journal of Botany*, pages 429–435, 1953.

[237] Adriana P Rightmyer and Sharon R Long. Pseudonodule formation by wild-type and symbiotic mutant medicago truncatula in response to auxin transport inhibitors. *Molecular plant-microbe interactions*, 24(11):1372–1384, 2011.

[238] Ben Scheres, Heather I McKhann, Andrei Zalensky, Marian Löbler, Ton Bisseling, and Ann M Hirsch. The psenod12 gene is expressed at two different sites in afghanistan pea pseudonodules induced by auxin transport inhibitors. *Plant physiology*, 100(4):1649–1655, 1992.

[239] Clemens Van de Wiel, Joanna H Norris, Birgit Bochenek, Rebecca Dickstein, Ton Bisseling, and Ann M Hirsch. Nodulin gene expression and enod2 localization in effective, nitrogen-fixing and ineffective, bacteria-free nodules of alfalfa. *The Plant Cell*, 2(10):1009–1017, 1990.

[240] Chunfa Wu, Rebecca Dickstein, Andrew J Cary, and J Hanks Norris. The auxin transport inhibitor n-(1-naphthyl) phthalamic acid elicits pseudonodules on nonnodulating mutants of white sweetclover. *Plant Physiology*, 110(2):501–510, 1996.

[241] Kojiro Takanashi, Akifumi Sugiyama, and Kazufumi Yazaki. Involvement of auxin distribution in root nodule development of lotus japonicus. *Planta*, 234(1):73–81, 2011.

[242] Jason LP Ng and Ulrike Mathesius. Acropetal auxin transport inhibition is involved in indeterminate but not determinate nodule formation. *Frontiers in plant science*, 9:169, 2018.

[243] Masayoshi Kawaguchi, Haruko Imaizumi-Anraku, Shungo Fukai, and Kunihiko Syono. Unusual branching in the seedlings of lotus japonicus-gibberellins reveal the nitrogen-sensitive cell divisions within the pericycle on roots. *Plant and cell physiology*, 37(4):461–470, 1996.

[244] William Teale and Klaus Palme. Naphthylphthalamic acid and the mechanism of polar auxin transport. *Journal of experimental botany*, 69(2):303–312, 2018.

[245] William D Teale, Taras Pasternak, Cristina Dal Bosco, Alexander Dovzhenko, Krystyna Kratzat, Wolfgang Bildl, Manuel Schwörer, Thorsten Falk, Benadetto Ruperti, Jonas V Schaefer, et al. Flavonol-mediated stabilization of pin efflux complexes regulates polar auxin transport. *The EMBO Journal*, page e104416, 2020.

[246] Bosl Noh, Angus S Murphy, and Edgar P Spalding. Multidrug resistance–like genes of arabidopsis required for auxin transport and auxin-mediated development. *The Plant Cell*, 13(11):2441–2454, 2001.

[247] Hans Depta, Karl-Heinz Eisele, and Rainer Hertel. Specific inhibitors of auxin transport: action on tissue segments and in vitro binding to membranes from maize coleoptiles. *Plant science letters*, 31(2-3):181–192, 1983.

[248] Klaus-Sten Thomson, Rainer Hertel, Sybille Müller, and James E Tavares. 1-n-naphthylphthalamic acid and 2, 3, 5-triiodobenzoic acid. *Planta*, 109(4):337–352, 1973.

[249] Mukesh Jain, Navneet Kaur, Akhilesh K Tyagi, and Jitendra P Khurana. The auxin-responsive gh3 gene family in rice (oryza sativa). *Functional & integrative genomics*, 6(1):36, 2006.

[250] Tim Ulmasov, Jane Murfett, Gretchen Hagen, and Tom J Guilfoyle. Aux/iaa proteins repress expression of reporter genes containing natural and highly active synthetic auxin response elements. *The Plant Cell*, 9(11):1963–1971, 1997.

[251] Eric M Kramer. Computer models of auxin transport: a review and commentary. *Journal of experimental botany*, 59(1):45–53, 2008.

[252] Anne-Gaëlle Rolland-Lagan and Przemyslaw Prusinkiewicz. Reviewing models of auxin canalization in the context of leaf vein pattern formation in arabidopsis. *The Plant Journal*, 44(5):854–865, 2005.

[253] GJ Mitchison, DE Hanke, and AR Sheldrake. The polar transport of auxin and vein patterns in plants [and discussion]. *Philosophical Transactions of the Royal Society of London B: Biological Sciences*, 295(1078):461–471, 1981.

[254] Pierre Barbier de Reuille, Isabelle Bohn-Courseau, Karin Ljung, Halima Morin, Nicola Carraro, Christophe Godin, and Jan Traas. Computer simulations reveal properties of the cell-cell signaling network at the shoot apex in arabidopsis. *Proceedings of the National Academy of Sciences*, 103(5):1627–1632, 2006.

[255] Katie Abley, Pierre Barbier De Reuille, David Strutt, Andrew Bangham, Przemyslaw Prusinkiewicz, Athanasius FM Marée, Verônica A Grieneisen, and Enrico Coen. An intracellular partitioning-based framework for tissue cell polarity in plants and animals. *Development*, 140(10):2061–2074, 2013.

[256] Krzysztof Wabnik, Jürgen Kleine-Vehn, Willy Govaerts, and Jiří Friml. Prototype cell-to-cell auxin transport mechanism by intracellular auxin compartmentalization. *Trends in plant science*, 16(9):468–475, 2011.

[257] Maria Simaskova, Jose Antonio O'Brien, Mamoona Khan, Giel Van Noorden, Krisztina Otvos, Anne Vieten, Inge De Clercq, Johanna Maria Adriana Van Haperen, Candela Cuesta, Klara Hoyerova, et al. Cytokinin response factors regulate pin-formed auxin transporters. *Nature communications*, 6, 2015.

[258] Peter Marhavỳ, Agnieszka Bielach, Lindy Abas, Anas Abuzeineh, Jerome Duclercq, Hirokazu Tanaka, Markéta Pařezová, Jan Petrášek, Jiří Friml, Jürgen Kleine-Vehn, et al. Cytokinin modulates endocytic trafficking of pin1 auxin efflux carrier to control plant organogenesis. *Developmental cell*, 21(4):796–804, 2011.

[259] Aurélien Bailly, Valpuri Sovero, Vincent Vincenzetti, Diana Santelia, Dirk Bartnik, Bernd W Koenig, Stefano Mancuso, Enrico Martinoia, and Markus Geisler. Modulation of p-glycoproteins by auxin transport inhibitors is mediated by interaction with immunophilins. *Journal of Biological Chemistry*, 283(31):21817–21826, 2008.

[260] Angus Murphy, Wendy Ann Peer, and Lincoln Taiz. Regulation of auxin transport by aminopeptidases and endogenous flavonoids. *Planta*, 211(3):315–324, 2000.

[261] Emmanuelle M Bayer, Richard S Smith, Therese Mandel, Naomi Nakayama, Michael Sauer, Przemyslaw Prusinkiewicz, and Cris Kuhlemeier. Integration of transport-based models for phyllotaxis and midvein formation. *Genes & development*, 23(3):373–384, 2009.

[262] Ann M Hirsch and Yiwen Fang. Plant hormones and nodulation: what's the connection? *Plant molecular biology*, 26(1):5–9, 1994.

[263] Che-Yang Liao, Wouter Smet, Geraldine Brunoud, Saiko Yoshida, Teva Vernoux, and Dolf Weijers. Reporters for sensitive and quantitative measurement of auxin response. *Nature methods*, 12(3):207–210, 2015.

[264] Eva Benková, Marta Michniewicz, Michael Sauer, Thomas Teichmann, Daniela Seifertová, Gerd Jürgens, and JiřıŽ Friml. Local, efflux-dependent auxin gradients as a common module for plant organ formation. *Cell*, 115(5):591–602, 2003.

[265] Justyna Wiśniewska, Jian Xu, Daniela Seifertova, Philip B Brewer, Kamil Ruzicka, Ikram Blilou, David Rouquile, Eva Benkova, Ben Scheres, and Jiri Friml. Polar pin localization directs auxin flow in plants. *Science*, 312(5775):883–883, 2006.

[266] Jian Xu and Ben Scheres. Dissection of arabidopsis adp-ribosylation factor 1 function in epidermal cell polarity. *The Plant Cell*, 17(2):525–536, 2005.

[267] Petra Žádníková, Jan Petrášek, Peter Marhavỳ, Vered Raz, Filip Vandenbussche, Zhaojun Ding, Kateřina Schwarzerová, Miyo T Morita, Masao Tasaka, Jan Hejátko, et al. Role of pin-mediated auxin efflux in apical hook development of arabidopsis thaliana. *Development*, 137(4):607–617, 2010.

[268] Anne Vieten, Steffen Vanneste, Justyna Wiśniewska, Eva Benková, René Benjamins, Tom Beeckman, Christian Luschnig, and Jiří Friml. Functional redundancy of pin proteins is accompanied by auxin-dependent cross-regulation of pin expression. *Development*, 132(20):4521–4531, 2005.

[269] Jurgen Kleine-Vehn, Fang Huang, Satoshi Naramoto, Jing Zhang, Marta Michniewicz, Remko Offringa, and Jiri Friml. Pin auxin efflux carrier polarity is regulated by pinoid kinase-mediated recruitment into gnom-independent trafficking in arabidopsis. *The Plant Cell*, 21(12):3839–3849, 2009.

[270] Ján Jásik, Boris Bokor, Stanislav Stuchlík, Karol Mičieta, Ján Turňa, and Elmon Schmelzer. Effects of auxins on pin-formed2 (pin2) dynamics are not mediated by inhibiting pin2 endocytosis. *Plant Physiology*, 172(2):1019–1031, 2016.

[271] Jason LP Ng, Astrid Welvaert, Jiangqi Wen, Rujin Chen, and Ulrike Mathesius. The medicago truncatula pin2 auxin transporter mediates basipetal auxin transport but is not necessary for nodulation. *Journal of Experimental Botany*, 71(4):1562–1573, 2020.

[272] N Kent Peters and Deborah K Crist-Estes. Nodule formation is stimulated by the ethylene inhibitor aminoethoxyvinylglycine. *Plant Physiology*, 91(2):690–693, 1989.

[273] David M Goodstein, Shengqiang Shu, Russell Howson, Rochak Neupane, Richard D Hayes, Joni Fazo, Therese Mitros, William Dirks, Uffe Hellsten, Nicholas Putnam, et al. Phytozome: a comparative platform for green plant genomics. *Nucleic acids research*, 40(D1):D1178–D1186, 2012.

[274] Jean-Philippe Combier, Florian Frugier, Françoise de Billy, Adnane Boualem, Fikri El-Yahyaoui, Sandra Moreau, Tatiana Vernié, Thomas Ott, Pascal Gamas, Martin Crespi, et al. Mthap2-1 is a key transcriptional regulator of symbiotic nodule development regulated by microrna169 in medicago truncatula. *Genes & development*, 20(22):3084–3088, 2006.

[275] Momoko Ikeuchi, Michitaro Shibata, Bart Rymen, Akira Iwase, Anne-Maarit Bågman, Lewis Watt, Duncan Coleman, David S Favero, Tatsuya Takahashi, Sebastian E Ahnert, et al. A gene regulatory network for cellular reprogramming in plant regeneration. *Plant and Cell Physiology*, 59(4):770–782, 2018.

[276] Rohan V Patel, Hardeep K Nahal, Robert Breit, and Nicholas J Provart. Bar expressolog identification: expression profile similarity ranking of homologous genes in plant species. *The Plant Journal*, 71(6):1038–1050, 2012.

[277] Jamie Waese, Jim Fan, Asher Pasha, Hans Yu, Geoffrey Fucile, Ruian Shi, Matthew Cumming, Lawrence A Kelley, Michael J Sternberg, Vivek Krishnakumar, et al. eplant: visualizing and exploring multiple levels of data for hypothesis generation in plant biology. *The Plant Cell*, 29(8):1806–1821, 2017.

[278] Ken Haga, Ken-ichiro Hayashi, and Tatsuya Sakai. Pinoid agc kinases are necessary for phytochrome-mediated enhancement of hypocotyl phototropism in arabidopsis. *Plant physiology*, 166(3):1535–1545, 2014.

[279] Albin Sandelin, Wynand Alkema, Pär Engström, Wyeth W Wasserman, and Boris Lenhard. Jaspar: an open-access database for eukaryotic transcription factor binding profiles. *Nucleic acids research*, 32(suppl_1):D91–D94, 2004.

[280] Timothy L Bailey, James Johnson, Charles E Grant, and William S Noble. The meme suite. *Nucleic acids research*, 43(W1):W39–W49, 2015.

[281] Luca Santuari, Gabino Sanchez-Perez, Marijn Luijten, Bas Rutjens, Inez Terpstra, Lidija Berke, Maartje Gorte, Kalika Prasad, Dongping Bao, Johanna LPM Timmermans-Hereijgers, et al. The plethora gene regulatory network guides growth and cell differentiation in arabidopsis roots. *The Plant Cell*, pages tpc–00656, 2016.

[282] Ning Sun, Jiajun Wang, Zhaoxu Gao, Jie Dong, Hang He, William Terzaghi, Ning Wei, Xing Wang Deng, and Haodong Chen. Arabidopsis saurs are critical for differential light regulation of the development of various organs. *Proceedings of the National Academy of Sciences*, 113(21):6071–6076, 2016.

[283] Hong Ren, Mee Yeon Park, Angela K Spartz, Jeh Haur Wong, and William M Gray. A subset of plasma membrane-localized pp2c. d phosphatases negatively regulate saur-mediated cell expansion in arabidopsis. *PLoS genetics*, 14(6):e1007455, 2018.

[284] Yi Li, Zhan-Bin Liu, Xiangyang Shi, Gretchen Hagen, and Tom J Guilfoyle. An auxin-inducible element in soybean saur promoters. *Plant physiology*, 106(1):37–43, 1994.

[285] Hilda van Mourik, Aalt DJ van Dijk, Niek Stortenbeker, Gerco C Angenent, and Marian Bemer. Divergent regulation of arabidopsis saur genes: a focus on the saur10-clade. *BMC plant biology*, 17(1):245, 2017.

[286] Tao Zhang, Bian Jiang, Ruxiu Xie, Mengfen Xu, Haili Li, and Kaidong Liu. Genome-wide identification and analysis of medicago truncatula small auxin upregulated rna (saur) gene family uncover their roles in nodule formation. *Journal of Plant Biochemistry and Biotechnology*, pages 1–12, 2020.

[287] Anna N Stepanova and Jose M Alonso. Auxin catabolism unplugged: Role of iaa oxidation in auxin homeostasis. *Proceedings of the National Academy of Sciences*, 113(39):10742–10744, 2016.

[288] Arina Shrestha, Sihui Zhong, Jasmine Therrien, Terry Huebert, Shusei Sato, Terry Mun, Stig Andersen, Jens Stougaard, Agnès Lepage, Andréas Niebel, et al. Lotus japonicus nuclear factor ya1, a nodule emergence stage-specific regulator of auxin signalling. *New Phytologist*, 2020.

[289] Priyanka Jha, Sergio J Ochatt, and Vijay Kumar. Wuschel: a master regulator in plant growth signaling. *Plant cell reports*, pages 1–14, 2020.

[290] Sandra L Stone, Siobhan A Braybrook, Stephanie L Paula, Linda W Kwong, Jonathan Meuser, Julie Pelletier, Tzung-Fu Hsieh, Robert L Fischer, Robert B Goldberg, and John J Harada. Arabidopsis leafy cotyledon2 induces maturation traits and auxin activity: implications for somatic embryogenesis. *Proceedings of the National Academy of Sciences*, 105(8):3151–3156, 2008.

[291] Siobhan A Braybrook, Sandra L Stone, Soomin Park, Anhthu Q Bui, Brandon H Le, Robert L Fischer, Robert B Goldberg, and John J Harada. Genes directly regulated by leafy cotyledon2 provide insight into the control of embryo maturation and somatic embryogenesis. *Proceedings of the National Academy of Sciences*, 103(9):3468–3473, 2006.

[292] Horllys Gomes Barreto, Solange Aparecida Ságio, Antonio Chalfun-Júnior, Pedro Fevereiro, and Vagner Augusto Benedito. Transcriptional profiling of the afl subfamily of b3-type transcription factors during the in vitro induction of somatic embryogenesis in the model legume medicago truncatula. *Plant Cell, Tissue and Organ Culture (PCTOC)*, 139(2):327–337, 2019.

[293] Barbara Wójcikowska, Karolina Jaskóła, Przemysław Gąsiorek, Magdalena Meus, Katarzyna Nowak, and Małgorzata D Gaj. Leafy cotyledon2 (lec2) promotes embryogenic induction in somatic tissues of arabidopsis, via yucca-mediated auxin biosynthesis. *Planta*, 238(3):425–440, 2013.

[294] Fengdan Guo, Chuanliang Liu, Han Xia, Yuping Bi, Chuanzhi Zhao, Shuzhen Zhao, Lei Hou, Fuguang Li, and Xingjun Wang. Induced expression of atlec1 and atlec2 differentially promotes somatic embryogenesis in transgenic tobacco plants. *PLoS One*, 8(8):e71714, 2013.

[295] Anneke Horstman, Mengfan Li, Iris Heidmann, Mieke Weemen, Baojian Chen, Jose M Muino, Gerco C Angenent, and Kim Boutilier. The baby boom transcription factor activates the lec1-abi3-fus3-lec2 network to induce somatic embryogenesis. *Plant Physiology*, 175(2):848–857, 2017.

[296] Brian CW Crawford, Jared Sewell, Greg Golembeski, Carmel Roshan, Jeff A Long, and Martin F Yanofsky. Genetic control of distal stem cell fate within root and embryonic meristems. *Science*, 347(6222):655–659, 2015.

[297] Katie Abley, Susanna Sauret-Güeto, Athanasius FM Marée, and Enrico Coen. Formation of polarity convergences underlying shoot outgrowths. *eLife*, 5:e18165, 2016.

[298] Mitsuhiro Aida, Tetsuya Ishida, Hidehiro Fukaki, Hisao Fujisawa, and Masao Tasaka. Genes involved in organ separation in arabidopsis: an analysis of the cup-shaped cotyledon mutant. *The plant cell*, 9(6):841–857, 1997.

[299] Alice Hasson, Anne Plessis, Thomas Blein, Bernard Adroher, Stephen Grigg, Miltos Tsiantis, Arezki Boudaoud, Catherine Damerval, and Patrick Laufs. Evolution and diverse roles of the cup-shaped cotyledon genes in arabidopsis leaf development. *The Plant Cell*, 23(1):54–68, 2011.

[300] Yassin Refahi, Argyris Zardilis, Gaël Michelin, Raymond Wightman, Bruno Leggio, Jonathan Legrand, Emmanuel Faure, Laetitia Vachez, Alessia Armezzani, Feng Zhao, et al. A multiscale analysis of early flower development in arabidopsis provides an integrated view of molecular regulation and growth control. *bioRxiv*, 2020.

[301] Haibao Tang, Vivek Krishnakumar, Shelby Bidwell, Benjamin Rosen, Agnes Chan, Shiguo Zhou, Laurent Gentzbittel, Kevin L Childs, Mark Yandell, Heidrun Gundlach, et al. An improved genome release (version mt4. 0) for the model legume medicago truncatula. *BMC genomics*, 15(1):312, 2014.

[302] Uritza von Groll, Dieter Berger, and Thomas Altmann. The subtilisin-like serine protease sdd1 mediates cell-to-cell signaling during arabidopsis stomatal development. *The Plant Cell*, 14(7):1527–1539, 2002.

[303] Fei Chen, Yue Hu, Alessandro Vannozzi, Kangcheng Wu, Hanyang Cai, Yuan Qin, Alison Mullis, Zhenguo Lin, and Liangsheng Zhang. The wrky transcription factor family in model plants and crops. *Critical Reviews in Plant Sciences*, 36(5-6):311–335, 2017.

[304] Peter Cressey and John Reeve. Metabolism of cyanogenic glycosides: A review. *Food and chemical toxicology*, 125:225–232, 2019.

[305] Zhou Du, Xin Zhou, Yi Ling, Zhenhai Zhang, and Zhen Su. agrigo: a go analysis toolkit for the agricultural community. *Nucleic acids research*, 38(suppl_2):W64–W70, 2010.

[306] Susan Y Fujimoto, Masaru Ohta, Akemi Usui, Hideaki Shinshi, and Masaru Ohme-Takagi. Arabidopsis ethylene-responsive element binding factors act as transcriptional activators or repressors of gcc box–mediated gene expression. *The Plant Cell*, 12(3):393–404, 2000.

[307] Patrick Favre, Laure Bapaume, Eligio Bossolini, Mauro Delorenzi, Laurent Falquet, and Didier Reinhardt. A novel bioinformatics pipeline to discover genes related to arbuscular mycorrhizal symbiosis based on their evolutionary conservation pattern among higher plants. *BMC plant biology*, 14(1):333, 2014.

[308] Katia Petroni, Roderick W Kumimoto, Nerina Gnesutta, Valentina Calvenzani, Monica Fornari, Chiara Tonelli, Ben F Holt, and Roberto Mantovani. The promiscuous life of plant nuclear factor y transcription factors. *The Plant Cell*, 24(12):4777–4792, 2012.

[309] José M Franco-Zorrilla, Irene López-Vidriero, José L Carrasco, Marta Godoy, Pablo Vera, and Roberto Solano. Dna-binding specificities of plant transcription factors and their potential to define target genes. *Proceedings of the National Academy of Sciences*, 111(6):2367–2372, 2014.

[310] Staci Nole-Wilson and Beth A Krizek. Dna binding properties of the arabidopsis floral development protein aintegumenta. *Nucleic Acids Research*, 28(21):4076–4082, 2000.

[311] D Roeland Boer, Alejandra Freire-Rios, Willy AM van den Berg, Terrens Saaki, Iain W Manfield, Stefan Kepinski, Irene López-Vidrieo, Jose Manuel Franco-Zorrilla, Sacco C de Vries, Roberto Solano, et al. Structural basis for dna binding specificity by the auxin-dependent arf transcription factors. *Cell*, 156(3):577–589, 2014.

[312] Ionas Erb, Juan R Gonzalez-Vallinas, Giovanni Bussotti, Enrique Blanco, Eduardo Eyras, and Cedric Notredame. Use of chip-seq data for the design of a multiple promoter-alignment method. *Nucleic acids research*, 40(7):e52–e52, 2012.

[313] Cedrik Magis, Jean-François Taly, Giovanni Bussotti, Jia-Ming Chang, Paolo Di Tommaso, Ionas Erb, José Espinosa-Carrasco, and Cedric Notredame. T-coffee: tree-based consistency objective function for alignment evaluation. In *Multiple Sequence Alignment Methods*, pages 117–129. Springer, 2014.

[314] Miguel A Moreno-Risueno, Rosangela Sozzani, Galip Gürkan Yardımcı, Jalean J Petricka, Teva Vernoux, Ikram Blilou, Jose Alonso, Cara M Winter, Uwe Ohler, Ben Scheres, et al. Transcriptional control of tissue formation throughout root development. *Science*, 350(6259):426–430, 2015.

[315] Sabrina Sabatini, Dimitris Beis, Harald Wolkenfelt, Jane Murfett, Tom Guilfoyle, Jocelyn Malamy, Philip Benfey, Ottoline Leyser, Nicole Bechtold, Peter Weisbeek, et al. An auxin-dependent distal organizer of pattern and polarity in the arabidopsis root. *Cell*, 99(5):463–472, 1999.

[316] Oliver Windram, Priyadharshini Madhou, Stuart McHattie, Claire Hill, Richard Hickman, Emma Cooke, Dafyd J Jenkins, Christopher A Penfold, Laura Baxter, Emily Breeze, et al. Arabidopsis defense against botrytis cinerea: chronology and regulation deciphered by high-resolution temporal transcriptomic analysis. *The Plant Cell*, 24(9):3530–3557, 2012.

[317] Bo Bai, Ying Hua Su, Jia Yuan, and Xian Sheng Zhang. Induction of somatic embryos in arabidopsis requires local yucca expression mediated by the down-regulation of ethylene biosynthesis. *Molecular plant*, 6(4):1247–1260, 2013.

[318] Sonja Kosuta, Mark Held, Md Shakhawat Hossain, Giulia Morieri, Amanda MacGillivary, Christopher Johansen, Meritxell Antolín-Llovera, Martin Parniske, Giles ED Oldroyd, Allan J Downie, et al. Lotus japonicus symrk-14 uncouples the cortical and epidermal symbiotic program. *The Plant Journal*, 67(5):929–940, 2011.

[319] Tom Denyer, Xiaoli Ma, Simon Klesen, Emanuele Scacchi, Kay Nieselt, and Marja CP Timmermans. Spatiotemporal developmental trajectories in the arabidopsis root revealed using high-throughput single-cell rna sequencing. *Developmental cell*, 48(6):840–852, 2019.

[320] Mireya Plass, Jordi Solana, F Alexander Wolf, Salah Ayoub, Aristotelis Misios, Petar Glažar, Benedikt Obermayer, Fabian J Theis, Christine Kocks, and Nikolaus Rajewsky. Cell type atlas and lineage tree of a whole complex animal by single-cell transcriptomics. *Science*, 360(6391), 2018.

[321] Vera Zywitza, Aristotelis Misios, Lena Bunatyan, Thomas E Willnow, and Nikolaus Rajewsky. Single-cell transcriptomics characterizes cell types in the subventricular zone and uncovers molecular defects impairing adult neurogenesis. *Cell Reports*, 25(9):2457–2469, 2018.

[322] Joko Prayitno, Barry G Rolfe, and Ulrike Mathesius. The ethylene-insensitive sickle mutant of medicago truncatula shows altered auxin transport regulation during nodulation. *Plant Physiology*, 142(1):168–180, 2006.

[323] Eric M Kramer. Auxin-regulated cell polarity: an inside job? *Trends in plant science*, 14(5):242–247, 2009.

[324] Krzysztof Wabnik, Jurgen Kleine-Vehn, Jozef Balla, Michael Sauer, Satoshi Naramoto, Vilem Reinohl, Roeland MH Merks, Willy Govaerts, and Jiri Friml. Emergence of tissue polarization from synergy of intracellular and extracellular auxin signaling. *Molecular systems biology*, 6(1):447, 2010.

[325] Mikolaj Cieslak, Adam Runions, and Przemyslaw Prusinkiewicz. Auxin-driven patterning with unidirectional fluxes. *Journal of experimental botany*, page erv262, 2015.

[326] GJ Mitchison. A model for vein formation in higher plants. *Proceedings of the Royal Society of London. Series B. Biological Sciences*, 207(1166):79–109, 1980.

[327] Krzysztof Wabnik, Willy Govaerts, Jiří Friml, and Jürgen Kleine-Vehn. Feedback models for polarized auxin transport: an emerging trend. *Molecular BioSystems*, 7(8):2352–2359, 2011.

[328] Jakub Hajnỳ, Tomáš Prát, Nikola Rydza, Lesia Rodriguez, Shutang Tan, Inge Verstraeten, David Domjan, Ewa Mazur, Elwira Smakowska-Luzan, Wouter Smet, et al. Receptor kinase module targets pin-dependent auxin transport during canalization. *Science*, 370(6516):550–557, 2020.

[329] Satoshi Naramoto. Polar transport in plants mediated by membrane transporters: focus on mechanisms of polar auxin transport. *Current Opinion in Plant Biology*, 40:8–14, 2017.

[330] Xueqing Geng and David Mackey. Dose–response to and systemic movement of dexamethasone in the gvg-inducible transgene system in arabidopsis. In *Plant Immunity*, pages 59–68. Springer, 2011.

[331] Lorenzo Borghi. Inducible gene expression systems for plants. *Plant Developmental Biology: Methods and Protocols*, pages 65–75, 2010.

[332] Shigeru Kondo and Takashi Miura. Reaction-diffusion model as a framework for understanding biological pattern formation. *science*, 329(5999):1616–1620, 2010.

[333] Alfred Gierer and Hans Meinhardt. A theory of biological pattern formation. *Kybernetik*, 12(1):30–39, 1972.

[334] Sara Díaz-Triviño, Yuchen Long, Ben Scheres, and Ikram Blilou. Analysis of a plant transcriptional regulatory network using transient expression systems. In *Plant Gene Regulatory Networks*, pages 83–103. Springer, 2017.

[335] Juan Dong, Cora A MacAlister, and Dominique C Bergmann. Basl controls asymmetric cell division in arabidopsis. *Cell*, 137(7):1320–1330, 2009.

[336] Saiko Yoshida, Alja Van Der Schuren, Maritza Van Dop, Luc Van Galen, Shunsuke Saiga, Milad Adibi, Barbara Möller, A Colette, Peter Marhavy, Richard Smith, et al. A

soseki-based coordinate system interprets global polarity cues in arabidopsis. *Nature plants*, 5(2):160–166, 2019.

[337] Jérémy Gruel, Benoit Landrein, Paul Tarr, Christoph Schuster, Yassin Refahi, Arun Sampathkumar, Olivier Hamant, Elliot M Meyerowitz, and Henrik Jönsson. An epidermis-driven mechanism positions and scales stem cell niches in plants. *Science advances*, 2(1):e1500989, 2016.

[338] Neha Bhatia, Behruz Bozorg, André Larsson, Carolyn Ohno, Henrik Jönsson, and Marcus G Heisler. Auxin acts through monopteros to regulate plant cell polarity and pattern phyllotaxis. *Current Biology*, 26(23):3202–3208, 2016.

[339] Marcin Nadzieja, Simon Kelly, Jens Stougaard, and Dugald Reid. Epidermal auxin biosynthesis facilitates rhizobial infection in lotus japonicus. *The Plant Journal*, 95(1):101–111, 2018.

[340] Takeshi Nishimura, Ken-ichiro Hayashi, Hiromi Suzuki, Atsuko Gyohda, Chihiro Takaoka, Yusuke Sakaguchi, Sachiko Matsumoto, Hiroyuki Kasahara, Tatsuya Sakai, Jun-ichi Kato, et al. Yucasin is a potent inhibitor of yucca, a key enzyme in auxin biosynthesis. *The Plant Journal*, 77(3):352–366, 2014.

[341] Shinichi Tsugafune, Kiyoshi Mashiguchi, Kosuke Fukui, Yumiko Takebayashi, Takeshi Nishimura, Tatsuya Sakai, Yukihisa Shimada, Hiroyuki Kasahara, Tomokazu Koshiba, and Ken-ichiro Hayashi. Yucasin df, a potent and persistent inhibitor of auxin biosynthesis in plants. *Scientific reports*, 7(1):1–13, 2017.

[342] Yusuke Kakei, Chiaki Yamazaki, Masashi Suzuki, Ayako Nakamura, Akiko Sato, Yosuke Ishida, Rie Kikuchi, Shouichi Higashi, Yumiko Kokudo, Takahiro Ishii, et al. Small-molecule auxin inhibitors that target yucca are powerful tools for studying auxin function. *The Plant Journal*, 84(4):827–837, 2015.

[343] D Marc Jones and Klaas Vandepoele. Identification and evolution of gene regulatory networks: Insights from comparative studies in plants. *Current opinion in plant biology*, 54:42–48, 2020.

[344] Beatriz Orosa-Puente, Nicola Leftley, Daniel von Wangenheim, Jason Banda, Anjil K Srivastava, Kristine Hill, Jekaterina Truskina, Rahul Bhosale, Emily Morris, Moumita Srivastava, et al. Root branching toward water involves posttranslational modification of transcription factor arf7. *Science*, 362(6421):1407–1410, 2018.

[345] Ioannis Tamvakis. Auxin and the nodule.

[346] Emiko Yoro, Takuya Suzaki, Koichi Toyokura, Hikota Miyazawa, Hidehiro Fukaki, and Masayoshi Kawaguchi. A positive regulator of nodule organogenesis, nodule inception, acts as a negative regulator of rhizobial infection in lotus japonicus. *Plant physiology*, 165(2):747–758, 2014.

[347] Takashi Soyano, Hideki Hirakawa, Shusei Sato, Makoto Hayashi, and Masayoshi Kawaguchi. Nodule inception creates a long-distance negative feedback loop involved in homeostatic regulation of nodule organ production. *Proceedings of the National Academy of Sciences*, 111(40):14607–14612, 2014.

[348] Christian Rogers and Giles ED Oldroyd. Synthetic biology approaches to engineering the nitrogen symbiosis in cereals. *Journal of experimental botany*, 65(8):1939–1946, 2014.

[349] Nicola J Patron, Diego Orzaez, Sylvestre Marillonnet, Heribert Warzecha, Colette Matthewman, Mark Youles, Oleg Raitskin, Aymeric Leveau, Gemma Farré, Christian Rogers, et al. Standards for plant synthetic biology: a common syntax for exchange of dna parts. *New Phytologist*, 208(1):13–19, 2015.

[350] Aurélien Boisson-Dernier, Mireille Chabaud, Fernand Garcia, Guillaume Bécard, Charles Rosenberg, and David G Barker. Agrobacterium rhizogenes-transformed roots of medicago truncatula for the study of nitrogen-fixing and endomycorrhizal symbiotic associations. *Molecular Plant-Microbe Interactions*, 14(6):695–700, 2001.

[351] GÖSTA FÅHRAEUS. The infection of clover root hairs by nodule bacteria studied by a simple glass slide technique. *Microbiology*, 16(2):374–381, 1957.

[352] Paula Korkuć, Jos HM Schippers, and Dirk Walther. Characterization and identification of cis-regulatory elements in arabidopsis based on single-nucleotide polymorphism information. *Plant Physiology*, 164(1):181–200, 2014.

[353] Si Quang Le and Olivier Gascuel. An improved general amino acid replacement matrix. *Molecular biology and evolution*, 25(7):1307–1320, 2008.

[354] Sudhir Kumar, Glen Stecher, and Koichiro Tamura. Mega7: molecular evolutionary genetics analysis version 7.0 for bigger datasets. *Molecular biology and evolution*, 33(7):1870–1874, 2016.

[355] Colin Smith, Przemyslaw Prusinkiewicz, and Faramarz Samavati. Local specification of surface subdivision algorithms. In *International Workshop on Applications of Graph Transformations with Industrial Relevance*, pages 313–327. Springer, 2003.